Xsuite physics manual

CERN - Geneva, Switzerland

Contents

1 Lattice modeling and particle coordinates **11**
- 1.1 Local reference system . . . 11
- 1.2 Global reference system . . . 12
- 1.3 Reference particle . . . 14
- 1.4 Electromagnetic potentials and fields . . . 15
- 1.5 Convention for multipole expansion of magnetic fields . . . 15
  - 1.5.1 Straight magnets ($h = 0$) . . . 15
  - 1.5.2 Curved magnets ($h \neq 0$) . . . 16
- 1.6 Particle coordinates . . . 17
- 1.7 Hamiltonian and equations of motion . . . 19
- 1.8 Expanded magnet body Hamiltonian . . . 19
  - 1.8.1 Approximation of the kinetic part of the Hamiltonian . . . 20
  - 1.8.2 Approximation of the magnetic part of the Hamiltonian . . . 20
- 1.9 Symplectic integrators and magnet models . . . 21
  - 1.9.1 Practical recommendations . . . 22

2 Beam element maps **25**
- 2.1 Drift . . . 25
- 2.2 Polar drift (sector curvature h) . . . 26
- 2.3 Curved exact bend . . . 27
- 2.4 Straight exact bend . . . 30
- 2.5 Rectangular bend - straight body . . . 31
- 2.6 Expanded Bend-Quadrupole (also used for Quadrupole) . . . 32
- 2.7 Exact path correction for mat-kick-mat . . . 35
- 2.8 Thin bend . . . 36
- 2.9 Thin Multipole . . . 36
- 2.10 Dipole fringe field . . . 37
  - 2.10.1 Geometry, coordinates and magnetic field . . . 37
  - 2.10.2 Lorentz equations near the mid-plane . . . 38
  - 2.10.3 Hard-edge limit and linear vertical focusing . . . 39
  - 2.10.4 Finite-width correction for zero incoming vertical slope . . . 40
  - 2.10.5 Momentum-dependent coefficient of the generating function . . . 42
  - 2.10.6 Constructing the corrected tangent form . . . 50
  - 2.10.7 Generating function and forward map . . . 51
  - 2.10.8 Additional cubic kick in the implementation . . . 52
  - 2.10.9 Complete generating function and forward map . . . 55

2.10.10 Derivatives used in tracking . . . 56
2.10.11 Exit face . . . 58
2.10.12 Backtracking . . . 59
2.11 Dipole wedge . . . 60
2.12 Multipole fringe field . . . 61
2.12.1 Backtracking . . . 62
2.13 Quadrupolar correction for wedge and Y rotation . . . 62
2.14 Accelerating Cavity . . . 63
2.15 RF-Multipole . . . 64
2.16 Solenoid . . . 65
2.16.1 Tilted solenoid . . . 68
2.16.2 Generalization to arbitrary tilt and dipolar components . . . 69
2.17 Wire . . . 70
2.18 Electron Lens . . . 71
2.18.1 Hollow electron lens - uniform annular profile . . . 72
2.19 Electron Cooler . . . 73
2.19.1 Electron beam space charge . . . 75
2.20 Rotations . . . 75
2.20.1 X Rotation . . . 76
2.20.2 Y Rotation . . . 76
2.20.3 S Rotation . . . 77
2.21 Cavity time, energy errors and acceleration . . . 77
2.21.1 Implementing energy errors . . . 77
2.21.2 Acceleration . . . 78

3 Misalignments **79**
3.1 Definitions . . . 79
3.2 Misalignment at arbitrary s without a tilt . . . 81
3.3 Misalignment at arbitrary s (the straight case) . . . 83
3.4 Misalignment at arbitrary s with a tilt . . . 85
3.5 Misalignment at arbitrary s with a tilt (straight case) . . . 86
3.6 S Shift – ζ correction . . . 86

4 Linear optics **89**
4.1 Linear normal form . . . 89
4.2 Twiss parameters . . . 93
4.3 Transformation to normalized coordinates . . . 95
4.4 Covariance matrix . . . 95
4.4.1 Normal-mode emittances . . . 96
4.4.2 Eigenvectors of the covariance matrix . . . 98
4.5 Action, amplitude and emittance . . . 99
4.6 Dispersion and crab dispersion . . . 100
4.6.1 Dispersion . . . 100
4.6.2 Crab dispersion . . . 101

5 Resonance Driving Terms **103**
5.1 Courant–Snyder normalized coordinates . . . 103
5.2 Complex Courant–Snyder coordinates . . . 103
5.3 Motion expressed through resonance driving terms . . . 103
5.4 Expression of RDTs from first-order perturbation theory . . . 104
5.5 Feed-down and misalignments . . . 104
5.5.1 Coordinate transformation . . . 105
5.5.2 Feed-down expansion . . . 105
5.5.3 Expansion around a closed orbit x_0, y_0 . . . 106

6 Linear coupling **107**
6.1 Scope and conventions . . . 107
6.2 Turn-by-turn motion in the Mais–Ripken formalism . . . 107
6.2.1 Linear normal form and the W matrix . . . 107
6.2.2 Mais–Ripken lattice functions from W . . . 108
6.2.3 Closest-tune-approach indicator . . . 109
6.3 Edwards–Teng decoupling and modal Twiss parameters . . . 110
6.3.1 Decoupled modal maps . . . 110
6.3.2 Relation between W and the Edwards–Teng transformation . . . 114
6.3.3 Relation between Edwards–Teng and Mais–Ripken functions . . . 117
6.3.4 Propagation of Edwards–Teng parameters . . . 118
6.4 Turn-by-turn motion in the RDT formalism . . . 119
6.4.1 Complex Courant–Snyder coordinates . . . 119
6.4.2 The four linear-coupling monomials . . . 120
6.5 Observable position and momentum amplitudes . . . 120
6.5.1 Normalized-coordinate signals . . . 120
6.5.2 Mais–Ripken and RDT amplitude identities . . . 121
6.5.3 Physical canonical-momentum ratios . . . 122
6.6 Exact matrix-equivalent RDTs from W . . . 123
6.6.1 Definition from the normalized coupling matrix . . . 123
6.6.2 Direct extraction of the coupling RDTs from the normal-form matrix . . . 124

7 Synchrotron motion **125**
7.1 Turn slippage for different particle species . . . 126
7.2 Linearized motion . . . 127
7.3 Smooth approximation . . . 128
7.4 Kick-drift model . . . 130
7.5 Hamiltonian of the synchrotron motion . . . 130
7.5.1 Fixed points . . . 131
7.6 RF-frequency change modeled as a shift in ζ . . . 132

8 Counter-rotating beams **135**
8.1 Reversed reference frame . . . 135
8.2 Transformation of beam elements . . . 135
8.2.1 Horizontal deflecting cavity . . . 136
8.2.2 Vertical deflecting cavity . . . 136

9 Synchrotron radiation **139**
9.1 Damping from synchrotron radiation . . . 140
9.2 Equilibrium emittance . . . 140
9.3 Radiation integrals . . . 142
9.3.1 Derivations . . . 145

10 Spin tracking and polarization **155**
10.1 Spin tracking . . . 155
10.2 Linear transport matrix including spin . . . 156
10.3 Invariant Spin Field - first order computation . . . 156
10.4 Equilibrium polarization and polarization time . . . 157
10.5 Monte Carlo method for equilibrium polarization . . . 158

11 Coasting beams and acceleration **159**
11.1 Simulation clock and arrival time . . . 159
11.2 Constant-energy frame construction . . . 160
11.3 Constant-energy ζ definition and update . . . 161
11.4 Handling particles jumping to the following frame . . . 162
11.5 Proofs for constant-energy frames . . . 163
11.6 Frames during acceleration . . . 165
11.6.1 Reference turns and frame boundaries . . . 165
11.6.2 Conditions on particle motion . . . 166
11.6.3 Coordinate changes and waiting particles . . . 166

12 Aperture Modelling and Calculation **169**
12.1 Overview and definitions . . . 169
12.1.1 Aperture model . . . 169
12.1.2 Aperture bounds . . . 169
12.1.3 Profile shapes . . . 170
12.1.4 Profiles . . . 171
12.1.5 Beam envelope . . . 171
12.2 Algorithms . . . 173
12.2.1 Aperture bounds . . . 173
12.2.2 Cross section interpolation . . . 173
12.2.3 Maximum beam sigma . . . 175

13 Modeling s-dependent magnetic fields **179**
13.1 Coordinates and field normalization . . . 179
13.1.1 Line element and differential operators . . . 179
13.1.2 Field normalization . . . 180
13.2 Field profiles and scalar-potential reconstruction . . . 181
13.2.1 Deriving the two seed functions . . . 181
13.2.2 Why two seeds determine the expansion . . . 182
13.2.3 Coefficient recurrence in a curved frame . . . 183
13.3 Vector potential and gauge . . . 183
13.3.1 Constructing the vector potential . . . 184
13.3.2 Checking the vertical field away from the midplane . . . 185

13.3.3 Evaluation and elementary examples . . . 185
13.4 Field representation in SplineBoris . . . 185
13.5 SplineBoris: spatial Boris integration . . . 186
13.5.1 Lorentz-force equations in spatial form . . . 186
13.5.2 Integration algorithm . . . 187
13.5.3 Phase-space volume preservation . . . 189
13.5.4 Reversibility and second-order accuracy . . . 193
13.5.5 Global symplectic defect at field-free boundaries . . . 199
13.5.6 Volume preservation of the exact spatial flow . . . 201
13.5.7 Divergence-free vector fields and volume preservation . . . 204
13.5.8 Consistency check for the parallel case . . . 204
13.5.9 Taylor expansion of the exact flow . . . 206
13.5.10 Discrete Gronwall lemma . . . 206
13.6 BFieldExpansion: RK4 tracking . . . 207
13.6.1 Polynomial profiles and additional strengths . . . 208
13.6.2 Expansion order and convergence . . . 208
13.6.3 Hamiltonian and equations of motion . . . 209
13.6.4 Numerical integration . . . 210
13.6.5 Canonical and kinetic momenta at boundaries . . . 210

14 Space charge and beam-beam forces 211
14.1 Fields generated by a bunch of particles . . . 211
14.1.1 2.5D approximation . . . 213
14.1.2 Modulated 2D . . . 213
14.2 Lorentz force . . . 214
14.3 Space charge . . . 215
14.4 Beam-beam interaction (4D model) . . . 216
14.5 Longitudinal profiles . . . 218
14.5.1 Gaussian profile . . . 218
14.5.2 q-Gaussian . . . 218
14.6 Beam-beam interaction (6D model, Hirata method) . . . 218
14.6.1 Direct Lorentz boost (for the weak beam) . . . 219
14.6.2 Synchro-beam mapping . . . 220
14.6.3 Propagation of the strong beam to the collision point . . . 221
14.6.4 Forces and kicks on weak beam particles . . . 228
14.6.5 Inverse Lorentz boost (for the weak beam) . . . 230
14.6.6 Additional material . . . 231
14.7 Beam-beam interaction (6d model, Particle In Cell) . . . 235
14.7.1 Propagation of particles during the interaction . . . 235
14.7.2 Time relation between the two beams . . . 236
14.7.3 Computation of the kick . . . 236
14.8 Configuration of beam-beam lenses for tracking simulations (weak-strong) . . . 236
14.8.1 Identification of the beam position and direction . . . 237
14.8.2 Computation of beam-beam separations . . . 238
14.8.3 Crossing plane and crossing angle . . . 238

14.8.4 The crossing plane . . . 239
14.8.5 The crossing angle . . . 240
14.8.6 Transformations for the anticlockwise beam (B4) . . . 242
14.8.7 Crab crossing . . . 242
14.8.8 Configuration of beam-beam lenses for beam 2 . . . 246
14.8.9 Step-by-step configuration procedure . . . 247

15 Bhabha scattering and beamstrahlung **249**
15.1 Bhabha scattering . . . 249
15.1.1 Luminosity Computation . . . 250
15.1.2 Virtual Photon Generation . . . 251
15.1.3 Inverse Compton Scattering of Virtual Photons . . . 251
15.2 Beamstrahlung . . . 252

16 Wakefields and impedances **255**
16.1 Transverse wakefields . . . 255
16.2 Transverse impedances . . . 256
16.3 Longitudinal wakefield . . . 257
16.4 Longitudinal impedance . . . 257
16.5 Integrated wakefields . . . 258
16.6 Analytical wakes . . . 260

17 Intra-Beam Scattering **263**
17.1 Analytical Growth Rates . . . 263
17.1.1 Nagaitsev Formalism . . . 264
17.1.2 Bjorken-Mtingwa Formalism . . . 266
17.2 Steady-state emittances . . . 269
17.2.1 Steady-state emittances with QE, SR, and IBS . . . 269
17.2.2 Steady-state emittances due to betatron coupling . . . 270
17.2.3 Steady-state emittances due to an external excitation . . . 270
17.3 IBS Kicks . . . 271
17.3.1 Analytical Kicks . . . 271
17.3.2 Kinetic Kicks . . . 271

18 Touschek scattering **275**
18.1 Touschek scattering rate . . . 275
18.2 Piwinski formula . . . 276
18.3 Monte Carlo evaluation of the scattering rate . . . 277
18.3.1 Sampling of the scattering pair . . . 278
18.3.2 Scattering kinematics . . . 279
18.3.3 Selection of the particles to be tracked . . . 279
18.3.4 Weighting of the scattered macroparticles . . . 279

19 FFT solvers and convolutions **281**
19.1 Notation for Discrete Fourier Transform . . . 281
19.2 FFT convolution - 1D case . . . 281
19.3 Extension to multiple dimensions . . . 286

19.4 Green functions for 2D and 3D Poisson problems 287
19.5 Generalization to observation interval different from source interval . 289
19.6 Compressed FFT convolution 293

Chapter 1

Lattice modeling and particle coordinates

The modeling of lattice and beam particles used in Xsuite is largely based on the experience of the MAD [1, 2] and SixTrack [3] programs.
More details on the derivation of the tracking maps and the Hamiltonian formalism can be found in the references [4, 5, 6, 7, 8, 9, 10, 11].

1.1 Local reference system

This section is adapted from [1].

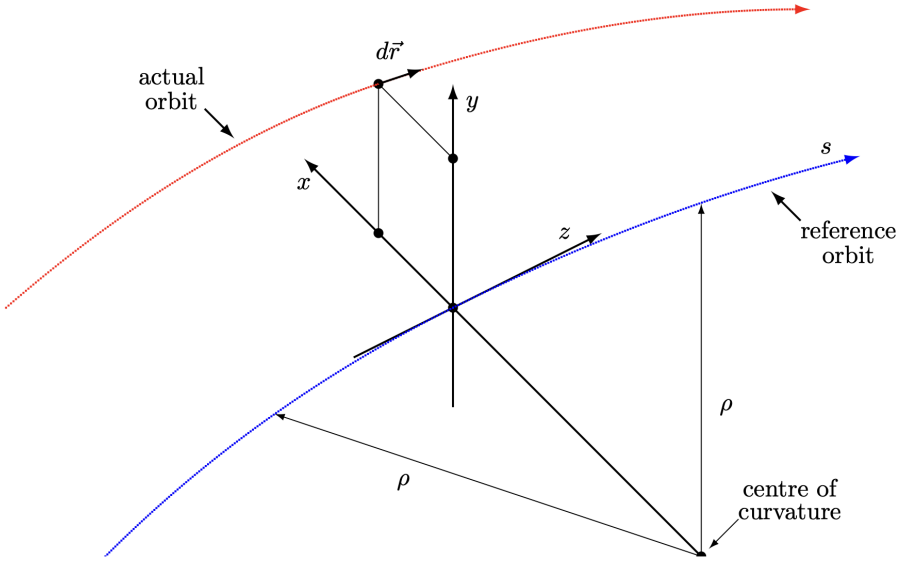


Figure 1.1: Local Reference System

The beam line or ring to be studied is described as a sequence of beam elements placed sequentially along a reference trajectory.

The reference trajectory consists of a series of straight line segments and circular arcs. The accompanying tripod, as shown in Fig. 1.1, spans a local curvilinear right-handed coordinate system (x, y, s). The local s-axis is the tangent to the reference orbit and x and y are perpendicular to s. Typically, x is horizontal and y vertical.
We call ρ the local radius of curvature of the reference trajectory and h the local curvature defined as:

$$h = \frac{1}{\rho} \tag{1.1.1}$$

1.2 Global reference system

This section is adapted from [1].

The local reference system (x, y, s) may thus be referred to a global Cartesian coordinate system (X, Y, Z) as shown in Fig. 1.2.

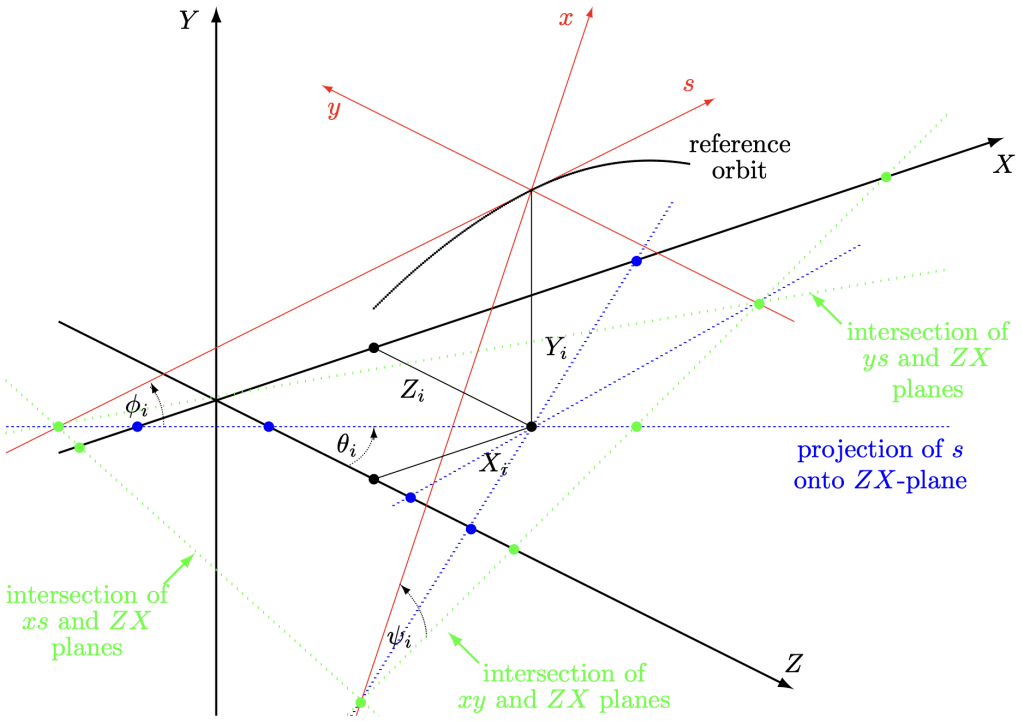


Figure 1.2: Global Reference System showing the global Cartesian system (X, Y, Z) in black and the local reference system (x, y, s) in red with the translation (X_i, Y_i, Z_i) and rotation $(\theta_i, \phi_i, \psi_i)$ relating the two.

The positions between beam elements are indexed with $i = 0, \ldots, n$. The local reference system (x_i, y_i, s_i) at position i, i.e. the displacement and direction of the reference orbit with respect to the system (X, Y, Z) are defined by three displacements (X_i, Y_i, Z_i) and three angles $(\theta_i, \phi_i, \psi_i)$.
The above quantities are defined more precisely as follows:

- X Displacement of the local origin in X-direction.
- Y Displacement of the local origin in Y-direction.
- Z Displacement of the local origin in Z-direction.
- θ is the angle of rotation (azimuth) about the global Y-axis, between the global Z-axis and the projection of the reference orbit onto the (Z, X)-plane. A positive angle θ forms a right-hand screw with the Y-axis.
- ϕ is the elevation angle, i.e. the angle between the reference orbit and its projection onto the (Z, X)-plane. A positive angle ϕ corresponds to increasing Y.

  If only horizontal bends are present, the reference orbit remains in the (Z, X)-plane and ϕ is always zero.
- ψ is the roll angle about the local s-axis, i.e. the angle between the line defined by the intersection of the (x, y)-plane and (Z, X)-plane on one hand, and the local x-axis on the other hand. A positive angle ψ forms a right-hand screw with the s-axis.

Note that the angles (θ, ϕ, ψ) do not follow the usual definition of Euler angles. The reference orbit starts at the origin and points by default in the direction of the positive Z-axis.
Internally the displacement is described by a vector $\mathbf{V}$ and the orientation by a unitary matrix $\mathbf{W}$. The column vectors of $\mathbf{W}$ are the unit vectors spanning the local coordinate axes in the order (x, y, s). $\mathbf{V}$ and $\mathbf{W}$ have the values:

$$\mathbf{V} = \begin{bmatrix} X \\ Y \\ Z \end{bmatrix}, \qquad \mathbf{W} = \Theta\Phi\Psi \tag{1.2.1}$$

where

$$\Theta = \begin{bmatrix} \cos\theta & 0 & \sin\theta \\ 0 & 1 & 0 \\ -\sin\theta & 0 & \cos\theta \end{bmatrix}, \quad \Phi = \begin{bmatrix} 1 & 0 & 0 \\ 0 & \cos\phi & \sin\phi \\ 0 & -\sin\phi & \cos\phi \end{bmatrix}, \quad \Psi = \begin{bmatrix} \cos\psi & -\sin\psi & 0 \\ \sin\psi & \cos\psi & 0 \\ 0 & 0 & 1 \end{bmatrix}. \tag{1.2.2}$$

When advancing through a beam element, Xsuite (like MAD) computes V_i and W_i by the recurrence relations

$$V_i = W_{i-1}R_i + V_{i-1}, \qquad W_i = W_{i-1}S_i \tag{1.2.3}$$

The vector R_i is the displacement and the matrix S_i is the rotation of the local reference system introduced by the element i with respect to the entrance of the same element. The values of R_i and S_i are listed below for different physical element types.

In straight elements the local reference system is simply translated by the length of the element along the local s-axis.
The corresponding R and S are

$$R = \begin{bmatrix} 0 \\ 0 \\ L \end{bmatrix}, \qquad S = \begin{bmatrix} 1 & 0 & 0 \\ 0 & 1 & 0 \\ 0 & 0 & 1 \end{bmatrix}. \tag{1.2.4}$$

A rotation of the element about the s-axis has no effect on R and S, since the rotations of the reference system before and after the element cancel.
Bending magnets have a curved reference orbit. For both rectangular and sector bending magnets, the R and S are expressed as functions of the bend angle α:

$$R = \begin{bmatrix} \rho(\cos\alpha - 1) \\ 0 \\ \rho\sin\alpha \end{bmatrix}, \qquad S = \begin{bmatrix} \cos\alpha & 0 & -\sin\alpha \\ 0 & 1 & 0 \\ \sin\alpha & 0 & \cos\alpha \end{bmatrix} \tag{1.2.5}$$

where we have assumed that the bending occurs in the horizontal plane. A positive bend angle represents a bend to the right, i.e. towards negative x values. For sector bending magnets, the bend radius is given by ρ, and for rectangular bending magnets it has the value $\rho = L/(2\sin(\alpha/2))$. If the magnet is rotated about the s-axis by an angle ψ, R and S are transformed by

$$R = TR, \qquad S = TST^{-1} \tag{1.2.6}$$

where T is the orthogonal rotation matrix

$$T = \begin{bmatrix} \cos\psi & -\sin\psi & 0 \\ \sin\psi & \cos\psi & 0 \\ 0 & 0 & 1 \end{bmatrix} \tag{1.2.7}$$

The special value $\psi = \pi/2$ represents a bend down.

1.3 Reference particle

We introduce a reference particle with rest mass m_0, charge q_0, total energy E_0, momentum P_0, and relativistic factors β_0, γ_0. These quantities satisfy

$$E_0^2 = (P_0 c)^2 + (m_0 c^2)^2, \tag{1.3.1}$$

$$E_0 = m_0 \gamma_0 c^2, \tag{1.3.2}$$

$$P_0 = m_0 \beta_0 \gamma_0 c, \tag{1.3.3}$$

$$\beta_0 = \frac{P_0 c}{E_0} = \sqrt{1 - \frac{1}{\gamma_0^2}}, \tag{1.3.4}$$

$$\gamma_0 = \frac{1}{\sqrt{1-\beta_0^2}}. \tag{1.3.5}$$

The reference particle will be used to normalize momentum and energy variables as well as electromagnetic fields and potentials. For this purpose we introduce the corresponding reference beam rigidity as

$$\mathrm{rig}_0 = \frac{P_0}{q_0}, \tag{1.3.6}$$

which is the momentum per unit charge used, for example, to normalize multipole strengths.

1.4 Electromagnetic potentials and fields

The electromagnetic fields **E** and **B** can be derived from the potentials $\Phi(x,y,s,t)$ and $\mathbf{A}(x,y,s,t)$, where

$$\mathbf{A}(x,y,s,t) = A_x(x,y,s,t)\hat{x}(s) + A_y(x,y,s,t)\hat{y}(s) + A_s(x,y,s,t)\hat{z}(s) \tag{1.4.1}$$

and for which:

$$\mathbf{E} = -\nabla\Phi - \frac{\partial \mathbf{A}}{\partial t} = -\partial_x\Phi\hat{x} - \partial_y\Phi\hat{y} - \frac{1}{1+hx}\partial_s\Phi\hat{z} - \partial_t\mathbf{A} \tag{1.4.2}$$

$$\mathbf{B} = \nabla\times\mathbf{A} = \left(\partial_y A_s - \frac{\partial_s A_y}{1+hx}\right)\hat{x} + \left(\frac{\partial_s A_x - \partial_x(1+hx)A_s}{1+hx}\right)\hat{y} + \left(\partial_x A_y - \partial_y A_x\right)\hat{z}. \tag{1.4.3}$$

We use the reference particle properties to define normalized potentials:

$$\mathbf{a}(x,y,s,t) = \frac{q_0}{P_0}\mathbf{A}(x,y,s,t) \tag{1.4.4}$$

$$\varphi(x,y,s,t) = \frac{q_0}{P_0 c}\Phi(x,y,s,t) \tag{1.4.5}$$

1.5 Convention for multipole expansion of magnetic fields

This section is adapted from [1].

1.5.1 Straight magnets ($h = 0$)

Xsuite, like MAD, uses the following Taylor expansion for the magnetic field components. Using a complex notation for the field $(B_y + iB_x)$ and the position $(x + iy)$ we write:

$$B_y + iB_x = \sum_{n=0}^{\infty} \frac{(B_n + iA_n)}{n!}(x+iy)^n \tag{1.5.1}$$

where, assuming that the field is piece-wise constant along s and that the local curvature h is zero, the coefficients B_n and A_n are the on-axis derivatives of the transverse field components:

$$B_n = \left.\frac{\partial^n B_y}{\partial x^n}\right|_{x=0,\,y=0}, \qquad A_n = \left.\frac{\partial^n B_x}{\partial x^n}\right|_{x=0,\,y=0}. \tag{1.5.2}$$

The associated longitudinal vector potential for straight elements can be written as

$$A_s(x,y) = -\,\Re\left(\sum_{n=0}^{\infty}\frac{(B_n + iA_n)}{(n+1)!}(x+iy)^{n+1}\right), \tag{1.5.3}$$

so that $B_y + iB_x = -(\partial_x - i\partial_y)A_s$ yields the field expansion above.
We define the normal multipole coefficients K_n and the skew multipole coefficients $\hat{K}_n$ using the reference beam rigidity from Eq. (1.3.6):

$$K_n = \frac{B_n}{\mathrm{rig}_0} \tag{1.5.4}$$

and

$$\hat{K}_n = \frac{A_n}{\mathrm{rig}_0} \tag{1.5.5}$$

Using these coefficients, the field expansion and the longitudinal vector potential can be written as

$$B_y + iB_x = \mathrm{rig}_0 \sum_{n=0}^{\infty}\frac{(K_n + i\hat{K}_n)}{n!}(x+iy)^n, \tag{1.5.6}$$

$$A_s(x,y) = -\,\mathrm{rig}_0\,\Re\left(\sum_{n=0}^{\infty}\frac{(K_n + i\hat{K}_n)}{(n+1)!}(x+iy)^{n+1}\right). \tag{1.5.7}$$

The normalized longitudinal potential a_s introduced in Sec. 1.4 is then

$$a_s(x,y) = \frac{q_0}{P_0}A_s(x,y) = -\,\Re\left(\sum_{n=0}^{\infty}\frac{(K_n + i\hat{K}_n)}{(n+1)!}(x+iy)^{n+1}\right). \tag{1.5.8}$$

In the special case where only K_0, K_1, and K_2 are non-zero (all $K_{n\geq 3} = 0$ and $\hat{K}_n = 0$), the normalized longitudinal potential reduces to

$$a_s(x,y) = -\left[K_0 x + \frac{K_1}{2}\left(x^2 - y^2\right) + \frac{K_2}{6}\left(x^3 - 3xy^2\right)\right]. \tag{1.5.9}$$

1.5.2 Curved magnets ($h \neq 0$)

In the case of curved magnets ($h \neq 0$), multipole components are still defined as the derivatives at the symmetry point of the magnet:

$$B_n = \left.\frac{\partial^n B_y}{\partial x^n}\right|_{x=0,\,y=0}, \tag{1.5.10}$$

$$A_n = \left.\frac{\partial^n B_x}{\partial x^n}\right|_{x=0,\, y=0}. \tag{1.5.11}$$

and the corresponding normalized multipole coefficients K_n and $\hat{K}_n$ are defined as before:

$$K_n = \frac{B_n}{\text{rig}_0}, \quad \hat{K}_n = \frac{A_n}{\text{rig}_0}. \tag{1.5.12}$$

The field and potential expansions are more complex than in the straight case as they must satisfy Eq. 1.4.3 together with the definitions (1.5.10) and (1.5.11).
For the special case where only K_0, K_1, and K_2 are non-zero, a truncated expansion for the normalized potential is:

$$\begin{aligned} a_s(x,y,s) = &-K_0\left(x - \frac{hx^2}{2(1+hx)}\right) - K_1\left(\frac{1}{2}(x^2-y^2) - \frac{h}{6}x^3\right) \\ &- K_2\left(\frac{1}{6}(x^3-3xy^2) - \frac{h}{24}(x^4-y^4)\right) \end{aligned} \tag{1.5.13}$$

1.6 Particle coordinates

Xsuite uses as independent variable the position along the reference trajectory s. We call t the time coordinate, i.e. the time at which the particle passes the position s.
Xsuite can track particles of different species within the same particle ensemble. We call m and q the rest mass and charge of the individual particle and we introduce the coefficient:

$$\chi = \frac{q}{q_0}\frac{m_0}{m} \tag{1.6.1}$$

In the "longitudinal plane", i.e. the space spanned by time and energy coordinates, we can use any of the following pairs of conjugate variables:

$$\xi = s\frac{\beta}{\beta_0} - \beta c t \qquad \tau = \frac{s}{\beta_0} - ct \qquad \zeta = s - \beta_0 c t \qquad \delta = \frac{P\frac{m_0}{m} - P_0}{P_0} \tag{1.6.2}$$

$$\delta = \frac{P\frac{m_0}{m} - P_0}{P_0} \qquad p_\tau = \frac{1}{\beta_0}\frac{E\frac{m_0}{m} - E_0}{E_0} \qquad p_\zeta = \frac{1}{\beta_0^2}\frac{E\frac{m_0}{m} - E_0}{E_0} \qquad \ell = \beta c t \tag{1.6.3}$$

where variables in the same column are canonically conjugate.
These variables can be easily related to each other:

$$E = m\gamma c^2 = P_0 c\left(p_\tau + \frac{1}{\beta_0}\right), \tag{1.6.4}$$

$$P = m\beta\gamma c = P_0(1+\delta) \tag{1.6.5}$$

$$\beta = \frac{Pc}{E} = \sqrt{1 - \frac{1}{\gamma^2}} = \sqrt{1 - \frac{1-\beta_0}{(1+\beta_0 p_\tau)^2}}, \tag{1.6.6}$$

$$\gamma = \frac{1}{\sqrt{1-\beta^2}} = \gamma_0(1+\beta_0 p_\tau) \tag{1.6.7}$$

$$\xi = s\frac{\beta}{\beta_0} - \ell = \beta\tau = \frac{\beta}{\beta_0}\zeta \tag{1.6.8}$$

$$\delta = \sqrt{p_\tau^2 + 2\frac{p_\tau}{\beta_0} + 1} - 1 = \beta p_\tau + \frac{\beta-\beta_0}{\beta_0} \tag{1.6.9}$$

$$\delta = \sqrt{\beta_0^2 p_\zeta^2 + 2p_\zeta + 1} - 1 = \beta\beta_0 p_\zeta + \frac{\beta-\beta_0}{\beta_0} \tag{1.6.10}$$

$$(1+\delta)^2 = \frac{P^2}{P_0^2} = \frac{E^2 - m_0^2c^4}{P_0^2c^2} = \frac{E^2}{c^2P_0^2} - \frac{1}{\beta_0^2\gamma_0^2} = \left(p_\tau + \frac{1}{\beta_0}\right)^2 - \frac{1}{\beta_0^2\gamma_0^2} \tag{1.6.11}$$

$$p_\tau = \beta_0 p_\zeta \tag{1.6.12}$$

$$p_\tau = \frac{\sqrt{1+\beta_0^2\,\delta(\delta+2)} - 1}{\beta_0} \tag{1.6.13}$$

and the following derivatives:

$$\frac{\partial\delta}{\partial p_\tau} = \frac{p_\tau + 1/\beta_0}{1+\delta} = \frac{1}{\beta} \tag{1.6.14}$$

$$\frac{\partial}{\partial\delta}\left(\frac{1+\delta}{\beta\beta_0}\right) = \frac{\beta}{\beta_0} \tag{1.6.15}$$

For small energy deviations ($\delta \ll 1$, $p_\tau \ll 1$, $p_\zeta \ll 1$), we can neglect the terms of order δ^2, p_τ^2, p_ζ^2 and higher, hence the following approximations hold:

$$\delta \simeq \frac{p_\tau}{\beta_0} \tag{1.6.16}$$

$$\delta \simeq p_\zeta \tag{1.6.17}$$

$$\beta \simeq \beta_0 + (1-\beta_0^2)p_\tau \tag{1.6.18}$$

In the transverse plane we use the coordinates x, p_x, y, p_y. The transverse canonical momenta are defined as:

$$p_x = \frac{m_0}{m}\frac{P_x}{P_0}, \qquad p_y = \frac{m_0}{m}\frac{P_y}{P_0}, \tag{1.6.19}$$

where:

$$P_x = m\gamma\dot{x} + qA_x, \qquad P_y = m\gamma\dot{y} + qA_y \tag{1.6.20}$$

in which $\dot{x}$ and $\dot{y}$ are the time derivatives of x and y.

1.7 Hamiltonian and equations of motion

The motion of a particle is described by one of the following Hamiltonian functions, depending on the choice of longitudinal coordinates:

$$H_\delta = \frac{1+\delta}{\beta\beta_0} - (1+hx)\left(\sqrt{\left(\frac{1+\delta}{\beta} - \chi\varphi\right)^2 - \frac{1}{\beta_0^2\gamma_0^2} - (p_x - \chi a_x)^2 - (p_y - \chi a_y)^2} + \chi a_s\right) \tag{1.7.1}$$

$$H_\tau = \frac{p_\tau}{\beta_0} - (1+hx)\left(\sqrt{\left(p_\tau + \frac{1}{\beta_0} - \chi\varphi\right)^2 - \frac{1}{\beta_0^2\gamma_0^2} - (p_x - \chi a_x)^2 - (p_y - \chi a_y)^2} + \chi a_s\right) \tag{1.7.2}$$

$$H_\zeta = p_\zeta - (1+hx)\left(\sqrt{\left(\beta_0 p_\zeta + \frac{1}{\beta_0} - \chi\varphi\right)^2 - \frac{1}{\beta_0^2\gamma_0^2} - (p_x - \chi a_x)^2 - (p_y - \chi a_y)^2} + \chi a_s\right) \tag{1.7.3}$$

Using τ and p_τ as longitudinal coordinates, the equations of motion are:

$$\frac{\mathrm{d}p_x}{\mathrm{d}s} = -\frac{\partial H_\tau}{\partial x} \tag{1.7.4}$$

$$\frac{\mathrm{d}p_y}{\mathrm{d}s} = -\frac{\partial H_\tau}{\partial y} \tag{1.7.5}$$

$$\frac{\mathrm{d}p_\tau}{\mathrm{d}s} = -\frac{\partial H_\tau}{\partial \tau} \tag{1.7.6}$$

$$\frac{\mathrm{d}x}{\mathrm{d}s} = \frac{\partial H_\tau}{\partial p_x} \tag{1.7.7}$$

$$\frac{\mathrm{d}y}{\mathrm{d}s} = \frac{\partial H_\tau}{\partial p_y} \tag{1.7.8}$$

$$\frac{\mathrm{d}\tau}{\mathrm{d}s} = \frac{\partial H_\tau}{\partial p_\tau} \tag{1.7.9}$$

The full derivation of the Hamiltonian and equations of motion can be found in Wolski [12] (note the different notation, as the symbol δ in [12] denotes the quantity that here we call p_τ).

1.8 Expanded magnet body Hamiltonian

For a magnet with piece-wise constant multipole components and curvature h, we can set $a_x = 0$ and $a_y = 0$ in Eq. (1.7.2):

$$H_\tau = H^{\mathrm{kin}} + H^{\mathrm{magn}} \tag{1.8.1}$$

where

$$H^{\mathrm{kin}} = \frac{p_\tau}{\beta_0} - (1+hx)\sqrt{\left(p_\tau + \frac{1}{\beta_0}\right)^2 - \frac{1}{\beta_0^2\gamma_0^2} - p_x^2 - p_y^2} \tag{1.8.2}$$

$$H^{\text{magn}} = -(1+hx)\chi a_s \tag{1.8.3}$$

1.8.1 Approximation of the kinetic part of the Hamiltonian

Using Eq. 1.6.11, the kinetic part can be rewritten as follows:

$$H^{\text{kin}} = \frac{p_\tau}{\beta_0} - (1+hx)\sqrt{(1+\delta)^2 - p_x^2 - p_y^2} \tag{1.8.4}$$

$$= \frac{p_\tau}{\beta_0} - \sqrt{(1+\delta)^2 - p_x^2 - p_y^2} - hx\sqrt{(1+\delta)^2 - p_x^2 - p_y^2} \tag{1.8.5}$$

Neglecting high-order terms $h^2x^2p_x^2$ and $h^2x^2p_y^2$ in the second square root, we can approximate:

$$H^{\text{kin}} = \frac{p_\tau}{\beta_0} - \sqrt{(1+\delta)^2 - p_x^2 - p_y^2} - hx(1+\delta) \tag{1.8.6}$$

$$= H_D - hx(1+\delta) \tag{1.8.7}$$

where

$$H_D = \frac{p_\tau}{\beta_0} - \sqrt{(1+\delta)^2 - p_x^2 - p_y^2} \tag{1.8.8}$$

is the Hamiltonian of a straight drift.
The Hamiltonian for the drift can in turn be expanded as follows:

$$H_D = \frac{p_\tau}{\beta_0} - (1+\delta)\sqrt{1 - \frac{p_x^2 + p_y^2}{(1+\delta)^2}} \tag{1.8.9}$$

$$\simeq \frac{p_\tau}{\beta_0} - (1+\delta) + \frac{1}{2}\frac{p_x^2 + p_y^2}{(1+\delta)} \tag{1.8.10}$$

Replacing Eq. (1.8.10) in Eq. (1.8.7) yields the following expression for the kinetic part of the Hamiltonian:

$$H^{\text{kin}} \simeq \frac{p_\tau}{\beta_0} - \left(1 + \delta - \frac{1}{2}\frac{p_x^2 + p_y^2}{(1+\delta)}\right) - hx\,(1+\delta) \tag{1.8.11}$$

1.8.2 Approximation of the magnetic part of the Hamiltonian

For the common case where only K_0, K_1, and K_2 are non-zero, inserting the curved-magnet potential from Eq. (1.5.13) in H^{magn} yields:

$$H^{\text{magn}} = (1+hx)\chi\left[K_0\left(x - \frac{hx^2}{2(1+hx)}\right) + K_1\left(\frac{1}{2}(x^2 - y^2) - \frac{h}{6}x^3\right)\right.$$
$$\left. + K_2\left(\frac{1}{6}(x^3 - 3xy^2) - \frac{h}{24}(x^4 - y^4)\right)\right]. \tag{1.8.12}$$

Discarding all terms nonlinear in h (i.e., keeping only $\mathcal{O}(h)$) yields

$$H^{\text{magn}} \simeq \chi\left[K_0 x + K_1\frac{x^2-y^2}{2} + K_2\frac{x^3-3xy^2}{6}\right] + \chi h\left[\frac{K_0}{2}x^2 + K_1\left(\frac{1}{3}x^3 - \frac{1}{2}xy^2\right) + K_2\left(\frac{1}{8}x^4 - \frac{1}{2}x^2y^2 + \frac{1}{24}y^4\right)\right]. \quad (1.8.13)$$

1.9 Symplectic integrators and magnet models

In Xsuite, magnets are modeled using symplectic integrators, splitting the Hamiltonian into a 'propagation' part and a 'kick' part, for which closed-form solutions of the equations of motion are available.
Hamiltonians for which closed-form solutions of the equations of motion exist and are implemented in Xsuite are reported in Table 1.1. The corresponding maps are reported in Chapter 2.
Different magnet models are available, which correspond to different ways of splitting the Hamiltonian. The available models are reported in Table 1.2 and the available integration schemes are reported in Table 1.3.

Map	**Params.**	**Description**	
D		Drift exact	$H_D = \frac{p_\tau}{\beta_0} - \sqrt{(1+\delta)^2 - p_x^2 - p_y^2}$
De		Drift expanded	$H_{De} = \frac{p_\tau}{\beta_0} - (1+\delta) + \frac{1}{2}\frac{p_x^2+p_y^2}{(1+\delta)}$
Dc		Exact drift correction	$H_{Dc} = H_D - H_{De}$
R	h	Curved drift	$H_R = \frac{p_\tau}{\beta_0} - (1+hx)\sqrt{(1+\delta)^2 - p_x^2 - p_y^2}$
Br	K_0	Rectangular bend	$H_{Br} = H_D + \chi K_0 x$
B	K_0, h	Exact Bend	$H_B = H_R + \chi K_0 x + \chi h K_0 \frac{x^2}{2}$
K0	K_0	Dipole kick	$H_{K0} = \chi K_0 x$
K1	K_1	Quadrupole kick	$H_{K1} = \chi K_1 \frac{x^2-y^2}{2}$
h	h	Curvature kick	$H_h = -hx(1+\delta)$
K0h	K_0	Weak focusing kick	$H_{K0h} = \chi h K_0 \frac{x^2}{2}$
K1h	K_1, h	Quad curv. correction	$H_{K1h} = \chi h K_1 \frac{2x^3-3xy^2}{6}$
Kn	K_n, $\hat{K}_n$	Multipole	$H_{Kn} = \chi\Re\left(\sum_{n=0}^{N}(K_n + i\hat{K}_n)\frac{(x+iy)^{n+1}}{(n+1)!}\right)$
M	K_0, K_1, h	Expanded bend-quad.	$H_M = H_{De} - hx(1+\delta) + \chi K_0 x + \chi K_1 \frac{x^2-y^2}{2} + \chi h K_0 \frac{x^2}{2}$
S	K_s	Solenoid	$H_S = \frac{p_\tau}{\beta_0} - \sqrt{(1+\delta)^2 - \left(p_x - \frac{K_s}{2}y\right)^2 - \left(p_y + \frac{K_s}{2}\right)^2}$

Table 1.1: Hamiltonians of the implemented maps.

Model	Propagation part	Kick part
rot-kick-rot-low-order	[R]	[K0 K0h K1 K1h Kn]
rot-kick-rot	[R, K0] - Yoshida 4	[K0h K1 K1h Kn]
rot-kick-rot-high-order	[R, K0] - Yoshida 6	[K0h K1 K1h Kn]
bend-kick-bend	[B]	[K1 K1h Kn]
mat-kick-mat	[M]	[K1h Kn]
mat-kick-mat-exact ($h = 0$)	[M]	[Dc/2, Kn, Dc/2]
drift-kick-drift-exact	[D]	[h K0 K0h K1 K1h Kn]
drift-kick-drift-expanded	[De]	[h K0 K0h K1 K1h Kn]

Table 1.2: Available magnet models. For `mat-kick-mat-exact`, the kick is bracketed by two half-length correction maps; see Sec. 2.7.

1.9.1 Practical recommendations

- The `bend-kick-bend` model is an exact map for a pure dipole (K_0) with curvature h, so if there is no `K1` or higher multipole component, the map is exact for any `nslice`, so `nslice=1` suffices and increasing the order or slicing will only increase the computational cost and numerical error.
- Otherwise (e.g. K_1, K_2, ..., or skew components present), prefer a higher-order integrator (`yoshida-6` is typically best) with as few slices as possible over a low-order one (`uniform`, `teapot`) with many slices: increasing the order is roughly equivalent, in terms of accuracy, to increasing `nslice` by a factor 10 while keeping a lower order (e.g. fourth order with `nslice=10` $\approx$ second order with `nslice=100`), but at a much lower computational cost.
- Fewer, higher-order slices are more numerically stable as each drift step has some numerical error, so more slices means more accumulated error, not less.

Integrator	$n_{\mathbf{kicks}}$	$n_{\mathbf{drifts}}$	**Order**	**Description**
uniform	1	2	2nd	Kicks uniformly distributed along the length of the element (leapfrog, eq. (2.10) of [13])
teapot	1	2	2nd	TEAPOT integration scheme [14, 15]
yoshida-4	3	4	4th	Fourth-order Yoshida integrator, eq. (2.11) of [13]
yoshida-6	7	8	6th	Sixth-order Yoshida integrator, table 1, variant A, of [13]. Default ("adaptive") integrator
yoshida-8	15	16	8th	Eighth-order Yoshida integrator, table 2, variant D, of [13], as also used by MAD-NG [16]

Table 1.3: Available integration schemes.

Chapter 2

Beam element maps

This chapter presents the maps used to transport particles through beam elements. Depending on the element and the chosen model, these maps are used individually or combined by the symplectic integrators described in Section 1.9. In the latter case, propagation and kick maps are composed to approximate the evolution under the full Hamiltonian.

2.1 Drift

Implemented in the Drift element.

A drift is a straight, field-free region ($h(x,y) = 0$, $V = 0$ and $\mathbf{A} = 0$). The exact and expanded Hamiltonians for a drift space are

$$H_\tau = \frac{p_\tau}{\beta_0} - \sqrt{(1+\delta)^2 - p_x^2 - p_y^2} \approx \frac{p_\tau}{\beta_0} - \delta + \frac{1}{2}\frac{p_x^2 + p_y^2}{1+\delta}. \tag{2.1.1}$$

The corresponding maps can be obtained by solving the equations of motion:

$$\frac{\mathrm{d}p_i}{\mathrm{d}s} = -\frac{\partial H}{\partial q_i} \qquad\qquad \frac{\mathrm{d}q_i}{\mathrm{d}s} = \frac{\partial H}{\partial p_i} \tag{2.1.2}$$

As there is no explicit dependency on the position coordinates in the Hamiltonian, the momenta remain unchanged in a drift.
For the position coordinates, we get:

$$(x)' = \frac{p_x}{p_z} \approx \frac{p_x}{1+\delta} \tag{2.1.3}$$

$$(y)' = \frac{p_y}{p_z} \approx \frac{p_y}{1+\delta} \tag{2.1.4}$$

$$(\tau)' = \frac{1}{\beta_0} - \frac{1}{\beta}\frac{1+\delta}{p_z} \approx \frac{1}{\beta_0} - \frac{1}{\beta} - \frac{1}{\beta}\frac{p_x^2 + p_y^2}{2} \tag{2.1.5}$$

$$p_z = \sqrt{(1+\delta)^2 - p_x^2 - p_y^2} \tag{2.1.6}$$

Hence, the map relative to the expanded Hamiltonian for a drift of length L is:

$$x_p = \frac{p_x}{1+\delta} \tag{2.1.7}$$
$$y_p = \frac{p_y}{1+\delta} \tag{2.1.8}$$
$$x \leftarrow x + x_p L \tag{2.1.9}$$
$$y \leftarrow y + y_p L \tag{2.1.10}$$
$$\zeta \leftarrow \zeta + l\left(1 - \frac{\beta_0}{\beta}\left(1 + \frac{x_p^2 + y_p^2}{2}\right)\right) \tag{2.1.11}$$

and the map relative to the exact Hamiltonian for a drift of length L is:

$$x \leftarrow x + \frac{p_x}{p_z} L \tag{2.1.12}$$
$$y \leftarrow y + \frac{p_y}{p_z} L \tag{2.1.13}$$
$$\zeta \leftarrow \zeta + L\left(1 - \frac{\beta_0}{\beta}\frac{1+\delta}{p_z}\right) \tag{2.1.14}$$

2.2 Polar drift (sector curvature h)

Used in the implementation of Bend and RBend elements when the model is "rot-kick-rot".
This map is ported from PTC and MAD-NG source codes.

The following map, corresponding to the motion of a particle in a field-free region in a reference frame with horizontal curvature h, is generated by the Hamiltonian:

$$H_R = \frac{p_\tau}{\beta_0} - (1+hx)\left(\sqrt{(1+\delta)^2 - p_x^2 - p_y^2}\right) \tag{2.2.1}$$

We call:

$$\delta_+ \equiv 1+\delta, \qquad \text{rvv} = v/c, \qquad s \equiv L.$$

Define the longitudinal momentum component

$$p_z \equiv \sqrt{\delta_+^2 - p_x^2 - p_y^2}. \tag{2.2.2}$$

Define the curvature radius

$$\rho \equiv \frac{1}{h}, \tag{2.2.3}$$

and the trigonometric abbreviations

$$c \equiv \cos(hs), \qquad s_a \equiv \sin(hs), \qquad s_{a2} \equiv \sin\left(\frac{hs}{2}\right). \tag{2.2.4}$$

Introduce

$$\frac{1}{p_z} \equiv p_z^{-1}, \qquad p_{x,t} \equiv \frac{p_x}{p_z}, \qquad \mathcal{D} \equiv c - s_a\, p_{x,t}, \qquad \mathcal{D}^{-1} \equiv \frac{1}{\mathcal{D}}. \tag{2.2.5}$$

Define also

$$p_s \equiv (x+\rho)\, s_a\, p_z^{-1}\, \mathcal{D}^{-1}. \tag{2.2.6}$$

Transverse map

$$x_1 = \left[x + \rho\left(2s_{a2}^2 + s_a\, p_{x,t}\right)\right] \mathcal{D}^{-1}, \tag{2.2.7}$$

$$p_{x1} = c\, p_x + s_a\, p_z, \tag{2.2.8}$$

$$y_1 = y + p_s\, p_y. \tag{2.2.9}$$

Path length / longitudinal map The quantity $\Delta\ell$ computed in the code is

$$\Delta\ell = \delta_+ \frac{(x+\rho)\, s_a}{c\, p_z \left(1 - \dfrac{p_x s_a}{c\, p_z}\right)}. \tag{2.2.10}$$

The longitudinal coordinate is updated as

$$\zeta_1 = \zeta + \left(L - \frac{\Delta\ell}{\mathrm{rvv}}\right), \tag{2.2.11}$$

and the reference longitudinal position as

$$s_{\mathrm{ref},1} = s_{\mathrm{ref}} + L. \tag{2.2.12}$$

2.3 Curved exact bend

Implemented in the Bend element.

The generating Hamiltonian is:

$$H_B = \frac{p_\tau}{\beta_0} - (1+hx)\left(\sqrt{(1+\delta)^2 - p_x^2 - p_y^2} - K_0\left(x - \frac{hx^2}{2(1+hx)}\right)\right) \tag{2.3.1}$$

For compactness, define

$$p_w = \sqrt{(1+\delta)^2 - p_y^2}, \tag{2.3.2}$$

$$p_z(0) = \sqrt{(1+\delta)^2 - p_x(0)^2 - p_y^2}, \tag{2.3.3}$$

$$p_z(s) = \sqrt{(1+\delta)^2 - p_x(s)^2 - p_y^2}, \tag{2.3.4}$$

$$\Delta a(s) = \sin^{-1}\left(\frac{p_x(0)}{p_w}\right) - \sin^{-1}\left(\frac{p_x(s)}{p_w}\right). \tag{2.3.5}$$

The corresponding map is adapted from [11]:

$$x(s) = \frac{1}{hK_0\chi}\left(hp_z(s) - \frac{dp_x(s)}{ds} - K_0\chi\right) \tag{2.3.6}$$

$$p_x(s) = p_x(0)\cos(hs) + \left(p_z(0) - K_0\chi\left(\frac{1}{h} + x(0)\right)\right)\sin(hs) \tag{2.3.7}$$

$$y(s) = y + \frac{p_y}{K_0\chi}\left[hs + \Delta a(s)\right] \tag{2.3.8}$$

$$p_y(s) = p_y \tag{2.3.9}$$

$$\delta(s) = \delta \tag{2.3.10}$$

$$\ell(s) = \ell + \frac{1+\delta}{K_0\chi}\left[hs + \Delta a(s)\right] \tag{2.3.11}$$

Numerically stable horizontal update The direct evaluation of the horizontal coordinate can involve the subtraction of large radius-like terms. In the implementation we compute the horizontal increment

$$\Delta x(s) \equiv x(s) - x(0), \tag{2.3.12}$$

and then update the coordinate as $x(s) = x(0) + \Delta x(s)$. To derive a stable expression for $\Delta x(s)$, define

$$C = p_z(0) - K_0\chi\left(\frac{1}{h} + x(0)\right). \tag{2.3.13}$$

Then

$$p_x(s) = p_x(0)\cos(hs) + C\sin(hs), \tag{2.3.14}$$

and

$$\frac{1}{h}\frac{dp_x(s)}{ds} = C\cos(hs) - p_x(0)\sin(hs). \tag{2.3.15}$$

The horizontal map can therefore be written as

$$x(s) = \frac{p_z(s) - \left[C\cos(hs) - p_x(0)\sin(hs)\right]}{K_0\chi} - \frac{1}{h}. \tag{2.3.16}$$

Using the definition of C, the initial coordinate satisfies

$$x(0) = \frac{p_z(0) - C}{K_0\chi} - \frac{1}{h}. \tag{2.3.17}$$

Subtracting these two expressions gives the increment directly and avoids reconstructing $x(s)$ as a difference of large radius-like terms:

$$\Delta p_z(s) \equiv p_z(s) - p_z(0), \tag{2.3.18}$$

$$\Delta D(s) \equiv C\cos(hs) - p_x(0)\sin(hs) - C. \tag{2.3.19}$$

Then

$$\Delta x(s) = \frac{\Delta p_z(s) - \Delta D(s)}{K_0\chi}. \tag{2.3.20}$$

The second term is evaluated as

$$\Delta D(s) = C\left[\cos(hs) - 1\right] - p_x(0)\sin(hs). \tag{2.3.21}$$

For small hs, the difference $\cos(hs) - 1$ is numerically inaccurate if evaluated directly. We therefore use

$$\cos(hs) - 1 = -2\sin^2\left(\frac{hs}{2}\right), \tag{2.3.22}$$

giving

$$\Delta D(s) = -2C\sin^2\left(\frac{hs}{2}\right) - p_x(0)\sin(hs). \tag{2.3.23}$$

The first term is also evaluated without subtracting two nearly equal square roots:

$$\Delta p_z(s) = \frac{p_z(s)^2 - p_z(0)^2}{p_z(s) + p_z(0)} \tag{2.3.24}$$

$$= \frac{p_x(0)^2 - p_x(s)^2}{p_z(s) + p_z(0)} \tag{2.3.25}$$

$$= \frac{\left[p_x(0) - p_x(s)\right]\left[p_x(0) + p_x(s)\right]}{p_z(s) + p_z(0)}. \tag{2.3.26}$$

The implemented increment uses the expression above, with $\Delta p_z(s)$ and $\Delta D(s)$ evaluated by the stable expressions given here. The horizontal coordinate is then updated as

$$x(s) = x(0) + \Delta x(s). \tag{2.3.27}$$

Numerically stable vertical and longitudinal update The vertical and longitudinal maps depend on the inverse-sine difference $\Delta a(s)$. Directly subtracting the two inverse sines can lose precision when their arguments are close. With

$$u = \frac{p_x(0)}{p_w}, \qquad v = \frac{p_x(s)}{p_w}, \tag{2.3.28}$$

we use

$$\sin^{-1}(u) - \sin^{-1}(v) = \operatorname{atan2}\left(u\sqrt{1-v^2} - v\sqrt{1-u^2}, \sqrt{1-u^2}\sqrt{1-v^2} + uv\right). \tag{2.3.29}$$

Since

$$\sqrt{1-u^2} = \frac{p_z(0)}{p_w}, \qquad \sqrt{1-v^2} = \frac{p_z(s)}{p_w}, \tag{2.3.30}$$

the common factor $1/p_w^2$ cancels, giving

$$\Delta a(s) = \operatorname{atan2}\left(p_x(0)p_z(s) - p_x(s)p_z(0), p_z(0)p_z(s) + p_x(0)p_x(s)\right). \tag{2.3.31}$$

The numerator is evaluated without subtracting two nearly equal products. Define

$$\Delta p_x(s) \equiv p_x(s) - p_x(0) = -2p_x(0)\sin^2\left(\frac{hs}{2}\right) + C\sin(hs). \tag{2.3.32}$$

Then

$$N_a(s) \equiv p_x(0)p_z(s) - p_x(s)p_z(0) \tag{2.3.33}$$
$$= p_x(0)\Delta p_z(s) - p_z(0)\Delta p_x(s), \tag{2.3.34}$$

and

$$D_a(s) \equiv p_z(0)p_z(s) + p_x(0)p_x(s). \tag{2.3.35}$$

The implemented inverse-sine difference is therefore

$$\Delta a(s) = \text{atan2}\left(N_a(s), D_a(s)\right). \tag{2.3.36}$$

Using

$$I(s) = \frac{hs + \Delta a(s)}{K_0\chi}, \tag{2.3.37}$$

the vertical and longitudinal updates are

$$y(s) = y + p_y I(s), \tag{2.3.38}$$
$$\ell(s) = \ell + (1+\delta)I(s). \tag{2.3.39}$$

2.4 Straight exact bend

Implemented in the Bend and RBend elements for specific configurations.

The generating Hamiltonian is:

$$H_{Br} = \frac{p_\tau}{\beta_0} - \sqrt{(1+\delta)^2 - p_x^2 - p_y^2} - K_0 x \tag{2.4.1}$$

The corresponding map is adapted from [11]:

$$x(L) = x + \frac{1}{K_0\chi}\left(\sqrt{(1+\delta)^2 - p_x(L)^2 - p_y^2} - \sqrt{(1+\delta)^2 - p_x^2 - p_y^2}\right) \tag{2.4.2}$$
$$p_x(L) = p_x - K_0\chi L \tag{2.4.3}$$
$$y(L) = y + \frac{p_y}{K_0\chi}\left(\sin^{-1}\left(\frac{p_x}{\sqrt{(1+\delta)^2 - p_y^2}}\right) - \sin^{-1}\left(\frac{p_x(L)}{\sqrt{(1+\delta)^2 - p_y^2}}\right)\right) \tag{2.4.4}$$
$$p_y(L) = p_y \tag{2.4.5}$$
$$\delta(L) = \delta \tag{2.4.6}$$
$$\ell(L) = \ell + \frac{1+\delta}{K_0\chi}\left(\sin^{-1}\left(\frac{p_x}{\sqrt{(1+\delta)^2 - p_y^2}}\right) - \sin^{-1}\left(\frac{p_x(L)}{\sqrt{(1+\delta)^2 - p_y^2}}\right)\right) \tag{2.4.7}$$

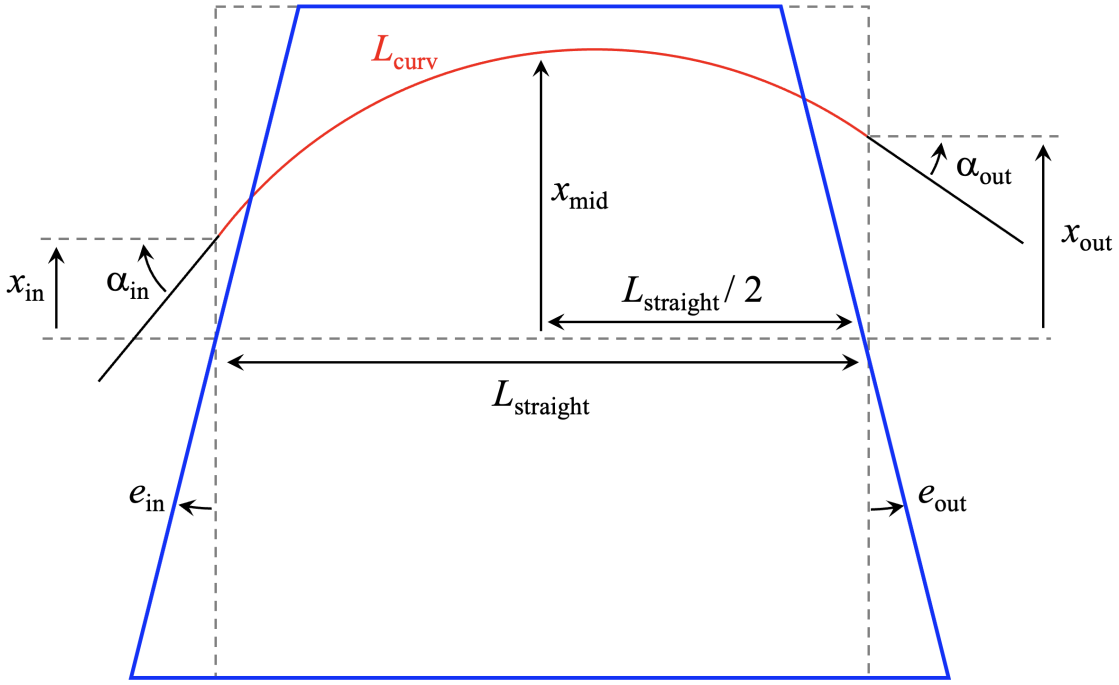


Figure 2.1: Rectangular bend.

2.5 Rectangular bend - straight body

Implemented in the RBend element.

Xsuite supports rectangular bends with generic shifts and angles at the entrance and exit faces as shown in Fig. 2.1. In this section we report relations among the quantities defining the geometry of the magnet with respect to the reference trajectory.
The code takes as input the total bending angle α and the difference α_{diff} between the angles at entrance and exit of the reference trajectory with respect to the magnet axis:

$$\alpha = \alpha_{\text{in}} + \alpha_{\text{out}} \tag{2.5.1}$$
$$\alpha_{\text{diff}} = \alpha_{\text{out}} - \alpha_{\text{in}} \tag{2.5.2}$$

from which:

$$\alpha_{\text{in}} = \frac{\alpha - \alpha_{\text{diff}}}{2} \tag{2.5.3}$$
$$\alpha_{\text{out}} = \frac{\alpha + \alpha_{\text{diff}}}{2} \tag{2.5.4}$$

In the reference frame of the magnet body, for an on-momentum particle on the reference trajectory we can write:

$$p_{x,\text{in}} = \sin(\alpha_{\text{in}}) \tag{2.5.5}$$
$$p_{x,\text{out}} = -\sin(\alpha_{\text{out}}) \tag{2.5.6}$$

Using Eq. (2.4.3) we can write:

$$-\sin(\alpha_{\text{out}}) = \sin(\alpha_{\text{in}}) - hL_{\text{straight}} \tag{2.5.7}$$

from which we can obtain the curvature of the reference trajectory:

$$h = \frac{\sin(\alpha_{\text{in}}) + \sin(\alpha_{\text{out}})}{L_{\text{straight}}} \tag{2.5.8}$$

Using Eqs. (2.4.2) and (2.4.3) we can write:

$$p_{x,\text{mid}} = p_{x,\text{in}} - hL_{\text{straight}}/2 \tag{2.5.9}$$

$$p_{x,\text{mid}} = p_{x,\text{out}} + hL_{\text{straight}}/2 \tag{2.5.10}$$

$$x_{\text{in}} = x_{\text{mid}} - \frac{1}{h}\left(\sqrt{1-p_{x,\text{mid}}^2} - \sqrt{1-p_{x,\text{in}}^2}\right) \tag{2.5.11}$$

$$x_{\text{out}} = x_{\text{mid}} + \frac{1}{h}\left(\sqrt{1-p_{x,\text{out}}^2} - \sqrt{1-p_{x,\text{mid}}^2}\right) \tag{2.5.12}$$

Using Eq. (2.4.7) we can write:

$$L_{\text{curv}} = \frac{1}{h}\left(\sin^{-1}(p_{x,\text{out}}) - \sin^{-1}(p_{x,\text{in}})\right) = \frac{\alpha_{\text{in}} + \alpha_{\text{out}}}{h} = \frac{\alpha}{h} \tag{2.5.13}$$

In the special case of a sector bend ($\alpha_{\text{diff}} = 0$) we have, summing Eqs. (2.5.9) and (2.5.10):

$$\alpha_{\text{in}} = \alpha_{\text{out}} = \frac{\alpha}{2} \tag{2.5.14}$$

$$p_{x,\text{in}} = -p_{x,\text{out}} = \sin(\alpha/2) \tag{2.5.15}$$

$$p_{x,\text{mid}} = 0 \tag{2.5.16}$$

$$h = \frac{2\sin(\alpha/2)}{L_{\text{straight}}} \tag{2.5.17}$$

$$L_{\text{curv}} = \frac{\alpha}{h} = \frac{L_{\text{straight}}}{\text{sinc}(\alpha/2)} \tag{2.5.18}$$

$$x_{\text{in}} = x_{\text{out}} = x_{\text{mid}} - \frac{1}{h}(1 - \cos(\alpha/2)) \tag{2.5.19}$$

The last gives the usual equation for the sagitta of a bending magnet.

2.6 Expanded Bend-Quadrupole (also used for Quadrupole)

Implemented in the Bend, RBend and Quadrupole elements, for the "mat-kick-mat" model.
This map is ported from the MAD-X source code.

The following map is generated by the Hamiltonian:

$$H_M = \frac{p_\tau}{\beta_0} + \frac{1}{2}\frac{p_x^2 + p_y^2}{(1+\delta)} + (K_0 - h)x + \frac{K_0 h x^2}{2} + K_1\frac{x^2 - y^2}{2} \tag{2.6.1}$$

We consider a particle with initial canonical coordinates

$$(x,\ p_x,\ y,\ p_y,\ \zeta),$$

relative momentum deviation δ, velocity factor rvv $= v/c$, and charge/sign factor χ. The element has length L, curvature h, and (input) strengths K_0 and K_1.

Definitions

Define

$$\delta_+ \equiv 1 + \delta, \tag{2.6.2}$$

$$x' = \frac{p_x}{\delta_+}, \qquad y' = \frac{p_y}{\delta_+}. \tag{2.6.3}$$

We introduce the momentum-scaled (effective) strengths

$$\bar{K}_0 = \frac{\chi K_0}{\delta_+}, \qquad \bar{K}_1 = \frac{\chi K_1}{\delta_+}, \tag{2.6.4}$$

and the corresponding focusing coefficients

$$K_x = \bar{K}_0\, h + \bar{K}_1, \tag{2.6.5}$$

$$K_y = -\bar{K}_1. \tag{2.6.6}$$

Auxiliary quantities:

$$A = -K_x x - \bar{K}_0 + h, \tag{2.6.7}$$

$$B = x', \tag{2.6.8}$$

$$C = -K_y y, \tag{2.6.9}$$

$$D = y'. \tag{2.6.10}$$

Transport Functions

For an element of length L, define

$$(C_x, S_x) = \begin{cases} \left(\cos(\sqrt{K_x}L), \dfrac{\sin(\sqrt{K_x}L)}{\sqrt{K_x}}\right), & K_x > 0, \\ \left(\cosh(\sqrt{-K_x}L), \dfrac{\sinh(\sqrt{-K_x}L)}{\sqrt{-K_x}}\right), & K_x < 0, \\ (1,\ L), & K_x = 0, \end{cases}$$

$$(C_y, S_y) = \begin{cases} \left(\cos(\sqrt{K_y}L), \dfrac{\sin(\sqrt{K_y}L)}{\sqrt{K_y}}\right), & K_y > 0, \\ \left(\cosh(\sqrt{-K_y}L), \dfrac{\sinh(\sqrt{-K_y}L)}{\sqrt{-K_y}}\right), & K_y < 0, \\ (1,\ L), & K_y = 0. \end{cases}$$

Transverse Map

Positions

$$x_1 = xC_x + x'S_x + \begin{cases} \dfrac{(\bar{K}_0 - h)(C_x - 1)}{K_x}, & K_x \neq 0, \\ -\dfrac{1}{2}(\bar{K}_0 - h)L^2, & K_x = 0, \end{cases} \tag{2.6.11}$$

$$y_1 = yC_y + y'S_y. \tag{2.6.12}$$

Momenta

$$p_{x1} = \delta_+ \left(AS_x + BC_x\right), \tag{2.6.13}$$

$$p_{y1} = \delta_+ \left(CS_y + DC_y\right). \tag{2.6.14}$$

Path Length

Let L_{tot} be the total path length traveled by the particle through the element.

Horizontal contribution For $K_x \neq 0$:

$$\begin{aligned} L_{\text{tot}} = L &- \frac{h\left[(C_x - 1)x' + S_x A + L(\bar{K}_0 - h)\right]}{K_x} \\ &+ \frac{1}{2}\left[- \frac{A^2 C_x S_x}{2K_x} + \frac{B^2 C_x S_x}{2} + \frac{A^2 L}{2K_x} + \frac{B^2 L}{2} \right. \\ &\left. - \frac{ABC_x^2}{K_x} + \frac{AB}{K_x} \right]. \end{aligned} \tag{2.6.15}$$

For $K_x = 0$:

$$L_{\text{tot}} = L + \frac{hL}{6}\left(3Lx' + 6x - (\bar{K}_0 - h)L^2\right) + \frac{1}{2}B^2 L. \tag{2.6.16}$$

Vertical contribution For $K_y \neq 0$:

$$\begin{aligned} L_{\text{tot}} \mathrel{+}= \frac{1}{2}\left[- \frac{C^2 C_y S_y}{2K_y} + \frac{D^2 C_y S_y}{2} + \frac{C^2 L}{2K_y} + \frac{D^2 L}{2} \right. \\ \left. - \frac{CDC_y^2}{K_y} + \frac{CD}{K_y} \right]. \end{aligned} \tag{2.6.17}$$

For $K_y = 0$:

$$L_{\text{tot}} \mathrel{+}= \frac{1}{2}D^2 L. \tag{2.6.18}$$

Longitudinal Map

The longitudinal coordinate update is

$$\Delta\zeta = L - \frac{L_{\text{tot}}}{\text{rvv}}. \tag{2.6.19}$$

Final Map

$$(x, p_x, y, p_y, \zeta) \longrightarrow (x_1, p_{x1}, y_1, p_{y1}, \zeta + \Delta\zeta), \qquad s \to s + L. \tag{2.6.20}$$

2.7 Exact path correction for mat-kick-mat

The `mat-kick-mat-exact` model extends `mat-kick-mat` for straight magnets ($h = 0$). Both propagate with the expanded bend–quadrupole map M described in Sec. 2.6, retaining its momentum dependence. The exact variant adds a correction depending only on momenta that restores the square-root kinetic Hamiltonian omitted by the expansion in transverse momentum. This follows the exact-model correction described by Forest, Schmidt and McIntosh in the PTC report [17], p. 69 and Secs. K.4.6–K.4.7, pp. 74–75.

With $p_z = \sqrt{(1+\delta)^2 - p_x^2 - p_y^2}$, the correction Hamiltonian is

$$H_{Dc} = H_D - H_{De} = 1 + \delta - p_z - \frac{p_x^2 + p_y^2}{2(1+\delta)}. \tag{2.7.1}$$

Thus, for $h = 0$, adding H_{Dc} to the expanded magnet Hamiltonian restores the exact kinetic term while retaining the same magnetic multipole potential. The factor $1/(1+\delta)$ in the expanded map is already retained exactly; the correction restores the higher powers of transverse momentum.

Since H_{Dc} has no position dependence, its map $C(\ell)$ over a signed integration length ℓ leaves p_x, p_y and δ unchanged. Define

$$d = \ell \left(\frac{1}{p_z} - \frac{1}{1+\delta} \right). \tag{2.7.2}$$

In Xtrack's longitudinal coordinate ζ, the coordinate updates are

$$x \leftarrow x + p_x d, \tag{2.7.3}$$

$$y \leftarrow y + p_y d, \tag{2.7.4}$$

$$\zeta \leftarrow \zeta + \frac{\beta_0}{\beta} \left(\frac{\ell(p_x^2 + p_y^2)}{2(1+\delta)^2} - (1+\delta)d \right). \tag{2.7.5}$$

This correction does not advance s; that advance belongs to the propagation map M. For each multipole kick with integration length ℓ, the implementation applies $C(\ell/2)$, the multipole kick, and $C(\ell/2)$, in that order. For example, one `uniform` step of length ℓ applies

$$M(\ell/2)\ ;\ C(\ell/2)\ ;\ K(\ell)\ ;\ C(\ell/2)\ ;\ M(\ell/2). \tag{2.7.6}$$

Here the operations are listed in tracking order; K contains the multipole terms not included in M. Other integrators use their own propagation and kick weights, including signed lengths. An empty magnetic kick still requires the correction: the two half-length maps combine into $C(\ell)$. With zero field, the resulting map is an exact drift.

2.8 Thin bend

Implemented in the Multipole element.

In a curvilinear reference system with a constant curvature h in the horizontal plane a uniform magnetic field can be derived from the vector potential:

$$A_x = 0, \qquad A_y = 0, \qquad A_s = -B_y \left(x - \frac{hx^2}{2(1+hx)} \right). \tag{2.8.1}$$

With the following normalization, $K_0 = \frac{q_0}{p} B_y$ is the inverse of the bending radius of the reference particle.
The exact and expanded Hamiltonians for a horizontal bending magnet are (eq. 2.12 in [5])

$$H = \frac{p_\tau}{\beta_0} - (1+hx)\sqrt{(1+\delta)^2 - p_x^2 - p_y^2} + \chi K_0 \left(x + \frac{hx^2}{2} \right) \tag{2.8.2}$$

$$\simeq \frac{p_\tau}{\beta_0} + \frac{1}{2}\frac{p_x^2 + p_y^2}{1+\delta} - (1+hx)(1+\delta) + \chi K_0 \left(x + \frac{hx^2}{2} \right) \tag{2.8.3}$$

The map for a thin dipole kick (horizontal or vertical) from the expanded Hamiltonian is (eq. 4.12 in [7]):

$$p_x \leftarrow p_x - \chi K_0 L + hL(1+\delta) - \chi K_0 hxL \tag{2.8.4}$$

$$\tau \leftarrow \tau - \frac{hx}{\beta} L. \tag{2.8.5}$$

2.9 Thin Multipole

Implemented in the Multipole element.

Multipolar components are defined according to the definition in Sec. 1.5.
A thin multipole models the effect of the field by taking the limit of the integration length going to zero while keeping constant the integrated strength. The Hamiltonian is:

$$H = \delta(s)\chi L \Re \left[\sum_{n=0} \frac{1}{(n+1)!} (K_n + i\hat{K}_n)(x+iy)^{n+1} \right]. \tag{2.9.1}$$

The corresponding map is:

$$p_x \leftarrow p_x - \chi L \cdot \Re\left[\sum_{n=0} \frac{1}{n!}(K_n + i\hat{K}_n)(x+iy)^n\right], \tag{2.9.2}$$

$$p_y \leftarrow p_y + \chi L \cdot \Im\left[\sum_{n=0} \frac{1}{n!}(K_n + i\hat{K}_n)(x+iy)^n\right], \tag{2.9.3}$$

where L is the length of the modeled multipole element.
The other coordinates (x, y, δ, ζ) remain unchanged.

2.10 Dipole fringe field

A dipole magnet bends a particle through its approximately uniform body field. Near an entrance or exit, the field changes between the body value and the external value. This transition is the *fringe field*. The transition also produces a longitudinal magnetic-field component away from the mid-plane, and that component can change the vertical momentum. An edge can therefore focus or defocus the vertical motion even when the uniform dipole body has no vertical focusing in Cartesian coordinates.
This section derives that effect starting from the Lorentz force. We first obtain the linear vertical kick of an ideal hard edge, then calculate the leading correction for a field transition of finite width. We next introduce a Hamiltonian description to extend the model to nonzero vertical slope and construct a consistent map of all phase-space coordinates. Finally, we explain the effective-angle form used in tracking, derive its corrected coefficient, and give the generating function and tracking derivatives.
The dipole fringe field map used in Xsuite is based on Ref. [18]; additional background is given in Refs. [19, 20]. The derivation below states the assumptions and intermediate steps needed here. In particular, the finite-width calculation is perturbative to second order in field strength. The resulting symplectic tracking model extends that calculation; it is not an exact solution for every fringe profile or every transverse amplitude.

2.10.1 Geometry, coordinates and magnetic field

We use a right-handed Cartesian frame (x, y, s), with s normal to the pole face, y vertical, and x horizontal. The nominal edge is at $s = 0$. The mid-plane is $y = 0$. A mid-plane particle trajectory lies in the (x, s) plane; to calculate its vertical focusing we consider a small vertical displacement and momentum about that trajectory. A particle exactly at $y = p_y = 0$ receives no vertical kick.
We derive an entrance edge: the field rises from zero before the magnet to its body value after the edge. Magnetic-field and incidence-angle signs are defined in this fixed frame. The derivation assumes the particle has the reference charge and mass, and there is no electric field. In the implementation, a particle of different charge or mass sees the body field K_0 multiplied by the rigidity factor $\chi = (q/q_0)(m_0/m)$ introduced with the particle coordinates; all formulas below then apply with $K_0 \rightarrow$

χK_0. Normalize mechanical momenta by the reference momentum, so that

$$p = 1 + \delta, \tag{2.10.1}$$

$$p_s = \sqrt{p^2 - p_x^2 - p_y^2}, \tag{2.10.2}$$

$$x' = \frac{dx}{ds} = \frac{p_x}{p_s}, \tag{2.10.3}$$

$$y' = \frac{dy}{ds} = \frac{p_y}{p_s}. \tag{2.10.4}$$

The positive square root selects forward motion, $p_s > 0$. The magnetic field changes the direction of the mechanical momentum but not its magnitude p. The slopes x', y' are ratios of momentum components; they are not angles measured in radians. Canonical momenta will be introduced explicitly when we construct the Hamiltonian. Let s_- and s_+ denote positions before and after the field transition. In the distributed-field derivation, arguments specify where a quantity is evaluated: $p_x(s)$ and $y(s)$ vary along the trajectory, whereas $p_x(s_-)$ and $y(s_-)$ denote their incoming values. We write the mechanical slopes as $x_p(s) = p_x(s)/p_s(s)$ and $y_p(s) = p_y(s)/p_s(s)$. These are particle quantities, not parameters of a fixed reference trajectory. Normal incidence is not assumed. For a thin map at the nominal plane, we instead use unadorned symbols for incoming coordinates and a subscript f for outgoing coordinates; this convention will also be used when inverting the map.
Let $b(s)$ be the mid-plane vertical magnetic field divided by the reference magnetic rigidity $(B\rho)_0$. It has units of inverse length. For an entrance fringe, $b(s_-) = 0$ and $b(s_+) = K_0$, where the endpoints lie outside the transition and K_0 is the signed normalized body field. We assume the ideal dipole field is independent of x, with $B_x = 0$ and mid-plane symmetry. In the current-free aperture, Maxwell's equations imply

$$\partial_y B_s = \partial_s B_y, \qquad \partial_y B_y = -\partial_s B_s. \tag{2.10.5}$$

Since $B_s(s, 0) = 0$ by symmetry, the first relation gives $B_s/(B\rho)_0 = yb'(s) + O(y^3)$. Inserting this in the second relation gives $B_y/(B\rho)_0 = b(s) - y^2 b''(s)/2 + O(y^4)$. Continuing in powers of y yields

$$\frac{B_y}{(B\rho)_0} = b(s) - \frac{y^2}{2} b''(s) + \cdots, \tag{2.10.6}$$

$$\frac{B_s}{(B\rho)_0} = yb'(s) - \frac{y^3}{6} b'''(s) + \cdots. \tag{2.10.7}$$

Primes denote derivatives with respect to s. Thus a changing vertical field necessarily produces a longitudinal field away from the mid-plane. This longitudinal component is the origin of the vertical edge kick.

2.10.2 Lorentz equations near the mid-plane

Writing the Lorentz force with s as the independent variable gives

$$\frac{d\boldsymbol{p}}{ds} = \left(\frac{p_x}{p_s}, \frac{p_y}{p_s}, 1\right) \times \frac{\boldsymbol{B}}{(B\rho)_0}, \tag{2.10.8}$$

where $\boldsymbol{p} = (p_x, p_y, p_s)$ is the normalized mechanical momentum. In particular,

$$\frac{dp_x}{ds} = \frac{p_y}{p_s}\frac{B_s}{(B\rho)_0} - \frac{B_y}{(B\rho)_0}, \tag{2.10.9}$$

$$\frac{dp_y}{ds} = \frac{B_x}{(B\rho)_0} - \frac{p_x}{p_s}\frac{B_s}{(B\rho)_0}. \tag{2.10.10}$$

Linearize in the vertical displacement and momentum, keeping the horizontal angle exact. The product $p_y B_s$ is second order in vertical amplitude, and p_y^2 does not enter p_s at linear order. Using the field expansion above gives

$$\frac{dp_x}{ds} = -b(s), \tag{2.10.11}$$

$$\frac{dy}{ds} = \frac{p_y}{p_s}, \tag{2.10.12}$$

$$\frac{dp_y}{ds} = -\frac{p_x}{p_s}\, b'(s) y, \tag{2.10.13}$$

$$p_s = \sqrt{p^2 - p_x^2}. \tag{2.10.14}$$

These equations are linear in the vertical variables but need not be expanded in field strength; they can also be integrated numerically for a specified smooth profile $b(s)$.

2.10.3 Hard-edge limit and linear vertical focusing

A hard edge idealizes the transition as having zero longitudinal width while keeping the field jump K_0 fixed. To derive its kick without multiplying singular fields, first use the linear vertical equations for a smooth transition of width L, and then take $L \to 0$. Equation (2.10.11) gives

$$p_x(s_+) - p_x(s_-) = -\int_{s_-}^{s_+} b(s)\, ds = O(K_0 L). \tag{2.10.15}$$

Thus the horizontal momentum change across the shrinking transition vanishes, so the horizontal slope tends to $x_p(s_-)$. The vertical position remains continuous. Integrating Eq. (2.10.12) over a vanishing length gives $y(s_+) \to y(s_-)$ for finite vertical momentum. The vertical momentum change, however, need not vanish, because the integral of b' is the fixed field jump:

$$\int_{s_-}^{s_+} b'(s)\, ds = b(s_+) - b(s_-) = K_0. \tag{2.10.16}$$

Integrating Eq. (2.10.13) in this limit therefore gives

$$\Delta p_y = -x_p(s_-) y(s_-) \int_{s_-}^{s_+} b'(s)\, ds \tag{2.10.17}$$

$$= -K_0 x_p(s_-)\, y(s_-). \tag{2.10.18}$$

This is the hard-edge vertical focusing law in the pole-face frame. Its linear map is

$$\begin{pmatrix} y(s_+) \\ p_y(s_+) \end{pmatrix} = \begin{pmatrix} 1 & 0 \\ -K_0 x_p(s_-) & 1 \end{pmatrix} \begin{pmatrix} y(s_-) \\ p_y(s_-) \end{pmatrix}. \tag{2.10.19}$$

It holds for any small incoming vertical momentum, including zero: at the linear order in the vertical variables used here, an incoming p_y does not alter the coefficient. The dependence on the vertical slope found in the Hamiltonian treatment below, the factor $1/(1+y_p^2)$ in Eq. (2.10.75), is quadratic in y_p and therefore lies beyond this linearization. When $K_0 x_p(s_-)$ is positive, a positive displacement receives a negative momentum kick, directed toward the mid-plane: the edge focuses. Reversing the sign of $K_0 x_p(s_-)$ makes it defocusing. At normal incidence, $x_p(s_-) = 0$, this hard-edge vertical kick vanishes.

The horizontal velocity couples to the longitudinal fringe field in the Lorentz force. Although the transition width tends to zero, that longitudinal field grows in proportion to b', so its integrated vertical impulse stays finite. This is why a hard edge can produce a kick. The derivation is a limit of the linearized equations; it does not assert that the off-mid-plane field of an infinitely sharp edge is regular.

The coefficient $K_0 x_p(s_-)$ has units of inverse length. At fixed incidence angle it has no explicit dependence on p when acting on the normalized momentum p_y. The slope change does have momentum dependence:

$$\Delta y' = \frac{\Delta p_y}{p_s(s_-)} = -\frac{K_0 x_p(s_-)}{p_s(s_-)} y(s_-). \tag{2.10.20}$$

This distinction matters when comparing formulas written in slopes and in normalized momenta. For a falling field transition, the same integration uses its signed field jump $-K_0$ instead of K_0, with the slope $x_p(s_-)$ measured in the frame whose s axis is normal to the exit face. The treatment of the exit face in the implementation is described in Section 2.10.11.

2.10.4 Finite-width correction for zero incoming vertical slope

We take $p_y(s_-) = 0$, hence zero incoming vertical slope, and retain a small incoming vertical displacement $y(s_-)$. The mid-plane itself is $y = 0$; a trajectory confined to it has both $y = 0$ and $p_y = 0$ and receives no vertical kick. Here we calculate the linear response to a displacement from that trajectory. The coefficient multiplying $y(s_-)$ in the resulting momentum kick is the vertical focusing coefficient. The vertical momentum generally becomes nonzero as the particle crosses the fringe.

For a finite transition width, p_x/p_s and y change while the particle crosses the fringe. Their first-order changes modify the vertical force and give the leading correction to Eq. (2.10.18). We now compute that correction to second order in field strength.

An equivalent thin fringe replaces the distributed transition by a map at its nominal plane. The ordinary drift before that plane and uniform-field bend after it are factored out. A uniform Cartesian dipole does not change p_y, so its removal leaves the vertical momentum kick unchanged.

The field-profile dependence of the correction can be expressed through

$$I = \int_{s_-}^{s_+} b(s)\big(K_0 - b(s)\big)\, ds. \tag{2.10.21}$$

The integrand vanishes both before the entrance and in the uniform body, so only the transition contributes. For a hard edge $I \to 0$; a finite transition generally gives a nonzero value. In tracking, this quantity is specified by the full magnet gap $g = 2\,\texttt{hgap}$ and the dimensionless fringe integral $F = \texttt{fint}$:

$$F = \frac{1}{gK_0^2}\int_{s_-}^{s_+} b(s)\big(K_0 - b(s)\big)\, ds, \qquad I = gK_0^2F. \tag{2.10.22}$$

The gap g is a transverse distance, not the longitudinal transition width L. The product gF encodes the profile integral; specifying it does not specify the complete field profile. For a fixed profile shape and width, I is proportional to K_0^2.
To extract the finite-width correction analytically, specify the incoming displacement $y(s_-)$ and take $p_y(s_-) = 0$. Introduce the accumulated normalized field integral

$$\mathcal{I}(s) = \int_{s_-}^{s} b(\sigma)\, d\sigma, \qquad p_x(s) = p_x(s_-) - \mathcal{I}(s). \tag{2.10.23}$$

The second relation follows by integrating Eq. (2.10.11), $dp_x/ds = -b(s)$, from s_- to s, with the incoming value $p_x(s_-)$. The integral $\mathcal{I}(s)$ is distinct from the quadratic fringe integral I in Eq. (2.10.22). Evaluating Eq. (2.10.14) at the entrance gives the incoming longitudinal momentum; the corresponding horizontal slope is

$$p_s(s_-) = \sqrt{p^2 - p_x(s_-)^2}, \qquad x_p(s_-) = \frac{p_x(s_-)}{p_s(s_-)}. \tag{2.10.24}$$

The magnetic field preserves the total momentum p, but both $p_x(s)$ and $p_s(s)$ vary along the trajectory. Using Eq. (2.10.14) to express their ratio as a function of $p_x(s)$, define, at fixed p,

$$f(a) = \frac{a}{\sqrt{p^2 - a^2}}, \qquad \frac{p_x(s)}{p_s(s)} = f\big(p_x(s_-) - \mathcal{I}(s)\big). \tag{2.10.25}$$

Differentiating the numerator and denominator gives

$$f'(a) = \frac{1}{\sqrt{p^2 - a^2}} + \frac{a^2}{(p^2 - a^2)^{3/2}} \tag{2.10.26}$$

$$= \frac{p^2}{(p^2 - a^2)^{3/2}}. \tag{2.10.27}$$

The first-order Taylor expansion about the incoming momentum $p_x(s_-)$ is therefore

$$f\big(p_x(s_-) - \mathcal{I}(s)\big) = f(p_x(s_-)) - \mathcal{I}(s)f'(p_x(s_-)) + O\big(\mathcal{I}(s)^2\big) \tag{2.10.28}$$

$$= x_p(s_-) - \frac{p^2}{p_s(s_-)^3}\mathcal{I}(s) + O\big(\mathcal{I}(s)^2\big). \tag{2.10.29}$$

For a fixed fringe shape and length, $b(s) = K_0\widehat{b}(s)$ with $\widehat{b}(s)$ independent of K_0, so $\mathcal{I}(s)$ is proportional to K_0. Holding p and $p_x(s_-)$ fixed while expanding in the field strength therefore gives

$$\frac{p_x(s)}{p_s(s)} = x_p(s_-) - \frac{p^2}{p_s(s_-)^3}\mathcal{I}(s) + O(K_0^2). \tag{2.10.30}$$

Since $b'(s)$ is already first order in K_0, the first-order vertical force uses the zero-field values $p_x/p_s = x_p(s_-)$ and $y = y(s_-)$ in Eq. (2.10.13). Integrating from s_-, where $p_y = 0$ and $b = 0$, gives

$$p_y^{(1)}(s) = -x_p(s_-)y(s_-)\int_{s_-}^{s} b'(\sigma)\,d\sigma = -x_p(s_-)b(s)y(s_-). \tag{2.10.31}$$

To obtain the first-order change in position, insert this result into Eq. (2.10.12) and use the zero-field denominator $p_s(s_-)$:

$$y^{(1)}(s) = \int_{s_-}^{s} \frac{p_y^{(1)}(\sigma)}{p_s(s_-)}\,d\sigma = -\frac{x_p(s_-)y(s_-)}{p_s(s_-)}\mathcal{I}(s). \tag{2.10.32}$$

The superscript (1) denotes the first-order change; the position itself is $y(s) = y(s_-) + y^{(1)}(s) + O(K_0^2)$. Substituting both corrections back into Eq. (2.10.13),

$$\begin{aligned}\frac{dp_y}{ds} &= -x_p(s_-)b'(s)y(s_-) \\ &\quad + \left(\frac{p^2}{p_s(s_-)^3} + \frac{x_p(s_-)^2}{p_s(s_-)}\right)\mathcal{I}(s)b'(s)y(s_-) + O(K_0^3 y(s_-)),\end{aligned} \tag{2.10.33}$$

$$\int \mathcal{I}(s)b'(s)\,ds = [\mathcal{I}(s)b(s)]_{s_-}^{s_+} - \int b(s)^2\,ds = \int b(s)\big(K_0 - b(s)\big)\,ds = I. \tag{2.10.34}$$

The resulting kick coefficient is therefore

$$\frac{\Delta p_y}{y(s_-)} = -K_0 x_p(s_-) + I\frac{1 + 2x_p(s_-)^2}{p_s(s_-)} + O(K_0^3). \tag{2.10.35}$$

The first term is the hard-edge focusing. The second is the leading correction due to the finite field transition. At fixed incoming slope, the finite-gap correction scales as $1/p$, since $p_s(s_-) = p/\sqrt{1 + x_p(s_-)^2}$. Its slope dependence must be preserved when correcting the momentum dependence.

2.10.5 Momentum-dependent coefficient of the generating function

Our aim is to determine the momentum-dependent focusing coefficient Φ of an equivalent thin fringe kick, written at the retained linear vertical order as

$$\Delta p_y = -\Phi(p_x, p_y, \delta)Y. \tag{2.10.36}$$

Here Y is the vertical position extrapolated to the nominal fringe plane along an unperturbed drift; its precise definition is given below. The preceding section obtained

the kick for zero incoming vertical momentum. We now seek the coefficient used in the operator model of Ref. [18], which also describes nonzero incoming vertical momentum. We construct the field Hamiltonian, remove the ordinary drift motion, and calculate the first- and second-order contributions in the field strength. The second-order calculation retains the terms needed for linear mid-plane focusing; their unexpanded momentum dependence defines the model's extension away from the mid-plane. The resulting Φ provides the coefficient that the generating-function model must reproduce to this order, rather than a description of every nonlinear fringe effect.

We first specify the vector potential and the momentum convention used in the Hamiltonian. The normalized vector potential is

$$\mathbf{a} = \frac{\mathbf{A}}{(B\rho)_0}. \tag{2.10.37}$$

Choose its components as

$$a_x = a(s, y), \tag{2.10.38}$$
$$a_y = 0, \tag{2.10.39}$$
$$a_s = -xb(s). \tag{2.10.40}$$

The scalar $a(s, y)$ therefore denotes the horizontal component of the normalized vector potential. Taking the curl in the Cartesian frame gives

$$\frac{B_x}{(B\rho)_0} = \partial_y a_s - \partial_s a_y = 0, \tag{2.10.41}$$
$$\frac{B_y}{(B\rho)_0} = \partial_s a_x - \partial_x a_s = b(s) + \partial_s a(s, y), \tag{2.10.42}$$
$$\frac{B_s}{(B\rho)_0} = \partial_x a_y - \partial_y a_x = -\partial_y a(s, y). \tag{2.10.43}$$

Thus a_s supplies the mid-plane vertical field, while a_x supplies its off-mid-plane corrections and the longitudinal fringe field.

To determine $a(s, y)$, impose Maxwell's equation $\partial_s B_y = \partial_y B_s$ in the current-free aperture. Substituting Eqs. (2.10.42) and (2.10.43) gives

$$b'(s) + \partial_s^2 a + \partial_y^2 a = 0. \tag{2.10.44}$$

Mid-plane symmetry allows an even series in y; choose $a(s, 0) = 0$ and write

$$a(s, y) = c_2(s)y^2 + c_4(s)y^4 + c_6(s)y^6 + \cdots. \tag{2.10.45}$$

Matching powers of y in Eq. (2.10.44) yields

$$b' + 2c_2 = 0, \tag{2.10.46}$$
$$c_2'' + 12c_4 = 0, \tag{2.10.47}$$
$$c_{2n}'' + (2n+2)(2n+1)c_{2n+2} = 0 \qquad (n \geq 1). \tag{2.10.48}$$

Consequently $c_2 = -b'/2$, $c_4 = b'''/24$, and in general

$$a(s,y) = \sum_{n=1}^{\infty} \frac{(-1)^n b^{(2n-1)}(s)}{(2n)!}\, y^{2n} = -\frac{b'(s)}{2} y^2 + \frac{b'''(s)}{24} y^4 - \cdots . \tag{2.10.49}$$

Here $b^{(n)}$ denotes the n-th derivative with respect to s. As a check, substituting this series into Eqs. (2.10.42) and (2.10.43) gives

$$\frac{B_y}{(B\rho)_0} = b(s) - \frac{b''(s)}{2} y^2 + \frac{b^{(4)}(s)}{24} y^4 - \cdots , \tag{2.10.50}$$

$$\frac{B_s}{(B\rho)_0} = b'(s) y - \frac{b'''(s)}{6} y^3 + \frac{b^{(5)}(s)}{120} y^5 - \cdots , \tag{2.10.51}$$

which reproduce the field expansion in Eq. (2.10.6).
We now use canonical momenta in the Hamiltonian. Their relation to the normalized mechanical momenta is

$$p_x^{\text{mech}} = p_x - a_x, \qquad p_y^{\text{mech}} = p_y - a_y, \qquad p_s^{\text{can}} = p_s^{\text{mech}} + a_s. \tag{2.10.52}$$

The preceding Lorentz-equation derivation used mechanical transverse momenta. Since $a_x = O(y^2)$ and $a_y = 0$, the transverse canonical and mechanical momenta agree to the linear vertical order used there. The symbol p continues to denote the conserved total mechanical momentum. For forward motion its longitudinal component is

$$p_s^{\text{mech}} = \sqrt{p^2 - (p_x - a_x)^2 - (p_y - a_y)^2}. \tag{2.10.53}$$

At fixed energy, using s as the independent variable gives the reduced Hamiltonian $H = -p_s^{\text{can}} = -p_s^{\text{mech}} - a_s$. Inserting the chosen vector potential therefore gives

$$H = -\sqrt{p^2 - (p_x - a)^2 - p_y^2} + b(s)x. \tag{2.10.54}$$

To identify the perturbation to the drift Hamiltonian, define

$$H_0 = -\sqrt{p^2 - p_x^2 - p_y^2}, \qquad p_s = \sqrt{p^2 - p_x^2 - p_y^2}. \tag{2.10.55}$$

For this unperturbed drift, denote the particle's slopes by $x_p = p_x/p_s$ and $y_p = p_y/p_s$. They are functions of the particle's canonical momenta, not fixed slopes of a reference trajectory. They remain constant along a free drift because its momenta are constant, but change when the incoming momenta are varied. In particular, their momentum derivatives must be retained in the tracking map.
Inside the magnetic field, these drift slopes must be distinguished from the actual mechanical slopes. For the chosen gauge, the latter are

$$\frac{dx}{ds} = \frac{p_x - a(s,y)}{p_s^{\text{mech}}}, \qquad \frac{dy}{ds} = \frac{p_y}{p_s^{\text{mech}}}. \tag{2.10.56}$$

At a field-free entrance, x_p evaluated at the incoming momenta equals the incoming mechanical slope $x_p(s_-)$ used above. Expanding Eq. (2.10.54) to first order in a gives

$$H = H_0 + b(s)x - \frac{p_x}{p_s} a(s,y) + O(a^2). \tag{2.10.57}$$

We denote the part of $H - H_0$ that is first order in field strength by V:

$$V(s, x, y, p_x, p_y) = b(s)x - x_p a(s, y), \qquad H = H_0 + V + O(K_0^2). \tag{2.10.58}$$

Both b and a are proportional to K_0 for a fixed field profile. At this stage V retains the full vertical-position series of $a(s, y)$; the expansion in field strength has not truncated that series.

The drift interaction frame removes the motion generated by H_0 before expanding in the fringe perturbation. To define it explicitly, Hamilton's equations for the unperturbed drift are

$$\frac{dx}{ds} = \frac{\partial H_0}{\partial p_x} = \frac{p_x}{p_s} = x_p, \tag{2.10.59}$$

$$\frac{dy}{ds} = \frac{\partial H_0}{\partial p_y} = \frac{p_y}{p_s} = y_p, \tag{2.10.60}$$

$$\frac{dp_x}{ds} = -\frac{\partial H_0}{\partial x} = 0, \tag{2.10.61}$$

$$\frac{dp_y}{ds} = -\frac{\partial H_0}{\partial y} = 0. \tag{2.10.62}$$

The slopes are therefore constant under this drift. Choose a reference plane $s = s_*$ and introduce coordinates X, Y by

$$X = x - (s - s_*)x_p, \tag{2.10.63}$$

$$Y = y - (s - s_*)y_p. \tag{2.10.64}$$

These are the positions obtained by extrapolating the instantaneous phase-space point back to s_* along a free drift; the transformation leaves the momenta unchanged. In the absence of the field perturbation, X, Y are constant. With the fringe present, they evolve because of that perturbation. Thus this change of coordinates does not assume that the actual trajectory through the fringe is a straight line.

The transformation is the inverse Hamiltonian flow of H_0 and is canonical. Its explicit dependence on s subtracts H_0 from the transformed Hamiltonian, leaving

$$H_I(s, X, Y, p_x, p_y) = (H - H_0)\big|_{x=X+(s-s_*)x_p,\; y=Y+(s-s_*)y_p}. \tag{2.10.65}$$

The subscript I denotes the interaction frame. Define V_I to be the same first-order perturbation V, evaluated at the physical positions corresponding to X, Y:

$$V_I(s, X, Y, p_x, p_y) = V\big(s, X + (s - s_*)x_p, Y + (s - s_*)y_p, p_x, p_y\big). \tag{2.10.66}$$

Substitution of Eq. (2.10.58) gives

$$V_I = b(s)\big[X + (s - s_*)x_p\big] - x_p a\big(s, Y + (s - s_*)y_p\big). \tag{2.10.67}$$

Thus $H_I = V_I + O(K_0^2)$: V_I is the first-order part of the interaction-frame Hamiltonian, not its full expression to all field orders. This explains the positive shifts in the arguments: the field perturbation must be evaluated at the physical position corresponding to X, Y at s. Choose the nominal fringe plane as the origin, $s_* = 0$. The

physical positions entering V are then $X + sx_p$ and $Y + sy_p$. We retain X, Y for the interaction-frame positions and x_p, y_p for the unperturbed drift slopes throughout the derivation.

To obtain the first-order vertical kick, use Hamilton's equation $dp_y/ds = -\partial H_I/\partial Y$ and retain V_I, the part first order in field strength. Integrating with the interaction-frame coordinates and momenta held at their unperturbed values gives

$$\Delta p_y^{(1)} = -\frac{\partial}{\partial Y} \int V_I \, ds. \tag{2.10.68}$$

The term $b(s)(X + sx_p)$ has no Y-dependence, so it contributes no vertical kick. Since x_p is independent of Y, this reduces to

$$\Delta p_y^{(1)} = x_p \frac{\partial}{\partial Y} \int a(s, Y + sy_p) \, ds. \tag{2.10.69}$$

The vector-potential integral is therefore an intermediate step toward the kick: its derivative with respect to Y, multiplied by x_p, gives the momentum change. To evaluate it, consider the n-th term of the series in Eq. (2.10.49). Integrating by parts $2n - 2$ times gives

$$\begin{aligned} &\int_{s_-}^{s_+} \frac{(-1)^n b^{(2n-1)}(s)}{(2n)!} (Y + sy_p)^{2n} \, ds \\ &\qquad = \frac{(-1)^n y_p^{2n-2}}{2} \int_{s_-}^{s_+} b'(s)(Y + sy_p)^2 \, ds. \end{aligned} \tag{2.10.70}$$

All boundary terms contain derivatives of b that vanish outside the transition. The remaining polynomial derivative supplies the factor $(2n)!/2$ and the power y_p^{2n-2}. Expanding the square gives

$$\int b'(s)(Y + sy_p)^2 \, ds = K_0 Y^2 + 2Y y_p \int b'(s)\, s \, ds + y_p^2 \int b'(s)\, s^2 \, ds. \tag{2.10.71}$$

The last term does not depend on Y and drops out of the derivative in Eq. (2.10.69). The middle term is removed by the choice of the nominal plane: we place $s = 0$ at the centroid of b',

$$\int_{s_-}^{s_+} b'(s)\, s \, ds = 0, \tag{2.10.72}$$

which is the midpoint of a transition that is antisymmetric about its centre, such as the hyperbolic-tangent profile used below. This convention fixes where the thin map is placed; it does not require the transition width to vanish. The part of the integral that contributes to the kick is therefore $K_0 Y^2$ for any width, and summing over n gives

$$\int a(s, Y + sy_p) \, ds \doteq \frac{K_0 Y^2}{2} \sum_{n=1}^{\infty} (-1)^n y_p^{2n-2} = -\frac{K_0 Y^2}{2(1 + y_p^2)}, \tag{2.10.73}$$

where $\doteq$ denotes equality up to terms independent of Y. The sum is first obtained where the geometric series converges and then used as its rational continuation. Substituting this result into Eq. (2.10.69) and differentiating at fixed momenta gives

$$\Delta p_y^{(1)} = x_p \frac{\partial}{\partial Y} \left[-\frac{K_0 Y^2}{2(1 + y_p^2)} \right] = -K_0 u Y, \tag{2.10.74}$$

where the dimensionless slope combination u is defined as

$$u = \frac{x_p}{1 + y_p^2}. \tag{2.10.75}$$

This is an auxiliary function of the two unperturbed drift slopes, not an independent coordinate. It is the factor entering the first-order vertical kick, $\Delta p_y^{(1)} = -K_0 u Y$, and thus gives the first-order focusing coefficient $\Phi^{(1)} = K_0 u$. On the mid-plane, $y_p = 0$, it reduces to $u = x_p$. For nonzero vertical slope, its denominator accounts for the vertical-slope dependence in this fringe model. This first-order result reduces to the hard-edge mid-plane kick derived directly from the Lorentz force in Eq. (2.10.18).
To calculate the contribution $C = O(K_0^2)$ to the focusing coefficient $\Phi = K_0 u - C$, we use the ordered second-order perturbation expansion. First expand the vertical-position dependence of V_I explicitly. Using $a(s, y) = -b'(s)y^2/2 + b'''(s)y^4/24 - \cdots$ in Eq. (2.10.67), with $s_* = 0$, gives

$$\begin{aligned} V_I = {} & b(s)(X + sx_p) + \frac{x_p}{2} b'(s)(Y + sy_p)^2 \\ & - \frac{x_p}{24} b'''(s)(Y + sy_p)^4 + \cdots . \end{aligned} \tag{2.10.76}$$

We denote by W the truncation of V_I that retains the horizontal term and the leading quadratic vertical term:

$$W(s) = b(s)(X + sx_p) + \frac{x_p}{2} b'(s)(Y + sy_p)^2. \tag{2.10.77}$$

Here $W(s)$ abbreviates $W(s, X, Y, p_x, p_y)$; it still depends on the transverse coordinates and momenta. It is not an additional physical interaction or a second-order Hamiltonian. Like V_I, W is first order in K_0, but it omits the fourth and higher powers of the physical vertical position $Y + sy_p$. Its two successive actions in the ordered expansion produce the second-order contribution C. Thus "second order" refers to the field strength, whereas "quadratic" refers to the vertical position. This truncation is part of the approximation used for linear mid-plane focusing; keeping the remaining momentum dependence unexpanded does not recover the omitted nonlinear terms. Define the transverse Poisson bracket by

$$\{f, h\} = f_X h_{p_x} - f_{p_x} h_X + f_Y h_{p_y} - f_{p_y} h_Y. \tag{2.10.78}$$

To see why a double integral appears, consider the motion generated by W and write the interaction-frame phase-space coordinates as $\mathbf{z} = (X, Y, p_x, p_y)$. Hamilton's equations are $dz_j/ds = \{z_j, W(s)\}$, in particular $dp_y/ds = \{p_y, W(s)\} = -\partial W(s)/\partial Y$. At first order, the force is evaluated at the unperturbed phase-space point, so only one integration is needed. The first-order change accumulated by the time the particle reaches s_1 is

$$z_j^{(1)}(s_1) = \int_{s_-}^{s_1} \{z_j, W(s_2)\}\, ds_2. \tag{2.10.79}$$

At second order, the vertical force at s_1 must account for this earlier change. To make the expansion explicit, denote the vertical momentum-change rate generated by W by

$$\mathcal{F}_y(s, \mathbf{z}) = \{p_y, W(s, \mathbf{z})\}. \tag{2.10.80}$$

Write the perturbed trajectory as

$$\mathbf{z}(s_1) = \mathbf{z}^{(0)} + \mathbf{z}^{(1)}(s_1) + O(K_0^2). \tag{2.10.81}$$

Here $\mathbf{z}^{(0)}$ is the constant unperturbed interaction-frame point, and $\mathbf{z}^{(1)}$ is its first-order change, not the full trajectory. A Taylor expansion of the force about $\mathbf{z}^{(0)}$ gives

$$\begin{aligned}\mathcal{F}_y(s_1, \mathbf{z}(s_1)) = \mathcal{F}_y(s_1, \mathbf{z}^{(0)}) \\ + \sum_j \frac{\partial \mathcal{F}_y(s_1, \mathbf{z})}{\partial z_j}\bigg|_{\mathbf{z}^{(0)}} z_j^{(1)}(s_1) + O(K_0^3).\end{aligned} \tag{2.10.82}$$

The first term is the first-order force. In the second term, $\partial \mathcal{F}_y / \partial z_j = O(K_0)$ and $z_j^{(1)} = O(K_0)$, so their product is second order in field strength. This contribution is therefore

$$\left(\frac{dp_y}{ds_1}\right)^{(2)} = \sum_j \frac{\partial \mathcal{F}_y(s_1)}{\partial z_j} z_j^{(1)}(s_1). \tag{2.10.83}$$

From here on, all brackets and derivatives are evaluated at $\mathbf{z}^{(0)}$ unless stated otherwise. Inserting Eq. (2.10.79) gives

$$\left(\frac{dp_y}{ds_1}\right)^{(2)} = \int_{s_-}^{s_1} \sum_j \frac{\partial \mathcal{F}_y(s_1)}{\partial z_j} \{z_j, W(s_2)\}\, ds_2. \tag{2.10.84}$$

The sum over the four coordinates is a Poisson bracket. Explicitly, writing $W_2 = W(s_2)$ and suppressing the argument s_1 of $\mathcal{F}_y$,

$$\begin{aligned}\sum_j \frac{\partial \mathcal{F}_y}{\partial z_j}\{z_j, W_2\} &= \frac{\partial \mathcal{F}_y}{\partial X}\frac{\partial W_2}{\partial p_x} + \frac{\partial \mathcal{F}_y}{\partial Y}\frac{\partial W_2}{\partial p_y} \\ &\quad - \frac{\partial \mathcal{F}_y}{\partial p_x}\frac{\partial W_2}{\partial X} - \frac{\partial \mathcal{F}_y}{\partial p_y}\frac{\partial W_2}{\partial Y} \\ &= \{\mathcal{F}_y, W_2\}.\end{aligned} \tag{2.10.85}$$

Restoring $\mathcal{F}_y(s_1) = \{p_y, W(s_1)\}$ then yields

$$\left(\frac{dp_y}{ds_1}\right)^{(2)} = \int_{s_-}^{s_1} \big\{\{p_y, W(s_1)\}, W(s_2)\big\}\, ds_2. \tag{2.10.86}$$

The inner bracket is the vertical force at s_1; the outer bracket gives its change due to the earlier interaction at s_2. Integrating the force over the later position s_1 therefore produces the ordered double integral

$$\Delta p_y^{(2)} = \int_{s_-}^{s_+} ds_1 \int_{s_-}^{s_1} ds_2 \,\big\{\{p_y, W(s_1)\}, W(s_2)\big\}. \tag{2.10.87}$$

The inner integration sums the earlier perturbations at s_2; the outer one sums their effects on the force at the later position s_1. The limit $s_2 < s_1$ enforces this ordering.

Each occurrence of W supplies one power of K_0, so this contribution is second order in field strength. It is the Hamiltonian counterpart of substituting the first-order trajectory changes back into the Lorentz force in the preceding derivation.
By antisymmetry of the Poisson bracket,

$$\big\{\{p_y, W(s_1)\}, W(s_2)\big\} = \big\{W(s_2), \{W(s_1), p_y\}\big\}. \tag{2.10.88}$$

In this integrand, the terms retained for linear mid-plane focusing are

$$Y\left[b(s_2)b'(s_1)\{X, x_p\} + x_p^2 b'(s_2)b'(s_1)(s_1 - s_2)\{Y, y_p\}\right]. \tag{2.10.89}$$

For example, the first term comes from the bracket of $b(s_2)X$ with $x_p b'(s_1)Y$. The second comes from the vertical-position and vertical-momentum derivatives of the two quadratic terms in W. Terms containing additional explicit powers of the vertical displacement or vertical slope are not retained in this step. Keeping the momentum derivatives $\{X, x_p\}$ and $\{Y, y_p\}$ unexpanded defines the conventional extension away from the mid-plane; it does not restore the other discarded terms. Integrating the retained expression over the ordered pair (s_2, s_1) in Eq. (2.10.87) gives $\Delta p_y^{(2)} = CY$, where

$$C = \{X, x_p\}J_0 + x_p^2\{Y, y_p\}(J_{10} - J_{01}), \tag{2.10.90}$$

where

$$J_0 = \int_{s_-}^{s_+} b'(s_1)\, ds_1 \int_{s_-}^{s_1} b(s_2)\, ds_2 = I, \tag{2.10.91}$$

$$J_{10} - J_{01} = \int_{s_-}^{s_+} b'(s_1)\, ds_1 \int_{s_-}^{s_1} b'(s_2)(s_1 - s_2)\, ds_2 = I. \tag{2.10.92}$$

For the second identity, the inner integral equals $\int_{s_-}^{s_1} b(s_2)\, ds_2$ by integration by parts, since $b(s_-) = 0$. The remaining momentum derivatives are explicit:

$$\{X, x_p\} = \frac{\partial(p_x/p_s)}{\partial p_x} = \frac{p^2 - p_y^2}{p_s^3} = \frac{1 + x_p^2}{p_s}, \tag{2.10.93}$$

$$\{Y, y_p\} = \frac{\partial(p_y/p_s)}{\partial p_y} = \frac{p^2 - p_x^2}{p_s^3} = \frac{1 + y_p^2}{p_s}. \tag{2.10.94}$$

Combining the first- and second-order kicks gives $\Delta p_y = -K_0 uY + CY = -\Phi Y$ at the retained order. Consequently, writing $A = 1 + x_p^2(2 + y_p^2)$, the coefficient to be matched is

$$\Phi = K_0 u - C = K_0 u - gK_0^2 F\frac{A}{p_s}. \tag{2.10.95}$$

This is Eq. (34) of Ref. [18] in the present notation. At $p_y = 0$, it reproduces the independent derivation in Eq. (2.10.35), with $\Delta p_y = -\Phi Y$. For general vertical slopes it specifies the chosen operator approximation; matching it does not establish an exact finite-width field map to all transverse orders.

2.10.6 Constructing the corrected tangent form

Denote by $\psi(p_x, p_y, \delta)$ the momentum-dependent focusing coefficient used in the tracking model. At the retained linear vertical order, its kick is $\Delta p_y = -\psi Y$. Thus ψ has units of inverse length; it is a focusing strength, not an angle. It will also supply the coefficient of the quadratic vertical term in the generating function below. The coefficient Φ derived in Eq. (2.10.95) is the perturbative result through second order in field strength. We require the model coefficient to reproduce that result:

$$\psi = \Phi + O(K_0^3). \tag{2.10.96}$$

Using distinct symbols distinguishes the derived expansion Φ from the unexpanded tracking-model expression ψ.
To connect the slope-based result to the existing effective-angle model, introduce the signed incoming mid-plane incidence angle e, measured from the s axis toward $+x$. For forward motion,

$$p_x = p \sin e, \qquad p_s = p \cos e, \qquad x_p = \tan e, \qquad p_y = 0. \tag{2.10.97}$$

Here the momenta are incoming values. At the field-free entrance, $x_p = x_p(s_-)$, connecting to the mechanical slope used above. Equation (2.10.18) therefore has focusing coefficient $K_0 \tan e$. The finite-width result in Eq. (2.10.35) can likewise be written

$$\frac{\Delta p_y}{y(s_-)} = -K_0 \tan e + \frac{g K_0^2 F}{p} \frac{1 + \sin^2 e}{\cos^3 e} + O(K_0^3). \tag{2.10.98}$$

The existing tracking model expresses the finite-fringe correction as a shift of an effective edge angle. On the mid-plane this means replacing e by $e - \epsilon$, giving a coefficient $K_0 \tan(e - \epsilon)$. For nonzero vertical slope, the first-order result is $K_0 u$, so the corresponding effective angle is $\arctan u$: it equals e on the mid-plane for forward motion, but in general it is a function of both slopes, not simply the geometric incidence angle. We retain this form of the existing model and determine the angle shift by requiring agreement with the derived focusing coefficient through second order in field strength. For the model coefficient ψ, write

$$\psi = K_0 \tan\big(\arctan u - \epsilon\big), \qquad \epsilon = O(K_0). \tag{2.10.99}$$

Expand the outer tangent, keeping the momenta fixed:

$$\tan(\arctan u - \epsilon) = u - (1 + u^2)\epsilon + O(\epsilon^2), \tag{2.10.100}$$

$$\psi = K_0 u - K_0(1 + u^2)\epsilon + O(K_0^3). \tag{2.10.101}$$

Agreement with Eq. (2.10.95) requires

$$\epsilon = g K_0 F \frac{A}{p_s(1 + u^2)}. \tag{2.10.102}$$

Thus the corrected expression used in the map is[1]

$$\boxed{\psi = K_0 \tan\left[\arctan u - gK_0F\frac{1+x_p^2(2+y_p^2)}{p_s(1+u^2)}\right], \qquad u = \frac{x_p}{1+y_p^2}.} \tag{2.10.103}$$

The tangent form is a model choice beyond the calculated order. The unexpanded tangent includes terms of order K_0^3 and higher whose accuracy has not been established by this matching. It is not required for symplecticity: that follows from using a single generating function consistently for all coordinates, as described below.
On the mid-plane, $y_p = 0$, so

$$\frac{1}{p_s(1+u^2)} = \frac{p_s}{p_s^2+p_x^2} = \frac{p_s}{(1+\delta)^2} = \frac{\cos e}{1+\delta}. \tag{2.10.104}$$

The mid-plane angle shift is therefore $\epsilon = gK_0F(1+\sin^2 e)/[(1+\delta)\cos e]$, the expression of SLAC-75 and MAD-X divided by $1+\delta$.

2.10.7 Generating function and forward map

The thin map acts at the nominal plane $s = 0$, where Eqs. (2.10.63) and (2.10.64) give $X = x$ and $Y = y$. We write its incoming and outgoing physical positions as (x, y) and (x_f, y_f). The coefficient ψ retains the slope notation $x_p = p_x/p_s$ and $y_p = p_y/p_s$, evaluated at the incoming canonical momenta.
A generating function is a scalar function whose derivatives define a canonical, and hence symplectic, transformation. Here we use a mixed generating function: its independent arguments are the incoming momenta and outgoing positions. With the longitudinal canonical pair $(\ell, -\delta)$, the defining relations are

$$x = \frac{\partial \mathcal{G}}{\partial p_x}, \qquad p_{x,f} = \frac{\partial \mathcal{G}}{\partial x_f}, \tag{2.10.105}$$

$$y = \frac{\partial \mathcal{G}}{\partial p_y}, \qquad p_{y,f} = \frac{\partial \mathcal{G}}{\partial y_f}, \tag{2.10.106}$$

$$\ell = -\frac{\partial \mathcal{G}}{\partial \delta}, \qquad \delta_f = -\frac{\partial \mathcal{G}}{\partial \ell_f}. \tag{2.10.107}$$

The function $p_x x_f + p_y y_f - \delta \ell_f$ gives the identity map. Adding $-\psi y_f^2/2$ generates the desired vertical kick, together with the position and longitudinal changes required by

[1] In the notation used here, the original PTC expression in Eq. (37) of Forest's fringe note, Ref. [18], is

$$\psi_{\mathrm{PTC}} = K_0 \tan[\arctan u - gK_0FAp_s], \qquad A = 1 + x_p^2(2+y_p^2).$$

Expanding the outer tangent gives $\psi_{\mathrm{PTC}} = K_0 u - gK_0^2FAp_s(1+u^2) + O(K_0^3)$, whereas Eq. (34) of that note requires $K_0 u - gK_0^2FA/p_s$ through second order. Thus Eqs. (34) and (37) do not agree to that order in general, contrary to the statement following Eq. (37). They agree for $\delta = 0$ and $p_y = 0$, where $p_s^2(1+u^2) = 1$. On the mid-plane at fixed incidence angle, the original PTC second-order correction scales as $p = 1+\delta$, instead of the required $1/p$. The factor $1/[p_s(1+u^2)]$ in Eq. (2.10.103) restores agreement with Eq. (34).

the momentum dependence of ψ. We first construct this map alone; the additional cubic kick present in the implementation is described separately in Section 2.10.8. We construct a symplectic thin-fringe map using the focusing coefficient ψ defined in Eq. (2.10.103). To generate the vertical kick $p_{y,f} = p_y - \psi y_f$, we choose the mixed generating function

$$\mathcal{G} = p_x x_f + p_y y_f - \delta \ell_f - \frac{1}{2}\psi(p_x, p_y, \delta) y_f^2. \tag{2.10.108}$$

The first three terms, $p_x x_f + p_y y_f - \delta \ell_f$, generate the identity map: without the last term, all positions and momenta remain unchanged. The last term introduces the fringe kick and its associated coordinate changes. Differentiating the generating function with respect to p_y and y_f gives

$$y = \frac{\partial \mathcal{G}}{\partial p_y} = y_f - \frac{1}{2}\psi_{p_y} y_f^2, \tag{2.10.109}$$

$$p_{y,f} = \frac{\partial \mathcal{G}}{\partial y_f} = p_y - \psi y_f. \tag{2.10.110}$$

Solving the quadratic equation for y_f using the root continuous at $y = 0$ gives the forward map:

$$\begin{aligned} p_s &= \sqrt{(1+\delta)^2 - p_x^2 - p_y^2} \\ x_f &= x + \frac{1}{2}\frac{\partial \psi}{\partial p_x} y_f^2 \\ p_{x,f} &= p_x \\ y_f &= \frac{2y}{1 + \sqrt{1 - 2\frac{\partial \psi}{\partial p_y} y}} \\ p_{y,f} &= p_y - \psi y_f \\ \ell_f &= \ell - \frac{1}{2}\frac{\partial \psi}{\partial \delta} y_f^2 \\ \delta_f &= \delta \end{aligned} \tag{2.10.111}$$

All derivatives are evaluated at the incoming momenta. The map is symplectic where this branch of the generating function is real and invertible; that property alone does not make the finite-width approximation exact.

2.10.8 Additional cubic kick in the implementation

Xtrack also applies a cubic vertical kick. The same term appears in the PTC dipole-fringe implementation. This term is separate from the focusing coefficient ψ derived above. Its coefficient, in the present notation, is

$$c_3 = \frac{K_0^2}{36 F g (1+\delta)}. \tag{2.10.112}$$

The same cubic coefficient is documented for the SAD soft-edge model in the Bmad Reference Manual [21].

We now derive it independently at normal incidence for a specified smooth field profile.

Take incoming mechanical momenta $p_x(s_-) = p_y(s_-) = 0$ and vertical displacement $y(s_-)$. Retain second order in field strength and third order in $y(s_-)$. Starting from $p_x(s_-) = 0$, the horizontal Lorentz equation, Eq. (2.10.9), generates $p_x = O(K_0)$. The vertical Lorentz equation, Eq. (2.10.10) with $B_x = 0$, contains the product $p_x B_s$. Since $B_s = O(K_0)$, the vertical force starts at $O(K_0^2)$. With incoming $p_y = 0$, the vertical momentum is therefore $O(K_0^2)$, and Eq. (2.10.12), $dy/ds = p_y/p_s$, shows that the vertical displacement change also starts at that order. In the force calculation at that order we can use $y(s) = y(s_-)$ and $p_s = p = 1 + \delta$.

It is essential to retain the off-mid-plane correction to B_y, as well as the cubic term of B_s:

$$\frac{B_y}{(B\rho)_0} = b(s) - \frac{y(s_-)^2}{2} b''(s) + O(y(s_-)^4), \tag{2.10.113}$$

$$\frac{B_s}{(B\rho)_0} = y(s_-) b'(s) - \frac{y(s_-)^3}{6} b'''(s) + O(y(s_-)^5). \tag{2.10.114}$$

Using mechanical momenta explicitly, the horizontal Lorentz equation at first order in field strength gives

$$\frac{dp_x^{\text{mech}}}{ds} = -b(s) + \frac{y(s_-)^2}{2} b''(s) + O(y(s_-)^4), \tag{2.10.115}$$

$$p_x^{\text{mech}}(s) = -\mathcal{I}(s) + \frac{y(s_-)^2}{2} b'(s) + O(y(s_-)^4), \qquad \mathcal{I}(s) = \int_{s_-}^{s} b(\sigma)\, d\sigma. \tag{2.10.116}$$

Here $b'(s_-) = 0$; the omitted field-strength orders are not needed below. Substituting this momentum into $dp_y^{\text{mech}}/ds = -(p_x^{\text{mech}}/p_s) B_s/(B\rho)_0$ gives, to second order in field strength,

$$\frac{dp_y^{\text{mech}}}{ds} = \frac{\mathcal{I}(s) b'(s)}{p} y(s_-) - \frac{y(s_-)^3}{p} \left[\frac{\mathcal{I}(s) b'''(s)}{6} + \frac{[b'(s)]^2}{2} \right] + O(y(s_-)^5). \tag{2.10.117}$$

Define the additional field-profile integral

$$J = \int_{s_-}^{s_+} [b'(s)]^2\, ds. \tag{2.10.118}$$

With b' and b'' vanishing at the endpoints, integration by parts twice gives

$$\int_{s_-}^{s_+} \mathcal{I}(s) b'''(s)\, ds = [\mathcal{I} b'']_{s_-}^{s_+} - \int_{s_-}^{s_+} b(s) b''(s)\, ds \tag{2.10.119}$$

$$= -[b b']_{s_-}^{s_+} + \int_{s_-}^{s_+} [b'(s)]^2\, ds = J. \tag{2.10.120}$$

Using also $\int \mathcal{I} b'\, ds = I$, we obtain the kick at the retained orders:

$$\Delta p_y = \frac{I}{p} y(s_-) - \frac{2J}{3p} y(s_-)^3. \tag{2.10.121}$$

The first term is the normal-incidence finite-width focusing term already derived. To represent the cubic term in the thin map, we add the quartic term $-c_3 y_f^4$ to the generating function. Its derivative with respect to the outgoing position y_f gives the additional momentum kick

$$\Delta p_y^{\text{cubic}} = \frac{\partial(-c_3 y_f^4)}{\partial y_f} = -4c_3 y_f^3. \tag{2.10.122}$$

At the order retained here, y_f can be replaced by the incoming displacement $y(s_-)$: their difference is second order in field strength, while c_3 is already second order. Matching this kick to the cubic term in Eq. (2.10.121) therefore gives

$$c_3 = \frac{J}{6p}. \tag{2.10.123}$$

The uniform-body map factored out of the fringe does not change p_y, so the derived momentum kick also applies to the equivalent thin map.
For a hyperbolic-tangent field profile with length scale $d > 0$,

$$b(s) = \frac{K_0}{2}\left[1 + \tanh(s/d)\right], \qquad b'(s) = \frac{K_0}{2d}\operatorname{sech}^2(s/d). \tag{2.10.124}$$

Integrating over the full transition, with $r = s/d$, gives

$$gF = \frac{d}{4}\int_{-\infty}^{\infty} \operatorname{sech}^2 r\, dr = \frac{d}{2}, \tag{2.10.125}$$

$$J = \frac{K_0^2}{4d}\int_{-\infty}^{\infty} \operatorname{sech}^4 r\, dr = \frac{K_0^2}{3d}. \tag{2.10.126}$$

For the second integral, $t = \tanh r$ gives $\int_{-1}^{1}(1 - t^2)\, dt = 4/3$. Equation (2.10.123) therefore becomes

$$c_3 = \frac{K_0^2}{18dp} = \frac{K_0^2}{36gF(1+\delta)}. \tag{2.10.127}$$

For a general profile, $J = \int [b']^2 ds$ is not determined by $gF = \int b(K_0 - b) ds / K_0^2$. The implemented expression effectively sets $J = K_0^2/(6gF)$, as for the hyperbolic-tangent profile. It should therefore not be interpreted as a universal coefficient for arbitrary fringe shapes. Nor does the normal-incidence calculation establish the complete cubic map at finite incidence angle or nonzero incoming vertical slope. Ref. [18], Eqs. (21)–(22), likewise identifies additional nonlinear profile integrals but leaves their further study aside. For the hyperbolic-tangent profile, the cubic coefficient grows as $1/d$ when the transition narrows. The displacement expansion requires $|y(s_-)| \ll d$, so its validity is not uniform in the limit $d \to 0$ at fixed nonzero $y(s_-)$. This nonlinear limit must be distinguished from the linearized hard-edge calculation above.
To include the implemented cubic kick in a symplectic map, augment Eq. (2.10.108) by a quartic term:

$$\mathcal{G}_{\text{extended}} = \mathcal{G} - c_3 y_f^4. \tag{2.10.128}$$

Differentiating with respect to y_f produces the extra kick $-4c_3y_f^3$. Since c_3 depends on δ, its derivative also produces a longitudinal-coordinate change. The two modified lines of Eq. (2.10.111) are

$$p_{y,f} = p_y - \psi y_f - 4c_3 y_f^3, \tag{2.10.129}$$

$$\ell_f = \ell - \frac{1}{2}\psi_\delta y_f^2 + \frac{c_3}{1+\delta} y_f^4. \tag{2.10.130}$$

Here $\partial c_3/\partial\delta = -c_3/(1+\delta)$; the quartic longitudinal term must accompany the cubic vertical kick. All other lines of the map, including the expression determining y_f, are unchanged because c_3 does not depend on p_x or p_y. In the tracking coordinate ζ, the extended longitudinal update is

$$\zeta_f = \zeta + \frac{\beta_0}{2}\psi_{p_\tau} y_f^2 - \beta_0 c_3 \frac{T}{p^2} y_f^4. \tag{2.10.131}$$

This extension does not change the linear vertical focusing about $y = 0$.

2.10.9 Complete generating function and forward map

Combining the focusing coefficient ψ from Eq. (2.10.103) with the cubic coefficient c_3 from Eq. (2.10.112), the complete generating function is

$$\mathcal{G}_{\text{extended}} = p_x x_f + p_y y_f - \delta\ell_f - \frac{1}{2}\psi(p_x, p_y, \delta) y_f^2 - c_3(\delta) y_f^4. \tag{2.10.132}$$

Its forward map is

$$\begin{aligned} y_f &= \frac{2y}{1 + \sqrt{1 - 2\psi_{p_y} y}}, \\ x_f &= x + \frac{1}{2}\psi_{p_x} y_f^2, \\ p_{x,f} &= p_x, \\ p_{y,f} &= p_y - \psi y_f - 4c_3 y_f^3, \\ \ell_f &= \ell - \frac{1}{2}\psi_\delta y_f^2 + \frac{c_3}{1+\delta} y_f^4, \\ \delta_f &= \delta. \end{aligned} \tag{2.10.133}$$

All coefficients and momentum derivatives are evaluated at the incoming momenta. Equivalently, in the longitudinal tracking coordinates,

$$\zeta_f = \zeta + \frac{\beta_0}{2}\psi_{p_\tau} y_f^2 - \beta_0 c_3 \frac{T}{p^2} y_f^4, \qquad p_{\tau,f} = p_\tau, \tag{2.10.134}$$

where $p = 1 + \delta$ and $T = 1/\beta_0 + p_\tau$. The next section details the derivatives of ψ; the additional coefficient satisfies $\partial c_3/\partial\delta = -c_3/p$ and has no dependence on p_x or p_y.

2.10.10 Derivatives used in tracking

The forward map in Eq. (2.10.111) needs three derivatives of ψ: $\partial\psi/\partial p_x$ determines the horizontal position change, $\partial\psi/\partial p_y$ enters the equation for y_f, and $\partial\psi/\partial\delta$ determines the longitudinal change. All are evaluated at the incoming momenta, holding the other incoming momenta and the magnet parameters K_0, g, F fixed.
The complication is that Eq. (2.10.103) is expressed through slopes and longitudinal momentum, rather than directly through (p_x, p_y, δ). Their dependence is

$$p = 1 + \delta, \qquad p_s = \sqrt{p^2 - p_x^2 - p_y^2}, \qquad x_p = \frac{p_x}{p_s}, \qquad y_p = \frac{p_y}{p_s}. \tag{2.10.135}$$

Changing p_x, for example, changes not only x_p but also p_s and y_p. We must include all three changes. We do this in two stages: first differentiate the focusing expression with respect to its three intermediate arguments, then apply the chain rule to the incoming momenta.

1. Write the focusing coefficient as a composite function. For the intermediate differentiation, write

$$\psi(p_x, p_y, \delta) = \Psi\big(x_p(p_x, p_y, \delta), y_p(p_x, p_y, \delta), p_s(p_x, p_y, \delta)\big). \tag{2.10.136}$$

The capital Ψ denotes the same focusing expression, with its three arguments temporarily treated as independent. It is not an additional physical coefficient. To organize its evaluation, define

$$u = \frac{x_p}{1 + y_p^2}, \tag{2.10.137}$$

$$A = 1 + x_p^2(2 + y_p^2), \tag{2.10.138}$$

$$R = \frac{A}{1 + u^2}, \tag{2.10.139}$$

$$\phi = \arctan u - \frac{gK_0F}{p_s}R, \tag{2.10.140}$$

$$\Psi = K_0 \tan\phi. \tag{2.10.141}$$

Here u is the slope combination already introduced, A is the numerator of the finite-gap correction, and R includes its compensating denominator $1 + u^2$. The angle ϕ is the argument of the outer tangent. These quantities are only intermediate steps in evaluating Eq. (2.10.103).

2. Differentiate with respect to the intermediate arguments. In this paragraph a subscript denotes a partial derivative with respect to that argument, holding the other two intermediate arguments fixed. For example, $u_{x_p} = \partial u/\partial x_p$ at fixed y_p and p_s. Direct differentiation gives

$$u_{x_p} = \frac{1}{1 + y_p^2}, \tag{2.10.142}$$

$$u_{y_p} = -\frac{2x_p y_p}{(1+y_p^2)^2}, \tag{2.10.143}$$

$$A_{x_p} = 2x_p(2+y_p^2), \tag{2.10.144}$$

$$A_{y_p} = 2x_p^2 y_p. \tag{2.10.145}$$

For either slope argument $a \in \{x_p, y_p\}$, the quotient rule gives

$$R_a = \frac{A_a(1+u^2) - A\,2uu_a}{(1+u^2)^2} = \frac{A_a - 2uRu_a}{1+u^2}. \tag{2.10.146}$$

Differentiating the arctangent and then the outer tangent gives

$$\phi_a = \frac{u_a}{1+u^2} - \frac{gK_0F}{p_s}R_a, \tag{2.10.147}$$

$$\Psi_a = K_0 \sec^2\phi\,\phi_a = K_0 \sec^2\phi\left(\frac{u_a}{1+u^2} - \frac{gK_0F}{p_s}R_a\right). \tag{2.10.148}$$

For the remaining argument p_s, the slopes are held fixed, so u and R are constant. Only the explicit factor $1/p_s$ changes:

$$\Psi_{p_s} = K_0 \sec^2\phi\,\frac{gK_0FR}{p_s^2}. \tag{2.10.149}$$

These three derivatives describe changes in the intermediate arguments. We next convert them to derivatives with respect to the incoming momenta.

3. Differentiate the slopes and longitudinal momentum. From Eq. (2.10.135), differentiation of the square root gives

$$\frac{\partial p_s}{\partial p_x} = -\frac{p_x}{p_s} = -x_p, \qquad \frac{\partial p_s}{\partial p_y} = -y_p, \qquad \frac{\partial p_s}{\partial \delta} = \frac{p}{p_s}. \tag{2.10.150}$$

The slope derivatives must include these denominator changes. For example,

$$\frac{\partial x_p}{\partial p_x} = \frac{1}{p_s} - \frac{p_x}{p_s^2}\frac{\partial p_s}{\partial p_x} = \frac{1+x_p^2}{p_s}, \tag{2.10.151}$$

$$\frac{\partial y_p}{\partial p_x} = -\frac{p_y}{p_s^2}\frac{\partial p_s}{\partial p_x} = \frac{x_p y_p}{p_s}. \tag{2.10.152}$$

All the required derivatives are collected below. Each column varies the indicated incoming momentum while holding the other two fixed.

	$\partial/\partial p_x$	$\partial/\partial p_y$	$\partial/\partial\delta$
x_p	$(1+x_p^2)/p_s$	$x_p y_p/p_s$	$-px_p/p_s^2$
y_p	$x_p y_p/p_s$	$(1+y_p^2)/p_s$	$-py_p/p_s^2$
p_s	$-x_p$	$-y_p$	p/p_s

(2.10.153)

4. Apply the chain rule to obtain the tracking derivatives. For any incoming momentum $m \in \{p_x, p_y, \delta\}$, the chain rule is

$$\frac{\partial \psi}{\partial m} = \Psi_{x_p} \frac{\partial x_p}{\partial m} + \Psi_{y_p} \frac{\partial y_p}{\partial m} + \Psi_{p_s} \frac{\partial p_s}{\partial m}. \tag{2.10.154}$$

Substituting the corresponding column of Eq. (2.10.153) gives

$$\psi_{p_x} = \Psi_{x_p} \frac{1 + x_p^2}{p_s} + \Psi_{y_p} \frac{x_p y_p}{p_s} - \Psi_{p_s} x_p, \tag{2.10.155}$$

$$\psi_{p_y} = \Psi_{x_p} \frac{x_p y_p}{p_s} + \Psi_{y_p} \frac{1 + y_p^2}{p_s} - \Psi_{p_s} y_p, \tag{2.10.156}$$

$$\psi_{\delta} = -\Psi_{x_p} \frac{p x_p}{p_s^2} - \Psi_{y_p} \frac{p y_p}{p_s^2} + \Psi_{p_s} \frac{p}{p_s}. \tag{2.10.157}$$

These are the derivatives to insert in Eq. (2.10.111). Every term follows from the same coefficient ψ; the map's coordinate changes must use its full momentum dependence.

5. Convert to the longitudinal tracking coordinates. The map above uses $(\ell, -\delta)$, while the tracking implementation uses the energy coordinate p_τ and the position coordinate ζ. The normalized energy–momentum relation gives

$$p^2 = (1 + \delta)^2 = 1 + \frac{2 p_\tau}{\beta_0} + p_\tau^2. \tag{2.10.158}$$

Differentiating this equation and defining $T = 1/\beta_0 + p_\tau$ gives

$$\frac{\partial \delta}{\partial p_\tau} = \frac{T}{p}, \qquad \psi_{p_\tau} = \frac{T}{p} \psi_\delta. \tag{2.10.159}$$

For the coordinate conversion, $\zeta = s - \beta_0 c t$ and $\ell = \beta c t$ imply $\Delta\zeta = -(\beta_0/\beta)\Delta\ell$ at fixed s and energy. Using $\beta = p/T$ and the longitudinal line of Eq. (2.10.111),

$$\Delta\zeta = \frac{\beta_0 T}{2p} \psi_\delta y_f^2 = \frac{\beta_0}{2} \psi_{p_\tau} y_f^2. \tag{2.10.160}$$

Thus the longitudinal update for this focusing model is

$$\zeta_f = \zeta + \frac{\beta_0}{2} \psi_{p_\tau} y_f^2. \tag{2.10.161}$$

2.10.11 Exit face

The map above was derived for an entrance face, where the field rises from zero to K_0. At the exit face the field falls from K_0 to zero. For the linear hard-edge kick, the Lorentz-force integration therefore uses $\int b' \, ds = -K_0$, giving

$$\Delta p_y = +K_0 x_p(s_-) y(s_-). \tag{2.10.162}$$

The incoming slope here is measured in the frame whose s axis is normal to the exit face. Thus a positive body field and a negative incoming horizontal slope give a focusing exit kick. Entrance and exit slopes must be evaluated in their respective pole-face frames.
For tracking, the implementation uses the complete generating-function map of Eq. (2.10.133) with K_0 replaced by $-K_0$. The gap g and fringe integral F retain their specified values. In particular, the cubic coefficient is unchanged because it depends on K_0^2. This prescription defines a symplectic nonlinear extension of the linear exit kick. The hard-edge sign argument alone does not establish that it is the exact nonlinear map of a finite-width exit field.
It is also important to distinguish this prescription from reversing an entrance map. Let R change the signs of x, p_y and ℓ, leaving y, p_x and δ unchanged. Although ψ and c_3 are even in p_y, the mixed generating-function map generally does not satisfy

$$R\, M_{\mathrm{ent}}(-K_0)^{-1} R = M_{\mathrm{ent}}(-K_0). \tag{2.10.163}$$

Inversion interchanges incoming and outgoing variables, whereas the forward map evaluates its coefficients at incoming momenta and its kick at the outgoing vertical position. The resulting differences can already be second order in K_0 for nonzero vertical slope, even when the finite-gap correction and cubic term are disabled. Thus the linear hard-edge agreement must not be interpreted as exact reversibility of the complete nonlinear extension under R. Backtracking instead uses the actual inverse of the chosen map, as described below.
In the implementation, the entrance face is treated by rotating the coordinates into the pole-face frame (Section 2.20.2), applying the dipole fringe map, and then applying the dipole wedge (Section 2.11), which moves the observation plane from the pole face to the plane normal to the reference trajectory inside the body. For the full edge model, the multipole fringe and the quadrupolar wedge correction are applied between the dipole fringe and the wedge. The exit face applies the same maps in the reverse order, with the exit face angle and with $-K_0$ in the dipole fringe map. Backtracking inverts each map in turn; the sign of K_0 seen by a given face does not depend on the direction of travel.

2.10.12 Backtracking

We invert the complete forward map in Eq. (2.10.133), including the cubic kick. As in the forward map, unadorned symbols denote incoming coordinates and the subscript f denotes outgoing coordinates. The outgoing coordinates are now known, and we recover the incoming ones. The conserved momenta give

$$p_x = p_{x,f}, \qquad \delta = \delta_f. \tag{2.10.164}$$

The remaining incoming momentum satisfies

$$p_y = p_{y,f} + \psi(p_{x,f}, p_y, \delta_f) y_f + 4c_3(\delta_f) y_f^3. \tag{2.10.165}$$

This equation is implicit because the corrected coefficient ψ in Eq. (2.10.103) depends on the unknown p_y. The coefficient c_3 is already known from δ_f.

The tracking implementation solves Eq. (2.10.165) by fixed-point iteration:

$$p_y^{(n+1)} = p_{y,f} + \psi(p_{x,f}, p_y^{(n)}, \delta_f) y_f + 4c_3(\delta_f) y_f^3, \qquad p_y^{(0)} = p_{y,f}. \tag{2.10.166}$$

At each iteration, ψ is evaluated at the current estimate of the incoming momentum. A sufficient condition for local convergence is

$$\left| y_f \frac{\partial \psi}{\partial p_y}(p_{x,f}, p_y, \delta_f) \right| < 1 \tag{2.10.167}$$

at the solution, with the initial estimate sufficiently close to it. A small momentum kick alone does not guarantee this condition.

Once p_y is recovered, evaluate ψ and its derivatives at the recovered incoming momenta. The remaining inverse updates are explicit:

$$x = x_f - \frac{1}{2}\psi_{p_x} y_f^2, \tag{2.10.168}$$

$$y = y_f - \frac{1}{2}\psi_{p_y} y_f^2, \tag{2.10.169}$$

$$\ell = \ell_f + \frac{1}{2}\psi_\delta y_f^2 - \frac{c_3}{1+\delta_f} y_f^4. \tag{2.10.170}$$

Equivalently, in the longitudinal tracking coordinates,

$$\zeta = \zeta_f - \frac{\beta_0}{2}\psi_{p_\tau} y_f^2 + \beta_0 c_3 \frac{T}{p^2} y_f^4, \qquad p_\tau = p_{\tau,f}, \tag{2.10.171}$$

where $p = 1 + \delta_f$ and $T = 1/\beta_0 + p_{\tau,f}$. Setting $c_3 = 0$ gives the inverse of the focusing-only map. These inverse relations apply on the real, invertible branch selected in the forward map.

The code makes at most 10 iterations, stopping when the change in p_y is at most $10^{-13}|p_y| + 10^{-20}$. Failure to converge marks the particle as lost.

2.11 Dipole wedge

The following map is used to move the observation plane by an angle θ around the y axis in a uniform dipole field [11]:

$$x(\theta) = x\cos\theta + \frac{x p_x \sin(2\theta) + \sin^2\theta \left(2x\sqrt{(1+\delta)^2 - p_x^2 - p_y^2} - K_0 x^2\right)}{\sqrt{(1+\delta)^2 - p_x(\theta)^2 - p_y^2} + \sqrt{(1+\delta)^2 - p_x^2 - p_y^2}\cos\theta - p_x \sin\theta} \tag{2.11.1}$$

$$p_x(\theta) = p_x\cos\theta + \left(\sqrt{(1+\delta)^2 - p_x^2 - p_y^2} - K_0 x\right)\sin\theta \tag{2.11.2}$$

$$y(\theta) = y + \frac{p_y}{K_0}\theta + \frac{p_y}{K_0}\left(\sin^{-1}\left(\frac{p_x}{\sqrt{(1+\delta)^2 - p_y^2}}\right) - \sin^{-1}\left(\frac{p_x(\theta)}{\sqrt{(1+\delta)^2 - p_y^2}}\right)\right) \tag{2.11.3}$$

$$p_y(\theta) = p_y \tag{2.11.4}$$

$$\delta(\theta) = \delta \tag{2.11.5}$$

$$\ell(\theta) = \ell + \frac{(1+\delta)}{K_0}\theta + \frac{(1+\delta)}{K_0}\left(\sin^{-1}\left(\frac{p_x}{\sqrt{(1+\delta)^2 - p_y^2}}\right) - \sin^{-1}\left(\frac{p_x(\theta)}{\sqrt{(1+\delta)^2 - p_y^2}}\right)\right) \tag{2.11.6}$$

where K_0 is the normalized magnetic field.

2.12 Multipole fringe field

The fringe field effect for multipole magnets is implemented as described in [11]. We introduce the following auxiliary quantities:

$$\begin{aligned} f_\pm &\approx \mp\Re\frac{c_n(x+iy)^n}{4(n+1)(1+\delta)}\left\{xp_x + yp_y + i\frac{n+2}{n}(xp_y - yp_x)\right\} \\ &= \frac{p_x f^x + p_y f^y}{1+\delta}. \end{aligned} \tag{2.12.1}$$

where $c_n = K_n + i\hat{K}_n$ is the complex multipole strength (see Sec. 1.5).
The functions f^x and f^y depend on position only. The characteristic function is chosen so as to depend on the final momenta:

$$S(\mathbf{x}, \mathbf{p}^f) = \mathbf{x}\cdot\mathbf{p}^f - \frac{p_x^f f^x + p_y^f f^y}{1+\delta}. \tag{2.12.2}$$

The following implicit solution is found:

$$x^f = x - \frac{f^x}{1+\delta} \tag{2.12.3a}$$

$$p_x = p_x^f - \frac{p_x^f(\partial_x f^x) + p_y^f(\partial_x f^y)}{1+\delta} \tag{2.12.3b}$$

$$y^f = y - \frac{f^y}{1+\delta} \tag{2.12.3c}$$

$$p_y = p_y^f - \frac{p_x^f(\partial_y f^x) + p_y^f(\partial_y f^y)}{1+\delta} \tag{2.12.3d}$$

$$\delta^f = \delta \tag{2.12.3e}$$

$$\ell = \ell^f + \frac{p_x^f f^x + p_y^f f^y}{(1+\delta)^2}. \tag{2.12.3f}$$

It is solved by inverting Eqs. (2.12.3b) and (2.12.3d) simultaneously to obtain the final transverse momenta.

2.12.1 Backtracking

As for the dipole fringe field (Sec. 2.10), the map relates the entrance and exit coordinates implicitly, here in x and y rather than in p_y, and so cannot be inverted analytically. As before, we describe the coordinates before entering the fringe map as $(x_0, p_{x,0}, y_0, p_{y,0})$ and the coordinates after the fringe map as $(x_1, p_{x,1}, y_1, p_{y,1})$.
The functions f^x, f^y and their derivatives are evaluated at the entrance position (x_0, y_0), which needs to be recovered when backtracking. Since Eqs. (2.12.3a) and (2.12.3c) couple the two planes through $f^x(x_0, y_0)$ and $f^y(x_0, y_0)$, they cannot be inverted one at a time as in the dipole fringe case, and we must instead solve the coupled system

$$\mathbf{F}(x_0, y_0) = \begin{pmatrix} x_0 - \dfrac{f^x(x_0, y_0)}{1+\delta} - x_1 \\ y_0 - \dfrac{f^y(x_0, y_0)}{1+\delta} - y_1 \end{pmatrix} = 0 \tag{2.12.4}$$

for (x_0, y_0), with (x_1, y_1) known. Its Jacobian is

$$J = \frac{\partial \mathbf{F}}{\partial(x_0, y_0)} = \begin{pmatrix} 1 - \dfrac{\partial_x f^x}{1+\delta} & -\dfrac{\partial_y f^x}{1+\delta} \\ -\dfrac{\partial_x f^y}{1+\delta} & 1 - \dfrac{\partial_y f^y}{1+\delta} \end{pmatrix}, \tag{2.12.5}$$

which is the Jacobian of the forward position map, so that Eq. (2.12.4) is solved by the Newton iteration

$$\begin{pmatrix} x_0 \\ y_0 \end{pmatrix}^{(n+1)} = \begin{pmatrix} x_0 \\ y_0 \end{pmatrix}^{(n)} - J^{-1}\mathbf{F}\Big|^{(n)}, \qquad (x_0, y_0)^{(0)} = (x_1, y_1), \tag{2.12.6}$$

where f^x, f^y and J are re-evaluated at $(x_0, y_0)^{(n)}$ at every step.
Once (x_0, y_0) has converged, the entrance momenta follow from Eqs. (2.12.3b) and (2.12.3d), which in matrix form read

$$\begin{pmatrix} p_{x,0} \\ p_{y,0} \end{pmatrix} = J^\top \begin{pmatrix} p_{x,1} \\ p_{y,1} \end{pmatrix}, \tag{2.12.7}$$

with J evaluated at the recovered entrance position.
The iteration is capped at 10 steps and is taken as converged when the change in both x_0 and y_0 between successive steps falls below a relative tolerance of 10^{-13}. If the iteration does not converge, an error is raised.

2.13 Quadrupolar correction for wedge and Y rotation

If a dipole wedge or rotation around the y axis in a field-free region takes place in the presence of a quadrupole field, the following correction is applied to the transverse momenta:

$$p_x^f = p_x - K_1 x^2 \theta + K_1 \frac{y^2}{2}\theta \tag{2.13.1}$$

$$p_y^f = p_y + K_1 xy\theta \tag{2.13.2}$$

This correction is a perturbation of the wedge or Y rotation, and can in theory be applied using any integration scheme. It is currently implemented as a kick-drift approximation.

Derivation

(derived by S. Van der Schueren based on the MAD-X/PTC [1] source code)
In a curved reference frame (dropping terms of order $\mathcal{O}(y^4)$):

$$H_\tau = \frac{p_\tau}{\beta_0} - (1+hx)\left(\sqrt{(1+\delta)^2 - p_x^2 - p_y^2} - \frac{x+\frac{h}{2}x^2}{1+hx}K_0 + K_1\frac{y^2}{2} - \frac{K_1 h x^3}{3} + \frac{K_1 x^2}{2(hx+1)}\right) \tag{2.13.3}$$

which we can split in perturbation theory into a drift-like part H_0 and a kick-like part H_1:

$$H_0 = \frac{p_\tau}{\beta_0} - (1+hx)\sqrt{(1+\delta)^2 - p_x^2 - p_y^2} + \left(x + \frac{h}{2}x^2\right)K_0 \tag{2.13.4}$$

$$H_1 = -(1+hx)K_1\frac{y^2}{2} + \left(K_1 h\frac{x^3}{3} + K_1\frac{x^2}{2}\right) \tag{2.13.5}$$

The Hamiltonian H_0 leads to the dipole wedge of Sec. 2.11 (or to a dynamical rotation, Sec. 2.20.2, if $b_0 = 0$) when taking the limit $1/h \to 0$, $s \to 0$, $sh \to \theta$. The Hamiltonian H_1 has equations of motion:

$$p_x' = -\frac{\partial H_1}{\partial x} = hK_1\frac{y^2}{2} - hK_1 x^2 - K_1 x \tag{2.13.6}$$

$$p_y' = -\frac{\partial H_1}{\partial y} = (1+hx)K_1 y \tag{2.13.7}$$

which gives integrated equations:

$$p_x(s) = p_x + hK_1\frac{y^2}{2}s - hK_1 x^2 s - K_1 xs \tag{2.13.8}$$

$$p_y(s) = p_y + (1+hx)K_1 ys \tag{2.13.9}$$

Taking the limit $1/h \to 0$, $s \to 0$, $sh \to \theta$ as for the dipole wedge we find the expressions for the quadrupole wedge.

2.14 Accelerating Cavity

Implemented in the Cavity element.

The approximated energy gain of a particle passing through an electric field of frequency $f = \frac{kc}{2\pi}$ for which:

$$V\sin(\phi - k\tau) = \int_{-l/2}^{l/2} E_s(0,0,t,s)\,\mathrm{d}s. \tag{2.14.1}$$

An equivalent vector potential can be derived and normalized as

$$A_s = -\frac{V}{\omega}\cos(\phi - k\tau) \qquad V_n = \frac{q_0}{P_0 c}V \tag{2.14.2}$$

from which one can derive the following map

$$p_\tau \leftarrow p_\tau + \chi V_n \sin(\phi - k\tau). \tag{2.14.3}$$

2.15 RF-Multipole

Implemented in the RFMultipole and Crab Cavity elements.

The RF-multipole generalizes the interaction of a particle with an electromagnetic field by assuming that

$$\Delta E(x,y,\tau) = q\int_{-L/2}^{L/2} E_z(x,y,t)\,\mathrm{d}s \tag{2.15.1}$$

$$\Delta P_x(x,y,\tau) = q\int_{-L/2}^{L/2} E_x(x,y,t) + \beta c B_y(x,y,t)\,\mathrm{d}s \tag{2.15.2}$$

$$\Delta P_y(x,y,\tau) = q\int_{-L/2}^{L/2} E_y(x,y,t) - \beta c B_x(x,y,t)\,\mathrm{d}s. \tag{2.15.3}$$

are harmonic in x, y and periodic in τ of frequency $f = \frac{k}{2\pi c}$ such that:

$$a_s(x,y,\tau) = \Re\left[\sum_{n=1}^{N}\left(k_n\cos(\phi_n - k\tau) + i\hat{k}_n\cos(\hat{\phi}_n - k\tau)\right)(x+iy)^n\right], \tag{2.15.4}$$

The map then follows:

$$\Delta p_x = -\sum_{n=1}^{N}\frac{\chi}{n!}\Re\left[(k_n C_n + i\hat{k}_n\hat{C}_n)(x+iy)^{(n-1)}\right], \tag{2.15.5}$$

$$\Delta p_y = \sum_{n=1}^{N}\frac{\chi}{n!}\Im\left[(k_n C_n + i\hat{k}_n\hat{C}_n)(x+iy)^{(n-1)}\right], \tag{2.15.6}$$

$$\Delta p_\tau = -\chi k\sum_{n=1}^{N}\Re\left[(k_n S_n + ik_n\hat{S}_n)(x+iy)^n\right], \tag{2.15.7}$$

where

$$C_n = \cos(\phi_n - \omega\Delta t) \qquad \hat{C}_n = \cos(\hat{\phi}_n - \omega\Delta t) \tag{2.15.8}$$

$$S_n = \sin(\phi_n - \omega\Delta t) \qquad \hat{S}_n = \sin(\hat{\phi}_n - \omega\Delta t). \tag{2.15.9}$$

2.16 Solenoid

Implemented in the UniformSolenoid and VariableSolenoid elements.

The derivation largely follows one by Forest [11], while the final map can be verified to be the same as the one by Wolski [12].
We can write the Hamiltonian for the solenoid as follows:

$$H = p_\zeta - \sqrt{(1+\delta)^2 - \left(p_x + \frac{b_z}{2}y\right)^2 - \left(p_y - \frac{b_z}{2}x\right)^2} \tag{2.16.1}$$

where we have defined the normalized quantities $b_z = B_z\frac{q_0}{P_0}$, $a_x = A_x\frac{q_0}{P_0}$, $a_y = A_y\frac{q_0}{P_0}$. This can be obtained knowing the general Hamiltonian

$$H = p_\zeta - \sqrt{(1+\delta)^2 - (p_x - a_x)^2 - (p_y - a_y)^2} - a_z, \tag{2.16.2}$$

from which we can extract the magnetic field potential and convince ourselves that H describes a magnetic field with only the longitudinal component equal to B_z, as expected of a solenoid:

$$\mathbf{A} = \begin{bmatrix} A_x \\ A_y \\ A_z \end{bmatrix} = \begin{bmatrix} -\frac{B_z}{2}y \\ \frac{B_z}{2}x \\ 0 \end{bmatrix} \implies \mathbf{B} = \nabla \times \mathbf{A} = \begin{bmatrix} \frac{\partial A_z}{\partial y} - \frac{\partial A_y}{\partial z} \\ \frac{\partial A_x}{\partial z} - \frac{\partial A_z}{\partial x} \\ \frac{\partial A_y}{\partial x} - \frac{\partial A_x}{\partial y} \end{bmatrix} = \begin{bmatrix} 0 \\ 0 \\ B_z \end{bmatrix}. \tag{2.16.3}$$

The Hamiltonian H can be simplified, by applying the following transformation, which should be understood as the change of reference from the general coordinate system $\mathbf{X}$ to a new $\mathbf{X}_{\text{new}}$:

$$T := \begin{bmatrix} -\frac{1}{2} & 0 & 0 & \frac{1}{b_z} \\ 0 & 1 & \frac{1}{2}b_z & 0 \\ -\frac{1}{2} & 0 & 0 & -\frac{1}{b_z} \\ 0 & 1 & -\frac{1}{2}b_z & 0 \end{bmatrix}.$$

In particular, note that if

$$\mathbf{X} = \begin{bmatrix} x \\ p_x \\ y \\ p_y \end{bmatrix} = T^{-1}\mathbf{X}_{\text{new}} = \begin{bmatrix} -x_{\text{new}} - y_{\text{new}} \\ \frac{1}{2}(p_{x,\text{new}} + p_{y,\text{new}}) \\ \frac{1}{b_z}(p_{x,\text{new}} - p_{y,\text{new}}) \\ \frac{b_z}{2}(x_{\text{new}} - y_{\text{new}}) \end{bmatrix},$$

then we can rewrite H in terms of $\mathbf{X}_{\text{new}}$ (dropping the 'new' suffix, while keeping it in mind) as

$$K := -\sqrt{(1+\delta)^2 - p_x^2 - b_z^2 x^2}.$$

We can simplify H even further, rewriting it in terms of the following action-angle variables:

$$x := \sqrt{\frac{2J}{|b_z|}}\cos(\phi) \quad \text{and} \quad p_x := \sqrt{2|b_z|J}\sin(\phi). \tag{2.16.4}$$

The new Hamiltonian with respect to J is the following:

$$\begin{aligned} K = -\sqrt{(1+\delta)^2 - p_x^2 - b_z^2 x^2} = \\ -\sqrt{(1+\delta)^2 - \left(\sqrt{2|b_z|J}\sin(\phi)\right)^2 - b_z^2\sqrt{\frac{2J}{|b_z|}}\cos(\phi)^2} = \\ -\sqrt{(1+\delta)^2 - \left(\sqrt{2|b_z|J}\sin(\phi)\right)^2 - \left(\sqrt{2|b_z|J}\cos(\phi)\right)^2} = \\ -\sqrt{(1+\delta)^2 - 2|b_z|J}. \end{aligned}$$

Then, using Hamilton's equations, we can solve for ϕ:

$$\frac{d\phi}{dz} = \frac{\partial K}{\partial J} \implies \phi(z) = \phi(0) + z\frac{\partial K}{\partial J} = \phi(0) - z\frac{|b_z|}{K}.$$

Let $\omega := -b_z/K$. Keeping in mind that we are still in the realm of $\mathbf{X}_{\text{new}}$, we can compute x_{new} and y_{new} substituting the above into (2.16.4). Note that we can drop the modulus on b_z in both ω and the equations below, as cos is an even function and, while sin is an odd function, the signs of $\sin(\omega z)$ and b_z will cancel out anyway.

$$\begin{aligned} x = \sqrt{\frac{2J}{|b_z|}}\cos\left(\phi(0) + \left(-z\frac{|b_z|}{K}\right)\right) = \\ \sqrt{\frac{2J}{|b_z|}}\cos\phi(0)\cos(\omega z) - \frac{\sqrt{2J|b_z|}}{|b_z|}\sin\phi(0)\sin\left(-z\frac{|b_z|}{K}\right) = \\ x_0\cos(\omega z) - \frac{p_{x,0}}{b_z}\sin(\omega z) \end{aligned}$$

$$\begin{aligned} p_x = \sqrt{2|b_z|J}\sin\left(\phi(0) + \left(-z\frac{|b_z|}{K}\right)\right) = \\ \sqrt{2|b_z|J}\sin\phi(0)\cos(\omega z) + |b_z|\sqrt{\frac{2J}{|b_z|}}\cos\phi(0)\sin\left(-z\frac{|b_z|}{K}\right) = \\ p_{x,0}\cos(\omega z) + b_z x_0\sin(\omega z) \end{aligned}$$

These equations give us the map for the solenoid in $\mathbf{X}_{\text{new}}$. We can write this transformation in the form of a matrix

$$R := \begin{bmatrix} \cos(\omega z) & -\frac{\sin(\omega z)}{b_z} & 0 & 0 \\ b_z\sin(\omega z) & \cos(\omega z) & 0 & 0 \\ 0 & 0 & 1 & 0 \\ 0 & 0 & 0 & 1 \end{bmatrix},$$

and therefore the whole solenoid map in **X** as follows (let $S := \sin(\omega z)$ and $C := \cos(\omega z)$):

$$M := T^{-1}RT = \begin{bmatrix} \frac{C+1}{2} & \frac{S}{b_z} & \frac{S}{2} & \frac{1-C}{b_z} \\ -\frac{b_z S}{4} & \frac{C+1}{2} & \frac{b_z(C-1)}{4} & \frac{S}{2} \\ -\frac{S}{2} & \frac{C-1}{b_z} & \frac{C+1}{2} & \frac{S}{b_z} \\ \frac{b_z(1-C)}{4} & -\frac{S}{2} & -\frac{b_z S}{4} & \frac{C+1}{2} \end{bmatrix}$$

In the tracking procedure of Xtrack (and MAD-X) the map is implemented with respect to a different quantity `sk`, which we will denote with k, and which represents half of the magnetic field strength b_z: $k = \frac{b_z}{2}$. Let $s := \sin(\frac{zk}{H}) = \sin(\frac{\omega z}{2})$ and $c := \cos(\frac{\omega z}{2})$; then we can rewrite M using the trigonometric identities:

$$\cos(2\theta) = 2\cos^2\theta - 1 = 1 - 2\sin^2\theta \implies c^2 = \frac{C+1}{2} \text{ and } s^2 = \frac{1-C}{2},$$
$$\sin(2\theta) = 2\cos\theta\sin\theta \implies sc = \frac{S}{2},$$

as the following transfer matrix

$$M = \begin{bmatrix} c^2 & \frac{cs}{k} & cs & \frac{s^2}{k} \\ -kcs & c^2 & -ks^2 & cs \\ -cs & -\frac{s^2}{k} & c^2 & \frac{cs}{k} \\ ks^2 & -cs & -kcs & c^2 \end{bmatrix},$$

which, with relatively little effort, can be verified to correspond to the implementation of the tracking procedure. We have the following map (note the change in ζ is analogous to the drift):

$$\begin{aligned} x &\leftarrow (x\cos(\theta) + y\sin(\theta))\cos(\theta) + \frac{2}{b_z}\big(p_x\cos(\theta) + p_y\sin(\theta)\big)\sin(\theta) \\ p_x &\leftarrow -\frac{1}{2}(x\cos(\theta) + y\sin(\theta))b_z\sin(\theta) + \big(p_x\cos(\theta) + p_y\sin(\theta)\big)\cos(\theta) \\ y &\leftarrow (y\cos(\theta) - x\sin(\theta))\cos(\theta) + \frac{2}{b_z}\big(p_y\cos(\theta) - p_x\sin(\theta)\big)\sin(\theta) \\ p_y &\leftarrow -\frac{1}{2}(y\cos(\theta) - x\sin(\theta))b_z\sin(\theta) + \big(p_y\cos(\theta) - p_x\sin(\theta)\big)\cos(\theta) \\ \zeta &\leftarrow \zeta + L\left(1 - \frac{\beta_0}{\beta}\frac{1+\delta}{p_z}\right), \end{aligned}$$

where $p_z := \sqrt{(\delta+1)^2 - \left(\frac{b_z}{2}x - p_y\right)^2 - \left(\frac{b_z}{2}y + p_x\right)^2}$, $\theta := \frac{b_z L}{2p_z}$, and L is the length of the thick solenoid.

2.16.1 Tilted solenoid

From the solenoid frame (x′-z′) to the beam frame (x-z) we have the following transformation:

$$x = x' \cos\theta - z' \sin\theta \tag{2.16.5}$$
$$z = x' \sin\theta + z' \cos\theta \tag{2.16.6}$$

The inverse transformation is:

$$x' = x \cos\theta + z \sin\theta \tag{2.16.7}$$
$$z' = -x \sin\theta + z \cos\theta \tag{2.16.8}$$

We write the potential for a solenoid with a longitudinal field dependent on z:

$$A_{x'} = -\frac{B_A(z')}{2} y' \tag{2.16.9}$$
$$A_{y'} = \frac{B_A(z')}{2} x' \tag{2.16.10}$$
$$A_{z'} = 0 \tag{2.16.11}$$

We compute the components in the beam frame:

$$A_x = \cos\theta \cdot A_{x'} - \sin\theta \cdot A_{z'} \tag{2.16.12}$$
$$A_y = A_{y'} \tag{2.16.13}$$
$$A_z = \sin\theta \cdot A_{x'} + \cos\theta \cdot A_{z'} \tag{2.16.14}$$

Replacing the coordinates x', y', z' we obtain:

$$A_x = -\frac{B_A(z\,/\cos\theta)}{2} y \cos\theta \tag{2.16.15}$$
$$A_y = \frac{B_A(z\,/\cos\theta)}{2} x \cos\theta + \frac{B_A(z\,/\cos\theta)}{2} z \sin\theta \tag{2.16.16}$$
$$A_z = -\frac{B_A(z\,/\cos\theta)}{2} y \sin\theta \tag{2.16.17}$$

We perform a change of gauge:

$$\mathbf{A}_{\text{new}} = \mathbf{A} + \nabla f \tag{2.16.18}$$

with:

$$f = -\frac{B_A(z\,/\cos\theta)}{2} yz \sin\theta \tag{2.16.19}$$

obtaining:

$$A_x = -\frac{B_A(z\,/\cos\theta)}{2} y \cos\theta \tag{2.16.20}$$
$$A_y = \frac{B_A(z\,/\cos\theta)}{2} x \cos\theta \tag{2.16.21}$$

$$A_z = -B_A(z\,/\,\cos\theta)\,y\sin\theta - \frac{1}{2}\frac{dB_A}{dz}\,zy\sin\theta \tag{2.16.22}$$

From this we compute the field $\mathbf{B} = \nabla \times \mathbf{A}$:

$$B_x(x,y,z) = -\frac{1}{2}\frac{d}{dz}\left[B_A(z\,/\,\cos\theta)\right]\,x\cos\theta - B_A(z\,/\,\cos\theta)\sin\theta - \frac{1}{2}\frac{d}{dz}\left[B_A(z\,/\,\cos\theta)\right]\,z\sin\theta \tag{2.16.23}$$

$$B_y(x,y,z) = -\frac{1}{2}\frac{d}{dz}\left[B_A(z\,/\,\cos\theta)\right]\,y\cos\theta \tag{2.16.24}$$

$$B_z(x,y,z) = B_A(z\,/\,\cos\theta)\cos\theta \tag{2.16.25}$$

We call

$$\boxed{B_{x0}(z) = B_x(0,0,z) = -B_A(z\,/\,\cos\theta)\sin\theta - \frac{1}{2}\frac{d}{dz}\left[B_A(z\,/\,\cos\theta)\right]\,z\sin\theta} \tag{2.16.26}$$

$$\boxed{B_{z0}(z) = B_z(0,0,z) = B_A(z\,/\,\cos\theta)\cos\theta} \tag{2.16.27}$$

We can use the above to express the field:

$$\boxed{B_x(x,y,z) = -\frac{1}{2}\frac{dB_{z0}}{dz}\,x + B_{x0}(z)} \tag{2.16.28}$$

$$\boxed{B_y(x,y,z) = -\frac{1}{2}\frac{dB_{z0}}{dz}\,y} \tag{2.16.29}$$

$$\boxed{B_z(x,y,z) = B_{z0}(z)} \tag{2.16.30}$$

and to express the vector potential:

$$\boxed{A_x = -\frac{B_{z0}(z)}{2}\,y} \tag{2.16.31}$$

$$\boxed{A_y = \frac{B_{z0}(z)}{2}\,x} \tag{2.16.32}$$

$$\boxed{A_z = B_{x0}(z)y} \tag{2.16.33}$$

2.16.2 Generalization to arbitrary tilt and dipolar components

If the tilt is not in the $x-z$ plane, and if additional dipolar components are present, we can generalize the above, obtaining the following vector potential:

$$\boxed{A_x = -\frac{B_{z0}(z)}{2}\,y} \tag{2.16.34}$$

$$\boxed{A_y = \frac{B_{z0}(z)}{2}\,x} \tag{2.16.35}$$

$$\boxed{A_z = B_{x0}(z)y - B_{y0}(z)x} \tag{2.16.36}$$

The corresponding magnetic field is:

$$\boxed{B_x(x,y,z) = -\frac{1}{2}\frac{dB_{z0}}{dz}\,x + B_{x0}(z)} \tag{2.16.37}$$

$$\boxed{B_y(x,y,z) = -\frac{1}{2}\frac{dB_{z0}}{dz}\,y + B_{y0}(z)} \tag{2.16.38}$$

$$\boxed{B_z(x,y,z) = B_{z0}(z)} \tag{2.16.39}$$

2.17 Wire

Implemented in the Wire element.

For each part we define $p_z = \sqrt{(1+\delta)^2 - x'^2 - y'^2}$, using the current values for x' and y'.
Step 1. Initial backwards drift of length $L = \frac{embl}{2}$.

$$x \to x - L \cdot \frac{x'}{p_z}$$
$$y \to y - L \cdot \frac{y'}{p_z}$$

Step 2.

$$y \to y - \frac{x \cdot \sin(t_x)}{\cos\left(\arctan\left(\frac{x'}{p_z}\right) - t_x\right)} \cdot \frac{y'}{\sqrt{(1+\delta)^2 - y'^2}}$$
$$x \to x \cdot \left[\cos(t_x) - \sin(t_x) \cdot \tan\left(\arctan\left(\frac{x'}{p_z}\right) - t_x\right)\right]$$
$$x' \to \sqrt{(1+\delta)^2 - y'^2} \cdot \sin\left(\arctan\left(\frac{x'}{p_z}\right) - t_x\right)$$
$$x \to x - \frac{y \cdot \sin(t_y)}{\cos\left(\arctan\left(\frac{y'}{p_z}\right) - t_y\right)} \cdot \frac{x'}{\sqrt{(1+\delta)^2 - x'^2}}$$
$$y \to y \left[\cos(t_y) - \sin(t_y) \cdot \tan\left(\arctan\left(\frac{y'}{p_z}\right) - t_y\right)\right]$$
$$y' \to \sqrt{(1+\delta)^2 - x'^2} \sin\left(\arctan\left(\frac{y'}{p_z}\right) - t_y\right)$$

Step 3. Drift part of length $L = lin$.

$$x \to x + L \cdot \frac{x'}{p_z}$$
$$y \to y + L \cdot \frac{y'}{p_z}$$

Step 4. Here $x_i = x - r_x$ and $y = y - r_y$.

$$x' \to x' - \frac{\frac{cur \cdot 10^{-7}}{chi}}{x_i^2 + y_i^2} \cdot x_i \left[\sqrt{(lin + l)^2 + x_i^2 + y_i^2} - \sqrt{(lin - l)^2 + x_i^2 + y_i^2} \right]$$
$$y' \to y' - \frac{\frac{cur \cdot 10^{-7}}{chi}}{x_i^2 + y_i^2} \cdot y_i \left[\sqrt{(lin + l)^2 + x_i^2 + y_i^2} - \sqrt{(lin - l)^2 + x_i^2 + y_i^2} \right]$$

Step 5. Drift of length $L = leff - lin$.

$$x \to x + L \frac{x'}{p_z}$$
$$y \to y + L \frac{y'}{p_z}$$

Step 6.

$$x \to x - \frac{y \cdot \sin(-t_y)}{\cos\left(\arctan\left(\frac{y'}{p_z}\right) + t_y\right)} \cdot \frac{x'}{\sqrt{(1+\delta)^2 - x'^2}}$$
$$y \to y \cdot \left[\cos(-t_y) - \sin(-t_y) \cdot \tan\left(\arctan\left(\frac{y'}{p_z}\right) + t_y\right) \right]$$
$$y' \to \sqrt{(1+\delta)^2 - x'^2} \cdot \sin\left(\arctan\left(\frac{y'}{p_z}\right) + t_y\right)$$
$$y \to y - \frac{x \cdot \sin(-t_x)}{\cos\left(\arctan\left(\frac{x'}{p_z}\right) + t_x\right)} \cdot \frac{y'}{\sqrt{(1+\delta)^2 - y'^2}}$$
$$x \to x \left[\cos(-t_x) - \sin(-t_x) \cdot \tan\left(\arctan\left(\frac{x'}{p_z}\right) + t_x\right) \right]$$
$$x' \to \sqrt{(1+\delta)^2 - y'^2} \cdot \sin\left(\arctan\left(\frac{x'}{p_z}\right) + t_x\right)$$

Step 7. Shift.

$$x \to x + embl \cdot \tan(t_x)$$
$$y \to y + embl \cdot \frac{\tan(t_y)}{\cos(t_x)}$$

Step 8. Negative drift of length $L = \frac{embl}{2}$.

$$x \to x - L \cdot \frac{x'}{p_z}$$
$$y \to y - L \cdot \frac{y'}{p_z}$$

2.18 Electron Lens

Implemented in the Elens element.

2.18.1 Hollow electron lens - uniform annular profile

For a uniform distribution of the electron beam between R_1 and R_2, the radial kick can be described by a shape function $f(r)$ and a maximum kick strength $\theta_{\max}$:

$$\theta(r) = \frac{f(r)}{(r/R_2)} \cdot \theta_{\max} \tag{2.18.1}$$

with $r = \sqrt{x^2 + y^2}$ and $\theta_{\max}$ independent of r. The shape function $f(r)$ is defined as

$$f(r) = \frac{I(r)}{I_T} = \frac{2\pi}{I_T} \int_0^r r\rho(r)dr \tag{2.18.2}$$

where I_T is the total electron beam current, $I(r)$ is the current enclosed in a radius r and $\rho(r)$ is the electron beam density distribution.
For a uniform profile one then obtains:

$$\begin{cases} 0 & , \quad r < R_1 \\ \frac{r^2 - R_1^2}{R_2^2 - R_1^2} & , \quad R_1 \leq r < R_2 \\ 1 & , \quad R_2 \leq r \end{cases} \tag{2.18.3}$$

and

$$\theta_{\max} = \theta(R_2) = \frac{2LI_T(1 \pm \beta_e\beta_p)}{4\pi\epsilon_0 \left(B\rho\right)_p \beta_e\beta_p c^2} \cdot \frac{1}{R_2} \tag{2.18.4}$$

where L is the length of the e-lens, I_T the total electron beam current, $\beta_{e/p}$ the relativistic β of the electron/proton beam, $B\rho$ the magnetic rigidity, c the speed of light and ϵ_0 the vacuum permittivity. The $\pm$-sign represents the two cases of the electron beam traveling in the direction of the proton beam $(+)$ or in the opposite direction $(-)$. For hollow electron beam collimation, electron and proton beams travel in the same direction.
The kick in (x', y') can then be expressed as (note $\frac{x}{r} = \cos(\phi)$, $\frac{y}{r} = \sin(\phi)$):

$$x' = x' - \theta_{\max} \cdot \frac{r_2}{r^2} \cdot f(r) \cdot x \tag{2.18.5}$$

$$y' = y' - \theta_{\max} \cdot \frac{r_2}{r^2} \cdot f(r) \cdot y \tag{2.18.6}$$

If the electron lens is offset by $(x_{\text{offset}}, y_{\text{offset}})$, the coordinates (x, y) are simply transformed to:

$$\tilde{x} = x + x_{\text{offset}} \tag{2.18.7}$$

$$\tilde{y} = y + y_{\text{offset}} \tag{2.18.8}$$

$$\tilde{r} = \sqrt{\tilde{x}^2 + \tilde{y}^2} \tag{2.18.9}$$

and the kick is then given by:

$$x' = x' - \theta_{\max} \cdot \frac{r_2}{\tilde{r}^2} \cdot f(\tilde{r}) \cdot \tilde{x} \tag{2.18.10}$$

$$y' = y' - \theta_{\max} \cdot \frac{r_2}{\tilde{r}^2} \cdot f(\tilde{r}) \cdot \tilde{y} \tag{2.18.11}$$

2.19 Electron Cooler

Implemented in the ElectronCooler element.

The Parkhomchuk electron cooler in Xsuite applies a kick to the circulating ion based on the following equation:

$$\mathbf{F} = -\frac{n_e q^2 e^4}{4\pi^2 \epsilon_0^2 m_e} \cdot \frac{d\mathbf{V}}{V_{\text{tot}}^3} \ln\left(\frac{\rho_{\max} + \rho_{\min} + \rho_{\text{L}}}{\rho_{\min} + \rho_{\text{L}}}\right), \tag{2.19.1}$$

where $\mathbf{F}$ is the friction force acting on the circulating particle, n_e is the electron density (per unit volume), q is the charge of the circulating particle, e is the elementary charge, m_e is the electron mass, $d\mathbf{V}$ is the velocity difference between the circulating particle and the local electron velocity. $\rho_{\max}$ and $\rho_{\min}$ are the maximum and minimum impact parameters, respectively, and ρ_{L} is the Larmor radius of the electrons (also known as the radius of gyration). V_{tot} represents the total velocity difference between the electrons and ion, which is given by:

$$V_{\text{tot}} = \sqrt{dV^2 + \Delta_{\parallel}^2 + \Delta_{\text{magnet}}^2}, \tag{2.19.2}$$

where $dV^2 = dV_x^2 + dV_y^2 + dV_z^2$ is the squared norm of the relative velocity difference between the ion and electron. To prevent the cooling force from diverging as $dV \to 0$, regularization terms are added. The most logical approach is to add the temperatures as regularization terms because they provide the RMS velocity difference when $dV = 0$. This is why $\Delta_{\parallel}$, the longitudinal electron velocity spread associated with their temperature, is added to Equation (2.19.2). Lastly, Δ_{magnet} is the additional velocity spread induced by imperfections in the magnetic field of the electron cooler solenoid, which is given by:

$$\Delta_{\text{magnet}} = c\gamma \frac{B_{\perp}}{B_{\parallel}} \tag{2.19.3}$$

where $\frac{B_{\perp}}{B_{\parallel}}$ is the ratio of the transverse component of the magnetic field to the longitudinal component. The transverse temperature is not included in Equation (2.19.2) because it is suppressed due to the gyration motion of the electrons in the magnetic field. The transverse temperature indirectly plays a role in the Parkhomchuk model via the Larmor radius ρ_{L}, which is given by:

$$\rho_{\text{L}} = \frac{m_e \Delta_{\perp}}{eB} \tag{2.19.4}$$

where $\Delta_{\perp}$ is the transverse velocity due to the transverse electron temperature and B is the magnetic field. The minimum impact parameter $\rho_{\min}$ is given by:

$$\rho_{\min} = \frac{Ze^2}{4\pi\varepsilon_0 m_e \mathbf{V}^2} \tag{2.19.5}$$

The maximum impact parameter determines the maximum length scale at which a Coulomb interaction takes place, which can be limited by various physical effects,

such as the Debye length, which is given by:

$$\rho_d = \frac{\Delta_\parallel}{\omega_p}, \tag{2.19.6}$$

where the longitudinal velocity spread of the electrons $\Delta_\parallel$ is given by:

$$\Delta_\parallel = \sqrt{\frac{k_B T}{m_e}} \tag{2.19.7}$$

The plasma frequency ω_p represents the natural oscillation frequency of the electron due to a perturbation in its charge distribution, which is given by:

$$\omega_\mathrm{p} = \sqrt{\frac{n_e e^2}{m_e \epsilon_0}}. \tag{2.19.8}$$

The Debye radius is not the only limitation for the maximum interaction length. In the case where the velocity difference between the ion and electron $d\mathbf{V}$ is sufficiently larger than the velocity spread of the electron $\Delta_\parallel$, then the maximum shielding radius ρ_s is given by:

$$\rho_\mathrm{s} = \frac{d\mathbf{V}}{\omega_p}. \tag{2.19.9}$$

In principle, it is necessary to compute both ρ_d and ρ_s and compare them to see which one is the bottleneck and use that as the maximum impact parameter, which is given by:

$$\rho_\mathrm{max} = \min(\rho_\mathrm{d}, \rho_\mathrm{s})$$

However, in the code, the two shielding impact parameters are merged into a single effective impact parameter, given by:

$$\rho_\mathrm{shield} = \frac{V_\mathrm{tot}}{\omega_p}. \tag{2.19.10}$$

Here, V_tot is the total velocity difference between the electron and ion from Equation 2.19.2. Combining these effects in one term ensures that the shielding parameter reflects the combined influence of the ion's motion and the internal velocity distribution of the electron beam, which is affected by the temperature of the electrons as well as the imperfections in the magnetic field. An advantage of this formulation is that it ensures that the impact parameter varies smoothly as a function of the relative ion velocity $d\mathbf{V}$, which changes continuously throughout the cooling process. By using the combined expression for ρ_shield from Equation (2.19.10), the code avoids any abrupt changes in the friction force that could arise from sharp transitions in the shielding distance.

In addition to ρ_shield, the maximum impact parameter can also be limited by the distance an ion travels inside the electron cooler. This distance-based limit is expressed as:

$$\rho_\mathrm{interaction} = V_\mathrm{tot}\tau \tag{2.19.11}$$

where τ is $\frac{L}{\beta_0 c \gamma_0}$, which is the time it takes for the ion to pass through the electron cooler. Finally, the maximum impact parameter in the Xsuite implementation is the minimum of $\rho_{\text{interaction}}$ and ρ_{shield}, which is given by:

$$\rho_{\max} = \min(\rho_{\text{shield}}, \rho_{\text{interaction}}) \tag{2.19.12}$$

2.19.1 Electron beam space charge

An additional effect of electron cooling that needs to be taken into consideration is the space charge of the electron beam. Moreover, the electron beam will assume a parabolic profile with respect to the radius, which is given by [22]:

$$\frac{\Delta E(r)}{E_0} = \frac{I r_{\text{e}}}{ec} \frac{\gamma + 1}{\beta_0^3 \gamma^2} \left(\frac{r}{r_0}\right)^2 \approx 1.2 \times 10^{-4} \frac{I}{\beta_0^3} \left(\frac{r}{r_{e-beam}}\right)^2 \tag{2.19.13}$$

Equation 2.19.13 says that the electrons at the edge of the electron beam have a larger momentum than the electrons at the center. This means that the ions at the edge of the beam pipe will reach a larger equilibrium momentum than the ions at the core because the ions will assume the momentum of the electrons.

The Xsuite electron cooler allows for the inclusion of an optional effect called "space charge neutralization," which is determined by the parameter "space charge factor." A value of 0 for this parameter indicates that there is no space charge in the electron beam, while a value of 1 indicates that the electron beam will follow a parabolic profile as described in Equation 2.19.13.

An additional effect due to space charge is the rotation of the electron beam around the beam axis due to the magnetic field of the electron cooler. The angular velocity of the rotation is given by [22]:

$$\omega = \frac{\mathbf{F} \times \mathbf{B}}{er|B|^2} = \frac{I}{2\pi\epsilon_0 c r_{\text{e- beam}}^2 \beta\gamma^2 B_{\parallel}} \approx 60 \frac{I}{r_{\text{e-beam}}^2 \beta\gamma^2 B_{\parallel}} \tag{2.19.14}$$

This effect can also be disabled by setting "space charge factor" to zero. A value of 0 indicates that there is no rotation of the electron beam, while a value of 1 indicates that the electron beam will rotate with the angular frequency described in Equation 2.19.14.

2.20 Rotations

We assume the conventions for the directions of rotation for compatibility with MAD-X, as visualized in Fig. 2.2, and give the maps to convert the particle coordinates to the reference frames rotated by ϕ, θ, and ψ, respectively.

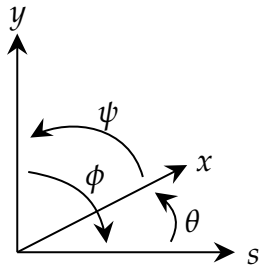


Figure 2.2: Rotation directions in the beam coordinate system (right-handed system).

The longitudinal momentum is

$$p_z = \sqrt{(1+\delta)^2 - p_x^2 - p_y^2}.$$

2.20.1 X Rotation

We define a scaling factor κ arising from the coordinate system being tilted by ϕ about the x-axis:

$$\kappa := 1 - \frac{\tan\phi\ p_y}{p_z}.$$

The coordinate updates can be described as follows:

$$y \leftarrow \frac{y}{\kappa\cos\phi}, \quad p_y \leftarrow p_y\cos\phi + p_z\sin\phi,$$

$$x \leftarrow x + \frac{y p_x \tan\phi}{\kappa p_z}, \quad \zeta \leftarrow \zeta - \frac{y\tan\phi\,(1+\beta_0 p_\tau)}{\kappa p_z}.$$

2.20.2 Y Rotation

We define a scaling factor κ arising from the coordinate system being tilted by θ about the y-axis:

$$\kappa := 1 + \frac{\tan\theta\ p_x}{p_z}.$$

The coordinate updates can be described as follows (which can be verified with [11], noting the opposite convention of the angle θ):

$$x \leftarrow \frac{x}{\kappa\cos\theta}, \quad p_x \leftarrow p_x\cos\theta - p_z\sin\theta,$$

$$y \leftarrow y - \frac{x\,p_y\,\tan\theta}{\kappa\,p_z}, \quad \zeta \leftarrow \zeta + \frac{x\,\tan\theta\,(1+\beta_0 p_\tau)}{\kappa\,p_z}.$$

2.20.3 S Rotation

We perform a rotation in the x-y plane by an angle ψ:

$$x \leftarrow x\cos\psi + y\sin\psi, \quad y \leftarrow -x\sin\psi + y\cos\psi,$$

$$p_x \leftarrow p_x\cos\psi + p_y\sin\psi, \quad p_y \leftarrow -p_x\sin\psi + p_y\cos\psi.$$

2.21 Cavity time, energy errors and acceleration

A cavity kick depends on:

$$\sin(2\pi fT + \phi) \tag{2.21.1}$$

where T is laboratory time.
For the most general case:

$$\sin(2\pi fT + \phi) = \sin\left(2\pi f\frac{s-\zeta}{\beta_0 c} + \phi\right) \tag{2.21.2}$$

Most codes drop the term $2\pi fs/(\beta_0 c)$ that is

$$\sin(2\pi fT + \phi) \to \sin\left(-2\pi f\frac{\zeta}{\beta_0 c} + \phi\right) \tag{2.21.3}$$

to make sure that a particle that is synchronous to the reference trajectory is in phase with the cavity.

2.21.1 Implementing energy errors

One can define

$$\begin{aligned} s &= s_0 + n(L_0 - L) + nL \\ f_{\text{rev}} &= \beta_0 c/L \\ f &= hf_{\text{rev}} \end{aligned} \tag{2.21.4}$$

where s_0 is the path length at the cavity turn at 0, L_0 is the design circumference, n is the turn number, h is the harmonic number, L is the new path length with an energy error. Indeed one could write $L = L_0(1 + \eta\delta_s)$ where η is a constant property of the lattice.
Multiple cavities can have their own defined L.
Using these definitions, then

$$\sin(2\pi fT + \phi) = \sin\left(2\pi hf_{\text{rev}}\frac{s_0 + n(L_0 - L) - \zeta}{\beta_0 c} + \phi\right) \tag{2.21.5}$$

$$= \sin\left(2\pi hf_{\text{rev}}\frac{n(L_0 - L) - \zeta}{\beta_0 c} + \phi'\right) \tag{2.21.6}$$

where $\phi' = \frac{2\pi h s_0}{L} + \phi$.
In MAD-X Twiss and MAD8, the longitudinal coordinate is directly $\zeta' = n(L_0 - L) - \zeta$ and the term $n(L_0 - L)$ is added smoothly in each thick element. This forces all the cavities to share the same L or $f_{\rm rev}$.
In SixTrack or MAD-X track, one could simply define a turn-dependent phase

$$\phi = \phi_0 + 2\pi h f_{\rm rev} n (L_0 - L) \tag{2.21.7}$$

which is very general, or alternatively add a special element that performs at each turn the following transformation:

$$\zeta_{\rm new} = (L_0 - L) - \zeta_{\rm old} \tag{2.21.8}$$

2.21.2 Acceleration

Acceleration can be achieved by renormalizing the relative variables using a new momentum reference. This has the side effect that the fields of the magnets (expressed in normalized strength) follow the energy ramp and that the cavity frequency (if expressed in terms of the harmonic number; NB we should perhaps change this in the Xtrack interface) is updated.
The re-normalization, if done once at each turn, is:

$$p_{x,\rm new} = p_{x,\rm old}\frac{P_{0,\rm old}}{P_{0,\rm new}} \qquad p_{y,\rm new} = p_{y,\rm old}\frac{P_{0,\rm old}}{P_{0,\rm new}} \tag{2.21.9}$$

$$\delta_{\rm new} = (\delta_{\rm old}+1)\frac{P_{0,\rm old}}{P_{0,\rm new}} - 1 \qquad p_{\tau,\rm new} = \frac{p_{\tau,\rm old}\,P_{0,\rm old}\,c + E_{0,\rm old} - E_{0,\rm new}}{P_{0,\rm new}c} \tag{2.21.10}$$

$$\zeta_{\rm new} = s\beta_0\left(\frac{1}{\beta_{0,\rm new}} - \frac{1}{\beta_{0,\rm old}}\right) - \zeta_{\rm old} \qquad \tau_{\rm new} = s\left(\frac{1}{\beta_{0,\rm new}} - \frac{1}{\beta_{0,\rm old}}\right) - \tau_{\rm old} \tag{2.21.11}$$

(2.21.12)

Chapter 3

Misalignments

3.1 Definitions

For defining the misalignments, we use the MAD-like coordinate system, where s is the axis tangent to the reference trajectory at the entrance to the element, and x and y are the transverse beam coordinates.
A misalignment of an element is characterized by seven quantities, as illustrated in Figs. 3.1, 3.2, and 3.3:

- A reference point (anchor) along the reference trajectory through the unperturbed element;
- 6 parameters specifying the shifts and rotations of the element with respect to the reference frame defined at the anchor point.

In the derivation we omit Δ in the naming of shifts and drifts and we call

$$f = \frac{\Delta s_{\text{anchor}}}{L} \tag{3.1.1}$$

the relative position of the anchor along the element of length L.
Note that the rotation about the y axis does not follow the classical right-handed approach: a positive ϕ rotation is clockwise when viewed from the positive x side, i.e., it goes from the s to the y axis, as opposed to from y to s.
For our calculations, we will represent the reference frame transformations using 4×4 augmented matrices. We shall assume the following notation convention: each matrix M consists of entries from M_{00} (top left corner), through M_{03} (top right corner), to M_{33} (bottom right corner). In particular, we distinguish 4 basic transformations:

$$\mathrm{T}(x, y, s) := \begin{bmatrix} 1 & 0 & 0 & x \\ 0 & 1 & 0 & y \\ 0 & 0 & 1 & s \\ 0 & 0 & 0 & 1 \end{bmatrix} \quad \text{(translation)}$$

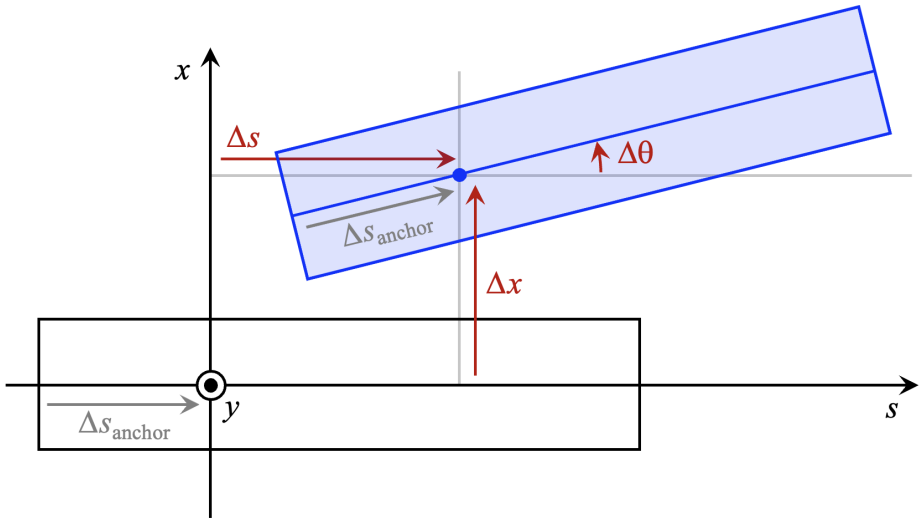


Figure 3.1: Misalignment in the s-x plane.

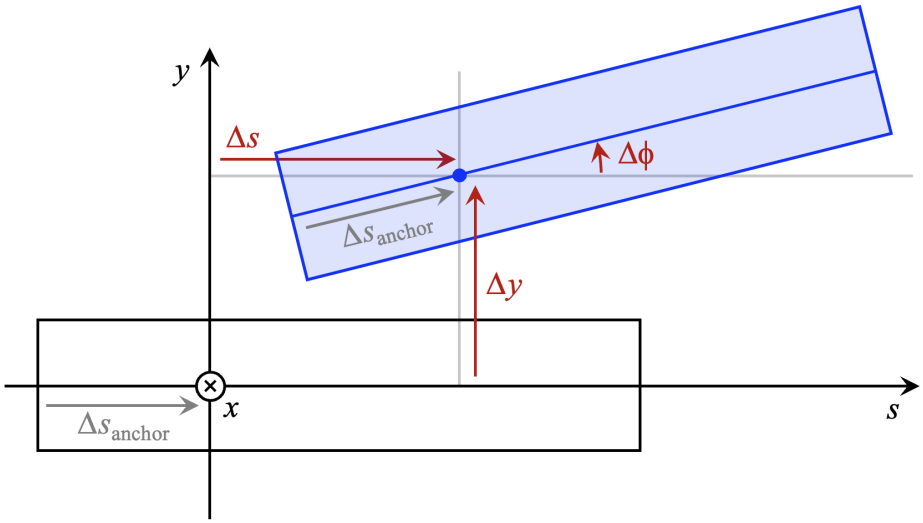


Figure 3.2: Misalignment in the s-y plane.

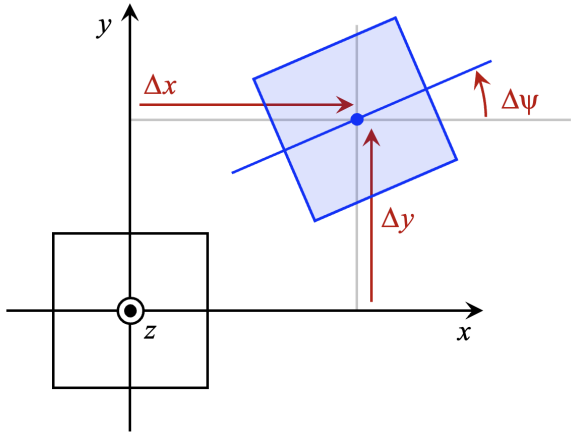


Figure 3.3: Misalignment in the x-y plane.

$$\mathrm{R}_x(\phi) := \begin{bmatrix} 1 & 0 & 0 & 0 \\ 0 & \cos(\phi) & \sin(\phi) & 0 \\ 0 & -\sin(\phi) & \cos(\phi) & 0 \\ 0 & 0 & 0 & 1 \end{bmatrix} \quad \text{(rotation around the } x \text{ axis)}$$

$$\mathrm{R}_y(\theta) := \begin{bmatrix} \cos(\theta) & 0 & \sin(\theta) & 0 \\ 0 & 1 & 0 & 0 \\ -\sin(\theta) & 0 & \cos(\theta) & 0 \\ 0 & 0 & 0 & 1 \end{bmatrix} \quad \text{(rotation around the } y \text{ axis)}$$

$$\mathrm{R}_s(\psi) := \begin{bmatrix} \cos(\psi) & -\sin(\psi) & 0 & 0 \\ \sin(\psi) & \cos(\psi) & 0 & 0 \\ 0 & 0 & 1 & 0 \\ 0 & 0 & 0 & 1 \end{bmatrix} \quad \text{(rotation around the } s \text{ axis)}$$

We allow the notation $T_x(\Delta x)$ to mean $T(\Delta x, 0, 0)$, and so on, for $T_y(\Delta y)$ and $T_s(\Delta s)$.

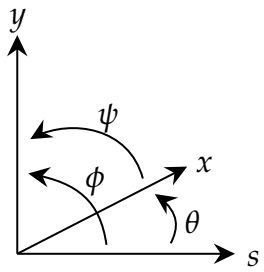


Figure 3.4: MAD-like coordinate system

3.2 Misalignment at arbitrary s without a tilt

We consider a potentially curved element misaligned with respect to an arbitrary position along its length.

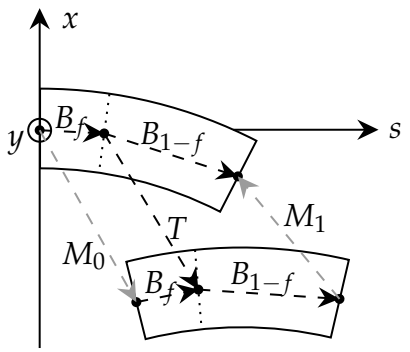


Figure 3.5: Transformations for a curved element misaligned at an arbitrary s.

Assuming a curved element of length L that bends the reference frame by α (and therefore a radius of curvature $\rho = L/\alpha$), we can represent B as a combination of a translation and a rotation, $B := T(\Delta x, 0, \Delta s)R_y(-\alpha)$, where

$$\begin{aligned} \Delta x &= \rho(\cos(\alpha) - 1) = -L\text{sinc}(\alpha/2)\sin(\alpha/2), \\ \Delta s &= \rho\sin(\alpha) = L\text{sinc}(\alpha). \end{aligned} \tag{3.2.1}$$

Note that the second formulations of Δx and Δs let us avoid division by zero if $\alpha = 0$, catering also to the case of a straight element for a truly general case.
Let us say that our element is misaligned at position ΔL along its length L. Then we can decompose our reference-frame-bending transformation B into parts B_f and B_{1-f} so that $B = B_f B_{1-f}$. The respective bending angles of the two parts are simply $f\alpha$ and $(1-f)\alpha$, where $f := \Delta L/L = \Delta L/(\rho\alpha)$ and ρ is the radius of curvature. Knowing these parameters, it is trivial to construct B_f and B_{1-f} analogously to B, as shown in Eq. 3.2.1.
Then, we compute the following transformation, which will take us from the normal to the misaligned element entry frame:

$$M_0 = B_f T B_f^{-1},$$

whereas for returning to the normal frame from the exit

$$\begin{aligned} B_f T B_{1-f} M_1 = B = B_f B_{1-f}, \\ M_1 = (TB_{1-f})^{-1} B_{1-f} = B_{1-f}^{-1} T^{-1} B_{1-f}. \end{aligned}$$

When evaluated, the matrix for the curved element in the general case is

$$B_f := \begin{bmatrix} \cos(\alpha f) & 0 & -\sin(\alpha f) & \rho(\cos(\alpha f) - 1) \\ 0 & 1 & 0 & 0 \\ \sin(\alpha f) & 0 & \cos(\alpha f) & \rho\sin(\alpha f) \\ 0 & 0 & 0 & 1 \end{bmatrix},$$

and so

$$B_f^{-1} := \begin{bmatrix} \cos(\alpha f) & 0 & \sin(\alpha f) & \rho(\cos(\alpha f) - 1) \\ 0 & 1 & 0 & 0 \\ -\sin(\alpha f) & 0 & \cos(\alpha f) & -\rho\sin(\alpha f) \\ 0 & 0 & 0 & 1 \end{bmatrix}.$$

Note that $B_{f,03} = (B_f^{-1})_{03} = -Lf\text{sinc}(\alpha f/2)\sin(\alpha f/2)$ and $B_{f,23} = -(B_f^{-1})_{23} = Lf\text{sinc}(\alpha f)$.
Meanwhile, the misalignment matrix is (let $s_\phi := \sin(\phi)$, $c_\psi := \cos(\psi)$, etc., for space-saving reasons)

$$T = \begin{bmatrix} -s_\phi s_\psi s_\theta + c_\psi c_\theta & -c_\psi s_\phi s_\theta - c_\theta s_\psi & c_\phi s_\theta & x \\ c_\phi s_\psi & c_\phi c_\psi & s_\phi & y \\ -c_\theta s_\phi s_\psi - c_\psi s_\theta & -c_\psi c_\theta s_\phi + s_\psi s_\theta & c_\phi c_\theta & s \\ 0 & 0 & 0 & 1 \end{bmatrix}$$

and its inverse, since T is a rigid affine transformation, can be computed with

$$T^{-1} = \begin{bmatrix} R^T & -R^T t \\ 0 & 1 \end{bmatrix}, \text{ given } \begin{bmatrix} R & t \\ 0 & 1 \end{bmatrix} := T.$$

For the conversion from M_0 and M_1 to the basic tracking transformations, we can use the decomposition, $M_0 = T(x_0, y_0, s_0)R_y(\theta_0)R_x(\phi_0)R_s(\psi_0)$, for which the parameters are as follows

$$\begin{aligned} \theta_0 &= \arctan_2(M_{0,02}, M_{0,22}), \\ \phi_0 &= \arctan_2(M_{0,12}, \sqrt{M_{0,10}^2 + M_{0,11}^2}), \\ \psi_0 &= \arctan_2(M_{0,10}, M_{0,11}), \\ x_0 &= M_{0,03}, \\ y_0 &= M_{0,13}, \\ s_0 &= M_{0,23}, \end{aligned}$$

and for the exit, $M_1 = T(x_1, y_1, s_1)R_y(\theta_1)R_x(\phi_1)R_s(\psi_1)$,

$$\begin{aligned} \theta_1 &= \arctan_2(M_{1,02}, M_{1,22}), \\ \phi_1 &= \arctan_2(M_{1,12}, \sqrt{M_{1,10}^2 + M_{1,11}^2}), \\ \psi_1 &= \arctan_2(M_{1,10}, M_{1,11}), \\ x_1 &= M_{1,03}, \\ y_1 &= M_{1,13}, \\ s_1 &= M_{1,23}. \end{aligned}$$

Note that many decompositions are possible, and their order can lead to more or less clean closed formulae for the parameters; in this case, however, we do not expect any 'nice' closed-form solutions (as opposed to the case of the subsequent section!). The above decomposition corresponds to the following tracking sequence:

- (M_0:) XYShift(x_0, y_0), SShift(s_0), YRot(θ_0), XRot(ϕ_0), SRot(ψ_0),
- (B:) Element(L, α),
- (M_1:) XYShift(x_1, y_1), SShift(s_1), YRot(θ_1), XRot(ϕ_1), SRot(ψ_1).

3.3 Misalignment at arbitrary s (the straight case)

Analogously to the previous section, we split D into $D_f D_{1-f}$:

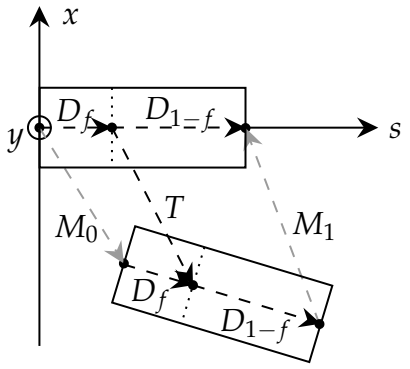


Figure 3.6: A straight element misaligned at an arbitrary location.

We simply have that $D_f := T(0,0,fL)$ and $D_{1-f} := T(0,0,(1-f)L)$. To get to the misaligned entry frame we have

$$M_0 := D_f T D_f^{-1} = T_s(fL)\ T\ T_s(-fL),$$

whereas for returning to the normal frame from the exit

$$M_1 := D_{1-f}^{-1} T^{-1} D_{1-f} = T_s((f-1)L)\ T^{-1}\ T_s((1-f)L).$$

It is intuitively obvious that, due to the lack of curvature, the entry and exit transformations should be possible to simplify. Specifically, we would want M_0 to involve some translation followed by rotations $R_y(\theta)R_x(\phi)R_s(\psi)$, and M_1, since it 'undoes' the effect of M_0, to involve rotations $R_s(-\psi)R_x(-\phi)R_y(-\theta)$ followed by some other translation.
First we decompose the entry matrix $M_0 = T(x_0,y_0,s_0)R_y(\theta_0)R_x(\phi_0)R_s(\psi_0)$, i.e. with the same method as in the previous section. After some algebra we observe that the angles and shifts indeed simplify:

$$\begin{aligned}
\theta_0 &= \arctan_2(M_{0,02}, M_{0,22}) = \theta,\\
\phi_0 &= \arctan_2(M_{0,12}, \sqrt{M_{0,10}^2 + M_{0,11}^2}) = \phi,\\
\psi_0 &= \arctan_2(M_{0,10}, M_{0,11}) = \psi,\\
x_0 &= T_{0,03} = x - Lf\cos(\phi)\sin(\theta),\\
y_0 &= T_{0,13} = y - Lf\sin(\phi),\\
s_0 &= T_{0,23} = s - Lf(\cos(\phi)\cos(\theta) - 1).
\end{aligned}$$

Let us now decompose the matrix M_1 into $R_s(\psi_1)R_x(\phi_1)R_y(\theta_1)T(x_1,y_1,s_1)$. To this end, let us write separately as M_{rot} and M_{tr} the rotation and translation part of the above decomposition, i.e. let $M_{rot} = R_s(\psi_1)R_x(\phi_1)R_y(\theta_1)$ and let $M_{tr} := T(x_1,y_1,s_1)$. In such a decomposition, the rotation part of M_{rot} is the same as that of M_1, and so we can simply extract it from there. Afterwards, knowing M_{rot} we can compute

$M_{tr} = M_{rot}^{-1} M_1$ to get the shifts. We indeed observe the angles and shifts simplifying:

$$\begin{aligned}
\theta_1 &= -\arctan_2(M_{1,20}, M_{1,22}) = -\theta, \\
\phi_1 &= -\arctan_2(M_{1,21}, \sqrt{M_{1,01}^2 + M_{1,11}^2}) = -\phi, \\
\psi_1 &= \arctan_2(M_{1,01}, M_{1,11}) = -\psi, \\
x_1 &= M_{tr,03} = (f-1)L\cos(\phi)\sin(\theta) - x, \\
y_1 &= M_{tr,13} = (f-1)L\sin(\phi) - y, \\
s_1 &= M_{tr,23} = (f-1)L(\cos(\phi)\cos(\theta) - 1) - s.
\end{aligned}$$

This way, our tracking procedure can be significantly less computationally expensive, compared to that of the preceding section, as no matrix operations are required:

- XYShift($x - Lf\cos(\phi)\sin(\theta)$, $y - Lf\sin(\phi)$)
- SShift($s - Lf(1 - \cos(\phi)\cos(\theta))$)
- YRot(θ), XRot(ϕ), SRot(ψ),
- Element(L),
- SRot($-\psi$), XRot($-\phi$), YRot($-\theta$),
- SShift($(f-1)L(\cos(\phi)\cos(\theta) - 1) - s$),
- XYShift($(f-1)L\cos(\phi)\sin(\theta) - x$, $(f-1)L\sin(\phi) - y$).

3.4 Misalignment at arbitrary s with a tilt

We consider a tilted curved element misaligned with respect to an arbitrary position along its length.

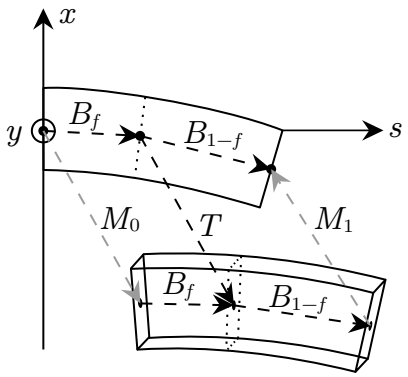


Figure 3.7: A tilted curved element misaligned at an arbitrary location.

Compared with the earlier discussion of misaligned curved elements (see Section 3.2), when considering a tilted element, we need to include the tilting in our transformation B (which, as before, is decomposed as $B_f B_{1-f}$ in Figure 3.7).

In order to include this effect we need to realize that in the previous case the curvature of the reference frame was only applied in the $s-x$ plane, whereas in the case of Figure 3.7, it will be applied in the plane obtained by tilting $s-x$ by some angle κ. Therefore, taking B_{sx} as the earlier transformation, i.e.,

$$B_{sx} := \begin{bmatrix} \cos(\alpha) & 0 & -\sin(\alpha) & \rho(\cos(\alpha)-1) \\ 0 & 1 & 0 & 0 \\ \sin(\alpha) & 0 & \cos(\alpha) & \rho\sin(\alpha) \\ 0 & 0 & 0 & 1 \end{bmatrix},$$

and taking $s_\alpha = \sin(\alpha)$, $c_\alpha = \cos(\alpha)$, etc. for space-saving reasons, we can express B as $R_s(\kappa)\ B_{sx}\ R_s(-\kappa)$, which evaluates to

$$B := \begin{bmatrix} (c_\alpha-1)c_\kappa^2+1 & (c_\alpha-1)c_\kappa s_\kappa & -c_\kappa s_\alpha & \rho(c_\alpha-1)c_\kappa \\ (c_\alpha-1)c_\kappa s_\kappa & (c_\alpha-1)s_\kappa^2+1 & -s_\alpha s_\kappa & \rho(c_\alpha-1)s_\kappa \\ c_\kappa s_\alpha & s_\alpha s_\kappa & c_\alpha & \rho s_\alpha \\ 0 & 0 & 0 & 1 \end{bmatrix}.$$

We can obtain the matrices B_f and B_{1-f} by substituting $f\alpha$ and $(1-f)\alpha$ for α in the above. To obtain the tracking procedure in this case it suffices to follow the steps of Section 3.2, substituting the new matrices.

3.5 Misalignment at arbitrary s with a tilt (straight case)

We can generalize the matrix of the above section to a straight case by recalling that $\rho(\cos(\alpha)-1) = -L\text{sinc}(\alpha/2)\sin(\alpha/2)$ and $\rho\sin(\alpha) = L\text{sinc}(\alpha)$. Then, we can see that when $\alpha = 0$, the matrix B of the preceding section simplifies to

$$B|_{\alpha=0} = \begin{bmatrix} 1 & 0 & 0 & 0 \\ 0 & 1 & 0 & 0 \\ 0 & 0 & 1 & L \\ 0 & 0 & 0 & 1 \end{bmatrix} = T_s(L) = D.$$

This means that the effect of the roll is disregarded in the calculation of the reference frame change for the purposes of a misalignment, and, therefore, that we can apply the exact procedure outlined in Section 3.3 also for tilted elements. This makes intuitive sense, as, in our setup, the tilt indeed only affects the direction of curvature of the element: if the element is straight, there is no work to be done for the misalignment, and the element map alone fully describes the effect of the tilt on the particles.

3.6 S Shift – ζ correction

In the tracking procedures shown in the preceding sections, we use the tracking map we refer to as an SShift, which we use to transport the particles in a straight line by a

displacement in s. We can presume the SShift to be a variant of DriftExact; however, there are special considerations that we need to take here, with respect to the path length s and the delay ζ of our particles.

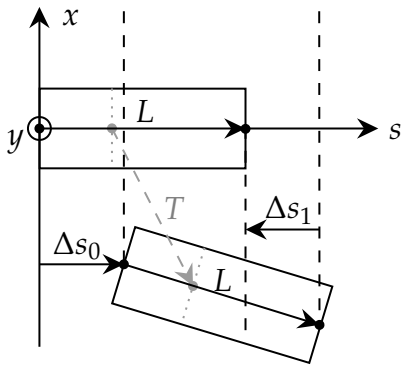


Figure 3.8: Visualization of the s-coordinate transformations without correction.

In the visualization in Fig. 3.8 we can see the different s-coordinate updates taking place when we track through a misalignment: in particular, we can see that the total path of the particle traveled, should SShift be simply a drift, is $\Delta s = \Delta s_0 + L + \Delta s_1$. Clearly, $\Delta s_0 \neq -\Delta s_1$, and so the path length changes between the aligned and misaligned element. However, what we desire is the opposite, i.e. that the path length does not change: it is inconvenient to have the length of our accelerator change due to a misalignment. Therefore, the simplest correction we can make in this instance is to disregard the update of the s coordinate in our drift/s-shift.
A further correction needs to be made with respect to the ζ coordinate. Since ζ is related to the path length by $\zeta = s - \beta_0 ct$, and since, in our setup, the synchronous particle arrival time is not expected to change between the normal and misaligned entry to the element, we expect that $\Delta\zeta = \Delta s$ between those two points. However, as we have already established for our correction of s, we expect the s coordinate to be unchanged, so we can adjust ζ in exactly the same fashion as we do s:

$$\text{SShift}(\Delta s) := (\text{DriftExact}(\Delta s),\ \ s \leftarrow s - \Delta s,\ \ \zeta \leftarrow \zeta - \Delta s).$$

Chapter 4

Linear optics

We define z as the vector of $2k$ coordinates,

$$z = (z_1, \ldots, z_{2k})^T = (x - x_0, p_x - p_{x0}, y - y_0, p_y - p_{y0}, \zeta - \zeta_0, p_\zeta - p_{\zeta 0})^T \tag{4.0.1}$$

One can define linear transfer maps (e.g. $R_{1\to 2}$ that propagates coordinates between two points s_1, s_2) and the one-turn map (e.g. R_1 that combines the effects for one turn starting from s_1):

$$z(s_2) = R_{1\to 2} z(s_1) \qquad\qquad z(C + s_1) = R_1 z(s_1). \tag{4.0.2}$$

In the following we will describe the optics calculation based on the Ripken formalism described in [23]. A good summary is also given in the MAD8 physics manual [2].

4.1 Linear normal form

Since the matrices derive from symplectic maps, the eigenvalue spectrum of the one-turn map R consists of $2k$ distinct eigenvalues and linearly independent eigenvectors. In addition, for the motion to be stable the eigenvalues $\lambda_k^\pm$ with eigenvectors $v_k^\pm$ have to be complex [23]:

$$R v_k^\pm = \lambda_k^\pm v_k^\pm,\ k = 1, \ldots, 3 \tag{4.1.1}$$

$$v_k^+ = (v_k^-)^*, \quad \lambda_k^+ = (\lambda_k^-)^*, \quad |\lambda_k^\pm| = 1 \tag{4.1.2}$$

As the eigenvectors are linearly independent, R can be diagonalized with

$$R = V \Lambda V^{-1}, \tag{4.1.3}$$

where V consists of the eigenvectors and Λ of the eigenvalues:

$$V = \begin{pmatrix} v_{1,1}^+ & v_{1,1}^- & \cdots & v_{3,1}^- \\ v_{1,2}^+ & v_{1,2}^- & \cdots & v_{3,2}^- \\ \vdots & \vdots & \vdots & \vdots \end{pmatrix} \qquad \Lambda = \begin{pmatrix} \lambda_1^+ & & & \\ & \lambda_1^- & & \\ & & \ddots & \\ & & & \lambda_3^- \end{pmatrix} \tag{4.1.4}$$

for which $v_{i,j}^{\pm}$ is the component j of eigenvector $v_i^{\pm}$.
The same calculation can be carried out with real numbers by the following definitions:

$$v_k^{\pm} = a_k \pm i b_k, \qquad \lambda_k^{\pm} = \cos\mu_k \pm i \sin\mu_k, \qquad \mu_k, a_k, b_k \in \mathbb{R} \tag{4.1.5}$$

such that:

$$R = W R_{\text{rot}} W^{-1} \tag{4.1.6}$$

with

$$R_{\text{rot}} = R_{\text{rot}}(\mu_k) = \begin{pmatrix} \cos\mu_1 & \sin\mu_1 & & & \\ -\sin\mu_1 & \cos\mu_1 & & & \\ & & \ddots & & \\ & & & \cos\mu_3 & \sin\mu_3 \\ & & & -\sin\mu_3 & \cos\mu_3 \end{pmatrix}, \tag{4.1.7}$$

$$W = \begin{pmatrix} a_{1,1} & b_{1,1} & \cdots & a_{3,1} & b_{3,1} \\ a_{1,2} & b_{1,2} & \cdots & a_{3,2} & b_{3,2} \\ \vdots & \vdots & \vdots & \vdots & \\ a_{1,6} & b_{1,6} & \cdots & a_{3,6} & b_{3,6} \end{pmatrix} \tag{4.1.8}$$

Equation 4.1.6 is called the linear normal form of the one-turn map R. The matrix R_{rot} describes a rotation in the 3 planes by angles μ_k.
Usually μ_k is written as $\mu_k = 2\pi Q_k$, where Q_k is then the tune of the mode k. By convention, the eigenvectors and values are normalized, sorted and rotated so that the following three conditions are fulfilled:

1. Plane 1 is associated with the horizontal, plane 2 with the vertical and plane 3 with the longitudinal plane. This is achieved by first normalizing the eigenvectors $v_k^{\pm}$ and then sorting them so that:

$$|v_{j,2j-1}^{+}| = |v_{j,2j-1}^{-}| = \max_{k=1,2,3} v_{k,j}, \quad j = 1, \ldots, 3 \tag{4.1.9}$$

2. The eigenvectors are then rotated with a phase term ψ_k

$$v_k \to v_k \exp(i\psi_k) \tag{4.1.10}$$

such that

$$\text{angle}(v_{k,2k-1}^{+}) = 0 \leftrightarrow \psi_k = -\text{angle}(v_{k,2k-1}^{+}) \tag{4.1.11}$$

In real space, Eqns. 4.1.9 and 4.1.11 then become equivalent to:

$$|a_{j,2j-1}| = \max_{k=1,2,3} |a_{k,j}|, \qquad b_{j,2j-1} = 0, \qquad j = 1, \ldots, 3 \tag{4.1.12}$$

This has the effect that a particle with $x = 0$ is transformed to $\tilde{x}$ in the normalized phase space.

3. The sign of $b_{k,j}$ is fixed by the symplectic condition on W

$$W^T S W = S \tag{4.1.13}$$

with S defined as

$$S = \begin{pmatrix} 0 & 1 & 0 & 0 & 0 & 0 \\ -1 & 0 & 0 & 0 & 0 & 0 \\ 0 & 0 & 0 & 1 & 0 & 0 \\ 0 & 0 & -1 & 0 & 0 & 0 \\ 0 & 0 & 0 & 0 & 0 & 1 \\ 0 & 0 & 0 & 0 & -1 & 0 \end{pmatrix} \tag{4.1.14}$$

which is equivalent to:

$$\begin{aligned} &a_k^T \cdot S \cdot b_k = 1, \quad b_k^T \cdot S \cdot a_k = -1, && \text{for } k = l \\ &a_k^T \cdot S \cdot b_l = 0, && \text{for } k \neq l \\ &a_k^T \cdot S \cdot a_l = 0, \quad b_k^T \cdot S \cdot b_l = 0, && k, l = 1, \ldots, 3 \end{aligned} \tag{4.1.15}$$

Eqn. 4.1.15 yields that in phase space a_k is thus obtained by an anticlockwise rotation of b_k by $\pi/2$ and a scaling of its length with $|a_k| = \frac{1}{|b_k|}$.

We will show in the following that in the normalized phase space the propagation of particle coordinates $z(s)$ from s_1 to s_2 is just a rotation by an angle ϕ_k in the $k = 1, \ldots, 3$ planes, while the amplitude I_k and initial phase $\phi_{k,0}$ stay constant, explicitly $z(s)$ is then given by:

$$z(s) = \sum_{k=1}^{3} \sqrt{2I_k} \left(a_k(s) \cos\left(\phi_{k,0} + \phi_k(s)\right) - b_k(s) \sin\left(\phi_{k,0} + \phi_k(s)\right) \right) \tag{4.1.16}$$

and

$$\begin{aligned} z(s_2) = W(s_2) R_{\text{rot}}(\phi_k) W(s_1)^{-1} z(s_1), \\ \text{with } \phi_k = \phi_k(s_2) - \phi_k(s_1) \end{aligned} \tag{4.1.17}$$

This implies that one turn is simply a rotation by $\phi_k = 2\pi Q_k$ where Q_k is the tune of the mode k. In the transverse plane the tune ($Q_{I,II}$) is usually positive and the particles rotate clockwise, while in the longitudinal plane the tune (Q_{III}) is negative above γ_T leading to an anticlockwise rotation.
For the derivation the following steps are needed:

1. The effect of one turn on the normalized variable $\tilde{z}(s) = W^{-1}(s) z(s)$ is a rotation:

$$\tilde{z}(C+s) = W^{-1} z(s+C) \overset{\text{(Eqn.4.1.6)}}{=} W^{-1} W R_{\text{rot}} W^{-1} z(s) = R_{\text{rot}} \tilde{z}(s), \tag{4.1.18}$$

As R and R_{rot} are symplectic, W is also symplectic, and its inverse is thus given by $S^{-1}W^TS$, explicitly:

$$W^{-1} = \begin{pmatrix} b_{12} & -b_{11} & b_{14} & -b_{13} & b_{16} & -b_{15} \\ -a_{12} & a_{11} & -a_{14} & a_{13} & -a_{16} & a_{15} \\ b_{22} & -b_{21} & b_{24} & -b_{23} & b_{26} & -b_{25} \\ -a_{22} & a_{21} & -a_{24} & a_{23} & -a_{26} & a_{25} \\ b_{32} & -b_{31} & b_{34} & -b_{33} & b_{36} & -b_{35} \\ -a_{32} & a_{31} & -a_{34} & a_{33} & -a_{36} & a_{35} \end{pmatrix} \tag{4.1.19}$$

2. The one-turn map and W-matrix can be propagated from s_1 to s_2 by

$$R_2 = R_{1\to 2}R_1R_{1\to 2}^{-1} \qquad\qquad W_2 = R_{1\to 2}W_1 \tag{4.1.20}$$

As Eqn. 4.1.18 represents a similarity transformation, the eigenvalues are thus independent of the position s and as the rotation matrix R_{rot} consists of the eigenvalues of R, the angle of the rotation $\mu_k = 2\pi Q_k$ is thus also independent of s.

3. As Eqn. 4.1.6 represents a basis transformation from the standard $\mathbb{R}^2$ basis to the eigenvector basis, the vectors a_k and b_k are projected onto (Eqn. 4.1.15):

$$\begin{aligned} \tilde{a}_1 = W^{-1}a_1 &= -SW^TSa_1 \\ &= -S(a_1Sa_1, b_1Sa_1, \ldots, b_3Sa_1)^T = (1,0,\ldots,0) \\ \tilde{b}_1 = W^{-1}b_1 &= -SW^TSb_1 \\ &= -S(a_1Sb_1, b_1Sb_1, \ldots, b_3Sb_1)^T = (0,1,\ldots,0) \\ &\ldots \\ \tilde{b}_3 = W^{-1}b_3 &= -SW^TSb_3 \\ &= -S(a_1Sb_3, b_1Sb_3, \ldots, b_3Sb_3)^T = (0,0,\ldots,1) \end{aligned} \tag{4.1.21}$$

in the normalized phase space.

4. From Eqn. 4.1.18 it follows that the amplitude I_k and initial phase ϕ_{k0} of $\tilde{z} = W^{-1}z = (\tilde{z}_{a_1}, \tilde{z}_{b_1}, \ldots, \tilde{z}_{b_3})$

$$I_k = \frac{(\tilde{z}_{a_k})^2 + (\tilde{z}_{b_k})^2}{2}, \quad k = 1,\ldots,3 \tag{4.1.22}$$

$$\tan\phi_{k0} = -\frac{\tilde{z}_{b_k}}{\tilde{z}_{a_k}} \tag{4.1.23}$$

are constants of the motion. The initial phase is defined with a minus sign in view of the definition of the Twiss parameters, where the initial phase is then

added (and not subtracted) to the phase advance. The components of $\tilde{z}$ are then explicitly given by:

$$\tilde{z}_{a_k} = \sum_{j=1}^{3} b_{k,2j} z_{2j-1} - b_{k,2j-1} z_{2j}, \quad k = 1, \ldots, 3 \tag{4.1.24}$$

$$\tilde{z}_{b_k} = \sum_{j=1}^{3} a_{k,2j-1} z_{2j} - a_{k,2j} z_{2j-1}, \quad k = 1, \ldots, 3. \tag{4.1.25}$$

An arbitrary vector $z(s)$ can thus be written in the following form:

$$\begin{aligned} z(s) &= W(s)\tilde{z}(s) \\ &= W(s) \left(\sum_{k=1}^{3} \tilde{z}_{a_k} \tilde{a}_k + \tilde{z}_{b_k} \tilde{b}_k \right) \\ &= \sum_{k=1}^{3} \tilde{z}_{a_k} W(s) \tilde{a}_k + \tilde{z}_{b_k} W(s) \tilde{b}_k \overset{\text{Eqn. 4.1.21}}{=} \sum_{k=1}^{3} \tilde{z}_{a_k} a_k + \tilde{z}_{b_k} b_k \\ &\overset{\text{Eqns. 4.1.22,4.1.23}}{=} \sum_{k=1}^{3} \sqrt{2I_k} \left(a_k \cos \phi_{k0} - b_k \sin \phi_{k0} \right) \end{aligned} \tag{4.1.26}$$

4.2 Twiss parameters

In the following the parameter k will always be used for the mode k and the parameter $j = 1, 2, 3$ for the horizontal (x, p_x), vertical (y, p_y) and longitudinal plane (ζ, p_ζ) in the phase space. z_{2j-1} then stands for the coordinates (x, y, ζ) and z_{2j} for $(p_{x,y}, p_\zeta)$.
The Twiss parameters can be introduced by writing the components of the eigenvector basis $(a_k(s), b_k(s))$ as the product of two envelope functions $\sqrt{\beta_{k,j}(s)}$, $\sqrt{\gamma_{k,j}(s)}$ and phase functions $\phi_{k,j}(s)$, $\bar{\phi}_{k,j}(s) = \phi_{k,j}(s) - \arctan(1/\alpha_{k,j})$, also called Twiss parameters or lattice functions, with

$$\begin{aligned} a_{k,2j-1}(s) &= \sqrt{\beta_{k,j}(s)} \cos \phi_{k,j}(s), \\ b_{k,2j-1}(s) &= \sqrt{\beta_{k,j}(s)} \sin \phi_{k,j}(s), \; k, j = 1, \ldots, 3, \end{aligned} \tag{4.2.1}$$

$$\begin{aligned} a_{k,2j}(s) &= \sqrt{\gamma_{k,j}(s)} \cos \bar{\phi}_{k,j}(s), \\ b_{k,2j}(s) &= \sqrt{\gamma_{k,j}(s)} \sin \bar{\phi}_{k,j}(s), \; k, j = 1, \ldots, 3 \end{aligned} \tag{4.2.2}$$

where $\beta_{k,j}(s), \alpha_{k,j}(s), \gamma_{k,j}(s)$ represent the projection of the ellipse of mode k on the plane of coordinates $z_{2k-1} - z_{2k}$.
Using Eqns. 4.1.16, 4.2.1, 4.2.2 and $\cos(x + y) = \cos x \cos y - \sin x \sin y$, the coordinates $z(s)$ can be expressed by:

$$z_{2j-1}(s) = \sum_{k=1}^{3} \sqrt{2I_k \beta_{k,j}(s)} \cos \left(\phi_{k,j}(s) + \phi_{k,0} \right) \tag{4.2.3}$$

$$z_{2j}(s) = \sum_{k=1}^{3} \sqrt{2I_k \gamma_{k,j}(s)} \cos\left(\bar{\phi}_{k,j}(s) + \phi_{k,0}\right),\ j = 1, \ldots, 3 \tag{4.2.4}$$

Conversely the lattice functions can also be expressed by a_k and b_k with

$$\beta_{k,j}(s) = a_{k,2j-1}(s)^2 + b_{k,2j-1}(s)^2 \tag{4.2.5}$$
$$\alpha_{k,j}(s) = -a_{k,2j-1}(s)a_{k,2j}(s) - b_{k,2j-1}(s)b_{k,2j}(s) \tag{4.2.6}$$
$$\gamma_{k,j}(s) = a_{k,2j}(s)^2 + b_{k,2j}(s)^2, \tag{4.2.7}$$

The well-known relations between the lattice functions

$$\sum_{j=1}^{3} \beta_{k,j}\phi'_{k,j} = 1 \tag{4.2.8}$$
$$\gamma_{k,j} = \frac{\beta_{k,j}^2 \phi_{k,j}'^2 + \alpha_{k,j}^2}{\beta_{k,j}}, \text{ with} \tag{4.2.9}$$
$$\alpha_{k,j} := -\frac{1}{2}\beta'_{k,j} \tag{4.2.10}$$

can then be derived with the help of the normalization condition (Eqn. 4.1.15)

$$a_k^T S b_k = 1 \tag{4.2.11}$$

by the following steps:

1. As $x' = \frac{dx}{ds}$, $y' = \frac{dy}{ds}$ the following relations hold also for a_k and b_k:

$$a_{k,2j} = a'_{k,2j-1} = \frac{d}{ds}(a_{k,2j-1}), \tag{4.2.12}$$
$$b_{k,2j} = b'_{k,2j-1} = \frac{d}{ds}(b_{k,2j-1}),\ k, j = 1, \ldots, 3 \tag{4.2.13}$$

2. The normalization condition Eqn. 4.1.15 can then be written as

$$\begin{aligned} a_k^T S b_k &= \sum_{j=1}^{3} \sqrt{\beta_{k,j}} \cos\phi_{k,j} \left(\sqrt{\beta_{k,j}} \sin\phi_{k,j}\right)' \\ &\quad - \left(\sqrt{\beta_{k,j}} \cos\phi_{k,j}\right)' \sqrt{\beta_{k,j}} \sin\phi_{k,j} \\ &= \sum_{j=1}^{3} \beta_{k,j}\phi'_{k,j} \\ &= 1 \end{aligned} \tag{4.2.14}$$

Note that Eqn. 4.2.14 yields the following relation between the phase advance ϕ and β in 2D:

$$\phi(s) = \phi(0) + \int_{s_0}^{s} \frac{1}{\beta(\bar{s})} d\bar{s} \tag{4.2.15}$$

3. Using the abbreviation $\alpha_{k,j} := -\frac{1}{2}\beta_{k,j}$, one finds for each mode k and plane j

$$\sqrt{\gamma_{k,j}}\cos\phi_{k,j} = a_{k,2j} = a'_{k,2j-1} = (\sqrt{\beta_{k,j}}\cos\phi_{k,j})' \tag{1}$$

$$\sqrt{\gamma_{k,j}}\sin\phi_{k,j} = b_{k,2j} = b'_{k,2j-1} = (\sqrt{\beta_{k,j}}\sin\phi_{k,j})' \tag{2}$$

$$\overset{(1)^2+(2)^2}{\Rightarrow} \gamma_{k,j} = \frac{\beta_{k,j}^2\phi_{k,j}'^2 + \alpha_{k,j}^2}{\beta_{k,j}}, \quad k,j = 1,\ldots,3 \tag{4.2.16}$$

which simplifies in the 2D case to:

$$\gamma \overset{\text{Eqn. 4.2.14}}{=} \frac{1+\alpha^2}{\beta} \tag{4.2.17}$$

4.3 Transformation to normalized coordinates

The W matrix can be used to transform normalized coordinates into physical coordinates relative to the closed orbit and vice versa:

$$\begin{pmatrix} x - x_0 \\ p_x - p_{x0} \\ y - y_0 \\ p_y - p_{y0} \\ \zeta - \zeta_0 \\ p_\zeta - p_{\zeta 0} \end{pmatrix} = W \begin{pmatrix} \hat{x} \\ \hat{p}_x \\ \hat{y} \\ \hat{p}_y \\ \hat{\zeta} \\ \hat{p}_\zeta \end{pmatrix} = W \begin{pmatrix} \sqrt{\varepsilon_x}\tilde{x} \\ \sqrt{\varepsilon_x}\tilde{p}_x \\ \sqrt{\varepsilon_y}\tilde{y} \\ \sqrt{\varepsilon_y}\tilde{p}_y \\ \sqrt{\varepsilon_\zeta}\tilde{\zeta} \\ \sqrt{\varepsilon_\zeta}\tilde{p}_\zeta \end{pmatrix} \tag{4.3.1}$$

where the subscript 0 denotes the closed orbit at the observation point, and

$$\begin{pmatrix} \tilde{x} & \tilde{p}_x & \tilde{y} & \tilde{p}_y & \tilde{\zeta} & \tilde{p}_\zeta \end{pmatrix} \tag{4.3.2}$$

are normalized coordinates in sigmas and ε_x, ε_y and ε_ζ are the geometric emittances.

4.4 Covariance matrix

The beam covariance matrix is defined from the central second moments of the phase-space coordinates

$$z = \begin{pmatrix} x & p_x & y & p_y & \zeta & p_\zeta \end{pmatrix}^T \tag{4.4.1}$$

as

$$\Sigma = \left\langle (z - \langle z\rangle)\,(z - \langle z\rangle)^T \right\rangle. \tag{4.4.2}$$

The subtraction of the centroid makes Σ independent of the closed-orbit offset of the distribution.

4.4.1 Normal-mode emittances

Let

$$\hat{z} = \begin{pmatrix} \hat{x} & \hat{p}_x & \hat{y} & \hat{p}_y & \hat{\zeta} & \hat{p}_\zeta \end{pmatrix}^T \tag{4.4.3}$$

be the normalized coordinates appearing in Eq. 4.3.1, so that $z - z_0 = W\hat{z}$, where z_0 is the closed orbit. We define $\Delta\hat{z} = \hat{z} - \langle\hat{z}\rangle$ and group the normalized coordinates by mode as

$$\Delta\hat{z}_x = \begin{pmatrix} \Delta\hat{x} \\ \Delta\hat{p}_x \end{pmatrix}, \quad \Delta\hat{z}_y = \begin{pmatrix} \Delta\hat{y} \\ \Delta\hat{p}_y \end{pmatrix}, \quad \Delta\hat{z}_\zeta = \begin{pmatrix} \Delta\hat{\zeta} \\ \Delta\hat{p}_\zeta \end{pmatrix}. \tag{4.4.4}$$

For a beam matched to the linear optics, the particles are distributed in each normal-mode plane with no preferred betatron phase. We write the centroid-subtracted coordinates of mode k as

$$\Delta\hat{q}_k = A_k \cos\phi_k, \qquad \Delta\hat{p}_k = -A_k \sin\phi_k, \tag{4.4.5}$$

where $(\Delta\hat{q}_k, \Delta\hat{p}_k)$ stands for $(\Delta\hat{x}, \Delta\hat{p}_x)$, $(\Delta\hat{y}, \Delta\hat{p}_y)$, or $(\Delta\hat{\zeta}, \Delta\hat{p}_\zeta)$. If the phase distribution is uniform and independent of the amplitude, then

$$\left\langle \cos^2\phi_k \right\rangle = \left\langle \sin^2\phi_k \right\rangle = \frac{1}{2}, \qquad \langle \sin\phi_k \cos\phi_k \rangle = 0, \tag{4.4.6}$$

and the covariance block of mode k is

$$\begin{aligned} C_k &= \left\langle \Delta\hat{z}_k \Delta\hat{z}_k^T \right\rangle \\ &= \begin{pmatrix} \left\langle A_k^2 \cos^2\phi_k \right\rangle & -\left\langle A_k^2 \sin\phi_k \cos\phi_k \right\rangle \\ -\left\langle A_k^2 \sin\phi_k \cos\phi_k \right\rangle & \left\langle A_k^2 \sin^2\phi_k \right\rangle \end{pmatrix} \\ &= \frac{\left\langle A_k^2 \right\rangle}{2} \begin{pmatrix} 1 & 0 \\ 0 & 1 \end{pmatrix}. \end{aligned} \tag{4.4.7}$$

Defining $\varepsilon_k = \left\langle A_k^2 \right\rangle / 2$, each normal-mode block is $C_k = \varepsilon_k I$. If the normal-mode variables are statistically independent, then the cross-covariances between different modes vanish:

$$\left\langle \Delta\hat{z}_j \Delta\hat{z}_k^T \right\rangle = 0, \qquad j \neq k. \tag{4.4.8}$$

It follows that the covariance of the normalized coordinates is

$$\left\langle \Delta\hat{z} \Delta\hat{z}^T \right\rangle = E, \tag{4.4.9}$$

with

$$E = \begin{pmatrix} \varepsilon_x & 0 & 0 & 0 & 0 & 0 \\ 0 & \varepsilon_x & 0 & 0 & 0 & 0 \\ 0 & 0 & \varepsilon_y & 0 & 0 & 0 \\ 0 & 0 & 0 & \varepsilon_y & 0 & 0 \\ 0 & 0 & 0 & 0 & \varepsilon_\zeta & 0 \\ 0 & 0 & 0 & 0 & 0 & \varepsilon_\zeta \end{pmatrix}. \tag{4.4.10}$$

Since W is a linear transformation, Eq. 4.3.1 gives

$$z - \langle z \rangle = W\left(\hat{z} - \langle \hat{z} \rangle\right). \tag{4.4.11}$$

Substituting this expression in Eq. 4.4.2 gives

$$\begin{aligned}\Sigma &= \left\langle W\left(\hat{z} - \langle \hat{z} \rangle\right)\left(W\left(\hat{z} - \langle \hat{z} \rangle\right)\right)^T \right\rangle \\ &= W\left\langle \left(\hat{z} - \langle \hat{z} \rangle\right)\left(\hat{z} - \langle \hat{z} \rangle\right)^T \right\rangle W^T \\ &= WEW^T. \end{aligned} \tag{4.4.12}$$

Since W is symplectic,

$$W^T S W = S, \tag{4.4.13}$$

and therefore

$$W^T S = S W^{-1}. \tag{4.4.14}$$

Multiplying Eq. 4.4.12 by S on the right gives

$$\Sigma S = WEW^T S = WESW^{-1}. \tag{4.4.15}$$

Thus ΣS is obtained from ES by a change of basis with matrix W. This implies that the two matrices have the same eigenvalues: if q is an eigenvector of ES with eigenvalue λ, then

$$\Sigma S\, Wq = WESW^{-1}Wq = WESq = \lambda Wq. \tag{4.4.16}$$

Therefore Wq is an eigenvector of ΣS with the same eigenvalue λ. Combining Eqs. 4.4.10 and 4.1.14 gives

$$ES = \begin{pmatrix} 0 & \varepsilon_x & 0 & 0 & 0 & 0 \\ -\varepsilon_x & 0 & 0 & 0 & 0 & 0 \\ 0 & 0 & 0 & \varepsilon_y & 0 & 0 \\ 0 & 0 & -\varepsilon_y & 0 & 0 & 0 \\ 0 & 0 & 0 & 0 & 0 & \varepsilon_\zeta \\ 0 & 0 & 0 & 0 & -\varepsilon_\zeta & 0 \end{pmatrix}, \tag{4.4.17}$$

which is block diagonal, with one block

$$\begin{pmatrix} 0 & \varepsilon_k \\ -\varepsilon_k & 0 \end{pmatrix} \tag{4.4.18}$$

for each normal mode $k = x, y, \zeta$. Each block has eigenvalues $\pm i\varepsilon_k$. The eigenvalues of ES in normalized coordinates, and equivalently of ΣS in physical coordinates, are therefore

$$\lambda_k^{\pm}(ES) = \lambda_k^{\pm}(\Sigma S) = \pm i\varepsilon_k. \tag{4.4.19}$$

The quantities ε_k are called **normal-mode emittances**. Their relation to the action variables is discussed in the following section.

4.4.2 Eigenvectors of the covariance matrix

The eigenvectors of ΣS are the same eigenvectors as those of the one-turn matrix R. This can be seen mode by mode. First work in normalized coordinates, where both $R_{\rm rot}$ and ES are block diagonal. Let q_k^+ be the vector whose only non-zero normal-mode block is

$$\begin{pmatrix} 1 \\ i \end{pmatrix} \tag{4.4.20}$$

in plane k. In this plane, the corresponding block of $R_{\rm rot}$ is

$$\begin{pmatrix} \cos\mu_k & \sin\mu_k \\ -\sin\mu_k & \cos\mu_k \end{pmatrix}, \tag{4.4.21}$$

and

$$\begin{pmatrix} \cos\mu_k & \sin\mu_k \\ -\sin\mu_k & \cos\mu_k \end{pmatrix} \begin{pmatrix} 1 \\ i \end{pmatrix} = \begin{pmatrix} \cos\mu_k + i\sin\mu_k \\ -\sin\mu_k + i\cos\mu_k \end{pmatrix} = \exp(i\mu_k) \begin{pmatrix} 1 \\ i \end{pmatrix}. \tag{4.4.22}$$

Therefore $R_{\rm rot} q_k^+ = \exp(i\mu_k) q_k^+$. The corresponding block of ES is

$$\begin{pmatrix} 0 & \varepsilon_k \\ -\varepsilon_k & 0 \end{pmatrix}, \tag{4.4.23}$$

and

$$\begin{pmatrix} 0 & \varepsilon_k \\ -\varepsilon_k & 0 \end{pmatrix} \begin{pmatrix} 1 \\ i \end{pmatrix} = \begin{pmatrix} i\varepsilon_k \\ -\varepsilon_k \end{pmatrix} = i\varepsilon_k \begin{pmatrix} 1 \\ i \end{pmatrix}. \tag{4.4.24}$$

Therefore $ES q_k^+ = i\varepsilon_k q_k^+$. Hence q_k^+ is an eigenvector of both $R_{\rm rot}$ and ES, with different eigenvalues.
Using

$$R = W R_{\rm rot} W^{-1}, \qquad \Sigma S = W E S W^{-1}, \tag{4.4.25}$$

define $v_k^+ = W q_k^+$. Then

$$\begin{aligned} R v_k^+ &= W R_{\rm rot} W^{-1} W q_k^+ \\ &= W R_{\rm rot} q_k^+ \\ &= W \exp(i\mu_k) q_k^+ \\ &= \exp(i\mu_k) v_k^+, \end{aligned} \tag{4.4.26}$$

and, in the same way,

$$\begin{aligned} \Sigma S v_k^+ &= W E S W^{-1} W q_k^+ \\ &= W E S q_k^+ \end{aligned}$$

$$\begin{aligned} &= Wi\varepsilon_k q_k^+ \\ &= i\varepsilon_k v_k^+. \end{aligned} \tag{4.4.27}$$

Thus the same physical vector v_k^+ is an eigenvector of both R and ΣS. The W matrix can therefore be obtained from the eigenvectors of ΣS by applying the same sorting, phase, and symplectic-normalization conventions described in Section 4.1. Once this W is known, the Twiss parameters and dispersions are obtained from the expressions in Sections 4.2 and 4.6.

4.5 Action, amplitude and emittance

We define the action associated with the three modes:

$$J_x = \frac{\hat{x}^2 + \hat{p}_x^2}{2}, \quad J_y = \frac{\hat{y}^2 + \hat{p}_y^2}{2}, \quad J_\zeta = \frac{\hat{\zeta}^2 + \hat{p}_\zeta^2}{2} \tag{4.5.1}$$

The corresponding amplitudes are defined such that:

$$A_x = \sqrt{\hat{x}^2 + \hat{p}_x^2} = \sqrt{2J_x}, \tag{4.5.2}$$

$$A_y = \sqrt{\hat{y}^2 + \hat{p}_y^2} = \sqrt{2J_y} \tag{4.5.3}$$

$$A_\zeta = \sqrt{\hat{\zeta}^2 + \hat{p}_\zeta^2} = \sqrt{2J_\zeta} \tag{4.5.4}$$

A Gaussian distribution is defined such that the density with respect to each action can be written as:

$$f(J_x) = Ke^{-J_x/\varepsilon_x} \tag{4.5.5}$$

The parameter ε_x is the same emittance defined from the eigenvalues of ΣS in Eq. 4.4.19. This can be seen from the covariance in normalized coordinates. Let $\Delta\hat{x} = \hat{x} - \langle\hat{x}\rangle$ and $\Delta\hat{p}_x = \hat{p}_x - \langle\hat{p}_x\rangle$. The x-mode block of Eq. 4.4.9 is

$$\left\langle \begin{pmatrix} \Delta\hat{x} \\ \Delta\hat{p}_x \end{pmatrix} \begin{pmatrix} \Delta\hat{x} & \Delta\hat{p}_x \end{pmatrix} \right\rangle = \begin{pmatrix} \varepsilon_x & 0 \\ 0 & \varepsilon_x \end{pmatrix}. \tag{4.5.6}$$

Reading the entries of this matrix gives

$$\left\langle \Delta\hat{x}^2 \right\rangle = \varepsilon_x, \qquad \left\langle \Delta\hat{p}_x^2 \right\rangle = \varepsilon_x, \qquad \langle \Delta\hat{x}\Delta\hat{p}_x \rangle = 0. \tag{4.5.7}$$

Therefore

$$\begin{aligned} \left\langle \frac{\Delta\hat{x}^2 + \Delta\hat{p}_x^2}{2} \right\rangle &= \frac{\left\langle \Delta\hat{x}^2 \right\rangle + \left\langle \Delta\hat{p}_x^2 \right\rangle}{2} \\ &= \varepsilon_x. \end{aligned} \tag{4.5.8}$$

For a distribution centered on the closed orbit, this is simply $\langle J_x \rangle = \varepsilon_x$. If the beam centroid is offset, the emittance is obtained from the centroid-subtracted action above,

while the raw average action also contains the coherent centroid contribution. Equivalently, for the exponential action density above,

$$\varepsilon_x = \langle J_x \rangle = \int J_x f(J_x)\, dJ_x. \tag{4.5.9}$$

The same argument applies to the other two normal modes.

4.6 Dispersion and crab dispersion

For a particle having no betatron amplitude ($\hat{x} = \hat{p}_x = \hat{y} = \hat{p}_y = 0$) we can write:

$$x = W_{15}\hat{\zeta} + W_{16}\hat{p}_\zeta \tag{4.6.1}$$
$$\zeta = W_{55}\hat{\zeta} + W_{56}\hat{p}_\zeta \tag{4.6.2}$$
$$p_\zeta = W_{65}\hat{\zeta} + W_{66}\hat{p}_\zeta \tag{4.6.3}$$

4.6.1 Dispersion

The dispersion is:

$$D_x^{p_\zeta} = \frac{dx}{dp_\zeta} \quad \text{for } \zeta = 0 \tag{4.6.4}$$

By imposing $\zeta = 0$ in Eq. 4.6.2 we obtain:

$$\hat{\zeta} = -\frac{W_{56}}{W_{55}}\hat{p}_\zeta \tag{4.6.5}$$

We replace in Eq. 4.6.3:

$$\hat{p}_\zeta = \left(W_{66} - \frac{W_{65}W_{56}}{W_{55}}\right)^{-1} p_\zeta \tag{4.6.6}$$

From Eq. 4.6.5 we obtain:

$$\hat{\zeta} = -\frac{W_{56}}{W_{55}}\left(W_{66} - \frac{W_{65}W_{56}}{W_{55}}\right)^{-1} p_\zeta \tag{4.6.7}$$

Replacing the last two into Eq. 4.6.1 we obtain:

$$x = \left(W_{16} - \frac{W_{15}W_{56}}{W_{55}}\right)\left(W_{66} - \frac{W_{65}W_{56}}{W_{55}}\right)^{-1} p_\zeta \tag{4.6.8}$$

which gives the dispersion:

$$D_x^{p_\zeta} = \left(W_{16} - \frac{W_{15}W_{56}}{W_{55}}\right)\left(W_{66} - \frac{W_{65}W_{56}}{W_{55}}\right)^{-1} \tag{4.6.9}$$

A similar type of calculation can be done for the other planes, and for the transverse momentum dispersion, obtaining $D_{px}^{p_\zeta}$:

$$D_{px}^{p_\zeta} = \left(W_{26} - \frac{W_{25}W_{56}}{W_{55}}\right)\left(W_{66} - \frac{W_{65}W_{56}}{W_{55}}\right)^{-1} \tag{4.6.10}$$

$$D_{y}^{p_\zeta} = \left(W_{36} - \frac{W_{35}W_{56}}{W_{55}}\right)\left(W_{66} - \frac{W_{65}W_{56}}{W_{55}}\right)^{-1} \tag{4.6.11}$$

$$D_{py}^{p_\zeta} = \left(W_{46} - \frac{W_{45}W_{56}}{W_{55}}\right)\left(W_{66} - \frac{W_{65}W_{56}}{W_{55}}\right)^{-1} \tag{4.6.12}$$

4.6.2 Crab dispersion

The crab dispersion is:

$$D_x^\zeta = \frac{dx}{dz} \quad \text{for } p_\zeta = 0 \tag{4.6.13}$$

By imposing $p_\zeta = 0$ in Eq. 4.6.3 we obtain:

$$\hat{p}_\zeta = -\frac{W_{65}}{W_{66}}\hat{\zeta} \tag{4.6.14}$$

We replace in Eq. 4.6.2:

$$\hat{\zeta} = \left(W_{55} - \frac{W_{56}W_{65}}{W_{66}}\right)^{-1}\zeta \tag{4.6.15}$$

From Eq. 4.6.14 we obtain:

$$\hat{p}_\zeta = -\frac{W_{65}}{W_{66}}\left(W_{55} - \frac{W_{56}W_{65}}{W_{66}}\right)^{-1}\zeta \tag{4.6.16}$$

Replacing the last two into Eq. 4.6.1 we obtain:

$$x = \left(W_{15} - \frac{W_{16}W_{65}}{W_{66}}\right)\left(W_{55} - \frac{W_{56}W_{65}}{W_{66}}\right)^{-1}\zeta \tag{4.6.17}$$

which gives the crab dispersion:

$$D_x^\zeta = \left(W_{15} - \frac{W_{16}W_{65}}{W_{66}}\right)\left(W_{55} - \frac{W_{56}W_{65}}{W_{66}}\right)^{-1} \tag{4.6.18}$$

A similar type of calculation can be done for the other planes, and for the transverse momentum crab dispersion, obtaining:

$$D_{p_x}^\zeta = \left(W_{25} - \frac{W_{26}W_{65}}{W_{66}}\right)\left(W_{55} - \frac{W_{56}W_{65}}{W_{66}}\right)^{-1} \tag{4.6.19}$$

$$D_{y}^\zeta = \left(W_{35} - \frac{W_{36}W_{65}}{W_{66}}\right)\left(W_{55} - \frac{W_{56}W_{65}}{W_{66}}\right)^{-1} \tag{4.6.20}$$

$$D_{p_y}^\zeta = \left(W_{45} - \frac{W_{46}W_{65}}{W_{66}}\right)\left(W_{55} - \frac{W_{56}W_{65}}{W_{66}}\right)^{-1} \tag{4.6.21}$$

Chapter 5

Resonance Driving Terms

This chapter follows the formulation in [24, 25].

5.1 Courant–Snyder normalized coordinates

We work in Courant–Snyder normalized transverse coordinates $(\tilde{u}, \tilde{p}_u)$ with $u \in \{x, y\}$, obtained from (u, p_u) via

$$\begin{pmatrix} \tilde{u} \\ \tilde{p}_u \end{pmatrix} = \begin{pmatrix} \beta_u^{-1/2} & 0 \\ \alpha_u \beta_u^{-1/2} & \beta_u^{1/2} \end{pmatrix} \begin{pmatrix} u \\ p_u \end{pmatrix}, \tag{5.1.1}$$

where the Twiss parameters (α_u, β_u) are evaluated at the observation point s.

5.2 Complex Courant–Snyder coordinates

For $q \in \{x, y\}$ we introduce the complex Courant–Snyder coordinates

$$h_{q,\pm} = \tilde{q} \pm i\tilde{p}_q = \sqrt{2I_q}\, e^{\mp i(\psi_q + \psi_{q,0})}, \tag{5.2.1}$$

where I_q is the action and ψ_q the betatron phase advance (with initial phase $\psi_{q,0}$). From $\tilde{q}$ and $\tilde{p}_q$ we recover

$$I_q = \frac{\tilde{q}^2 + \tilde{p}_q^2}{2}, \tag{5.2.2}$$

$$\psi_q = -\psi_{q,0} - \operatorname{atan2}\left(\tilde{p}_q, \tilde{q}\right). \tag{5.2.3}$$

5.3 Motion expressed through resonance driving terms

The transverse motion written in terms of resonance driving terms (RDTs) reads

$$h_{x,-}(s, N) = \sqrt{2I_x}\, e^{i(2\pi Q_x N + \psi_{s,x,0})} - 2i \sum_{pqrt} p\, f_{pqrt}^{(s)}\, (2I_x)^{\frac{p+q-1}{2}} (2I_y)^{\frac{r+t}{2}}$$

$$\times\, e^{i\left[(1-p+q)(2\pi Q_x N+\psi_{s,x,0})+(t-r)\left(2\pi Q_y N+\psi_{s,y,0}\right)\right]}, \tag{5.3.1}$$

$$h_{y,-}(s,N) = \sqrt{2I_y}\, e^{i\left(2\pi Q_y N+\psi_{s,y,0}\right)} - 2i \sum_{pqrt} r\, f^{(s)}_{pqrt}\, (2I_x)^{\frac{p+q}{2}} (2I_y)^{\frac{r+t-1}{2}}$$
$$\times\, e^{i\left[(q-p)(2\pi Q_x N+\psi_{s,x,0})+(1-r+t)\left(2\pi Q_y N+\psi_{s,y,0}\right)\right]}, \tag{5.3.2}$$

where N is the turn number, $Q_{x,y}$ the tunes, $I_{x,y}$ the invariants and $\psi_{s,x,0}$, $\psi_{s,y,0}$ the initial phases at the observation point s.

5.4 Expression of RDTs from first-order perturbation theory

The coefficients f_{pqrt} at the element j are computed from first-order perturbation theory obtaining:

$$f_{pqrt}(j) = \frac{\sum_{m=1}^{M} h_{m,pqrt}\, e^{i\left[(p-q)\Delta\phi_{x,mj}+(r-t)\Delta\phi_{y,mj}\right]}}{1 - e^{2\pi i\left[(p-q)Q_x+(r-t)Q_y\right]}}, \tag{5.4.1}$$

where the numerator runs over the M elements of the ring and where

$$h_{m,pqrt} = -\frac{K_{m,n-1}\,\Omega(r+t) + i\,\hat{K}_{m,n-1}\,\Omega(r+t+1)}{p!\,q!\,r!\,t!\,2^{p+q+r+t}}\; i^{r+t}\,(\beta_{m,x})^{\frac{p+q}{2}}(\beta_{m,y})^{\frac{r+t}{2}}, \tag{5.4.2}$$

with $n = p+q+r+t$ and where $K_{m,n-1}$ and $\hat{K}_{m,n-1}$ are the normal and skew multipole strengths of order $n-1$ in element m. The parity selector is

$$\Omega(i) = \begin{cases} 1, & \text{if } i \text{ is even,} \\ 0, & \text{if } i \text{ is odd.} \end{cases} \tag{5.4.3}$$

The phase advances between element m and observation point j follow

$$\Delta\phi_{x,mj} = \begin{cases} \phi_{x,j} - \phi_{x,m}, & \phi_{x,j} > \phi_{x,m}, \\ \phi_{x,j} - \phi_{x,m} + 2\pi Q_x, & \phi_{x,j} < \phi_{x,m}, \end{cases} \tag{5.4.4}$$

$$\Delta\phi_{y,mj} = \begin{cases} \phi_{y,j} - \phi_{y,m}, & \phi_{y,j} > \phi_{y,m}, \\ \phi_{y,j} - \phi_{y,m} + 2\pi Q_y, & \phi_{y,j} < \phi_{y,m}. \end{cases} \tag{5.4.5}$$

Note that $h_{m,pqrt}$ in Eq. (5.4.2) is a Hamiltonian coefficient and shall not be confused with the complex Courant–Snyder coordinates $h_{x,y}$ appearing in Eqs. (5.3.1)–(5.3.2).

5.5 Feed-down and misalignments

When evaluating RDTs, the multipole strengths must be taken on the closed orbit and corrected for magnet tilts and transverse shifts. Using the complex transverse

coordinate $z = x + iy$ (lab frame), the normalized longitudinal potential is

$$a_s(z) = -\Re\left[\sum_{n=0}^{\infty} \frac{K_n + i\hat{K}_n}{(n+1)!}\, z^{n+1}\right], \tag{5.5.1}$$

where K_n and $\hat{K}_n$ are the normal and skew multipole coefficients of order n (dipole $n = 0$, quadrupole $n = 1$, etc.) in the magnet reference frame. We consider a magnet whose center is transversely shifted by $\Delta = \Delta x + i\Delta y$ and tilted by an angle ψ around the longitudinal axis (positive ψ rotates the magnet frame counter-clockwise relative to the lab frame).

5.5.1 Coordinate transformation

From the lab coordinate z, the coordinate in the magnet frame is obtained by first translating by $-\Delta$ and then rotating by $-\psi$:

$$z_{\text{mag}} = e^{-i\psi}\,(z - \Delta). \tag{5.5.2}$$

Substituting (5.5.2) into (5.5.1) gives

$$a_s(z) = -\Re\left[\sum_{n=0}^{\infty} \frac{K_n + i\hat{K}_n}{(n+1)!}\, e^{-i(n+1)\psi}\,(z - \Delta)^{n+1}\right]. \tag{5.5.3}$$

5.5.2 Feed-down expansion

Expanding the shifted power with the binomial theorem,

$$(z - \Delta)^{n+1} = \sum_{m=0}^{n+1} \binom{n+1}{m+1} z^{m+1} (-\Delta)^{n-m}, \tag{5.5.4}$$

and re-collecting terms proportional to z^{m+1}, we write

$$a_s(z) = -\Re\left[\sum_{m=0}^{\infty} \frac{K'_m + i\hat{K}'_m}{(m+1)!}\, z^{m+1}\right], \tag{5.5.5}$$

with effective (feed-down) multipole coefficients

$$K'_m + i\hat{K}'_m = \sum_{n=m}^{\infty} \frac{K_n + i\hat{K}_n}{(n-m)!}\,(-\Delta)^{n-m}\, e^{-i(n+1)\psi}. \tag{5.5.6}$$

Expressing the transverse shift in the magnet frame, $\tilde{\Delta} = e^{-i\psi}\Delta$, and using $n = m + p$ gives

$$K'_m + i\hat{K}'_m = e^{-i(m+1)\psi} \sum_{p=0}^{\infty} \frac{K_{m+p} + i\hat{K}_{m+p}}{p!}\,(-\tilde{\Delta})^{p}. \tag{5.5.7}$$

5.5.3 Expansion around a closed orbit x_0, y_0

Let $z_0 = x_0 + iy_0$ denote the closed orbit in the lab frame and write $z = z_0 + u$, where u is the small transverse excursion. The magnet-frame coordinate becomes

$$z_{\text{mag}} = e^{-i\psi}\,(z_0 - \Delta + u) = \tilde{b} + e^{-i\psi}u, \quad \text{with} \quad \tilde{b} \equiv e^{-i\psi}(z_0 - \Delta). \tag{5.5.8}$$

Expanding the potential in powers of u as in (5.5.5) yields effective multipoles around the closed orbit:

$$K_m^{(\text{orb})} + i\hat{K}_m^{(\text{orb})} = e^{-i(m+1)\psi} \sum_{p=0}^{\infty} \frac{K_{m+p} + i\hat{K}_{m+p}}{p!}\,(\tilde{b})^{\,p}. \tag{5.5.9}$$

This is the same feed-down structure as (5.5.7), with $\tilde{\Delta}$ replaced by the orbit-corrected offset $\tilde{b} = e^{-i\psi}(z_0 - \Delta)$. For $z_0 = 0$ the result reduces to (5.5.7); for a centered magnet ($\Delta = 0$), $\tilde{b}$ captures the intrinsic feed-down from the closed-orbit displacement.

Chapter 6

Linear coupling

6.1 Scope and conventions

We restrict the discussion to the transverse canonical phase-space vector

$$\boldsymbol{z} = (x, p_x, y, p_y)^T, \tag{6.1.1}$$

with symplectic matrix

$$\boldsymbol{S} = \mathrm{diag}(\boldsymbol{J}, \boldsymbol{J}), \qquad \boldsymbol{J} = \begin{pmatrix} 0 & 1 \\ -1 & 0 \end{pmatrix}. \tag{6.1.2}$$

The one-turn map is assumed stable and symplectic. Mode 1 is labeled horizontal-like and mode 2 vertical-like. A superscript $*$ denotes complex conjugation. Following the notation of the Xsuite physics manual, for a real 2×2 matrix A we write

$$\bar{A} \equiv -\boldsymbol{J} A^T \boldsymbol{J} \tag{6.1.3}$$

for its symplectic conjugate; the overbar must not be confused with complex conjugation.
The exact matrix relations below apply to a purely transverse 4×4 symplectic problem. Longitudinal coupling, radiation damping, non-symplectic maps, and the distinction between canonical momentum and geometric slope require additional terms. The complex-variable and RDT signs follow the convention introduced in chapter 5.

6.2 Turn-by-turn motion in the Mais–Ripken formalism

6.2.1 Linear normal form and the W matrix

At observation point s, let $R(s)$ be the one-turn map. Its real linear normal form is written as

$$R(s) = W(s)\, R_{\mathrm{rot}}(\mu_1, \mu_2)\, W^{-1}(s), \tag{6.2.1}$$

where

$$R_{\mathrm{rot}}(\mu_1,\mu_2)=\mathrm{diag}(R_2(\mu_1),R_2(\mu_2))\,,\qquad R_2(\mu)=\begin{pmatrix}\cos\mu & \sin\mu\\ -\sin\mu & \cos\mu\end{pmatrix}, \tag{6.2.2}$$

and

$$W^T\boldsymbol{S}W=\boldsymbol{S}. \tag{6.2.3}$$

The normal-mode phases at turn N are

$$\Phi_j(N)=2\pi Q_jN+\phi_{j0},\qquad j=1,2. \tag{6.2.4}$$

Using actions J_j, the normalized mode coordinates are chosen as

$$\widehat{\boldsymbol{z}}(N)=\begin{pmatrix}\sqrt{2J_1}\cos\Phi_1\\ -\sqrt{2J_1}\sin\Phi_1\\ \sqrt{2J_2}\cos\Phi_2\\ -\sqrt{2J_2}\sin\Phi_2\end{pmatrix},\qquad \boldsymbol{z}(N)=W\widehat{\boldsymbol{z}}(N). \tag{6.2.5}$$

Define the complex eigenvectors

$$\boldsymbol{v}_j=W_{:,2j-1}+\mathrm{i}W_{:,2j}. \tag{6.2.6}$$

Then the complete turn-by-turn orbit is

$$\boxed{\boldsymbol{z}(N)=\sum_{j=1}^{2}\sqrt{2J_j}\;\mathrm{Re}\left[\boldsymbol{v}_j\mathrm{e}^{\mathrm{i}\Phi_j(N)}\right].} \tag{6.2.7}$$

This form is independent of the phase gauge used for each eigenvector, provided the same gauge is used consistently in W and in Φ_j.

6.2.2 Mais–Ripken lattice functions from W

Partition W into 2×2 blocks by physical plane and normal mode,

$$W=\begin{pmatrix}W_{x1} & W_{x2}\\ W_{y1} & W_{y2}\end{pmatrix}. \tag{6.2.8}$$

For $q\in\{x,y\}$ and $j\in\{1,2\}$, define the projected mode matrix

$$\Sigma_{qj}\equiv W_{qj}W_{qj}^T=\begin{pmatrix}\beta_{qj} & -\alpha_{qj}\\ -\alpha_{qj} & \gamma_{qj}\end{pmatrix}. \tag{6.2.9}$$

Equivalently, if the two columns of W_{qj} are denoted by $(w_{q,2j-1},w_{q,2j})$ and $(w_{p_q,2j-1},w_{p_q,2j})$, then

$$\beta_{qj}=w_{q,2j-1}^2+w_{q,2j}^2, \tag{6.2.10}$$

$$\alpha_{qj} = -w_{q,2j-1}w_{p_q,2j-1} - w_{q,2j}w_{p_q,2j}, \tag{6.2.11}$$

$$\gamma_{qj} = w^2_{p_q,2j-1} + w^2_{p_q,2j}. \tag{6.2.12}$$

Unlike an uncoupled Courant–Snyder triplet, an individual projected triplet need not satisfy $\beta\gamma - \alpha^2 = 1$. These projected functions are the Mais–Ripken lattice functions [26, 27].
Writing

$$v_{qj} = W_{q,2j-1} + \mathrm{i}W_{q,2j} = \sqrt{\beta_{qj}}\mathrm{e}^{\mathrm{i}\chi_{qj}}, \tag{6.2.13}$$

the position and canonical-momentum signals are

$$q(N) = \sum_{j=1}^{2} \sqrt{2J_j\beta_{qj}}\cos\left(\Phi_j + \chi_{qj}\right), \tag{6.2.14}$$

$$p_q(N) = \sum_{j=1}^{2} \sqrt{2J_j\gamma_{qj}}\cos\left(\Phi_j + \chi_{p_qj}\right), \tag{6.2.15}$$

where $\chi_{p_qj} = \arg(W_{p_q,2j-1} + \mathrm{i}W_{p_q,2j})$. To avoid confusion with the ET normalizing matrices A_q, let $\mathcal{A}_u(Q_j)$ denote the amplitude of the Fourier line at tune Q_j in a signal $u(N)$. The position and canonical-momentum line amplitudes are therefore

$$\mathcal{A}_q(Q_j) = \sqrt{2J_j\beta_{qj}}, \qquad \mathcal{A}_{p_q}(Q_j) = \sqrt{2J_j\gamma_{qj}}. \tag{6.2.16}$$

6.2.3 Closest-tune-approach indicator

A commonly used global coupling indicator can be obtained from the relative amplitudes and phases of the two tune lines [28, 29]. For the horizontal-like and vertical-like modes, respectively, define

$$r_1 \equiv \frac{\mathcal{A}_y(Q_1)}{\mathcal{A}_x(Q_1)} = \sqrt{\frac{\beta_{y1}}{\beta_{x1}}}, \qquad r_2 \equiv \frac{\mathcal{A}_x(Q_2)}{\mathcal{A}_y(Q_2)} = \sqrt{\frac{\beta_{x2}}{\beta_{y2}}}, \tag{6.2.17}$$

and the cross-plane phase differences

$$\Delta\phi_1 = \chi_{y1} - \chi_{x1}, \qquad \Delta\phi_2 = \chi_{x2} - \chi_{y2}. \tag{6.2.18}$$

The closest-tune-approach magnitude is then [29]

$$\left|C^-\right| = \frac{2\sqrt{r_1r_2}\,|Q_1 - Q_2|}{1 + r_1r_2}. \tag{6.2.19}$$

Together with $\chi(s) = \Delta\phi_1(s)$, this defines the local complex quantity

$$C^-(s) = |C^-|\mathrm{e}^{\mathrm{i}\chi(s)}. \tag{6.2.20}$$

Only its phase depends on the observation point s. In first-order perturbation theory it is related to the skew-quadrupole distribution by

$$C^- = \frac{1}{2\pi}\int_0^L \sqrt{\beta_x\beta_y}\,k_s\mathrm{e}^{\mathrm{i}[\Phi_x - \Phi_y - 2\pi\Delta s/L]}\,\mathrm{d}l, \tag{6.2.21}$$

where Δ is the difference of the uncoupled fractional tunes. For a more robust scalar estimate, equation (6.2.19) can be evaluated at every observation point and averaged around the ring [30].

6.3 Edwards–Teng decoupling and modal Twiss parameters

6.3.1 Decoupled modal maps

The Edwards–Teng construction decouples the physical four-dimensional map into two stable two-dimensional modal maps [31, 32, 33]. Following the notation used throughout this manual, partition the one-turn map as

$$R = \begin{pmatrix} A & B \\ C & D \end{pmatrix}, \tag{6.3.1}$$

and denote the horizontal-like and vertical-like decoupled maps by E and F, respectively. The purpose of the Edwards–Teng transformation is to find a symplectic matrix T_{ET} such that

$$T_{\mathrm{ET}}^{-1} R T_{\mathrm{ET}} = \begin{pmatrix} E & 0 \\ 0 & F \end{pmatrix}, \tag{6.3.2}$$

or, equivalently,

$$R = T_{\mathrm{ET}} \begin{pmatrix} E & 0 \\ 0 & F \end{pmatrix} T_{\mathrm{ET}}^{-1}. \tag{6.3.3}$$

Thus E and F are the diagonal blocks of the transformed, decoupled map; in a coupled lattice they are not the physical diagonal blocks A and D of R.
Here and below,

$$I_2 = \begin{pmatrix} 1 & 0 \\ 0 & 1 \end{pmatrix} \tag{6.3.4}$$

denotes the 2×2 identity matrix. In the Edwards–Teng convention used here [31], the decoupling matrix is parametrized as

$$T_{\mathrm{ET}} = g \begin{pmatrix} I_2 & \bar{R}_{\mathrm{ET}} \\ -R_{\mathrm{ET}} & I_2 \end{pmatrix}, \qquad g = \frac{1}{\sqrt{1 + \det R_{\mathrm{ET}}}} > 0. \tag{6.3.5}$$

We now derive R_{ET} from the physical map. Extend the symplectic conjugate to the full four-dimensional map. Since R is symplectic,

$$\overline{R} \equiv -\boldsymbol{S} R^T \boldsymbol{S} = R^{-1}. \tag{6.3.6}$$

For any real 2×2 matrix Z,

$$Z + \bar{Z} = (\operatorname{tr} Z) I_2, \qquad \bar{Z} Z = Z \bar{Z} = (\det Z) I_2. \tag{6.3.7}$$

The reason for considering $R + \overline{R}$ is that it exposes the ET modal planes. Indeed, using equation (6.3.3) and $\overline{R} = R^{-1}$ gives

$$R + \overline{R} = T_{\mathrm{ET}} \begin{pmatrix} E + E^{-1} & 0 \\ 0 & F + F^{-1} \end{pmatrix} T_{\mathrm{ET}}^{-1}. \tag{6.3.8}$$

Because E and F are 2×2 symplectic matrices, equation (6.3.7) implies

$$E + E^{-1} = (\operatorname{tr} E) I_2, \qquad F + F^{-1} = (\operatorname{tr} F) I_2. \tag{6.3.9}$$

Consequently, provided $\operatorname{tr} E \neq \operatorname{tr} F$, the two eigenspaces of $R + \overline{R}$ are precisely the two ET modal planes. The first block column of equation (6.3.5) shows that every vector in the horizontal-like plane has the form

$$T_{\mathrm{ET}} \begin{pmatrix} \boldsymbol{x} \\ 0 \end{pmatrix} = g \begin{pmatrix} \boldsymbol{x} \\ -R_{\mathrm{ET}} \boldsymbol{x} \end{pmatrix}. \tag{6.3.10}$$

Thus, if an eigenvector of $R + \overline{R}$ in this plane is written as $(\boldsymbol{x}, \boldsymbol{y})^T$, its two blocks satisfy

$$\boldsymbol{y} = -R_{\mathrm{ET}} \boldsymbol{x}. \tag{6.3.11}$$

We can therefore obtain R_{ET} by calculating the same eigenspace directly from the physical blocks of R and comparing its $\boldsymbol{y}$ and $\boldsymbol{x}$ components.
Therefore, on defining

$$a \equiv \operatorname{tr} A, \qquad d \equiv \operatorname{tr} D, \qquad X \equiv C + \bar{B}, \tag{6.3.12}$$

one obtains

$$R + \overline{R} = \begin{pmatrix} A + \bar{A} & B + \bar{C} \\ C + \bar{B} & D + \bar{D} \end{pmatrix} = \begin{pmatrix} a I_2 & \bar{X} \\ X & d I_2 \end{pmatrix}. \tag{6.3.13}$$

Let Λ be an eigenvalue of $R + \overline{R}$ and write a corresponding two-block eigenvector as $(\boldsymbol{x}, \boldsymbol{y})^T$. Equation (6.3.13) gives

$$(a - \Lambda)\boldsymbol{x} + \bar{X}\boldsymbol{y} = 0, \tag{6.3.14}$$

$$X\boldsymbol{x} + (d - \Lambda)\boldsymbol{y} = 0. \tag{6.3.15}$$

For $\Lambda \neq d$, the second equation gives

$$\boldsymbol{y} = \frac{X}{\Lambda - d} \boldsymbol{x}. \tag{6.3.16}$$

Substitution into the first equation, together with $\bar{X}X = (\det X) I_2$, yields the scalar characteristic equation

$$(a - \Lambda)(d - \Lambda) - \det X = 0. \tag{6.3.17}$$

Expanding the product makes this an ordinary quadratic equation in Λ:

$$\Lambda^2 - (a + d)\Lambda + ad - \det X = 0. \tag{6.3.18}$$

The quadratic formula therefore gives

$$\Lambda_{\pm} = \frac{a + d \pm \sqrt{(a + d)^2 - 4(ad - \det X)}}{2}$$

$$= \frac{a+d}{2} \pm \sqrt{\Delta}, \qquad \Delta \equiv \frac{1}{4}(a-d)^2 + \det X, \tag{6.3.19}$$

where the second line follows because

$$(a+d)^2 - 4(ad - \det X) = (a-d)^2 + 4\det X = 4\Delta. \tag{6.3.20}$$

The horizontal-like root must approach $a = \operatorname{tr} A$ when the coupling block X tends to zero. In that limit $\det X \to 0$ and hence

$$\sqrt{\Delta} \longrightarrow \frac{|a-d|}{2}. \tag{6.3.21}$$

Consequently, the sign that selects the horizontal-like root depends on the ordering of a and d:

$$\begin{aligned} a > d: &\qquad \Lambda_+ \longrightarrow a, \quad \Lambda_- \longrightarrow d, \\ a < d: &\qquad \Lambda_- \longrightarrow a, \quad \Lambda_+ \longrightarrow d. \end{aligned} \tag{6.3.22}$$

Both cases are encoded by $\operatorname{sign}(a-d)$. Thus, for $a \neq d$,

$$\begin{aligned} \Lambda_1 &= \frac{a+d}{2} + \operatorname{sign}(a-d)\sqrt{\Delta}, \quad \Lambda_1 - d = \frac{a-d}{2} + \operatorname{sign}(a-d)\sqrt{\Delta}, \\ \Lambda_2 &= \frac{a+d}{2} - \operatorname{sign}(a-d)\sqrt{\Delta}, \quad \Lambda_2 - a = \frac{d-a}{2} - \operatorname{sign}(a-d)\sqrt{\Delta}. \end{aligned} \tag{6.3.23}$$

The first modal subspace in T_{ET} consists of vectors $(\boldsymbol{x}, -R_{\mathrm{ET}}\boldsymbol{x})^T$. Comparing this with equation (6.3.16) for $\Lambda = \Lambda_1$ therefore gives

$$\boxed{R_{\mathrm{ET}} = -\left[\frac{1}{2}(\operatorname{tr} A - \operatorname{tr} D) + \operatorname{sign}(\operatorname{tr} A - \operatorname{tr} D)\sqrt{\Delta}\right]^{-1}(C + \bar{B}).} \tag{6.3.24}$$

This eigenvector construction also proves the block diagonalization. Indeed, R commutes with $R + R^{-1}$, so each nondegenerate eigenspace of $R + R^{-1}$ is invariant under R. Writing $K = R_{\mathrm{ET}}$, invariance of the first subspace gives

$$R\begin{pmatrix} I_2 \\ -K \end{pmatrix} = \begin{pmatrix} I_2 \\ -K \end{pmatrix} E, \qquad E = A - BK, \tag{6.3.25}$$

whose lower block is the matrix Riccati equation

$$C + KA - DK - KBK = 0. \tag{6.3.26}$$

The second modal eigenspace similarly gives

$$R\begin{pmatrix} \bar{K} \\ I_2 \end{pmatrix} = \begin{pmatrix} \bar{K} \\ I_2 \end{pmatrix} F, \qquad F = D + C\bar{K} = D + KB. \tag{6.3.27}$$

The equality $C\bar{K} = KB$ follows from $K = -X/(\Lambda_1 - d)$ and $\det B = \det C$. The latter is itself an immediate consequence of the symplectic block identities $A\bar{A} + B\bar{B} = I_2 =$

$A\bar{A} + C\bar{C}$ and equation (6.3.7). The two block columns in these equations are precisely the two block columns of T_{ET}/g, so together they imply equation (6.3.2). Moreover,

$$\left(\frac{T_{\mathrm{ET}}}{g}\right)^{T} \boldsymbol{S} \left(\frac{T_{\mathrm{ET}}}{g}\right) = (1 + \det K)\, \boldsymbol{S}, \tag{6.3.28}$$

which explains the normalization $g = (1 + \det K)^{-1/2}$ in equation (6.3.5). At a degeneracy the separation into the two modal subspaces is not unique, and the branch must instead be selected by continuity from a neighboring lattice point. By construction, T_{ET} maps modal coordinates $\boldsymbol{z}_{\mathrm{ET}}$ to physical coordinates $\boldsymbol{z}$:

$$\boldsymbol{z} = T_{\mathrm{ET}} \boldsymbol{z}_{\mathrm{ET}}. \tag{6.3.29}$$

Write the two stable modal maps as

$$E = A_x R_2(\mu_1) A_x^{-1}, \qquad F = A_y R_2(\mu_2) A_y^{-1}, \tag{6.3.30}$$

where R_2 is the rotation matrix defined above and

$$A_q = \begin{pmatrix} \sqrt{\beta_q} & 0 \\ -\alpha_q/\sqrt{\beta_q} & 1/\sqrt{\beta_q} \end{pmatrix}. \tag{6.3.31}$$

For $q \in \{x, y\}$, set $\gamma_q = (1 + \alpha_q^2)/\beta_q$. The entries of the horizontal-like map are then

$$E = \begin{pmatrix} E_{11} & E_{12} \\ E_{21} & E_{22} \end{pmatrix} = \begin{pmatrix} \cos\mu_1 + \alpha_x \sin\mu_1 & \beta_x \sin\mu_1 \\ -\gamma_x \sin\mu_1 & \cos\mu_1 - \alpha_x \sin\mu_1 \end{pmatrix}. \tag{6.3.32}$$

Consequently, its phase advance and Twiss parameters can be recovered directly from E:

$$\cos\mu_1 = \frac{1}{2}\operatorname{tr} E, \tag{6.3.33}$$

$$\sin\mu_1 = \operatorname{sign}(E_{12}) \sqrt{-E_{12}E_{21} - \left(\frac{E_{11} - E_{22}}{2}\right)^2}, \tag{6.3.34}$$

$$\beta_x = \frac{E_{12}}{\sin\mu_1}, \qquad \gamma_x = -\frac{E_{21}}{\sin\mu_1}, \quad \alpha_x = \frac{E_{11} - E_{22}}{2\sin\mu_1}. \tag{6.3.35}$$

The vertical-like quantities follow from the same equations with $E \to F$, $(\beta_x, \alpha_x, \gamma_x) \to (\beta_y, \alpha_y, \gamma_y)$, and $\mu_1 \to \mu_2$.

Following the propagation subsection of the Xsuite physics manual, the Edwards–Teng Twiss parameters are denoted by (β_x, α_x) for the horizontal-like mode and (β_y, α_y) for the vertical-like mode. They are not the projected Mais–Ripken functions $(\beta_{x1}, \alpha_{x1})$ and $(\beta_{y2}, \alpha_{y2})$.

The inverse of the normalizing matrix is

$$A_q^{-1} = \begin{pmatrix} \beta_q^{-1/2} & 0 \\ \alpha_q \beta_q^{-1/2} & \beta_q^{1/2} \end{pmatrix} \tag{6.3.36}$$

and maps physical modal coordinates in plane q to Edwards–Teng normalized coordinates:

$$\begin{pmatrix} \widetilde{q} \\ \widetilde{p}_q \end{pmatrix} = A_q^{-1} \begin{pmatrix} q \\ p_q \end{pmatrix}. \tag{6.3.37}$$

In the uncoupled limit, these modal Twiss parameters reduce to the usual horizontal and vertical Courant–Snyder Twiss parameters.

6.3.2 Relation between W and the Edwards–Teng transformation

The matrix A_q^{-1} maps modal coordinates to normalized coordinates, whereas A_q performs the inverse operation. Throughout this subsection and all that follows, we assume that the phases of the two transverse eigenvectors of W have already been chosen such that $v_{1,x}$ and $v_{2,y}$ are real and positive. With

$$\boldsymbol{v}_1 = W_{:,1} + \mathrm{i}W_{:,2}, \qquad \boldsymbol{v}_2 = W_{:,3} + \mathrm{i}W_{:,4}, \tag{6.3.38}$$

this means explicitly

$$\mathrm{Im}(v_{1,x}) = 0, \qquad \mathrm{Re}(v_{1,x}) > 0, \qquad \mathrm{Im}(v_{2,y}) = 0, \qquad \mathrm{Re}(v_{2,y}) > 0. \tag{6.3.39}$$

This is the Edwards–Teng phase gauge used in the implementation.
We shall now prove that this phase choice makes the normalized coordinates associated with W and with the ET construction identical. Initially denote them separately by

$$\widehat{\boldsymbol{z}}_W = W^{-1}\boldsymbol{z}, \qquad \widehat{\boldsymbol{z}}_{\mathrm{ET}} = \mathrm{diag}(A_x^{-1}, A_y^{-1})T_{\mathrm{ET}}^{-1}\boldsymbol{z}. \tag{6.3.40}$$

Define

$$\mathcal{A} \equiv \mathrm{diag}(A_x, A_y), \qquad U \equiv T_{\mathrm{ET}}\mathcal{A}. \tag{6.3.41}$$

The second definition in equation (6.3.40) is then equivalent to

$$\boldsymbol{z} = U\widehat{\boldsymbol{z}}_{\mathrm{ET}}. \tag{6.3.42}$$

Both U and W reduce the physical map to the same block rotation. To see this explicitly, use $U^{-1} = \mathcal{A}^{-1}T_{\mathrm{ET}}^{-1}$ and substitute the ET block-diagonalization from equation (6.3.2):

$$\begin{aligned} U^{-1}RU &= \mathcal{A}^{-1}T_{\mathrm{ET}}^{-1}RT_{\mathrm{ET}}\mathcal{A} \\ &= \mathcal{A}^{-1}\,\mathrm{diag}(E,F)\mathcal{A} \\ &= \mathrm{diag}(A_x^{-1}EA_x, A_y^{-1}FA_y) \\ &= \mathrm{diag}(R_2(\mu_1), R_2(\mu_2)) \\ &= R_{\mathrm{rot}}(\mu_1,\mu_2). \end{aligned} \tag{6.3.43}$$

The penultimate equality follows directly from $E = A_xR_2(\mu_1)A_x^{-1}$ and $F = A_yR_2(\mu_2)A_y^{-1}$ in equation (6.3.30). Likewise, equation (6.2.1) gives

$$W^{-1}RW = R_{\mathrm{rot}}(\mu_1,\mu_2). \tag{6.3.44}$$

Define the change of normalized basis

$$D \equiv U^{-1}W \tag{6.3.45}$$

so that $W = UD$. Substituting this relation into the preceding normal-form equation gives

$$\begin{aligned} R_{\mathrm{rot}}(\mu_1, \mu_2) &= W^{-1}RW \\ &= (UD)^{-1}R(UD) \\ &= D^{-1}(U^{-1}RU)D \\ &= D^{-1}R_{\mathrm{rot}}(\mu_1, \mu_2)D. \end{aligned} \tag{6.3.46}$$

Multiplication from the left by D therefore shows explicitly that D commutes with the block rotation:

$$DR_{\mathrm{rot}}(\mu_1, \mu_2) = R_{\mathrm{rot}}(\mu_1, \mu_2)D. \tag{6.3.47}$$

For distinct, nondegenerate tunes and a fixed ordering of the two modes, a symplectic matrix with this property consists of an independent phase rotation in each mode:

$$D = \mathrm{diag}(R_2(\delta_1), R_2(\delta_2))\,. \tag{6.3.48}$$

It follows from $W = UD$ that the two normalized vectors are related by

$$\widehat{\boldsymbol{z}}_{\mathrm{ET}} = D\widehat{\boldsymbol{z}}_W. \tag{6.3.49}$$

It remains to use the phase convention in equation (6.3.39) to determine D.
Substituting the explicit form of T_{ET} from equation (6.3.5) into the definition of U in equation (6.3.41) shows that its upper-left and lower-right blocks are gA_x and gA_y, respectively. Because the first row of each A_q is $(\sqrt{\beta_q}, 0)$, the corresponding complex position components of U are the positive real numbers $g\sqrt{\beta_x}$ and $g\sqrt{\beta_y}$. Right multiplication of a real column pair by $R_2(\delta)$ multiplies its associated complex vector by $e^{\mathrm{i}\delta}$. Since $W = UD$, it follows that

$$v_{1,x} = g\sqrt{\beta_x}\, e^{\mathrm{i}\delta_1}, \qquad v_{2,y} = g\sqrt{\beta_y}\, e^{\mathrm{i}\delta_2}. \tag{6.3.50}$$

The factors $g\sqrt{\beta_x}$ and $g\sqrt{\beta_y}$ are positive. Since the left-hand sides are also real and positive by equation (6.3.39),

$$e^{\mathrm{i}\delta_1} = e^{\mathrm{i}\delta_2} = 1, \qquad D = \mathrm{diag}(I_2, I_2). \tag{6.3.51}$$

Therefore $W = UD = U$, and equation (6.3.49) gives

$$\boxed{\widehat{\boldsymbol{z}}_{\mathrm{ET}} = \widehat{\boldsymbol{z}}_W \equiv \widehat{\boldsymbol{z}}.} \tag{6.3.52}$$

Finally, $W = U$ and equation (6.3.41) give

$$\boxed{W = T_{\mathrm{ET}}\,\mathrm{diag}(A_x, A_y).} \tag{6.3.53}$$

All equations below that involve the individual columns or blocks of W use this explicitly rephased matrix. Substituting the explicit ET matrix from equation (6.3.5) into equation (6.3.53) first gives

$$\begin{aligned} W &= g \begin{pmatrix} I_2 & \bar{R}_{\mathrm{ET}} \\ -R_{\mathrm{ET}} & I_2 \end{pmatrix} \begin{pmatrix} A_x & 0 \\ 0 & A_y \end{pmatrix} \\ &= \begin{pmatrix} gA_x & g\bar{R}_{\mathrm{ET}}A_y \\ -gR_{\mathrm{ET}}A_x & gA_y \end{pmatrix}. \end{aligned} \tag{6.3.54}$$

To factor the modal normalizers A_x and A_y from the left, define the ET-normalized coupling matrix

$$\boxed{\mathcal{C} = gA_x^{-1}\bar{R}_{\mathrm{ET}}A_y.} \tag{6.3.55}$$

The upper-right block in equation (6.3.54) is consequently

$$A_x\mathcal{C} = g\bar{R}_{\mathrm{ET}}A_y. \tag{6.3.56}$$

For the lower-left block, use

$$\overline{PQ} = \bar{Q}\,\bar{P}, \qquad \overline{\bar{R}_{\mathrm{ET}}} = R_{\mathrm{ET}}, \qquad \bar{A}_q = A_q^{-1}, \tag{6.3.57}$$

where the last identity follows because A_q is symplectic. Taking the symplectic conjugate of equation (6.3.55) gives

$$\begin{aligned} \bar{\mathcal{C}} &= g\overline{A_x^{-1}\bar{R}_{\mathrm{ET}}A_y} \\ &= gA_y^{-1}R_{\mathrm{ET}}A_x, \end{aligned} \tag{6.3.58}$$

and therefore

$$A_y\bar{\mathcal{C}} = gR_{\mathrm{ET}}A_x. \tag{6.3.59}$$

Using these two block identities, equation (6.3.54) becomes

$$\boxed{W = \begin{pmatrix} A_x & 0 \\ 0 & A_y \end{pmatrix} \begin{pmatrix} gI_2 & \mathcal{C} \\ -\bar{\mathcal{C}} & gI_2 \end{pmatrix}.} \tag{6.3.60}$$

Symplecticity requires

$$g^2 + \det\mathcal{C} = 1. \tag{6.3.61}$$

Equivalently, if W is partitioned as in equation (6.3.60), its phase-gauged blocks obey

$$\boxed{A_x^{-1}W_{x1} = gI_2, \qquad A_x^{-1}W_{x2} = \mathcal{C}, \qquad A_y^{-1}W_{y1} = -\bar{\mathcal{C}}, \qquad A_y^{-1}W_{y2} = gI_2.} \tag{6.3.62}$$

For later use, define

$$u \equiv \det\mathcal{C} = \frac{\det R_{\mathrm{ET}}}{1 + \det R_{\mathrm{ET}}} = 1 - g^2. \tag{6.3.63}$$

For the ordinary trigonometric ET branch, $u = \sin^2\phi$ and $g^2 = \cos^2\phi$, where ϕ is the Teng rotation angle.

6.3.3 Relation between Edwards–Teng and Mais–Ripken functions

Using the definition $\Sigma_{qj} = W_{qj}W_{qj}^T$ from equation (6.2.9) and substituting the four blocks of W from equation (6.3.60) gives

$$\Sigma_{x1} = g^2 A_x A_x^T, \qquad \Sigma_{x2} = A_x \mathcal{C}\mathcal{C}^T A_x^T, \tag{6.3.64}$$

$$\Sigma_{y1} = A_y \bar{\mathcal{C}}(\bar{\mathcal{C}})^T A_y^T, \qquad \Sigma_{y2} = g^2 A_y A_y^T. \tag{6.3.65}$$

The principal Mais–Ripken functions are therefore

$$\beta_{x1} = g^2\beta_x, \qquad \alpha_{x1} = g^2\alpha_x, \qquad \gamma_{x1} = g^2\gamma_x, \tag{6.3.66}$$

$$\beta_{y2} = g^2\beta_y, \qquad \alpha_{y2} = g^2\alpha_y, \qquad \gamma_{y2} = g^2\gamma_y. \tag{6.3.67}$$

The determinant of either principal projected block is therefore

$$\beta_{x1}\gamma_{x1} - \alpha_{x1}^2 = \beta_{y2}\gamma_{y2} - \alpha_{y2}^2 = g^4. \tag{6.3.68}$$

Consequently, g is obtained directly from the principal Mais–Ripken functions:

$$\boxed{g^2 = \sqrt{\beta_{x1}\gamma_{x1} - \alpha_{x1}^2} = \sqrt{\beta_{y2}\gamma_{y2} - \alpha_{y2}^2}.} \tag{6.3.69}$$

The ET modal Twiss parameters then follow by division by g^2:

$$\boxed{\beta_x = \frac{\beta_{x1}}{g^2}, \quad \alpha_x = \frac{\alpha_{x1}}{g^2}, \qquad \beta_y = \frac{\beta_{y2}}{g^2}, \quad \alpha_y = \frac{\alpha_{y2}}{g^2}.} \tag{6.3.70}$$

To make the remaining Mais–Ripken functions equally explicit, write

$$\mathcal{C} = \begin{pmatrix} c_{11} & c_{12} \\ c_{21} & c_{22} \end{pmatrix}. \tag{6.3.71}$$

Then

$$\beta_{x2} = \beta_x(c_{11}^2 + c_{12}^2), \tag{6.3.72}$$

$$\alpha_{x2} = \alpha_x(c_{11}^2 + c_{12}^2) - (c_{11}c_{21} + c_{12}c_{22}), \tag{6.3.73}$$

$$\gamma_{x2} = \frac{(c_{21} - \alpha_x c_{11})^2 + (c_{22} - \alpha_x c_{12})^2}{\beta_x}, \tag{6.3.74}$$

and, since

$$-\bar{\mathcal{C}} = \begin{pmatrix} -c_{22} & c_{12} \\ c_{21} & -c_{11} \end{pmatrix}, \tag{6.3.75}$$

one also has

$$\beta_{y1} = \beta_y(c_{22}^2 + c_{12}^2), \tag{6.3.76}$$

$$\alpha_{y1} = \alpha_y(c_{22}^2 + c_{12}^2) + c_{21}c_{22} + c_{11}c_{12}, \tag{6.3.77}$$

$$\gamma_{y1} = \frac{(c_{21} + \alpha_y c_{22})^2 + (c_{11} + \alpha_y c_{12})^2}{\beta_y}. \tag{6.3.78}$$

The cross-plane projected determinants satisfy

$$\begin{aligned} \beta_{x2}\gamma_{x2} - \alpha_{x2}^2 &= \beta_{y1}\gamma_{y1} - \alpha_{y1}^2 \\ &= (1 - g^2)^2. \end{aligned} \tag{6.3.79}$$

6.3.4 Propagation of Edwards–Teng parameters

Let the transfer map from location a to location b be partitioned as

$$R^{ab} = \begin{pmatrix} A^{ab} & B^{ab} \\ C^{ab} & D^{ab} \end{pmatrix}. \tag{6.3.80}$$

Given the ET quantities E^a, F^a, and R^a_{ET} at a, define the two effective modal transfer matrices

$$E^{ab} = A^{ab} - B^{ab} R^a_{\mathrm{ET}}, \tag{6.3.81}$$

$$F^{ab} = D^{ab} + C^{ab} \bar{R}^a_{\mathrm{ET}}. \tag{6.3.82}$$

The decoupled one-turn maps and the ET coupling matrix at b are then

$$E^b = E^{ab} E^a \bar{E}^{ab} / \det E^{ab}, \tag{6.3.83}$$

$$F^b = F^{ab} F^a \bar{F}^{ab} / \det F^{ab}, \tag{6.3.84}$$

$$R^b_{\mathrm{ET}} = -\left(C^{ab} - D^{ab} R^a_{\mathrm{ET}}\right) \bar{E}^{ab} / \det E^{ab}. \tag{6.3.85}$$

The factors $\bar{E}^{ab} / \det E^{ab}$ and $\bar{F}^{ab} / \det F^{ab}$ are simply $(E^{ab})^{-1}$ and $(F^{ab})^{-1}$, respectively. Writing E^{ab}_{ij} for the entries of E^{ab}, the horizontal ET Twiss parameters and phase propagate according to

$$\beta_x^b = \frac{\left(E^{ab}_{11}\beta_x^a - E^{ab}_{12}\alpha_x^a\right)^2 + \left(E^{ab}_{12}\right)^2}{\det(E^{ab})\,\beta_x^a}, \tag{6.3.86}$$

$$\alpha_x^b = -\frac{1}{\det(E^{ab})\,\beta_x^a}\left[\left(E^{ab}_{21}\beta_x^a - E^{ab}_{22}\alpha_x^a\right)\left(E^{ab}_{11}\beta_x^a - E^{ab}_{12}\alpha_x^a\right) + E^{ab}_{12}E^{ab}_{22}\right], \tag{6.3.87}$$

$$\mu_1^b = \mu_1^a + operatornameatan2\left(E^{ab}_{12}, E^{ab}_{11}\beta_x^a - E^{ab}_{12}\alpha_x^a\right), \tag{6.3.88}$$

$$\gamma_x^b = \frac{1 + (\alpha_x^b)^2}{\beta_x^b}. \tag{6.3.89}$$

The vertical formulas follow by replacing E^{ab} with F^{ab}, x with y, and mode 1 with mode 2.

6.4 Turn-by-turn motion in the RDT formalism

6.4.1 Complex Courant–Snyder coordinates

Using the Edwards–Teng normalized coordinates defined in equation (6.3.37), the complex Courant–Snyder variables are

$$h_{q,\pm} = \widetilde{q} \pm \mathrm{i}\widetilde{p}_q = \sqrt{2I_q}\mathrm{e}^{\mp \mathrm{i}\Phi_q}. \tag{6.4.1}$$

Thus $h_{q,-} = \widetilde{q} - \mathrm{i}\widetilde{p}_q$ and

$$\widetilde{q} = \mathrm{Re}(h_{q,-}), \qquad \widetilde{p}_q = -\,\mathrm{Im}(h_{q,-}). \tag{6.4.2}$$

The normal-form generating function is expanded as

$$F = \sum_{jklm} f_{jklm} h_{x,+}^{j} h_{x,-}^{k} h_{y,+}^{l} h_{y,-}^{m}. \tag{6.4.3}$$

To first order in the RDTs, the turn-by-turn motion is

$$\begin{aligned} h_{x,-}(s,N) = \sqrt{2I_x}\mathrm{e}^{\mathrm{i}\Phi_x} - 2\mathrm{i}\sum_{jklm} j f_{jklm}^{(s)} (2I_x)^{(j+k-1)/2} (2I_y)^{(l+m)/2} \\ \times \mathrm{e}^{\mathrm{i}[(1-j+k)\Phi_x + (m-l)\Phi_y]}, \end{aligned} \tag{6.4.4}$$

$$\begin{aligned} h_{y,-}(s,N) = \sqrt{2I_y}\mathrm{e}^{\mathrm{i}\Phi_y} - 2\mathrm{i}\sum_{jklm} l f_{jklm}^{(s)} (2I_x)^{(j+k)/2} (2I_y)^{(l+m-1)/2} \\ \times \mathrm{e}^{\mathrm{i}[(k-j)\Phi_x + (1-l+m)\Phi_y]}. \end{aligned} \tag{6.4.5}$$

Here $\Phi_x = 2\pi Q_x N + \psi_{x,s,0}$ and similarly for y.
At first order in lattice perturbation theory, the local RDT at observation point s can be written as

$$f_{jklm}(s) = \frac{\sum_w h_{w,jklm}\mathrm{e}^{\mathrm{i}[(j-k)\Delta\phi_{x,w\to s} + (l-m)\Delta\phi_{y,w\to s}]}}{1 - \mathrm{e}^{2\pi\mathrm{i}[(j-k)Q_x + (l-m)Q_y]}}. \tag{6.4.6}$$

The coefficient $h_{w,jklm}$ is the corresponding Hamiltonian coefficient of source w. For a thin skew quadrupole, $h_{w,1001}$ and $h_{w,1010}$ have the same local strength factor, proportional to

$$K_{1s,w}\sqrt{\beta_{x,w}\beta_{y,w}}/4;$$

their different global behavior comes from their phase factors and resonance denominators in equation (5.4.1).
In particular,

$$f_{1001}(s) = \frac{\sum_w h_{w,1001}\mathrm{e}^{\mathrm{i}(\Delta\phi_{x,w\to s} - \Delta\phi_{y,w\to s})}}{1 - \mathrm{e}^{2\pi\mathrm{i}(Q_x - Q_y)}}, \tag{6.4.7}$$

$$f_{1010}(s) = \frac{\sum_w h_{w,1010}\mathrm{e}^{\mathrm{i}(\Delta\phi_{x,w\to s} + \Delta\phi_{y,w\to s})}}{1 - \mathrm{e}^{2\pi\mathrm{i}(Q_x + Q_y)}}. \tag{6.4.8}$$

6.4.2 The four linear-coupling monomials

Reality of the Hamiltonian implies

$$f^*_{jklm} = f_{kjml}. \tag{6.4.9}$$

Hence

$$\boxed{f_{0110} = f^*_{1001}, \qquad f_{0101} = f^*_{1010}.} \tag{6.4.10}$$

In the reversed local reference frame used by Xtrack, $x \mapsto -x$, $p_x \mapsto p_x$, $y \mapsto y$, and $p_y \mapsto -p_y$. Reversal conjugates the phase factors in equations (6.4.7) and (6.4.8); at the same time the skew-quadrupole strength changes sign, $K^{\mathrm{rev}}_{1s} = -K_{1s}$. This second sign cancels the minus sign arising from the conjugated resonance denominator. Therefore

$$\begin{aligned} f^{\mathrm{rev}}_{1001} &= f^*_{1001} = f_{0110}, & f^{\mathrm{rev}}_{1010} &= f^*_{1010} = f_{0101}, \\ f^{\mathrm{rev}}_{0110} &= f_{1001}, & f^{\mathrm{rev}}_{0101} &= f_{1010}. \end{aligned} \tag{6.4.11}$$

Only terms with $j > 0$ enter $h_{x,-}$, whereas only terms with $l > 0$ enter $h_{y,-}$. Equations (6.4.4) and (6.4.5) give

$$\boxed{h_{x,-} = \sqrt{2I_x}\mathrm{e}^{\mathrm{i}\Phi_x} - 2\mathrm{i}\sqrt{2I_y}\left(f_{1001}\mathrm{e}^{\mathrm{i}\Phi_y} + f_{1010}\mathrm{e}^{-\mathrm{i}\Phi_y}\right)} \tag{6.4.12}$$

$$\boxed{h_{y,-} = \sqrt{2I_y}\mathrm{e}^{\mathrm{i}\Phi_y} - 2\mathrm{i}\sqrt{2I_x}\left(f^*_{1001}\mathrm{e}^{\mathrm{i}\Phi_x} + f_{1010}\mathrm{e}^{-\mathrm{i}\Phi_x}\right).} \tag{6.4.13}$$

The difference-resonance term f_{1001} produces the opposite-plane line with the same sign of frequency; the sum-resonance term f_{1010} produces the negative-frequency contribution. In a real position signal these two contributions interfere at the same observed tune line.

6.5 Observable position and momentum amplitudes

6.5.1 Normalized-coordinate signals

Using $\widetilde{q} = \mathrm{Re}\, h_{q,-}$ and $\widetilde{p}_q = -\,\mathrm{Im}\, h_{q,-}$, the horizontal signal becomes

$$\widetilde{x}(N) = \sqrt{2I_x}\cos\Phi_x + 2\sqrt{2I_y}\ \mathrm{Im}\left[(f_{1001} - f^*_{1010})\mathrm{e}^{\mathrm{i}\Phi_y}\right], \tag{6.5.1}$$

$$\widetilde{p}_x(N) = -\sqrt{2I_x}\sin\Phi_x + 2\sqrt{2I_y}\ \mathrm{Re}\left[(f_{1001} + f^*_{1010})\mathrm{e}^{\mathrm{i}\Phi_y}\right]. \tag{6.5.2}$$

Similarly,

$$\widetilde{y}(N) = \sqrt{2I_y}\cos\Phi_y + 2\sqrt{2I_x}\ \mathrm{Im}\left[(f^*_{1001} - f^*_{1010})\mathrm{e}^{\mathrm{i}\Phi_x}\right], \tag{6.5.3}$$

$$\widetilde{p}_y(N) = -\sqrt{2I_y}\sin\Phi_y + 2\sqrt{2I_x}\ \mathrm{Re}\left[(f^*_{1001} + f^*_{1010})\mathrm{e}^{\mathrm{i}\Phi_x}\right]. \tag{6.5.4}$$

The four basic combinations are summarized in table 6.1.

Observable	Cross-mode complex coefficient
x from mode 2	$f_{1001} - f_{1010}^{*}$
$\widetilde{p}_x$ from mode 2	$f_{1001} + f_{1010}^{*}$
y from mode 1	$(f_{1001} - f_{1010})^{*}$
$\widetilde{p}_y$ from mode 1	$(f_{1001} + f_{1010})^{*}$

Table 6.1: RDT combinations controlling the cross-plane mode projection.

For a particle carrying both mode actions, the measured position-line ratios are therefore

$$\frac{\mathcal{A}_x(Q_2)}{\mathcal{A}_x(Q_1)} = 2\sqrt{\frac{I_y}{I_x}}\,|f_{1001} - f_{1010}^{*}|, \tag{6.5.5}$$

$$\frac{\mathcal{A}_y(Q_1)}{\mathcal{A}_y(Q_2)} = 2\sqrt{\frac{I_x}{I_y}}\,|f_{1001} - f_{1010}|. \tag{6.5.6}$$

The corresponding normalized-momentum ratios are

$$\frac{\mathcal{A}_{\widetilde{p}_x}(Q_2)}{\mathcal{A}_{\widetilde{p}_x}(Q_1)} = 2\sqrt{\frac{I_y}{I_x}}\,|f_{1001} + f_{1010}^{*}|, \tag{6.5.7}$$

$$\frac{\mathcal{A}_{\widetilde{p}_y}(Q_1)}{\mathcal{A}_{\widetilde{p}_y}(Q_2)} = 2\sqrt{\frac{I_x}{I_y}}\,|f_{1001} + f_{1010}|. \tag{6.5.8}$$

6.5.2 Mais–Ripken and RDT amplitude identities

From equation (6.2.16),

$$\frac{\mathcal{A}_x(Q_2)}{\mathcal{A}_x(Q_1)} = \sqrt{\frac{J_2}{J_1}}\sqrt{\frac{\beta_{x2}}{\beta_{x1}}}, \tag{6.5.9}$$

$$\frac{\mathcal{A}_y(Q_1)}{\mathcal{A}_y(Q_2)} = \sqrt{\frac{J_1}{J_2}}\sqrt{\frac{\beta_{y1}}{\beta_{y2}}}. \tag{6.5.10}$$

Identifying $J_1 = I_x$ and $J_2 = I_y$ to the working order gives

$$\boxed{r_x \equiv \frac{1}{2}\sqrt{\frac{\beta_{x2}}{\beta_{x1}}} = |f_{1001} - f_{1010}^{*}|} \tag{6.5.11}$$

$$\boxed{r_y \equiv \frac{1}{2}\sqrt{\frac{\beta_{y1}}{\beta_{y2}}} = |f_{1001} - f_{1010}|.} \tag{6.5.12}$$

These are exact identities for the matrix-equivalent RDTs defined in section 6.6; for the source-summed perturbative RDTs they hold to first order in the coupling.
The normalized momentum in plane q is

$$\widetilde{p}_q = \frac{\alpha_q q + \beta_q p_q}{\sqrt{\beta_q}}. \tag{6.5.13}$$

Using the Mais–Ripken projection matrices, define

$$r_{\widetilde{p}_x} \equiv \frac{1}{2}\sqrt{\frac{\alpha_x^2\beta_{x2} - 2\alpha_x\beta_x\alpha_{x2} + \beta_x^2\gamma_{x2}}{\beta_{x1}}}, \tag{6.5.14}$$

$$r_{\widetilde{p}_y} \equiv \frac{1}{2}\sqrt{\frac{\alpha_y^2\beta_{y1} - 2\alpha_y\beta_y\alpha_{y1} + \beta_y^2\gamma_{y1}}{\beta_{y2}}}. \tag{6.5.15}$$

Then

$$\boxed{r_{\widetilde{p}_x} = |f_{1001} + f_{1010}^*|,} \tag{6.5.16}$$

$$\boxed{r_{\widetilde{p}_y} = |f_{1001} + f_{1010}|.} \tag{6.5.17}$$

Thus the position projection selects the difference of the two complex coupling terms, while the normalized-momentum projection selects their sum.
The interference structure is explicit:

$$r_x^2 = |f_{1001}|^2 + |f_{1010}|^2 - 2\,\mathrm{Re}(f_{1001}f_{1010}), \tag{6.5.18}$$

$$r_{\widetilde{p}_x}^2 = |f_{1001}|^2 + |f_{1010}|^2 + 2\,\mathrm{Re}(f_{1001}f_{1010}), \tag{6.5.19}$$

$$r_y^2 = |f_{1001}|^2 + |f_{1010}|^2 - 2\,\mathrm{Re}(f_{1001}f_{1010}^*), \tag{6.5.20}$$

$$r_{\widetilde{p}_y}^2 = |f_{1001}|^2 + |f_{1010}|^2 + 2\,\mathrm{Re}(f_{1001}f_{1010}^*). \tag{6.5.21}$$

Consequently, even a relatively small f_{1010} produces a first-order modulation of a Mais–Ripken position ratio around $|f_{1001}|$.

6.5.3 Physical canonical-momentum ratios

The Mais–Ripken functions give directly

$$\frac{\mathcal{A}_{p_x}(Q_2)}{\mathcal{A}_{p_x}(Q_1)} = \sqrt{\frac{J_2}{J_1}}\sqrt{\frac{\gamma_{x2}}{\gamma_{x1}}}, \tag{6.5.22}$$

$$\frac{\mathcal{A}_{p_y}(Q_1)}{\mathcal{A}_{p_y}(Q_2)} = \sqrt{\frac{J_1}{J_2}}\sqrt{\frac{\gamma_{y1}}{\gamma_{y2}}}. \tag{6.5.23}$$

Because $p_q = (\widetilde{p}_q - \alpha_q\widetilde{q})/\sqrt{\beta_q}$, the pure RDT combinations are mixed by α_q. The corresponding lattice ratios are

$$\boxed{\frac{1}{2}\sqrt{\frac{\gamma_{x2}}{\gamma_{x1}}} = \frac{\left|f_{1001} + f_{1010}^* + \mathrm{i}\alpha_x(f_{1001} - f_{1010}^*)\right|}{\sqrt{1+\alpha_x^2}}} \tag{6.5.24}$$

$$\boxed{\frac{1}{2}\sqrt{\frac{\gamma_{y1}}{\gamma_{y2}}} = \frac{\left|f_{1001} + f_{1010} - \mathrm{i}\alpha_y(f_{1001} - f_{1010})\right|}{\sqrt{1+\alpha_y^2}}.} \tag{6.5.25}$$

At an ET waist, where $\alpha_q = 0$, the physical and normalized momentum ratios coincide.

6.6 Exact matrix-equivalent RDTs from W

6.6.1 Definition from the normalized coupling matrix

The Edwards–Teng construction in section 6.3 provides g and the normalized coupling matrix $\mathcal{C}$ directly from W, before any RDT is introduced. In the Xsuite RDT convention, the corresponding exact matrix-equivalent linear coupling RDTs are

$$\boxed{f_{1001} = \frac{c_{21} - c_{12} + \mathrm{i}(c_{11} + c_{22})}{4g}} \tag{6.6.1}$$

$$\boxed{f_{1010} = \frac{c_{12} + c_{21} + \mathrm{i}(c_{11} - c_{22})}{4g}.} \tag{6.6.2}$$

Relative to the convention used in the original matrix–Hamiltonian formulas of Calaga, Tomás, and Franchi [34], the Xsuite convention applies an overall minus complex conjugation to each of these two RDTs.
Conversely,

$$\boxed{\mathcal{C} = 2g \begin{pmatrix} \mathrm{Im}(f_{1001} + f_{1010}) & \mathrm{Re}(f_{1010} - f_{1001}) \\ \mathrm{Re}(f_{1001} + f_{1010}) & \mathrm{Im}(f_{1001} - f_{1010}) \end{pmatrix}.} \tag{6.6.3}$$

Its complex row combinations are

$$c_{11} + \mathrm{i}c_{12} = -2\mathrm{i}g(f_{1001} - f_{1010}^*), \tag{6.6.4}$$
$$c_{21} + \mathrm{i}c_{22} = 2g(f_{1001} + f_{1010}^*), \tag{6.6.5}$$
$$(-\bar{\mathcal{C}})_{11} + \mathrm{i}(-\bar{\mathcal{C}})_{12} = -2\mathrm{i}g(f_{1001}^* - f_{1010}^*), \tag{6.6.6}$$
$$(-\bar{\mathcal{C}})_{21} + \mathrm{i}(-\bar{\mathcal{C}})_{22} = 2g(f_{1001}^* + f_{1010}^*). \tag{6.6.7}$$

These four identities are the matrix counterpart of equations (6.5.1) to (6.5.4).
Equation (6.3.61) becomes

$$\det\mathcal{C} = 4g^2\left(|f_{1001}|^2 - |f_{1010}|^2\right), \qquad \boxed{g^2 = \frac{1}{1 + 4(|f_{1001}|^2 - |f_{1010}|^2)}.} \tag{6.6.8}$$

Thus $g = 1 + \mathcal{O}(f_{1001}^2, f_{1010}^2)$, explaining why it is absent in the first-order orbit formulas while canceling exactly from the amplitude ratios. Combining equations (6.3.64) and (6.3.65) with equations (6.6.4) to (6.6.7) immediately yields the exact amplitude identities in equations (6.5.11), (6.5.12), (6.5.16) and (6.5.17).

6.6.2 Direct extraction of the coupling RDTs from the normal-form matrix

The matrix-equivalent RDTs can be obtained directly from W without first reconstructing all four real entries of $\mathcal{C}$. Assume the coordinate order (x, p_x, y, p_y) and that columns 3 and 4 of W belong to the vertical-like mode 2. As stated in equation (6.3.39), W is already assumed to be in the ET phase gauge.
The complex mode-2 eigenvector is therefore

$$\boldsymbol{v}_2 = W_{:,3} + \mathrm{i}W_{:,4}, \qquad v_{2,y} > 0, \tag{6.6.9}$$

with a real, positive physical y component. The mode-1 phase does not enter the following calculation because its Mais–Ripken functions are phase invariant.
Next obtain g from the principal horizontal Mais–Ripken functions and recover the horizontal ET Twiss parameters:

$$g^2 = \sqrt{\beta_{x1}\gamma_{x1} - \alpha_{x1}^2}, \qquad g = \sqrt{g^2}, \tag{6.6.10}$$

$$\beta_x = \frac{\beta_{x1}}{g^2}, \qquad \alpha_x = \frac{\alpha_{x1}}{g^2}. \tag{6.6.11}$$

The quantities β_{x1}, α_{x1}, and γ_{x1} are obtained from the first two columns of W through equation (6.2.12).
Apply the inverse horizontal ET normalizer to the horizontal components of $\boldsymbol{v}_2$:

$$\begin{pmatrix} u_x \\ u_{p_x} \end{pmatrix} = A_x^{-1} \begin{pmatrix} v_{2,x} \\ v_{2,p_x} \end{pmatrix} = \begin{pmatrix} v_{2,x}/\sqrt{\beta_x} \\ (\alpha_x v_{2,x} + \beta_x v_{2,p_x})/\sqrt{\beta_x} \end{pmatrix}. \tag{6.6.12}$$

By equation (6.3.62), $A_x^{-1} W_{x2} = \mathcal{C}$, so these two complex numbers are

$$u_x = c_{11} + \mathrm{i}c_{12}, \qquad u_{p_x} = c_{21} + \mathrm{i}c_{22}. \tag{6.6.13}$$

Substitution into equations (6.6.1) and (6.6.2) finally gives

$$\boxed{f_{1001} = \frac{u_{p_x} + \mathrm{i}u_x}{4g}} \tag{6.6.14}$$

$$\boxed{f_{1010} = \frac{(u_{p_x} - \mathrm{i}u_x)^*}{4g}}. \tag{6.6.15}$$

This is the direct route used by an implementation based on the complex mode-2 eigenvector of W.

Chapter 7

Synchrotron motion

We collect here some relevant properties and quantities of the longitudinal particle motion. Unless stated otherwise, we consider particles with the same mass and charge as the reference particle. The extension of momentum compaction and slip factor to other species is discussed in Section 7.1.
To first order in the momentum deviation, the momentum compaction factor is defined as:

$$\alpha_c = \frac{\Delta C/C}{\delta} \tag{7.0.1}$$

where C is the closed orbit path length. The slip factor is defined as (positive above transition):

$$\eta = -\frac{\Delta f/f_0}{\delta} = \alpha_c - \frac{1}{\gamma_0^2} = \frac{1}{\gamma_t^2} - \frac{1}{\gamma_0^2} \tag{7.0.2}$$

The slippage over a single turn is given by:

$$\Delta\zeta = -\beta_0 c\Delta T = -\beta_0 c(T - T_0) = -\beta_0 c\left(\frac{1}{f} - \frac{1}{f_0}\right) \tag{7.0.3}$$

$$= -\frac{\beta_0 c}{f_0}\left(\frac{1}{1+\Delta f/f_0} - 1\right) \simeq \frac{\beta_0 c}{f_0}\frac{\Delta f}{f_0} = -\eta\frac{\beta_0 c}{f_0}\delta = -\eta C\delta \tag{7.0.4}$$

The kick in energy from an RF cavity is given by:

$$\Delta E = qV_{RF}\sin\left(2\pi h_{RF} f_0 t + \phi_{RF}\right) \tag{7.0.5}$$

$$= qV_{RF}\sin\left(-2\pi h_{RF}\frac{\zeta}{C} + \phi_{RF}\right) \tag{7.0.6}$$

$$= qV_{RF}\sin\left(-2\pi f_{RF}\frac{\zeta}{\beta_0 c} + \phi_{RF}\right) \tag{7.0.7}$$

from which:

$$\Delta p_\zeta = \frac{\Delta E}{\beta_0^2 E_0} = \frac{qV_{RF}}{\beta_0^2 E_0}\sin\left(-2\pi f_{RF}\frac{\zeta}{\beta_0 c} + \phi_{RF}\right) \tag{7.0.8}$$

7.1 Turn slippage for different particle species

For a particle with mass m and charge q different from those of the reference particle, the turn slippage depends on both δ and χ. Recalling

$$1+\delta = \frac{P}{P_0}\frac{m_0}{m} = \frac{\beta\gamma}{\beta_0\gamma_0}, \qquad \chi = \frac{q}{q_0}\frac{m_0}{m}, \tag{7.1.1}$$

the relative rigidity offset is exactly

$$\delta_{\mathrm{rig}} = \frac{P/q}{P_0/q_0} - 1 = \frac{1+\delta}{\chi} - 1. \tag{7.1.2}$$

We assume a static magnetic lattice with constant momentum around the orbit. The magnetic force changes the direction of the momentum but not its magnitude. In a transverse magnetic field, the local bending radius satisfies $\rho = P/(|q|B_\perp)$, while the sign of q determines the bending direction. The closed-orbit length C is therefore determined by P/q. In Xsuite coordinates, this ratio is

$$\frac{P}{q} = \frac{P_0}{q_0}\frac{1+\delta}{\chi}.$$

The transverse closed orbit is also determined by the rigidity. Let $x_0(s)$ be the reference closed orbit and $D_x(s)$ the horizontal dispersion evaluated for the reference species on that orbit at $\delta = 0$. To first order in the rigidity offset,

$$x(s) - x_0(s) \simeq D_x(s)\delta_{\mathrm{rig}} = D_x(s)\left(\frac{1+\delta}{\chi} - 1\right). \tag{7.1.3}$$

Expanding also in δ and $\chi - 1$, and assuming a centered reference orbit, $x_0(s) = 0$, gives

$$x(s) \simeq D_x(s)\big[\delta - (\chi - 1)\big]. \tag{7.1.4}$$

Both $|\delta| \ll 1$ and $|\chi - 1| \ll 1$ are required for this expansion.
The speed, on the other hand, follows from $P = mc\beta\gamma$, or

$$\beta = \frac{P/(mc)}{\sqrt{1+[P/(mc)]^2}}, \qquad \frac{P}{m} = \frac{P_0}{m_0}(1+\delta).$$

It therefore depends on P/m, independently of the charge: particles with the same δ have the same speed, even if their masses and charges differ. In particular, at $\delta = 0$ the speed is $\beta_0 c$, but the rigidity differs from the reference value when $\chi \neq 1$. Such a particle can take a different time to complete a turn because its closed orbit has a different length. Both effects enter the revolution period $T = C/(\beta c)$ and frequency $f = 1/T$.
Let C_0 be the reference closed-orbit length, $T_0 = C_0/(\beta_0 c)$, and $f_0 = 1/T_0$. Denote by α_{c0} and $\eta_0 = \alpha_{c0} - 1/\gamma_0^2$ the coefficients evaluated for the reference species on that orbit. To first order in both δ and $\chi - 1$,

$$\frac{C - C_0}{C_0} \simeq \alpha_{c0}\delta_{\mathrm{rig}} \simeq \alpha_{c0}\big[\delta - (\chi - 1)\big], \tag{7.1.5}$$

$$\frac{\beta - \beta_0}{\beta_0} \simeq \frac{\delta}{\gamma_0^2}. \tag{7.1.6}$$

Combining the changes in orbit length and speed gives

$$\boxed{\frac{T - T_0}{T_0} \simeq -\frac{f - f_0}{f_0} \simeq \eta_0 \delta - \alpha_{c0}(\chi - 1).} \tag{7.1.7}$$

and the slippage over one turn is

$$\boxed{\Delta\zeta = -\beta_0 c(T - T_0) \simeq -C_0\big[\eta_0 \delta - \alpha_{c0}(\chi - 1)\big].} \tag{7.1.8}$$

The momentum offset for which the particle has the same revolution period as the reference particle is obtained by setting $T = T_0$, or equivalently $\Delta\zeta = 0$:

$$\boxed{\delta_{T=T_0} \simeq \frac{\alpha_{c0}}{\eta_0}(\chi - 1) = \frac{\alpha_{c0}}{\eta_0}\left(\frac{q}{q_0}\frac{m_0}{m} - 1\right).} \tag{7.1.9}$$

This result requires $\eta_0 \neq 0$ and a sufficiently small resulting δ. At transition ($\eta_0 = 0$), the term proportional to δ in the first-order slippage vanishes, so this approximation cannot determine the required momentum offset.
For $\chi = 1$, the usual first-order expressions for orbit length and slippage therefore apply even when $m \neq m_0$ and $q \neq q_0$, provided mass and charge scale by the same factor. For $\chi \neq 1$, a particle at $\delta = 0$ has the reference speed but a different rigidity, giving a turn slippage through the change in orbit length. These expressions require both $|\delta| \ll 1$ and $|\chi - 1| \ll 1$; larger offsets require evaluating the actual closed-orbit length and revolution period.

7.2 Linearized motion

We expand around the synchronous fixed point at longitudinal position ζ_0, where the RF frequency is $f_{RF} = h_{RF} f_0 = h_{RF}\beta_0 c/C$:

$$\Delta p_\zeta \approx \frac{qV_{RF}}{\beta_0^2 E_0} \sin\left(-2\pi f_{RF}\frac{\zeta_0}{\beta_0 c} + \phi_{RF}\right) - \frac{2\pi q f_{RF} V_{RF}}{\beta_0^3 E_0 c}(\zeta - \zeta_0)\cos\left(-2\pi f_{RF}\frac{\zeta_0}{\beta_0 c} + \phi_{RF}\right) \tag{7.2.1}$$

We define the synchronous phase as

$$\phi_s = -2\pi f_{RF}\frac{\zeta_0}{\beta_0 c} + \phi_{RF} \tag{7.2.2}$$

and the longitudinal displacement as

$$\bar{\zeta} = \zeta - \zeta_0 \tag{7.2.3}$$

obtaining:

$$\Delta p_\zeta \approx \frac{qV_{RF}}{\beta_0^2 E_0}\sin\phi_s - \frac{2\pi q f_{RF} V_{RF}}{\beta_0^3 E_0 c}\bar{\zeta}\cos\phi_s \tag{7.2.4}$$

We assume that the energy deviation of the stable fixed point is zero, giving

$$\Delta p_\zeta \approx -\frac{2\pi q f_{RF} V_{RF}}{\beta_0^3 E_0 c} \cos\phi_s \bar{\zeta} \tag{7.2.5}$$

7.3 Smooth approximation

In the smooth approximation we smear the RF kicks and the slippage uniformly along the ring. The equations of motion become:

$$\frac{dp_\zeta}{ds} = \frac{\Delta p_\zeta}{C} = K_s \bar{\zeta} \tag{7.3.1}$$

$$\frac{d\bar{\zeta}}{ds} = \frac{\Delta \zeta}{C} = -\eta p_\zeta \tag{7.3.2}$$

where we have used the approximation from Eq. 1.6.17:

$$\delta \ll 1 \Rightarrow \delta \simeq p_\zeta \tag{7.3.3}$$

and we have defined the smooth-approximation longitudinal focusing factor:

$$K_s = -\frac{2\pi q V_{RF} f_{RF}}{\beta_0^3 C E_0 c} \cos\phi_s \tag{7.3.4}$$

We differentiate the second equation and substitute the first:

$$\frac{d^2\bar{\zeta}}{ds^2} + \eta K_s \bar{\zeta} = 0 \tag{7.3.5}$$

The motion is stable if

$$\eta K_s > 0 \quad \Leftrightarrow \quad \eta \cos\phi_s < 0 \tag{7.3.6}$$

In that case the solution is harmonic:

$$\begin{aligned} \bar{\zeta}(s) &= \bar{\zeta}_A \cos\left(\sqrt{\eta K_s}\, s\right) + B \sin\left(\sqrt{\eta K_s}\, s\right) \\ &= \bar{\zeta}_A \cos\left(2\pi Q_s s/C\right) + B \sin\left(2\pi Q_s s/C\right) \end{aligned} \tag{7.3.7}$$

where $\bar{\zeta}_A = \bar{\zeta}(0)$ and $p_{\zeta_A} = p_\zeta(0)$ denote the initial conditions. The synchrotron tune is

$$Q_s = \sqrt{\eta K_s}\frac{C}{2\pi} = \sqrt{-\frac{q\eta f_{RF} C V_{RF}}{2\pi\beta_0^3 E_0 c}\cos\phi_s} \tag{7.3.8}$$

We replace

$$f_{RF} = \frac{h_{RF}\beta_0 c}{C} \tag{7.3.9}$$

obtaining:

$$Q_s = \sqrt{-\frac{q\eta h_{RF} V_{RF}}{2\pi\beta_0^2 E_0}\cos\phi_s} \tag{7.3.10}$$

Replacing Eq. 7.3.7 in Eq. 7.3.2:

$$p_\zeta = -\frac{2\pi Q_s}{\eta C}\left(-\bar{\zeta}_A \sin\left(2\pi Q_s s/C\right) + B\cos\left(2\pi Q_s s/C\right)\right) \tag{7.3.11}$$

Replacing $s = 0$:

$$p_{\zeta_A} = -\frac{2\pi Q_s}{\eta C} B \tag{7.3.12}$$

from which:

$$B = -\frac{\eta C}{2\pi Q_s} p_{\zeta_A} = -\beta_\zeta p_{\zeta_A}, \tag{7.3.13}$$

where we have defined:

$$\beta_\zeta = \frac{\eta C}{2\pi Q_s} \tag{7.3.14}$$

Replacing

$$\bar{\zeta}(s) = \bar{\zeta}_A \cos\left(2\pi Q_s \frac{s}{C}\right) - p_{\zeta_A}\beta_\zeta \sin\left(2\pi Q_s \frac{s}{C}\right) \tag{7.3.15}$$

$$p_\zeta(s) = \frac{\bar{\zeta}_A}{\beta_\zeta} \sin\left(2\pi Q_s \frac{s}{C}\right) + p_{\zeta_A} \cos\left(2\pi Q_s \frac{s}{C}\right) \tag{7.3.16}$$

These expressions can be recast in Courant–Snyder form:

$$\bar{\zeta}(s) = \sqrt{\beta_\zeta\, \varepsilon_s}\, \cos\left(2\pi Q_s \frac{s}{C} + \Phi_{s,\bar{\zeta}}\right) \tag{7.3.17}$$

$$p_\zeta(s) = \sqrt{\frac{\varepsilon_s}{\beta_\zeta}}\, \cos\left(2\pi Q_s \frac{s}{C} + \Phi_{s,p_\zeta}\right) \tag{7.3.18}$$

with the longitudinal emittance and phases determined by the initial conditions $\bar{\zeta}_A = \bar{\zeta}(0)$ and $p_{\zeta_A} = p_\zeta(0)$:

$$\varepsilon_s = \frac{\bar{\zeta}_A^2}{\beta_\zeta} + \beta_\zeta p_{\zeta_A}^2 \tag{7.3.19}$$

$$\Phi_{s,\bar{\zeta}} = \mathrm{atan2}\left(\beta_\zeta p_{\zeta_A},\, \bar{\zeta}_A\right) \tag{7.3.20}$$

$$\Phi_{s,p_\zeta} = \mathrm{atan2}\left(-\bar{\zeta}_A/\beta_\zeta,\, p_{\zeta_A}\right) \tag{7.3.21}$$

The two phase offsets differ by $\pi/2$ (modulo 2π), consistently with the sine/cosine quadrature between coordinate and momentum in a simple harmonic oscillator.

In the longitudinal plane we can take the Twiss parameter $\alpha_\zeta = 0$, since the longitudinal focusing is weak compared to the revolution scale and can be treated as constant around the ring.
For a matched bunch with longitudinal emittance ε_s, the rms beam sizes read

$$\sigma_{\bar{\zeta}} = \sqrt{\beta_\zeta \, \varepsilon_s} \tag{7.3.22}$$

$$\sigma_{p_\zeta} = \sqrt{\frac{\varepsilon_s}{\beta_\zeta}} \tag{7.3.23}$$

so that

$$\sigma_{\bar{\zeta}} \sigma_{p_\zeta} = \varepsilon_s \tag{7.3.24}$$

and equivalently

$$\beta_\zeta = \frac{\sigma_{\bar{\zeta}}}{\sigma_{p_\zeta}} \tag{7.3.25}$$

and the longitudinal envelope rotates in phase space with tune Q_s.

7.4 Kick-drift model

For the kick-drift model we want to rewrite Eq. 7.2.5:

$$\Delta p_\zeta = C K_s \bar{\zeta} \tag{7.4.1}$$

7.5 Hamiltonian of the synchrotron motion

In this section we use the time in the laboratory frame as independent variable as done in the PyHEADTAIL longitudinal treatment. In this section we also include the effect of a reference momentum change of ΔP_0 per turn.
We assume small energy deviations, hence we can consider the coordinates (ζ, δ) to be canonically conjugate ($\delta \ll 1 \Rightarrow \delta \simeq p_\zeta$ – see Eq. 1.6.17).
The longitudinal motion can be described by the following Hamiltonian:

$$H(\zeta, \delta) = -\frac{1}{2}\eta \beta_0 c \delta^2 + \frac{\beta_0 c}{C}\frac{\Delta P_0}{P_0}\zeta - \frac{q_0}{P_0}\sum_i \frac{1}{2\pi h_i} V_i \cos\left(-2\pi h_i \frac{\zeta}{C} + \phi_i\right) \tag{7.5.1}$$

This can be proven using Hamilton's equations:

$$\frac{d\zeta}{dt} = \frac{\partial H}{\partial \delta} = -\eta \beta_0 c \delta \tag{7.5.2}$$

$$\frac{d\delta}{dt} = -\frac{\partial H}{\partial \zeta} = -\frac{\beta_0 c}{C}\frac{\Delta P_0}{P_0} + \frac{q_0}{P_0 C}\sum_i V_i \sin\left(-2\pi h_i \frac{\zeta}{C} + \phi_i\right) \tag{7.5.3}$$

The coordinate change over one revolution is:

$$\Delta\zeta = \frac{d\zeta}{dt}\frac{C}{\beta_0 c} = -\eta C\delta \tag{7.5.4}$$

$$\Delta\delta = \frac{d\delta}{dt}\frac{C}{\beta_0 c} = -\frac{\Delta P_0}{P_0} + \frac{q_0}{\beta_0 c P_0}\sum_i V_i \sin\left(-2\pi h_i \frac{\zeta}{C} + \phi_i\right) \tag{7.5.5}$$

which are consistent with those found in Sec. 7.

7.5.1 Fixed points

The fixed points can be found by imposing $\Delta\zeta = 0$ and $\Delta\delta = 0$. If only a single harmonic is present a closed solution can be found:

$$-\frac{\Delta P_0}{P_0} + \frac{q_0}{\beta_0 c P_0} V_{\mathrm{RF}} \sin\left(-2\pi h_{\mathrm{RF}} \frac{\zeta}{C} + \phi_i\right) = 0 \tag{7.5.6}$$

We want to get an explicit expression for ζ:

$$\frac{\Delta P_0 \beta_0 c}{q_0 V_{\mathrm{RF}}} = \sin\left(-2\pi h_{\mathrm{RF}} \frac{\zeta}{C} + \phi_i\right) \tag{7.5.7}$$

There are two families of solutions:

$$\arcsin\left(\frac{\Delta P_0 \beta_0 c}{q_0 V_{\mathrm{RF}}}\right) + 2n\pi = -2\pi h_{\mathrm{RF}} \frac{\zeta}{C} + \phi_{\mathrm{RF}} \tag{7.5.8}$$

$$\pi - \arcsin\left(\frac{\Delta P_0 \beta_0 c}{q_0 V_{\mathrm{RF}}}\right) + 2n\pi = -2\pi h_{\mathrm{RF}} \frac{\zeta}{C} + \phi_{\mathrm{RF}} \tag{7.5.9}$$

where n is an integer number. Depending on the sign of η only one family of fixed points is stable.
We solve for ζ:

$$\zeta = \frac{C}{2\pi h_{\mathrm{RF}}}\left(\phi_{\mathrm{RF}} - \arcsin\left(\frac{\Delta P_0 \beta_0 c}{q_0 V_{\mathrm{RF}}}\right) + 2n\pi\right) \tag{7.5.10}$$

$$\zeta = \frac{C}{2\pi h_{\mathrm{RF}}}\left(\phi_{\mathrm{RF}} + \pi + \arcsin\left(\frac{\Delta P_0 \beta_0 c}{q_0 V_{\mathrm{RF}}}\right) + 2n\pi\right) \tag{7.5.11}$$

It is possible to set ϕ_{RF} to place a fixed point of either family at $\zeta = 0$:

$$\phi_{\mathrm{RF}} = \arcsin\left(\frac{\Delta P_0 \beta_0 c}{q_0 V_{\mathrm{RF}}}\right) \tag{7.5.12}$$

$$\phi_{\mathrm{RF}} = \pi - \arcsin\left(\frac{\Delta P_0 \beta_0 c}{q_0 V_{\mathrm{RF}}}\right) \tag{7.5.13}$$

It can be shown that, to have a stable fixed point at $\zeta = 0$, one needs to use Eq. 7.5.12 when $\eta < 0$ (below transition) and Eq. 7.5.13 when $\eta > 0$ (above transition).

7.6 RF-frequency change modeled as a shift in ζ

The standard cavity map is synchronized with the reference particle on every turn. Consequently, changing the frequency in this map changes the variation of the RF phase within the bunch, but does not by itself introduce the turn-by-turn phase slip associated with an RF-frequency change. This phase slip can be represented by a shift in ζ.
Let m be the turn number and let

$$T_0 = \frac{C}{\beta_0 c} = \frac{1}{f_0}. \tag{7.6.1}$$

At a cavity located at $s = s_{RF}$, the definition

$$\zeta = s - \beta_0 c\,(t - mT_0) \tag{7.6.2}$$

gives

$$t = \frac{s_{RF} - \zeta}{\beta_0 c} + mT_0. \tag{7.6.3}$$

The energy kick from a cavity with frequency f_{RF} can therefore be written as

$$\Delta E = qV_{RF} \sin\left(2\pi f_{RF} t + \widetilde{\phi}_{RF}\right) \tag{7.6.4}$$

$$= qV_{RF} \sin\left(-2\pi f_{RF}\frac{\zeta}{\beta_0 c} + 2\pi m\frac{f_{RF}}{f_0} + \phi_{RF}\right), \tag{7.6.5}$$

where the phase at the cavity location has been absorbed into

$$\phi_{RF} = \widetilde{\phi}_{RF} + 2\pi f_{RF}\frac{s_{RF}}{\beta_0 c}. \tag{7.6.6}$$

For $f_{RF} = h_{RF} f_0$, with integer h_{RF}, the turn-dependent term in Eq. 7.6.5 is an integer multiple of 2π and the standard cavity map is recovered:

$$\Delta E = qV_{RF} \sin\left(-2\pi f_{RF}\frac{\zeta}{\beta_0 c} + \phi_{RF}\right). \tag{7.6.7}$$

Consider instead the frequency change

$$f_{RF} = h_{RF} f_0 + \Delta f_{RF}. \tag{7.6.8}$$

Substituting this expression into Eq. 7.6.5 gives

$$\Delta E = qV_{RF} \sin\left(-2\pi f_{RF}\frac{\zeta}{\beta_0 c} + 2\pi m\frac{h_{RF} f_0 + \Delta f_{RF}}{f_0} + \phi_{RF}\right) \tag{7.6.9}$$

$$= qV_{RF} \sin\left(-2\pi f_{RF}\frac{\zeta}{\beta_0 c} + 2\pi m h_{RF} + 2\pi m\frac{\Delta f_{RF}}{f_0} + \phi_{RF}\right) \tag{7.6.10}$$

$$= qV_{RF} \sin\left(-2\pi f_{RF}\frac{\zeta}{\beta_0 c} + 2\pi m\frac{\Delta f_{RF}}{f_0} + \phi_{RF}\right). \tag{7.6.11}$$

where the third line follows from $m, h_{RF} \in \mathbb{Z}$ and the 2π-periodicity of the sine. We define

$$\boxed{\Delta\zeta_{RF} = \frac{\beta_0 c}{f_0}\frac{\Delta f_{RF}}{f_{RF}} = C\frac{\Delta f_{RF}}{f_{RF}}.} \tag{7.6.12}$$

Replacing Eq. 7.6.12 in Eq. 7.6.11 gives

$$\Delta E = qV_{RF}\sin\left[-2\pi f_{RF}\frac{\zeta - m\Delta\zeta_{RF}}{\beta_0 c} + \phi_{RF}\right]. \tag{7.6.13}$$

We therefore find that the RF phase slip accumulated over m turns is equivalent to applying the following transformation once per turn, immediately before a cavity using the standard relative-time map:

$$\boxed{\zeta \longleftarrow \zeta - \Delta\zeta_{RF}.} \tag{7.6.14}$$

In Xtrack, the `TimeDelay` element implements this transformation. Its `shift_zeta` parameter is set to $\Delta\zeta_{RF}$.
For a small frequency change,

$$\Delta\zeta_{RF} \simeq C\frac{\Delta f_{RF}}{h_{RF} f_0}. \tag{7.6.15}$$

Since the RF frequency and revolution frequency have the same fractional change, the definition of the slip factor gives

$$\frac{\Delta f_{RF}}{f_{RF}} = \frac{\Delta f}{f_0} = -\eta\delta. \tag{7.6.16}$$

The corresponding equilibrium momentum offset is therefore

$$\boxed{\delta = -\frac{1}{\eta}\frac{\Delta f_{RF}}{f_{RF}},} \tag{7.6.17}$$

and Eq. 7.6.12 can equivalently be written as

$$\Delta\zeta_{RF} = -\eta C\delta. \tag{7.6.18}$$

Chapter 8

Counter-rotating beams

In machines having counter-rotating beams, such as the LHC, it is useful to be able to express beam coordinates for one of the beams in the reference frame of the other. Furthermore it is also useful to be able to define the two sequences using the same orientation. For the LHC, for example, the sequence of the LHC Beam 2 is defined following the orientation of the LHC Beam 1. In this case the properties of the elements are specified in such a way that the built sequence is able to backtrack the physical beam and the sequence required to track the physical beam (usually called Beam 4 sequence) can be obtained with suitable transformations.

8.1 Reversed reference frame

The reference frames for Beam 4 and Beam 2 are related by the following transformations:

$$\tilde{x} = -x \tag{8.1.1}$$
$$\tilde{y} = y \tag{8.1.2}$$
$$\tilde{s} = -s \tag{8.1.3}$$
$$\tilde{t} = -t \tag{8.1.4}$$
$$\tilde{\zeta} = -\zeta \tag{8.1.5}$$
$$\tilde{p_x} = p_x \tag{8.1.6}$$
$$\tilde{p_y} = -p_y \tag{8.1.7}$$
$$\tilde{p_\zeta} = p_\zeta \tag{8.1.8}$$
$$\tilde{\delta} = \delta \tag{8.1.9}$$

where the tilde indicates the coordinates in the reversed reference frame.

8.2 Transformation of beam elements

The elements are transformed in such a way that the map implements the backtrack of the physical beam as seen in the reversed reference frame.

8.2.1 Horizontal deflecting cavity

In the case of a horizontal deflecting cavity we can proceed as follows.
For Beam 4 we can write:

$$\Delta p_x = V_x \sin(\phi - \omega t) \tag{8.2.1}$$

and for Beam 2 we can write:

$$\Delta \tilde{p}_x = \tilde{V}_x \sin(\tilde{\phi} - \omega \tilde{t}), \tag{8.2.2}$$

Since we define the element as backtracking we can write:

$$\Delta \tilde{p}_x = -\Delta p_x \tag{8.2.3}$$

where the minus sign comes from the backtracking and no additional sign change comes from the reference frame transformation (see Eq. 8.1.6).
Combining the equations above we obtain:

$$\tilde{V}_x \sin(\tilde{\phi} - \omega \tilde{t}) = -V_x \sin(\phi - \omega t) \tag{8.2.4}$$

Using Eq. 8.1.4 we can write:

$$\tilde{V}_x \sin(\tilde{\phi} + \omega t) = -V_x \sin(\phi - \omega t) \tag{8.2.5}$$

We choose to reverse the voltage definition since the electric field is also expressed in the reversed reference frame:

$$\boxed{\tilde{V}_x = -V_x} \tag{8.2.6}$$

obtaining:

$$\sin(\tilde{\phi} + \omega t) = \sin(\phi - \omega t) \tag{8.2.7}$$

Using trigonometric properties we can write:

$$-\sin(-\tilde{\phi} - \omega t) = \sin(\phi - \omega t) \tag{8.2.8}$$

and then:

$$\sin(\pi - \tilde{\phi} - \omega t) = \sin(\phi - \omega t) \tag{8.2.9}$$

From this we obtain:

$$\boxed{\tilde{\phi} = \pi - \phi} \tag{8.2.10}$$

8.2.2 Vertical deflecting cavity

The case of a vertical deflecting cavity is similar but not identical.
For Beam 4 we can write:

$$\Delta p_y = V_y \sin(\phi - \omega t) \tag{8.2.11}$$

and for Beam 2 we can write:

$$\Delta \tilde{p}_y = \tilde{V}_y \sin(\tilde{\phi} - \omega \tilde{t}), \tag{8.2.12}$$

Since we define the element as backtracking we can write:

$$\Delta\tilde{p}_y = -(-\Delta p_y) \tag{8.2.13}$$

where one minus sign comes from the backtracking and an additional sign change comes from the reference frame transformation (see Eq. 8.1.7).
Combining the equations above we obtain:

$$\tilde{V}_y \sin(\tilde{\phi} - \omega\tilde{t}) = V_y \sin(\phi - \omega t) \tag{8.2.14}$$

Using Eq. 8.1.4 we can write:

$$\tilde{V}_y \sin(\tilde{\phi} + \omega t) = -V_y \sin(\phi - \omega t) \tag{8.2.15}$$

We do not reverse the voltage definition as the vertical component of the electric field does not change sign due to the reference frame transformation:

$$\boxed{\tilde{V}_y = V_y} \tag{8.2.16}$$

Hence we obtain:

$$\sin(\tilde{\phi} + \omega t) = \sin(\phi - \omega t) \tag{8.2.17}$$

Using trigonometric properties we can write:

$$-\sin(-\tilde{\phi} - \omega t) = \sin(\phi - \omega t) \tag{8.2.18}$$

and then:

$$\sin(\pi - \tilde{\phi} - \omega t) = \sin(\phi - \omega t) \tag{8.2.19}$$

From this we obtain:

$$\boxed{\tilde{\phi} = \pi - \phi} \tag{8.2.20}$$

Chapter 9

Synchrotron radiation

We collect here some relevant properties of synchrotron radiation [35]:
We assume $B = |B_\perp|$.
Classical particle radius:

$$r_0 = Q^2 / \left(4\pi\epsilon_0 m_0 c^2\right) \tag{9.0.1}$$

Curvature, rigidity, field:

$$\frac{1}{\rho} = \frac{QB}{p} = \frac{QB}{m_0 c\beta\gamma} \tag{9.0.2}$$

Emitted power:

$$P_\mathrm{s} = \frac{2r_0 c^3 Q^2 \beta^2 \gamma^2 B^2}{3m_0 c^2} \tag{9.0.3}$$

Critical frequency:

$$\omega_\mathrm{c} = \frac{3Q\beta^2\gamma^2 B}{2m_0} \tag{9.0.4}$$

Critical energy:

$$E_{\gamma\mathrm{c}} = \hbar\omega_\mathrm{c} = \frac{3Q\hbar\beta^2\gamma^2 B}{2m_0} \tag{9.0.5}$$

Number of photons per unit time:

$$\dot{n}_\mathrm{s} = \frac{15\sqrt{3}}{8}\frac{P_\mathrm{s}}{E_{\gamma\mathrm{c}}} = \frac{60\sqrt{3}}{72}\frac{r_0 cQB}{\hbar} \tag{9.0.6}$$

Average photon energy:

$$\langle E_\gamma \rangle = \frac{8\sqrt{3}}{45}E_{\gamma\mathrm{c}} = \frac{8\sqrt{3}}{15}\frac{Q\hbar\beta^2\gamma^2 B}{2m_0} \tag{9.0.7}$$

Photon energy variance:

$$\left\langle E_\gamma^2 \right\rangle = \frac{11}{27}E_{\gamma\mathrm{c}}^2 = \frac{11}{12}\frac{Q^2\hbar^2\beta^4\gamma^4 B^2}{m_0^2} \tag{9.0.8}$$

$$\left\langle \dot{n}_s \Delta\delta^2 \right\rangle = \frac{\left\langle \dot{n}_s E_\gamma^2 \right\rangle}{E_0^2} = \frac{11}{12}\frac{1}{m_0^2 c^4 \gamma_0^2}\frac{Q^2\hbar^2\beta^4\gamma^4 B^2}{m_0^2}\frac{60\sqrt{3}}{72}\frac{cQB}{\hbar}\frac{Q^2}{4\pi\epsilon_0 m_0 c^2} \tag{9.0.9}$$

The algorithm to generate photon energies with the appropriate distribution is described in [36].

9.1 Damping from synchrotron radiation

The damping constants from synchrotron radiation can be easily obtained from the magnitude of the eigenvalues of the one-turn matrix:

$$\alpha_x = -\log(|\lambda_x|) \tag{9.1.1}$$
$$\alpha_y = -\log(|\lambda_y|) \tag{9.1.2}$$
$$\alpha_\zeta = -\log(|\lambda_\zeta|) \tag{9.1.3}$$

The damping acts such that:

$$\frac{1}{A_x}\frac{dA_x}{dt} = -\frac{\alpha_x}{T_0} \tag{9.1.4}$$

where T_0 is the revolution period. From Eq. 4.5.2 we obtain:

$$\frac{dJ_x}{dt} = -\frac{2\alpha_x}{T_0}J_x \tag{9.1.5}$$

By averaging over the beam distribution we obtain:

$$\frac{d\varepsilon_x}{dt} = -\frac{2\alpha_x}{T_0}\varepsilon_x \tag{9.1.6}$$

9.2 Equilibrium emittance

This section is based on the approach described in [37].
To account for the kicks experienced by the particles due to quantum excitation we note that the transverse momentum change due to an energy kick in the direction of the particle motion can be written as:

$$P_{x,y}^{\text{new}} = P_{x,y}^{\text{old}}\frac{P^{\text{new}}}{P^{\text{old}}} \tag{9.2.1}$$

From this:

$$P_{x,y}^{\text{new}} - P_{x,y}^{\text{old}} = P_{x,y}^{\text{old}}\left(\frac{P^{\text{new}} - P^{\text{old}}}{P^{\text{old}}}\right) \tag{9.2.2}$$

Dividing by P_0:

$$\frac{P_{x,y}^{\text{new}} - P_{x,y}^{\text{old}}}{P_0} = \frac{P_{x,y}^{\text{old}}}{P_0}\left(\frac{P^{\text{new}} - P^{\text{old}}}{P_0}\right)\frac{P_0}{P^{\text{old}}} \tag{9.2.3}$$

Using the accelerator coordinates definitions (Eqs. 1.6.2 and 1.6.3), we obtain:

$$\Delta p_{x,y} = \frac{p_{x,y}}{1+\delta}\Delta\delta \tag{9.2.4}$$

The corresponding change in normalized coordinates can be computed from Eq. 4.3.1:

$$\begin{pmatrix} \Delta\tilde{x} \\ \Delta\tilde{p}_x \\ \Delta\tilde{y} \\ \Delta\tilde{p}_y \\ \Delta\tilde{\zeta} \\ \Delta\tilde{p}_\zeta \end{pmatrix} = W^{-1} \begin{pmatrix} 0 \\ \frac{p_x}{1+\delta}\Delta\delta \\ 0 \\ \frac{p_y}{1+\delta}\Delta\delta \\ 0 \\ \Delta\delta \end{pmatrix} \tag{9.2.5}$$

Using Eq. 4.1.19 we obtain:

$$\Delta\hat{x} = \mathcal{K}_x\Delta\delta \tag{9.2.6}$$
$$\Delta\hat{p}_x = \mathcal{K}_{p_x}\Delta\delta \tag{9.2.7}$$
$$\Delta\hat{y} = \mathcal{K}_y\Delta\delta \tag{9.2.8}$$
$$\Delta\hat{p}_y = \mathcal{K}_{p_y}\Delta\delta \tag{9.2.9}$$
$$\Delta\hat{\zeta} = \mathcal{K}_\zeta\Delta\delta \tag{9.2.10}$$
$$\Delta\hat{p}_\zeta = \mathcal{K}_{p_\zeta}\Delta\delta \tag{9.2.11}$$

where:

$$\mathcal{K}_x = \left(\frac{a_{11}p_x + a_{13}p_y}{1+\delta} + a_{15}\right) \tag{9.2.12}$$
$$\mathcal{K}_{p_x} = \left(\frac{b_{11}p_x + b_{13}p_y}{1+\delta} + b_{15}\right) \tag{9.2.13}$$
$$\mathcal{K}_y = \left(\frac{a_{21}p_x + a_{23}p_y}{1+\delta} + a_{25}\right) \tag{9.2.14}$$
$$\mathcal{K}_{p_y} = \left(\frac{b_{21}p_x + b_{23}p_y}{1+\delta} + b_{25}\right) \tag{9.2.15}$$
$$\mathcal{K}_\zeta = \left(\frac{a_{31}p_x + a_{33}p_y}{1+\delta} + a_{35}\right) \tag{9.2.16}$$
$$\mathcal{K}_{p_\zeta} = \left(\frac{b_{31}p_x + b_{33}p_y}{1+\delta} + b_{35}\right) \tag{9.2.17}$$

The change in action (see Eq. 4.5.1) associated with the first mode, due to the emission of a photon, can be written as:

$$\Delta J_x = \frac{1}{2}\left[(\hat{x}+\Delta\hat{x})^2 + (\hat{p}_x+\Delta\hat{p}_x)^2 - \hat{x}^2 - \hat{p}_x^2\right] \tag{9.2.18}$$

$$= \frac{1}{2}\left[\Delta\hat{x}^2 + \Delta\hat{p}_x^2 + 2\hat{x}\Delta\hat{x} + 2\hat{p}_x\Delta\hat{p}_x\right] \tag{9.2.19}$$

Averaging over all particles in the beam we obtain:

$$\Delta\varepsilon_x = \langle\Delta J_x\rangle = \frac{1}{2}\left(\langle\Delta\hat{x}^2\rangle + \langle\Delta\hat{p}_x^2\rangle\right) \tag{9.2.20}$$

Using Eqs. 9.2.6 and 9.2.7 we obtain:

$$\Delta\varepsilon_x = \langle\Delta J_x\rangle = \frac{1}{2}\left(\mathcal{K}_x^2 + \mathcal{K}_{p_x}^2\right)\langle\Delta\delta^2\rangle \tag{9.2.21}$$

Assuming that the kicks are uncorrelated we can obtain the emittance growth rate from quantum excitation by integrating over a full turn:

$$\left(\frac{d\varepsilon_x}{dt}\right)_{\text{quant}} = \frac{1}{2T_0c}\int_0^C \left(\mathcal{K}_x^2 + \mathcal{K}_{p_x}^2\right)\langle\dot{N}\Delta\delta^2\rangle\, ds \tag{9.2.22}$$

where $\dot{N}$ is the photon emission rate (number of photons per unit time), T_0 is the revolution period, and C is the circumference.
By summing Eqs. 9.1.6 and 9.2.22 we obtain the total instantaneous growth rate:

$$\frac{d\varepsilon_x}{dt} = \left(\frac{d\varepsilon_x}{dt}\right)_{\text{damp}} + \left(\frac{d\varepsilon_x}{dt}\right)_{\text{quant}} = -\frac{2\alpha_x}{T_0}\varepsilon_x + \frac{1}{2T_0c}\int_0^C \left(\mathcal{K}_x^2 + \mathcal{K}_{p_x}^2\right)\langle\dot{N}\Delta\delta^2\rangle\, ds \tag{9.2.23}$$

By setting the derivative to zero we obtain the value of the equilibrium emittance:

$$\varepsilon_x = \frac{1}{4\alpha_x c}\int_0^C \left(\mathcal{K}_x^2 + \mathcal{K}_{p_x}^2\right)\langle\dot{N}\Delta\delta^2\rangle\, ds \tag{9.2.24}$$

In the ultra-relativistic approximation:

$$\langle\dot{N}\Delta\delta^2\rangle = \frac{\langle\dot{N}(\Delta E)^2\rangle}{E_0^2} \tag{9.2.25}$$

9.3 Radiation integrals

Xsuite can compute the following radiation integrals:

$$I_1 = \oint \left(h_{0x}D_x + h_{0y}D_y\right)\, \mathrm{d}s \tag{9.3.1}$$

$$I_2 = \oint |h|^2\, \mathrm{d}s \tag{9.3.2}$$

$$I_3 = \oint |h|^3\, \mathrm{d}s \tag{9.3.3}$$

$$I_{4x} = \oint \left(|h|^2 h_{0x} + 2h_x k_1\right) D_x\, \mathrm{d}s \tag{9.3.4}$$

$$I_{4y} = \oint \left(|h|^2 h_{0y} - 2h_y k_1 \right) D_y \, \mathrm{d}s \tag{9.3.5}$$

$$I_4 = I_{4x} + I_{4y} = \oint \left[2k_1 \left(h_x D_x - h_y D_y \right) + |h|^2 (h_{0x} D_x + h_{0y} D_y) \right] \, \mathrm{d}s \tag{9.3.6}$$

$$I_{5x} = \oint h^3 \mathcal{H}_x \, \mathrm{d}s \tag{9.3.7}$$

$$I_{5y} = \oint h^3 \mathcal{H}_y \, \mathrm{d}s \tag{9.3.8}$$

The following quantities are used in the calculation.

- Horizontal and vertical curvature of the particle trajectory:

$$h_x = \frac{B_y Q}{m_0 c \gamma} \tag{9.3.9}$$

$$h_y = -\frac{B_x Q}{m_0 c \gamma} \tag{9.3.10}$$

- Total transverse curvature and relation to the transverse magnetic field:

$$h = \sqrt{h_x^2 + h_y^2} \tag{9.3.11}$$

  which is related to the transverse magnetic field by:

$$B = \sqrt{B_x^2 + B_y^2} = h \frac{m_0 \beta c \gamma}{Q} \tag{9.3.12}$$

- "Curly H" functions:

$$\mathcal{H}_x = \gamma_x D_x^2 + 2\alpha_x D_x D_x' + \beta_x D_x'^2 \tag{9.3.13}$$

$$\mathcal{H}_y = \gamma_y D_y^2 + 2\alpha_y D_y D_y' + \beta_y D_y'^2 \tag{9.3.14}$$

- The derivative of the dispersion $D'_{x,y}$ can be obtained from the transverse momentum dispersion $D_{p_{x,y}}$ using the relation:

$$D'_{x,y} = \frac{\mathrm{d}D_{x,y}}{\mathrm{d}s} = \frac{\mathrm{d}x'}{\mathrm{d}\delta} = \frac{\mathrm{d}}{\mathrm{d}\delta} \frac{p_{x,y}}{1+\delta} = (1-\delta) D_{p_{x,y}} - p_{x,y} \tag{9.3.15}$$

- h_{0x} and h_{0y} are the curvatures of the reference trajectory. The path length on the particle trajectory is related to the path length on the reference trajectory by:

$$\mathrm{d}s' = (1 + h_{0x} x + h_{0y} y) \, \mathrm{d}s \tag{9.3.16}$$

The radiation integrals can be used to compute the following quantities (where C_0 is the ring circumference, r_0 is the classical particle radius, $\hbar$ is the reduced Planck's constant) :

- Momentum compaction factor (unitless):

$$\alpha_c = \frac{I_1}{C_0} \tag{9.3.17}$$

- Energy loss per turn:

$$U_s = \frac{2}{3} r_0 E_0 \gamma^3 I_2 \tag{9.3.18}$$

- Damping partition numbers:

$$J_x = 1 - \frac{I_{4x}}{I_2} \tag{9.3.19}$$

$$J_y = 1 - \frac{I_{4y}}{I_2} \tag{9.3.20}$$

$$J_z = 2 + \frac{I_4}{I_2} \tag{9.3.21}$$

  which satisfy Robinson's theorem:

$$J_x + J_y + J_z = 4 \tag{9.3.22}$$

- Longitudinal damping rate in [s^{-1}]:

$$\alpha_\epsilon = \frac{c r_0 \gamma^3}{3 C_0} (2 I_2 + I_4) \tag{9.3.23}$$

- Transverse damping rates in [s^{-1}]:

$$\alpha_x = \frac{c r_0 \gamma^3}{3 C_0} (I_2 - I_{4x}) \tag{9.3.24}$$

$$\alpha_y = \frac{c r_0 \gamma^3}{3 C_0} (I_2 - I_{4y}) \tag{9.3.25}$$

- Energy spread (unitless):

$$\sigma_\delta^2 = \frac{55\sqrt{3}}{96} \frac{\hbar \gamma^2}{m_0 c} \frac{I_3}{2 I_2 + I_4} \tag{9.3.26}$$

- Transverse equilibrium emittances in [m rad]:

$$\epsilon_x = \frac{55\sqrt{3}}{96} \frac{\hbar \gamma^2}{m_0 c} \frac{I_{5x}}{I_2 - I_{4x}} \tag{9.3.27}$$

$$\epsilon_y = \frac{55\sqrt{3}}{96} \frac{\hbar \gamma^2}{m_0 c} \frac{I_{5y}}{I_2 - I_{4y}} \tag{9.3.28}$$

9.3.1 Derivations

9.3.1.1 Energy Loss and Second Radiation Integral

From the instantaneous radiated power,

$$P_s = \frac{2}{3}\frac{c^3 r_0 Q^2 E^2 B^2}{(m_0 c^2)^3} = \frac{2}{3} c r_0 E \gamma^3 |h|^2 \tag{9.3.29}$$

The energy loss per turn is obtained by integration around one turn.

$$U_s = \int P_s(t)\,\mathrm{d}t \approx \frac{1}{c}\oint P_s(s')\,\mathrm{d}s' = \frac{2}{3} r_0 E \gamma^3 \oint |h|^2\,\mathrm{d}s' \tag{9.3.30}$$

We can assume $(h_{0x}x + h_{0y}y) \ll 1$, obtaining:

$$U_s = \frac{2}{3} r_0 E \gamma^3 I_2 \tag{9.3.31}$$

where we have defined the second radiation integral:

$$I_2 = \oint |h|^2\,\mathrm{d}s \tag{9.3.32}$$

9.3.1.2 Longitudinal Damping Rate and Fourth Radiation Integral

Following Hofmann's analysis, the longitudinal damping rate can be written as [35]:

$$\alpha_\epsilon = \frac{1}{2}\frac{1}{T_{\mathrm{rev}}}\frac{\mathrm{d}U_s}{\mathrm{d}E} \tag{9.3.33}$$

We calculate:

$$\frac{\mathrm{d}U_s}{\mathrm{d}E} = \frac{1}{c}\frac{\mathrm{d}}{\mathrm{d}E}\oint P_s(s')\,\mathrm{d}s' = \frac{1}{c}\frac{\mathrm{d}}{\mathrm{d}E}\oint P_s\,(1 + h_{0x}x(E) + h_{0y}y(E))\,\mathrm{d}s \tag{9.3.34}$$

Using the dispersion to express $x(E)$ and $y(E)$:

$$\frac{\mathrm{d}U_s}{\mathrm{d}E} = \frac{\mathrm{d}}{\mathrm{d}E}\frac{1}{c}\oint P_s\,(1 + h_{0x}D_x\delta + h_{0y}D_y\delta)\,\mathrm{d}s \tag{9.3.35}$$

The derivative w.r.t. E is related to the derivative w.r.t. δ by:

$$\frac{\mathrm{d}}{\mathrm{d}E} = \frac{\mathrm{d}\delta}{\mathrm{d}E}\frac{\mathrm{d}}{\mathrm{d}\delta} = \frac{\mathrm{d}}{\mathrm{d}E}\left(\frac{E - E_0}{E_0}\right)\frac{\mathrm{d}}{\mathrm{d}\delta} = \frac{1}{E_0}\frac{\mathrm{d}}{\mathrm{d}\delta} \tag{9.3.36}$$

Writing out the derivative then gives:

$$\begin{aligned}\frac{\mathrm{d}U_s}{\mathrm{d}E} &= \frac{1}{c}\oint \frac{\mathrm{d}P_s}{\mathrm{d}E}(1 + h_{0x}D_x\delta + h_{0y}D_y\delta) + \frac{P_s}{E_0}\frac{\mathrm{d}}{\mathrm{d}\delta}(1 + h_{0x}D_x\delta + h_{0y}D_y\delta)\,\mathrm{d}s \\ &= \frac{1}{c}\oint \frac{\mathrm{d}P_s}{\mathrm{d}E}(1 + h_{0x}D_x\delta + h_{0y}D_y\delta) + \frac{P_s}{E_0}(h_{0x}D_x + h_{0y}D_y)\,\mathrm{d}s\end{aligned} \tag{9.3.37}$$

The derivative of P_s w.r.t. E can be rewritten as:

$$\frac{\mathrm{d}P_s}{\mathrm{d}E} = 2P_s \left[\frac{1}{E} + \frac{1}{B} \left(\frac{\partial B}{\partial x} \frac{\mathrm{d}x}{\mathrm{d}E} + \frac{\partial B}{\partial y} \frac{\mathrm{d}y}{\mathrm{d}E} \right) \right] \tag{9.3.38}$$

The derivatives of the positions w.r.t. E are related to the dispersions through Eq. 9.3.36

$$\frac{\mathrm{d}x}{\mathrm{d}E} = \frac{1}{E_0} \frac{\mathrm{d}x}{\mathrm{d}\delta} = \frac{1}{E_0} D_x \tag{9.3.39}$$

$$\frac{\mathrm{d}y}{\mathrm{d}E} = \frac{1}{E_0} \frac{\mathrm{d}y}{\mathrm{d}\delta} = \frac{1}{E_0} D_y \tag{9.3.40}$$

Using the fact that $B = \sqrt{B_x^2 + B_y^2}$, the derivatives of B w.r.t. x and y are:

$$\frac{\partial B}{\partial x} = \frac{B_x}{B} \frac{\partial B_x}{\partial x} + \frac{B_y}{B} \frac{\partial B_y}{\partial x} \tag{9.3.41}$$

$$\frac{\partial B}{\partial y} = \frac{B_x}{B} \frac{\partial B_x}{\partial y} + \frac{B_y}{B} \frac{\partial B_y}{\partial y} \tag{9.3.42}$$

The magnetic field gradients are defined as:

$$\frac{\partial B_y}{\partial x} = \frac{\partial B_x}{\partial y} = G = \frac{\gamma_0 m_0 c}{Q_0} k_1 \tag{9.3.43}$$

$$\frac{\partial B_x}{\partial x} = -\frac{\partial B_y}{\partial y} = \bar{G} = \frac{\gamma_0 m_0 c}{Q_0} \bar{K}_1 \tag{9.3.44}$$

Here, k_1 is the normalized normal quadrupole strength and $\bar{K}_1$ is the normalized skew quadrupole strength, both in units of $1/m^2$. In the following we neglect the skew quadrupole component and we assume that for the closed orbit $\gamma \simeq \gamma_0$, obtaining:

$$\frac{\mathrm{d}P_s}{\mathrm{d}E} = 2P_s \left[\frac{1}{E} + \frac{1}{E_0} \frac{\gamma m_0 c}{Q_0} \frac{k_1}{B^2} \left(B_y D_x + B_x D_y \right) \right] \tag{9.3.45}$$

The curvatures in Eqs. (9.3.9), (9.3.10) and (9.3.12) can be substituted, which gives:

$$\frac{\mathrm{d}P_s}{\mathrm{d}E} = 2\frac{P_s}{E} \left[\frac{1}{E} + \frac{1}{E_0} \frac{k_1}{h^2} \left(h_x D_x - h_y D_y \right) \right] \tag{9.3.46}$$

Substituting Eq. (9.3.29) gives:

$$\frac{\mathrm{d}P_s}{\mathrm{d}E} = \frac{4}{3} c r_0 E \gamma^3 \left[\frac{|h|^2}{E} + \frac{1}{E_0} k_1 \left(h_x D_x - h_y D_y \right) \right] \tag{9.3.47}$$

Substituting this expression back in Eq. (9.3.34) gives:

$$\frac{\mathrm{d}U_s}{\mathrm{d}E} = \frac{2}{3} \frac{c r_0 E \gamma^3}{c} \oint \left[2\frac{|h|^2}{E} (1 + h_{0x} x + h_{0y} y) + 2\frac{k_1}{E_0} \left(h_x D_x - h_y D_y \right) (1 + h_{0x} x + h_{0y} y) \right.$$
$$\left. + \frac{|h|^2}{E_0} (h_{0x} D_x + h_{0y} D_y) \right] \mathrm{d}s \tag{9.3.48}$$

The first term can be identified as I_2; again we assume that $h_{0x}x + h_{0y}y \ll 1$ and, as stated above, on the closed orbit we assume $E/E_0 \approx 1$. Hence, we can write:

$$\frac{\mathrm{d}U_s}{\mathrm{d}E} = \frac{2}{3} r_0 \gamma^3 \left[2I_2 + \oint \left[2k_1 \left(h_x D_x - h_y D_y \right) + |h|^2 (h_{0x} D_x + h_{0y} D_y) \right] \mathrm{d}s \right] \tag{9.3.49}$$

The last integral is identified as the fourth radiation integral, I_4, given by:

$$I_4 = \oint \left[2k_1 \left(h_x D_x - h_y D_y \right) + |h|^2 (h_{0x} D_x + h_{0y} D_y) \right] \mathrm{d}s \tag{9.3.50}$$

Hence we can write:

$$\frac{\mathrm{d}U_s}{\mathrm{d}E} = \frac{2}{3} r_0 \gamma^3 (2I_2 + I_4) \tag{9.3.51}$$

The longitudinal damping rate is obtained by substituting this expression in Eq. (9.3.33):

$$\alpha_\epsilon = \frac{1}{3} \frac{r_0 \gamma^3}{T_{\mathrm{rev}}} (2I_2 + I_4) \tag{9.3.52}$$

9.3.1.3 Energy Spread and Third Radiation Integral

From Hofmann, the variance in the amplitude of a damped oscillator that is excited by a short pulse $a\delta(t)$ is given by [35]:

$$\left\langle x^2 \right\rangle = \frac{\dot{n} \left\langle a^2 \right\rangle}{4\alpha} \tag{9.3.53}$$

Here, x is the deflection of the oscillator, $\dot{n}$ is the average rate at which excitation occurs, a is the amplitude of the excitation and α is the damping rate of the oscillator. For quantum excitation of the longitudinal emittance, we identify x as the RMS energy $\mathrm{d}E$, $\dot{n}$ as the average rate of photon emission, a as the photon energy and α as α_ϵ, the longitudinal damping rate. The normalized variance is then:

$$\frac{\left\langle \mathrm{d}E^2 \right\rangle}{E_0^2} = \frac{\dot{n} \left\langle E_\gamma^2 \right\rangle}{4\alpha_\epsilon E_0^2} \tag{9.3.54}$$

The rate of photon emission is given by:

$$\dot{n} = \frac{60\sqrt{3}}{72} \frac{r_0 c Q B}{\hbar} \tag{9.3.55}$$

The variance in the photon energy is given by:

$$\left\langle E_\gamma^2 \right\rangle = \frac{11}{12} \frac{Q^2 \hbar^2 \gamma^4 B^2}{m_0^2} \tag{9.3.56}$$

and the longitudinal damping rate is given by Eq. (9.3.52). Combining all these terms leads to

$$\frac{\left\langle \mathrm{d}E^2 \right\rangle}{E_0^2} = \frac{60\sqrt{3}}{72} \frac{11}{12} \frac{3}{4} \frac{r_0 c Q B}{\hbar} \frac{Q^2 \hbar^2 \gamma^4 B^2}{m_0^2 E_0^2} \frac{C_0}{c r_0 \gamma^3} \frac{1}{2I_2 + I_4} \tag{9.3.57}$$

This simplifies to

$$\frac{\langle \mathrm{d}E^2 \rangle}{E_0^2} = \frac{55\sqrt{3}}{96} \frac{Q^3 \hbar \gamma B^3 C_0}{m_0^2 E_0^2} \frac{1}{2I_2 + I_4} \tag{9.3.58}$$

The curvature h can be substituted for B, which gives

$$\frac{\langle \mathrm{d}E^2 \rangle}{E_0^2} = \frac{55\sqrt{3}}{96} \frac{\hbar m_0 \gamma^4 c^3 C_0}{E_0^2} \frac{h^3}{2I_2 + I_4} \tag{9.3.59}$$

Now averaging over the entire circumference of the ring gives

$$\left\langle \frac{\langle \mathrm{d}E^2 \rangle}{E_0^2} \right\rangle_{\text{ring}} = \frac{55\sqrt{3}}{96} \frac{\hbar \gamma^2 C_0}{m_0 c} \frac{\frac{1}{C_0} \oint h^3 \, \mathrm{d}s'}{2I_2 + I_4} = \frac{55\sqrt{3}}{96} \frac{\hbar \gamma^2}{m_0 c} \frac{\oint h^3 \, \mathrm{d}s'}{2I_2 + I_4} \tag{9.3.60}$$

The integral in the numerator can be defined as

$$I_3 = \oint |h|^3 \, \mathrm{d}s' = \oint |h|^3 (1 + h_{0x} x + h_{0y} y) \, \mathrm{d}s \tag{9.3.61}$$

This is the third radiation integral. This way, the energy spread becomes

$$\left\langle \frac{\langle \mathrm{d}E^2 \rangle}{E_0^2} \right\rangle_{\text{ring}} = \frac{55\sqrt{3}}{96} \frac{\hbar \gamma^2}{m_0 c} \frac{I_3}{2I_2 + I_4} \tag{9.3.62}$$

9.3.1.4 Transverse Damping Rates

The derivation in this section is valid for either x or y. To this end, u will be used as a substitute for either x or y. The goal is to find the rate at which the transverse emittance, ϵ_u, decreases. The emittance is given by

$$\epsilon_u = \gamma_u u_\beta^2 + 2\alpha_u u_\beta u'_\beta + \beta_u u'^2_\beta \tag{9.3.63}$$

Here, the subscript β indicates the betatron component of the coordinate value. The total coordinates, u and u', are a combination of the betatron and the energy deviation δ parts, that is

$$u = u_\beta + u_\delta \tag{9.3.64}$$

$$u' = u'_\beta + u'_\delta \tag{9.3.65}$$

When a photon is emitted, the coordinate does not change. This means that

$$\mathrm{d}u = \mathrm{d}u_\beta + \mathrm{d}u_\delta = 0 \tag{9.3.66}$$

The change in position due to an energy deviation is related to the dispersion through

$$\mathrm{d}u_\delta = D_u \mathrm{d}\delta = D_u \frac{\mathrm{d}E}{E_0} = -D_u \frac{\mathrm{d}E_\gamma}{E_0} \tag{9.3.67}$$

Therefore

$$\mathrm{d}u_\beta = -\mathrm{d}u_\delta = D_u \frac{\mathrm{d}E_\gamma}{E_0} \tag{9.3.68}$$

where $\mathrm{d}E_\gamma$ is the energy of the emitted photon. The angle is allowed to change due to the photon emission, that is

$$\mathrm{d}u' = \mathrm{d}u'_\beta + \mathrm{d}u'_\delta \tag{9.3.69}$$

We want to express $\mathrm{d}u'$ in terms of the photon energy. To this end, assume that the particle before photon emission is on-momentum, such that

$$u'_1 = u'_\beta \tag{9.3.70}$$

Following Hofmann we can write [35]:

$$u'_{2\beta} - u'_{1\beta} = \mathrm{d}u_\beta = -\left(u'_{1\beta} - D'\right)\frac{\mathrm{d}E_\gamma}{E_0} \tag{9.3.71}$$

Note that the emittance only depends on u_β and u'_β. The change in emittance is:

$$\mathrm{d}\epsilon_u = 2\left(\gamma_u u_\beta\, \mathrm{d}u_\beta + \alpha_u(u_\beta\, \mathrm{d}u'_\beta + u'_\beta\, \mathrm{d}u_\beta) + \gamma_u u'_\beta\, \mathrm{d}u'_\beta\right) \tag{9.3.72}$$

Substituting Equations (9.3.68) and (9.3.71) gives

$$\mathrm{d}\epsilon_u = 2\left[\gamma_u u_\beta\, D_u\frac{\mathrm{d}E_\gamma}{E_0} + \alpha_u\left(-u_\beta\,\left(u'_\beta - D'\right)\frac{\mathrm{d}E_\gamma}{E_0} + u'_\beta\, D_u\frac{\mathrm{d}E_\gamma}{E_0}\right) - \beta_u u'_\beta\,\left(u'_\beta - D'\right)\frac{\mathrm{d}E_\gamma}{E_0}\right] \tag{9.3.73}$$

$$= -2\frac{\mathrm{d}E_\gamma}{E_0}\left[\left(\alpha_u u_\beta u'_\beta + \beta_u u'^2_\beta\right) - \left(\gamma_u D_u u_\beta + \alpha_x(D_u u'_\beta + D'_u u_\beta) + \beta_u D'_u u'_\beta\right)\right] \tag{9.3.74}$$

The instantaneous power radiated by a particle undergoing betatron oscillations can be expressed as:

$$P_{s'} = P_s + \frac{\mathrm{d}P_s}{\mathrm{d}u}u_\beta \tag{9.3.75}$$

Using the chain rule for the derivative gives:

$$\frac{\mathrm{d}P_s}{\mathrm{d}u} = \frac{\mathrm{d}P_s}{\mathrm{d}B}\frac{\mathrm{d}B}{\mathrm{d}u} = 2\frac{P_s}{B}\left(\frac{\mathrm{d}B}{\mathrm{d}B_w}\frac{\partial B_w}{\partial u} + \frac{\mathrm{d}B}{\mathrm{d}B_u}\frac{\partial B_u}{\partial u}\right) = 2\frac{P_s}{B^2}\left(B_w\frac{\partial B_w}{\partial u} + B_u\frac{\partial B_u}{\partial u}\right) \tag{9.3.76}$$

Here, w denotes the component other than u. That is, if u is chosen to be x, then $w = y$ and vice versa. As has been done in Section 9.3.1.2, $\frac{\partial B_u}{\partial u}$ represents the skew quadrupole gradients, whereas $\frac{\partial B_w}{\partial u}$ represents the normal quadrupole gradients. The following step is similar to the derivation of Eq. 9.3.46, which results in

$$\frac{\mathrm{d}P_s}{\mathrm{d}u} = 2\frac{P_s}{B^2}B_w\frac{\partial B_w}{\partial u} = 2P_s\frac{h_u}{h^2}k_1 \tag{9.3.77}$$

The radiated power then becomes

$$P_{s'} = P_s \left[1 + 2\frac{h_u}{h^2} k_1 u_\beta\right] \tag{9.3.78}$$

The energy radiated in a time interval $\mathrm{d}s'/c$ is then given by

$$\begin{aligned} \mathrm{d}E_\gamma = P_{s'}\frac{\mathrm{d}s'}{c} &= \frac{P_s}{c}\left[1 + 2\frac{h_u}{h^2} k_1 u_\beta\right]\ \mathrm{d}s' \\ &= \frac{P_s}{c}\left[1 + 2\frac{h_u}{h^2} k_1 u_\beta\right]\ (1 + h_{0u} u_\beta)\ \mathrm{d}s \\ &= \frac{P_s}{c}\left[1 + \left(h_{0u} + 2\frac{h_u}{h^2} k_1\right) u_\beta\right]\ \mathrm{d}s \end{aligned} \tag{9.3.79}$$

Here, only the u-component of h_0 was used, because we study betatron oscillations only in the selected plane. Furthermore, terms of second order in u_β were neglected. This result can be substituted back in Eq. 9.3.74, which gives

$$\begin{aligned} \mathrm{d}\epsilon_u = -2\frac{P_s}{cE_0}&\left[1 + \left(h_{0u} + 2\frac{h_u}{h^2} k_1\right) u_\beta\right] \\ &\times \left[\left(\alpha_u u_\beta u'_\beta + \beta_u u'^2_\beta\right) - \left(\gamma_u D_u u_\beta + \alpha_x (D_u u'_\beta + D'_u u_\beta) + \beta_u D'_u u'_\beta\right)\right]\ \mathrm{d}s \end{aligned} \tag{9.3.80}$$

Using the same reasoning as before, the odd terms average to zero. This means only the even terms need to be kept. This results in

$$\begin{aligned} \mathrm{d}\epsilon_u = -2\frac{P_s}{cE_0}&\left[\left(\alpha_u u_\beta u'_\beta + \beta_u u'^2_\beta\right)\right. \\ &\left. - \left(h_{0u} + 2\frac{h_u}{h^2} k_1\right)\left(\gamma_u D_u u^2_\beta + \alpha_x (D_u u_\beta u'_\beta + D'_u u^2_\beta) + \beta_u D'_u u_\beta u'_\beta\right)\right]\ \mathrm{d}s \end{aligned} \tag{9.3.81}$$

The averages of the squared terms are

$$\left\langle u^2_\beta \right\rangle = \frac{1}{2}\epsilon_u \beta_u \tag{9.3.82}$$

$$\left\langle u_\beta u'_\beta \right\rangle = -\frac{1}{2}\epsilon_u \alpha_u \tag{9.3.83}$$

$$\left\langle u'^2_\beta \right\rangle = \frac{1}{2}\epsilon_u \gamma_u \tag{9.3.84}$$

Substituting these averages gives

$$\begin{aligned} \mathrm{d}\epsilon_u = -2\frac{P_s}{cE_0}&\left[\left(-\frac{1}{2}\alpha^2_u \epsilon_u + \frac{1}{2}\beta_u \gamma_u \epsilon_u\right)\right. \\ &\left. - \left(h_{0u} + 2\frac{h_u}{h^2} k_1\right)\left(\frac{1}{2}\gamma_u \beta_u \epsilon_u D_u + \alpha_x\left(-\frac{1}{2}\alpha_u \epsilon_u D_u + \frac{1}{2}\beta_u \epsilon_u D'_u\right) - \frac{1}{2}\alpha_u \beta_u \epsilon_u D'_u\right)\right]\ \mathrm{d}s \end{aligned} \tag{9.3.85}$$

Note that $\beta_u\gamma_u - \alpha_u^2 = 1$ and that the cross terms between $\alpha_u\beta_u$ cancel. This way, the expression simplifies to

$$\mathrm{d}\epsilon_u = -\epsilon_u \frac{P_s}{E_0}\left[1 - \left(h_{0u} + 2\frac{h_u}{h^2}k_1\right) D_u\right] \mathrm{d}s \tag{9.3.86}$$

To arrive at the change in emittance per unit time, we divide by T_{rev}

$$\frac{\mathrm{d}\epsilon_u}{dt} = -\epsilon_u \oint \frac{P_s}{C_0 E_0}\left[1 - \left(h_{0u} + 2\frac{h_u}{h^2}k_1\right) D_u\right] \mathrm{d}s \tag{9.3.87}$$

Finally, Eq. 9.3.29 may be substituted, which results in

$$\frac{\mathrm{d}\epsilon_u}{dt} = -\epsilon_u \frac{2}{3}\frac{cr_0\gamma^3}{C_0} \oint \left[h^2 - \left(h^2 h_{0u} + 2h_u k_1\right) D_u\right] \mathrm{d}s \tag{9.3.88}$$

Here, the second radiation integral is identified. Furthermore, the u-component of the fourth radiation integral is found to be

$$I_{4u} = \oint \left(h^2 h_{0u} + 2h_u k_1\right) D_u \, \mathrm{d}s \tag{9.3.89}$$

Thus,

$$\frac{\mathrm{d}\epsilon_u}{dt} = -\epsilon_u \frac{2}{3}\frac{cr_0\gamma^3}{C_0}(I_2 - I_{4u}) \tag{9.3.90}$$

This is a first-order ODE, with a damping rate given by

$$\frac{2}{3}\frac{cr_0\gamma^3}{C_0}(I_2 - I_{4u}) \tag{9.3.91}$$

Since the betatron amplitude is proportional to $\sqrt{\epsilon_u}$, the 2 in the numerator disappears. This leads to the damping constant

$$\alpha_u = \frac{cr_0\gamma^3}{3C_0}(I_2 - I_{4u}) \tag{9.3.92}$$

9.3.1.5 Transverse Equilibrium Emittances and the Fifth Radiation Integral

The derivation in this section is valid for either x or y. To this end, u will be used as a substitute for either x or y. The changes in betatron position and angle when a photon is emitted, denoted by u_β and u'_β respectively, are given by

$$\delta u_\beta = D_u \frac{\delta E\gamma}{E_0} \tag{9.3.93}$$

$$\delta u'_\beta = D'_u \frac{\delta E\gamma}{E_0} \tag{9.3.94}$$

Here, δE is the energy carried away by the photon. The emittance before the emission of the photon, ϵ_{u1}, is given by

$$\epsilon_{u1} = \gamma_u u_\beta^2 + 2\alpha_u u_\beta u'_\beta + \beta_u u'^2_\beta \tag{9.3.95}$$

After the emission of the photon, the emittance has increased. The resulting emittance, ϵ_{u2}, is

$$\begin{aligned}\epsilon_{u2} &= \gamma_u(u_\beta + \delta u_\beta)^2 + 2\alpha_u(u_\beta + \delta u_\beta)(u'_\beta + \delta u'_\beta) + \beta_u(u'_\beta + \delta u'_\beta)^2 \\ &= \epsilon_{u1} + 2\left(\gamma_u u_\beta \delta u_\beta + \alpha_u(u_\beta \delta u'_\beta + u'_\beta \delta u_\beta) + \beta_u u'_\beta \delta u'_\beta\right) \\ &+ \gamma_u \delta u_\beta^2 + 2\alpha_u \delta u_\beta \delta u'_\beta + \beta_u \delta u_\beta^2\end{aligned} \tag{9.3.96}$$

The change in the emittance is then

$$\begin{aligned}\mathrm{d}\epsilon_u = \epsilon_{u2} - \epsilon_{u1} &= 2\left(\gamma_u u_\beta \mathrm{d}u_\beta + \alpha_u(u_\beta \mathrm{d}u'_\beta + u'_\beta \mathrm{d}u_\beta) + \beta_u u'_\beta \mathrm{d}u'_\beta\right) \\ &+ \gamma_u \mathrm{d}u_\beta^2 + 2\alpha_u \mathrm{d}u_\beta \mathrm{d}u'_\beta + \beta_u \mathrm{d}u'^2_\beta\end{aligned} \tag{9.3.97}$$

Equations (9.3.93) and (9.3.94) can now be substituted, which results in

$$\begin{aligned}\mathrm{d}\epsilon_u &= \left(\gamma_u D_u^2 + 2\alpha_u D_u D'_u + \beta_u D'^2_u\right)\left(\frac{\mathrm{d}E_\gamma}{E_0}\right)^2 \\ &+ 2\left(\gamma_u u_\beta D_x + \alpha_u\left(u_\beta D'_x + u'_\beta D_x\right) + \beta_u u'_\beta D'_x\right)\frac{\mathrm{d}E_\gamma}{E_0}\end{aligned} \tag{9.3.98}$$

The terms that are linear in u_β and u'_β will average to zero over many photon emissions. Hence:

$$\langle \mathrm{d}\epsilon_u \rangle = \left(\gamma_u D_u^2 + 2\alpha_u D_u D'_u + \beta_u D'^2_u\right)\frac{\left\langle \mathrm{d}E_\gamma^2 \right\rangle}{E_0^2} \tag{9.3.99}$$

To this end, we define $\mathcal{H}_u$ as

$$\mathcal{H}_u = \gamma_u D_u^2 + 2\alpha_u D_u D'_u + \beta_u D'^2_u \tag{9.3.100}$$

Thus, the expectation of the change in emittance is

$$\langle \mathrm{d}\epsilon_u \rangle = \mathcal{H}_u \frac{\left\langle \mathrm{d}E_\gamma^2 \right\rangle}{E_0^2} \tag{9.3.101}$$

Now, Eq. 9.3.54 can be used, on the transverse coordinate [35]:

$$\langle \mathrm{d}\epsilon_u \rangle = \mathcal{H}_u \frac{\left\langle \mathrm{d}E^2 \right\rangle}{E_0^2} = \mathcal{H}_u \frac{\dot{n}\left\langle E_\gamma^2 \right\rangle}{4\alpha_u E_0^2} \tag{9.3.102}$$

This gives a result very similar to Eq. 9.3.59

$$\langle \mathrm{d}\epsilon_u \rangle = \frac{55\sqrt{3}}{96}\frac{\hbar\gamma^2}{m_0 c}\frac{h^3 \mathcal{H}_u}{I_2 - I_{4u}} \tag{9.3.103}$$

Integrating over the entire ring gives

$$\begin{aligned}\langle \epsilon_u \rangle &= \frac{55\sqrt{3}}{96}\frac{\hbar\gamma^2}{m_0 c}\frac{1}{I_2 - I_{4u}}\oint h^3 \mathcal{H}_u \, \mathrm{d}s' \\ &= \frac{55\sqrt{3}}{96}\frac{\hbar\gamma^2}{m_0 c}\frac{1}{I_2 - I_{4u}}\oint h^3 \mathcal{H}_u \, (1 + h_{0u}u) \, \mathrm{d}s \end{aligned} \tag{9.3.104}$$

Again we assume $h_{0u}u \ll 1$. We can then define the fifth radiation integral, I_{5u}, as follows:

$$I_{5u} = \oint h^3 \mathcal{H}_u \, \mathrm{d}s \tag{9.3.105}$$

The expectation value of the emittance can be written as:

$$\langle \epsilon_u \rangle = \frac{55\sqrt{3}}{96}\frac{\hbar\gamma^2}{m_0 c}\frac{I_{5u}}{I_2 - I_{4u}} \tag{9.3.106}$$

Chapter 10

Spin tracking and polarization

10.1 Spin tracking

This section is based on [38, 21].
The spin precession for a particle traveling in a magnetic field $\boldsymbol{B}$ can be written in terms of the precession angular velocity:

$$\boldsymbol{\Omega}_{\mathrm{BMT}} = -\frac{1}{B\rho_{\mathrm{part}}}\left[(1+a\gamma)\boldsymbol{B}_{\perp} + (1+a)\boldsymbol{B}_{\parallel}\right] \tag{10.1.1}$$

where a is the anomalous magnetic moment and $\boldsymbol{B}_{\parallel}$ and $\boldsymbol{B}_{\perp}$ are referred to the velocity of the particle.
The precession angle for a particle traveling a path length ℓ is given by:

$$\phi = |\boldsymbol{\Omega}|\ell \tag{10.1.2}$$

We call:

$$\boldsymbol{\omega} = \frac{\boldsymbol{\Omega}}{|\boldsymbol{\Omega}|} \tag{10.1.3}$$

and we define:

$$t_0 = \cos\left(\frac{\phi}{2}\right) \tag{10.1.4}$$

$$t_x = \omega_x \sin\left(\frac{\phi}{2}\right) \tag{10.1.5}$$

$$t_y = \omega_y \sin\left(\frac{\phi}{2}\right) \tag{10.1.6}$$

$$t_s = \omega_z \sin\left(\frac{\phi}{2}\right) \tag{10.1.7}$$

The spin vector of the particle is transformed by the following rotation matrix:

$$M = \begin{bmatrix} (t_0^2+t_x^2)-(t_s^2+t_y^2) & 2(t_xt_y - t_0t_s) & 2(t_xt_s + t_0t_y) \\ 2(t_xt_y + t_0t_s) & (t_0^2+t_y^2)-(t_x^2+t_s^2) & 2(t_st_y - t_0t_x) \\ 2(t_xt_s - t_0t_y) & 2(t_st_y + t_0t_x) & (t_0^2+t_s^2)-(t_x^2+t_y^2) \end{bmatrix} \tag{10.1.8}$$

10.2 Linear transport matrix including spin

The coordinate vector including the spin is defined as:

$$\boldsymbol{z} = \begin{pmatrix} x \\ p_x \\ y \\ p_y \\ \zeta \\ \delta \\ s_x \\ s_y \\ s_z \end{pmatrix} \quad \text{We call } \boldsymbol{z}_{\text{orb}} = \begin{pmatrix} x \\ p_x \\ y \\ p_y \\ \zeta \\ \delta \end{pmatrix}, \quad \boldsymbol{z}_{\text{spin}} = \begin{pmatrix} s_x \\ s_y \\ s_z \end{pmatrix} \tag{10.2.1}$$

The corresponding 9D transport matrix can be written as

$$\mathbf{R} = \begin{pmatrix} \mathbf{R}_{\text{orb}} & 0 \\ \mathbf{D} & \mathbf{A} \end{pmatrix} \tag{10.2.2}$$

We call $\boldsymbol{e}_1, \ldots, \boldsymbol{e}_9$ the eigenvectors and $\lambda_1, \ldots, \lambda_9$ the eigenvalues so that

$$\mathbf{R}\boldsymbol{e}_i = \lambda_i \boldsymbol{e}_i \tag{10.2.3}$$

From the definition of eigenvectors (doing the matrix product in blocks), we can write:

$$\mathbf{R}_{\text{orb}}\, \boldsymbol{e}_{i,\text{orb}} = \lambda_i \boldsymbol{e}_{i,\text{orb}} \tag{10.2.4}$$

$$\mathbf{D}\, \boldsymbol{e}_{i,\text{orb}} + \mathbf{A}\, \boldsymbol{e}_{i,\text{spin}} = \lambda_i \boldsymbol{e}_{i,\text{spin}} \tag{10.2.5}$$

From this:

$$\mathbf{D}\, \boldsymbol{e}_{i,\text{orb}} = (\lambda_i \boldsymbol{I} - \mathbf{A})\, \boldsymbol{e}_{i,\text{spin}} \tag{10.2.6}$$

$$\boldsymbol{e}_{i,\text{spin}} = (\lambda_i \boldsymbol{I} - \mathbf{A})^{-1}\, \mathbf{D}\, \boldsymbol{e}_{i,\text{orb}} \tag{10.2.7}$$

10.3 Invariant Spin Field - first order computation

This section is based on [39].
We expand the Invariant Spin Field [38] function to first order

$$\boldsymbol{n}(\boldsymbol{z}_{\text{orb}}) = \boldsymbol{n}_0 + \mathbf{N}\left(\boldsymbol{z}_{\text{orb}} - \boldsymbol{z}_{\text{orb}}^{\text{CO}}\right) \tag{10.3.1}$$

In the following we drop all the constant terms so we simply write $\boldsymbol{n}(\boldsymbol{z}_{\text{orb}}) = \mathbf{N}\boldsymbol{z}_{\text{orb}}$.
We now call $\boldsymbol{z}_1^{\text{spin}}$ the ISF at $\boldsymbol{z}_1^{\text{orb}}$, i.e.

$$\boldsymbol{z}_1^{\text{spin}} = \mathbf{N}\boldsymbol{z}_1^{\text{orb}} \tag{10.3.2}$$

We call $\boldsymbol{z}_2$ the coordinate after one revolution. By definition of the ISF, the spin part of $\boldsymbol{z}_2$ is the ISF at $\boldsymbol{z}_2^{\text{orb}}$, i.e.

$$\boldsymbol{z}_2^{\text{spin}} = \mathbf{N}\boldsymbol{z}_2^{\text{orb}} \tag{10.3.3}$$

We know from the structure of the one-turn matrix:

$$\boldsymbol{z}_2^{\text{orb}} = \mathbf{R}_{\text{orb}}\boldsymbol{z}_1^{\text{orb}} \tag{10.3.4}$$

$$\boldsymbol{z}_2^{\text{spin}} = \mathbf{D}\boldsymbol{z}_1^{\text{orb}} + \mathbf{A}\boldsymbol{z}_1^{\text{spin}} \tag{10.3.5}$$

Combining Eqs. 10.3.3, 10.3.4 and 10.3.5, we obtain:

$$\mathbf{N}\mathbf{R}_{\text{orb}}\boldsymbol{z}_1^{\text{orb}} = \mathbf{D}\boldsymbol{z}_1^{\text{orb}} + \mathbf{A}\mathbf{N}\boldsymbol{z}_1^{\text{orb}} \tag{10.3.6}$$

We specialize it for the case $\boldsymbol{z}_1^{\text{orb}} = \boldsymbol{e}_1^{\text{orb}}$ obtaining:

$$\lambda_1\mathbf{N}\boldsymbol{e}_1^{\text{orb}} = \mathbf{D}\boldsymbol{e}_1^{\text{orb}} + \mathbf{A}\mathbf{N}\boldsymbol{e}_1^{\text{orb}} \tag{10.3.7}$$

From Eq. 10.2.4, we obtain:

$$\mathbf{D}\boldsymbol{e}_1^{\text{orb}} = \lambda_1\boldsymbol{e}_1^{\text{spin}} - \mathbf{A}\boldsymbol{e}_1^{\text{spin}} \tag{10.3.8}$$

Replacing into Eq. 10.2.4, we obtain:

$$(\lambda_1\mathbf{I} - \mathbf{A})\mathbf{N}\boldsymbol{e}_1^{\text{orb}} = (\lambda_1\mathbf{I} - \mathbf{A})\boldsymbol{e}_1^{\text{spin}} \tag{10.3.9}$$

If $(\lambda_1\mathbf{I} - \mathbf{A})$ is not singular:

$$\mathbf{N}\boldsymbol{e}_1^{\text{orb}} = \boldsymbol{e}_1^{\text{spin}} \tag{10.3.10}$$

Combining this result for the six orbital eigenvectors:

$$\begin{pmatrix}\mathbf{N}\boldsymbol{e}_1^{\text{orb}} & \cdots & \mathbf{N}\boldsymbol{e}_6^{\text{orb}}\end{pmatrix} = \begin{pmatrix}\boldsymbol{e}_1^{\text{spin}} & \cdots & \boldsymbol{e}_6^{\text{spin}}\end{pmatrix} \tag{10.3.11}$$

In matrix form:

$$\mathbf{N}\mathbf{E}^{\text{orb}} = \mathbf{E}^{\text{spin}} \quad \Rightarrow \quad \mathbf{N} = \mathbf{E}^{\text{spin}}\left(\mathbf{E}^{\text{orb}}\right)^{-1} \tag{10.3.12}$$

We note that the last column of the matrix $\boldsymbol{N}$ provides the derivative $\frac{d\boldsymbol{n}}{d\delta}$ which is relevant for the computation of equilibrium polarization.

10.4 Equilibrium polarization and polarization time

This section is based on [39, 40, 41, 21, 42, 43].
In the presence of photon emission, the polarization of the beam evolves following the equation:

$$P(t) = P(0)e^{-\frac{t}{\tau_{\text{tot}}}} + P_{\text{eq}}\left(1 - e^{-\frac{t}{\tau_{\text{tot}}}}\right) \tag{10.4.1}$$

The equilibrium polarization and the buildup time can be computed as:

$$P_{\text{eq}} = \frac{8}{5\sqrt{3}} \frac{\alpha_-}{\alpha_+} \tag{10.4.2}$$

$$\tau_{\text{tot}}^{-1} = \frac{5\sqrt{3}}{8} \frac{r_e \hbar \gamma^5}{m_e} \cdot \alpha_+ \tag{10.4.3}$$

where, truncating to the first order the dependence of the ISF on the phase space coordinates, we have:

$$\alpha_+ \simeq \frac{1}{C} \oint \frac{ds}{|\rho(s)|^3} \left[1 - \frac{2}{9} (\boldsymbol{n_0} \cdot \hat{\boldsymbol{i}}_v)^2 + \frac{11}{18} \left| \frac{\partial \boldsymbol{n}}{\partial \delta} \right|^2 \right]_s \tag{10.4.4}$$

$$\alpha_- \simeq \frac{1}{C} \oint \frac{ds}{|\rho(s)|^3} \left[\hat{\boldsymbol{i}}_B \cdot (\boldsymbol{n}_0 - \frac{\partial \boldsymbol{n}}{\partial \delta}) \right]_s \tag{10.4.5}$$

The buildup time can be decomposed into two terms:

$$\tau_{\text{tot}}^{-1} = \tau_{\text{pol}}^{-1} + \tau_{\text{depol}}^{-1} \tag{10.4.6}$$

where:

$$\tau_{\text{pol}}^{-1} = \frac{5\sqrt{3}}{8} \frac{r_e \hbar \gamma^5}{m_e} \frac{1}{C} \oint \frac{ds}{|\rho(s)|^3} \left[1 - \frac{2}{9} (\boldsymbol{n_0} \cdot \hat{\boldsymbol{i}}_v)^2 \right]_s \tag{10.4.7}$$

$$\tau_{\text{depol}}^{-1} = \frac{5\sqrt{3}}{8} \frac{r_e \hbar \gamma^5}{m_e} \frac{1}{C} \oint \frac{ds}{|\rho(s)|^3} \left[\frac{11}{18} \left| \frac{\partial \boldsymbol{n}}{\partial \delta} \right|^2 \right]_s \tag{10.4.8}$$

10.5 Monte Carlo method for equilibrium polarization

This section is based on [41, 44].
We can define:

$$P_\infty = \frac{8}{5\sqrt{3}} \frac{\oint \frac{ds}{|\rho(s)|^3} \left[\hat{\boldsymbol{i}}_B \cdot (\boldsymbol{n}_0) \right]_s}{\oint \frac{ds}{|\rho(s)|^3} \left[1 - \frac{2}{9} (\boldsymbol{n_0} \cdot \hat{\boldsymbol{i}}_v)^2 \right]_s} \tag{10.5.1}$$

The equilibrium polarization and the buildup rate can be written as follows:

$$P_{\text{eq}} = P_\infty \frac{1}{1 + \frac{\tau_{\text{pol}}}{\tau_{\text{depol}}}} \tag{10.5.2}$$

$$\tau_{\text{tot}}^{-1} = \tau_{\text{pol}}^{-1} + \tau_{\text{depol}}^{-1} \tag{10.5.3}$$

The term τ_{depol} can be evaluated using particle tracking, accounting for quantum excitation from synchrotron radiation. Unlike the approach used in the previous section, this method accounts for the nonlinear dependence of the ISF on the phase space coordinates. Using τ_{depol} we can get from Eqs. 10.5.2 and 10.5.3 estimates for P_{eq} and τ_{tot} that include nonlinear effects.

Chapter 11

Coasting beams and acceleration

Tracking with time-dependent fields requires a consistent relation between the simulation clock, the longitudinal coordinates, and the particles' arrival times. During acceleration, the reference velocity and revolution period change, so the time associated with a turn must follow the evolving reference motion. This matters for both coasting and bunched beams.
Coasting beams also require care when grouping particles for collective interactions. Particles with different revolution frequencies can complete different numbers of revolutions in the same time interval. At a given location, a collective interaction must therefore use particles belonging to the same arrival-time window. The `SyncTime` scheme organizes tracking into such windows, pausing particles that arrive beyond the current window until a later simulation frame.
This chapter introduces the common clock and arrival-time convention, develops the frame construction at constant reference energy, and extends it to acceleration. The coordinate updates preserve physical arrival times when the clock advances or the reference velocity changes. Acceleration alone does not require `SyncTime`; the same clock convention also applies to ordinary turn-by-turn tracking with an active `EnergyProgram`.

11.1 Simulation clock and arrival time

A simulated "turn" is one pass through the ordered list of elements, advancing one time frame. It need not correspond to one revolution of every particle. We denote the common clock at the start of frame n by T_n, and its advance by $\Delta T_n = T_{n+1} - T_n$. The longitudinal coordinate is defined by

$$\boxed{\zeta = s - \beta_0 c(t - T_n), \qquad t = T_n + \frac{s - \zeta}{\beta_0 c}.} \tag{11.1.1}$$

Here t is the particle's arrival time at its current position s, and β_0 is its current reference velocity divided by c. The clock T_n is common to the ensemble; the arrival times and completed revolution counts are not.
In Xsuite, T_n is stored in `Particles.time_s`, while ΔT_n is stored in `Particles.t_sim`. In particular, `t_sim` is a duration, not the absolute simulation time. With `SyncTime`,

the requested `num_turns` counts frames, whereas each particle's `at_turn` counts its completed revolutions.
The following construction first assumes constant reference energy and a constant frame duration, with $T_n = n\Delta T$. Section 11.6 extends it to an accelerating reference using a common reference-turn/time map.

11.2 Constant-energy frame construction

We define for each particle and for any pair of positions $s_1 < s_2$:

$$\hat{\beta}(s_1, s_2) = \frac{1}{c}\frac{s_2 - s_1}{t(s_2) - t(s_1)} \tag{11.2.1}$$

We choose an auxiliary value β_{sim} such that at all times:

$$\hat{\beta}(s_1, s_2) < \beta_{\text{sim}} \quad \text{for all particles and any } s_1, s_2 \tag{11.2.2}$$

$$\hat{\beta}(s_1, s_2) > \frac{\beta_{\text{sim}}}{2} \quad \text{for all particles and any } s_1, s_2 \tag{11.2.3}$$

From β_{sim} we define an auxiliary time interval ΔT as:

$$\Delta T = \frac{L}{\beta_{\text{sim}} c} \tag{11.2.4}$$

At each "turn" n we want to simulate at any collective element the time frame $F_n(s)$ given by:

$$F_n(s) = \left[T_n(s) - \frac{\Delta T}{2}, T_n(s) + \frac{\Delta T}{2} \right) \tag{11.2.5}$$

where:

$$T_n(s) = T_n + \frac{s}{\beta_{\text{sim}} c} = n\Delta T + \frac{s}{\beta_{\text{sim}} c} \tag{11.2.6}$$

The intervals are contiguous; hence at any location over N frames we simulate a time interval of length $N\Delta T$. We include the lower boundary and exclude the upper boundary, so an arrival at a shared edge belongs to the later frame.
From Eq. 11.2.6 we can simply derive the following relations, which will be useful in the following:

$$T_{n+1}(s) - T_n(s) = \Delta T \tag{11.2.7}$$

$$T_n(s_2) - T_n(s_1) = \frac{s_2 - s_1}{\beta_{\text{sim}} c} \tag{11.2.8}$$

We also note that the condition $t(s) \in F_n(s)$ can be rewritten as:

$$-\frac{\Delta T}{2} \leq t - n\Delta T - \frac{s}{\beta_{\text{sim}} c} < \frac{\Delta T}{2} \tag{11.2.9}$$

We can prove the following propositions (see Sec. 11.5):

Proposition 1: If the time $t_k(s_1)$ defining the k-th arrival of a particle at location s_1

falls in the frame $F_n(s_1)$, then the particle arrives at location $s_2 > s_1$ either in the frame $F_n(s_2)$ or in the following frame $F_{n+1}(s_2)$. In symbols:

$$t_k(s_1) \in F_n(s_1) \Rightarrow t_k(s_2) \in F_n(s_2) \cup F_{n+1}(s_2) \quad \text{for any } s_1 < s_2 \tag{11.2.10}$$

Proposition 2: If the time $t_k(s_2)$ defining the k-th arrival of a particle at location s_2 falls in the frame $F_n(s_2)$, then the time of $(k+1)$-th arrival at any location $s_1 < s_2$ falls in the frame $F_{n+1}(s_1)$ or in the following frame $F_{n+2}(s_1)$. In symbols:

$$t_k(s_2) \in F_n(s_2) \Rightarrow t_{k+1}(s_1) \in F_{n+1}(s_1) \cup F_{n+2}(s_1) \quad \text{for any } s_1 < s_2 \tag{11.2.11}$$

Proposition 3: If the time $t_k(L)$ defining the k-th arrival of a particle at the end of the line falls in the frame $F_n(L)$, then the time $t_{k+1}(0) = t_k(L)$ of the $(k+1)$-th arrival of the particle at $s = 0$ falls in the interval $F_{n+1}(0)$. In symbols:

$$t_k(L) \in F_n(L) \Rightarrow t_{k+1}(0) \in F_{n+1}(0) \tag{11.2.12}$$

11.3 Constant-energy ζ definition and update

For constant reference energy and $T_n = n\Delta T$, Eq. 11.1.1 becomes:

$$\zeta = s - \beta_0 c(t - n\Delta T) \tag{11.3.1}$$

where s is the distance from the start of the line for the present turn, t is the absolute time since the start of the simulation, n is the index of the present simulated time frame.
We can write t in terms of ζ as:

$$t = \frac{s}{\beta_0 c} - \frac{\zeta}{\beta_0 c} + n\Delta T \tag{11.3.2}$$

With this definition the ζ coordinate needs to be updated each time the particle passes at the start of the line since across $s = 0$ we can write:

$$\zeta^- = L - \beta_0 c(t - n\Delta T) \tag{11.3.3}$$
$$\zeta^+ = 0 - \beta_0 c(t - (n+1)\Delta T) \tag{11.3.4}$$

where t is the time at which the particle passes zero (which is the same in both equations).
Combining the two equations we can write:

$$\zeta^+ = \zeta^- - (L - \beta_0 c\Delta T) \tag{11.3.5}$$

In standard simulations for bunched beams at constant reference energy the simulated frame is $\Delta T = L/(\beta_0 c)$, hence the ζ coordinate is continuous.

For coasting beams ΔT is given by Eq. 11.2.4, hence ζ needs to be updated at each turn using:

$$\boxed{\zeta^+ = \zeta^- - L\left(1 - \frac{\beta_0}{\beta_{\text{sim}}}\right)} \tag{11.3.6}$$

We want to translate the condition Eq. 11.2.9 into a condition on ζ. Replacing Eq. 11.3.2 into Eq. 11.2.9 we obtain:

$$-\frac{\Delta T}{2} \leq \left(\frac{s}{\beta_0 c} - \frac{\zeta}{\beta_0 c} + n\Delta T\right) - n\Delta T - \frac{s}{\beta_{\text{sim}} c} < \frac{\Delta T}{2} \tag{11.3.7}$$

We change signs:

$$\frac{\Delta T}{2} \geq -\frac{s}{\beta_0 c} + \frac{\zeta}{\beta_0 c} + \frac{s}{\beta_{\text{sim}} c} > -\frac{\Delta T}{2} \tag{11.3.8}$$

We rearrange:

$$-\frac{\Delta T}{2} < -\frac{s}{\beta_0 c} + \frac{\zeta}{\beta_0 c} + \frac{s}{\beta_{\text{sim}} c} \leq \frac{\Delta T}{2} \tag{11.3.9}$$

$$-\beta_0 c\frac{\Delta T}{2} < \zeta - s\left(1 - \frac{\beta_0}{\beta_{\text{sim}}}\right) \leq \beta_0 c\frac{\Delta T}{2} \tag{11.3.10}$$

from which we can write:

$$\boxed{t \in F_n(s) \quad \Leftrightarrow \quad -\frac{\Delta\zeta}{2} < \zeta - s\left(1 - \frac{\beta_0}{\beta_{\text{sim}}}\right) \leq \frac{\Delta\zeta}{2}} \tag{11.3.11}$$

where we have defined:

$$\boxed{\Delta\zeta = \beta_0 c\Delta T = \frac{\beta_0}{\beta_{\text{sim}}} L} \tag{11.3.12}$$

11.4 Handling particles jumping to the following frame

From Proposition 1 we know that during tracking particles will either stay in the present frame or "jump" to the following one.
From Eqs. 11.2.5 and 11.3.11, we know that the jump occurs when:

$$t \geq T_n(s) + \frac{\Delta T}{2} \;\Leftrightarrow\; \zeta \leq -\frac{\Delta\zeta}{2} + s\left(1 - \frac{\beta_0}{\beta_{\text{sim}}}\right) \tag{11.4.1}$$

When this condition is met, the particle tracking needs to be paused for the remainder of the frame n (based on Proposition 1 it cannot go back to frame n) and, based on Proposition 2, its tracking needs to be resumed from the same location where the tracking was paused when tracking the following frame. As the frame index is increased, ζ needs to be updated to preserve the time of arrival:

$$\zeta_{\text{before jump}} = s - \beta_0 c\,(t - n\Delta T) \tag{11.4.2}$$

$$\zeta_{\text{after jump}} = s - \beta_0 c\,(t - (n+1)\Delta T) \tag{11.4.3}$$

from which we obtain:

$$\boxed{\zeta_{\text{after jump}} = \zeta_{\text{before jump}} + \beta_0 c\Delta T = \zeta_{\text{before jump}} + \Delta\zeta} \tag{11.4.4}$$

11.5 Proofs for constant-energy frames

We notice that from Eqs. 11.2.2 and 11.2.3 we can write

$$\hat{\beta} < \beta_{\text{sim}} \quad \Rightarrow \quad \frac{1}{\hat{\beta}} > \frac{1}{\beta_{\text{sim}}} \quad \Rightarrow \quad \left(\frac{1}{\hat{\beta}} - \frac{1}{\beta_{\text{sim}}}\right) > 0 \tag{11.5.1}$$

$$\hat{\beta} > \frac{\beta_{\text{sim}}}{2} \quad \Rightarrow \quad \frac{1}{\hat{\beta}} < \frac{2}{\beta_{\text{sim}}} \quad \Rightarrow \quad \left(\frac{1}{\hat{\beta}} - \frac{1}{\beta_{\text{sim}}}\right) < \frac{1}{\beta_{\text{sim}}} \tag{11.5.2}$$

Combining the two we obtain

$$0 < \left(\frac{1}{\hat{\beta}} - \frac{1}{\beta_{\text{sim}}}\right) < \frac{1}{\beta_{\text{sim}}} \tag{11.5.3}$$

Proof of proposition 1

By definition of $\hat{\beta}$ we can write:

$$t_k(s_2) = t_k(s_1) + \frac{s_2 - s_1}{\hat{\beta}c} \tag{11.5.4}$$

By the hypothesis:

$$t_k(s_1) \geq T_n(s_1) - \frac{\Delta T}{2} \tag{11.5.5}$$

hence:

$$t_k(s_2) \geq T_n(s_1) - \frac{\Delta T}{2} + \frac{s_2 - s_1}{\hat{\beta}c} \tag{11.5.6}$$

Using Eq. 11.2.8 we can write:

$$t_k(s_2) \geq T_n(s_2) - \frac{s_2 - s_1}{\beta_{\text{sim}}c} - \frac{\Delta T}{2} + \frac{s_2 - s_1}{\hat{\beta}c} \tag{11.5.7}$$

Rearranging:

$$t_k(s_2) \geq T_n(s_2) - \frac{\Delta T}{2} + \frac{s_2 - s_1}{c}\left(\frac{1}{\hat{\beta}(s_1, s_2)} - \frac{1}{\beta_{\text{sim}}}\right) \tag{11.5.8}$$

Using Eq. 11.5.3 and the fact that, by hypothesis, $s_2 > s_1$, we know that the last term is positive. Therefore we can write:

$$t_k(s_2) > T_n(s_2) - \frac{\Delta T}{2} \tag{11.5.9}$$

Similarly from the hypothesis we know:

$$t_k(s_1) < T_n(s_1) + \frac{\Delta T}{2} \tag{11.5.10}$$

From Eq. 11.5.4 we can write:

$$t_k(s_2) < T_n(s_1) + \frac{\Delta T}{2} + \frac{s_2 - s_1}{\hat{\beta} c} \tag{11.5.11}$$

Again, using Eq. 11.2.8 we obtain:

$$t_k(s_2) < T_n(s_2) - \frac{s_2 - s_1}{\beta_{\text{sim}} c} + \frac{\Delta T}{2} + \frac{s_2 - s_1}{\hat{\beta} c} \tag{11.5.12}$$

Rearranging:

$$t_k(s_2) < T_n(s_2) + \frac{\Delta T}{2} + \frac{s_2 - s_1}{c}\left(\frac{1}{\hat{\beta}(s_1, s_2)} - \frac{1}{\beta_{\text{sim}}}\right) \tag{11.5.13}$$

Using Eq. 11.5.3 we obtain:

$$t_k(s_2) < T_n(s_2) + \frac{\Delta T}{2} + \frac{s_2 - s_1}{\beta_{\text{sim}} c} \tag{11.5.14}$$

Using the fact that $s_2 - s_1 \leq L$ and Eq. 11.2.4 we can write:

$$\frac{s_2 - s_1}{\beta_{\text{sim}} c} \leq \frac{L}{\beta_{\text{sim}} c} = \Delta T \tag{11.5.15}$$

Replacing in Eq. 11.5.14 we obtain:

$$t_k(s_2) < T_n(s_2) + \frac{\Delta T}{2} + \Delta T \tag{11.5.16}$$

Using Eq. 11.2.7 we obtain:

$$t_k(s_2) < T_{n+1}(s_2) + \frac{\Delta T}{2} \tag{11.5.17}$$

Combining Eq. 11.5.9 with this upper bound gives:

$$T_n(s_2) - \frac{\Delta T}{2} < t_k(s_2) < T_{n+1}(s_2) + \frac{\Delta T}{2} \tag{11.5.18}$$

which is what we wanted to prove.

Proof of proposition 2

For $s_2 = L$ and $s_1 = 0$, the claim follows directly from Proposition 3. Otherwise, the path from s_2 to the next arrival at $s_1 < s_2$ has length $D = L - s_2 + s_1$, with $0 < D < L$. Applying the speed bounds along this path gives

$$\frac{D}{\beta_{\text{sim}} c} < t_{k+1}(s_1) - t_k(s_2) < \frac{2D}{\beta_{\text{sim}} c}. \tag{11.5.19}$$

The frame centres satisfy

$$T_{n+1}(s_1) - T_n(s_2) = \frac{D}{\beta_{\text{sim}} c}. \tag{11.5.20}$$

Therefore, if $\epsilon = t_k(s_2) - T_n(s_2)$ is in the current frame,

$$\epsilon < t_{k+1}(s_1) - T_{n+1}(s_1) < \epsilon + \frac{D}{\beta_{\text{sim}} c} < \epsilon + \Delta T. \tag{11.5.21}$$

Using $-\Delta T/2 \leq \epsilon < \Delta T/2$, the next arrival is in $F_{n+1}(s_1)$ or $F_{n+2}(s_1)$, as claimed.

Proof of proposition 3

The two descriptions of the ring boundary refer to the same arrival: $t_{k+1}(0) = t_k(L)$. Moreover,

$$T_n(L) = (n+1)\Delta T = T_{n+1}(0), \qquad F_n(L) = F_{n+1}(0). \tag{11.5.22}$$

Thus membership in either frame is exactly equivalent to membership in the other, including their shared-edge convention.

11.6 Frames during acceleration

11.6.1 Reference turns and frame boundaries

For a fixed circumference L, define the accumulated reference revolutions by

$$u(t) = u(t_0) + \int_{t_0}^{t} \frac{\beta_0(t')c}{L}\,\mathrm{d}t'. \tag{11.6.1}$$

Assuming a moving reference beam over the time interval considered, $u(t)$ is strictly increasing, and we denote its inverse by $\mathcal{T}$:

$$t = \mathcal{T}(u). \tag{11.6.2}$$

An `EnergyProgram` supplies this map and its inverse from the programmed reference energy. The persistent value $u_n = u(T_n)$ corresponds to `Particles.reference_turns`; it is not an individual particle's revolution count.
Let f be the fraction of a reference revolution per frame, with $0 < f \leq 1$. In Xsuite it is set by `frame_relative_length`, whose default is 0.9. Then

$$u_{n+1} = u_n + f, \qquad T_n = \mathcal{T}(u_n), \qquad \Delta T_n = \mathcal{T}(u_n + f) - \mathcal{T}(u_n). \tag{11.6.3}$$

At position s, define the window by mapping both edges to time:

$$\boxed{F_n(s) = \left[\mathcal{T}\left(u_n + f\left(\frac{s}{L} - \frac{1}{2}\right)\right), \mathcal{T}\left(u_n + f\left(\frac{s}{L} + \frac{1}{2}\right)\right)\right).} \tag{11.6.4}$$

The upper edge of $F_n(s)$ equals the lower edge of $F_{n+1}(s)$. Also $F_n(L) = F_{n+1}(0)$, so both descriptions of the ring boundary use exactly the same window, even while the reference accelerates.
The frame is symmetric in reference-turn coordinates, not generally in time. Its time width can depend on both n and s and need not equal ΔT_n. Consequently, replacing ΔT in Eq. 11.2.5 by a turn-dependent duration would not give the same construction.
At constant reference energy, $\mathcal{T}$ is linear and these definitions reduce to the previous ones, with

$$\Delta T_n = \Delta T = \frac{fL}{\beta_0 c}, \qquad \beta_{\mathrm{sim}} = \frac{\beta_0}{f}. \tag{11.6.5}$$

The auxiliary β_{sim} specifies the motion of the window; it is not the speed of a physical particle and need not be smaller than one.

11.6.2 Conditions on particle motion

Contiguity of windows follows directly from Eq. 11.6.4. The bounds on which frame a particle can reach additionally require a restriction on its flight time. A sufficient generalization of Eqs. 11.2.2 and 11.2.3 is

$$\boxed{\frac{fd}{L} < u(t_2) - u(t_1) < \frac{2fd}{L}} \tag{11.6.6}$$

for every particle and every forward path segment of length $0 < d \leq L$ between arrivals at t_1 and t_2, including segments crossing the ring boundary. Here d is the advance along the reference orbit, as in the definition of $\hat{\beta}$. For constant reference energy this is exactly $\beta_{\text{sim}}/2 < \hat{\beta} < \beta_{\text{sim}}$.
To see why this condition suffices, write

$$w = u(t) - \frac{fs}{L}, \qquad t \in F_n(s) \iff u_n - \frac{f}{2} \leq w < u_n + \frac{f}{2}. \tag{11.6.7}$$

Along a segment without a ring-boundary crossing, Eq. 11.6.6 gives $0 < w_2 - w_1 < fd/L \leq f$. An arrival in frame n can therefore remain in frame n or enter frame $n+1$, but cannot return to an earlier frame. For a path from s_2 to the next arrival at $s_1 < s_2$, the reset of s adds f to this difference, giving $f < w_2 - w_1 < 2f$. The arrival is consequently in frame $n+1$ or $n+2$. Together with $F_n(L) = F_{n+1}(0)$, this establishes the accelerating counterparts of the three propositions under the stated bound.
The choice of f must respect this bound throughout the ramp and over the particle distribution being simulated. A fraction suitable at injection is not automatically suitable for an arbitrary energy program. In particular, an arrival before the lower window edge signals that the window is too slow for that particle.

11.6.3 Coordinate changes and waiting particles

The updates follow by keeping the physical arrival time in Eq. 11.1.1 unchanged when the clock or reference coordinates change. At fixed β_0, the arrival times expressed in the coordinates before and after the update are

$$t^- = T_n + \frac{s^- - \zeta^-}{\beta_0 c}, \tag{11.6.8}$$

$$t^+ = T_{n+1} + \frac{s^+ - \zeta^+}{\beta_0 c} = T_n + \Delta T_n + \frac{s^- + \Delta s - \zeta^+}{\beta_0 c}. \tag{11.6.9}$$

Here $T_{n+1} = T_n + \Delta T_n$ and $s^+ = s^- + \Delta s$. Imposing $t^+ = t^-$ gives

$$\frac{s^- - \zeta^-}{\beta_0 c} = \Delta T_n + \frac{s^- + \Delta s - \zeta^+}{\beta_0 c}. \tag{11.6.10}$$

Solving for ζ^+ yields

$$\boxed{\zeta^+ = \zeta^- + \Delta s + \beta_0 c \Delta T_n.} \tag{11.6.11}$$

For a particle completing the line with s reset from L to zero, $\Delta s = -L$. For a particle paused at a synchronization location, s stays fixed and $\Delta s = 0$. The updates are therefore

$$\zeta^+_{\text{crossing}} = \zeta^-_{\text{crossing}} - L + \beta_0 c \Delta T_n, \tag{11.6.12}$$

$$\zeta^+_{\text{waiting}} = \zeta^-_{\text{waiting}} + \beta_0 c \Delta T_n. \tag{11.6.13}$$

If s is not reset at the end of the line, its update also uses $\Delta s = 0$. These are changes of coordinates, not additional physical drifts or energy kicks.
A change of reference velocity at fixed s, T_n, and physical arrival time instead requires

$$\boxed{\zeta^+ = s + \frac{\beta_0^+}{\beta_0^-}(\zeta^- - s).} \tag{11.6.14}$$

The reference change applies to waiting particles as well as active particles; being paused does not remove a particle from the beam. In combination with the usual momentum-coordinate transformation, it preserves its physical momentum and arrival time.
At a synchronization location, particles at or beyond the upper window edge are paused. They are reconsidered at that same location in the following frame, and remain paused if their arrival is still beyond the window. The waiting-particle coordinate shift is applied once per frame, even if the particle has not completed a revolution.
In Xsuite, `SyncTime` elements bracket the complete line and precede collective elements, RF cavities, and any additional synchronization locations requested by the user. The first boundary establishes the windows for the new frame; the last accounts for all waiting particles before the common clock advances. This construction uses complete frames. Time-dependent expressions and the `EnergyProgram` follow the common clock when `line.enable_time_dependent_vars` is enabled.

Chapter 12

Aperture Modelling and Calculation

12.1 Overview and definitions

12.1.1 Aperture model

The aperture module in `xtrack/aperture` provides a geometric model of machine acceptance along an accelerator and tools to compare this acceptance with a beam envelope derived from Twiss data and a halo prescription. The model is built from:

- logical *profile* shapes such as ellipses, rectangles, racetracks, etc.;
- placements of these profiles inside a model of a *pipe* section, which can be either straight or curved (an arc segment);
- placements of pipes, *pipe positions*, along the survey of the machine.

When placing a profile in a pipe, or the pipe in the survey, transformations can be given. In particular, the aperture model stores:

- $(\Delta x, \Delta y, \Delta s, \phi, \theta, \psi)$ for each profile position within the pipe, where Δs is the shift along the possibly curved frame of the pipe, and where the angles follow the usual conventions (see Chapter 3 on misalignments);
- a 4×4 homogeneous transformation matrix for each pipe position, which specifies the placement of the pipe instance relative to the relevant survey reference point in the survey reference frame (X, Y, Z).

12.1.2 Aperture bounds

Building the aperture model pre-computes so-called *aperture bounds*. This is a database associating every *installed aperture* (a concrete instance of a profile in the model, i.e. a particular *profile position* within a pipe installed at a particular *pipe position* in the line) with its location along the survey. Aperture queries automatically build the model if it has not yet been built. For every installed profile the survey s positions spanning it are computed and memorised; this is illustrated in Figure 12.1. For the common case of an aperture i orthogonal to the survey, the bound will simply be $\{s_i\}$. Aperture bounds are used for checking the validity of the model as well as for aperture interpolation.

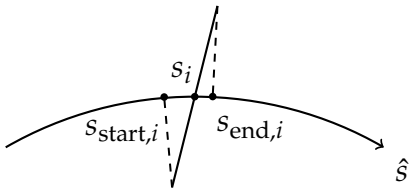
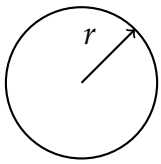


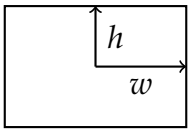
Figure 12.1: Visualisation of an aperture bound for some installed aperture i.

12.1.3 Profile shapes

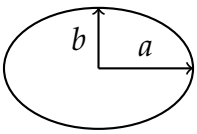
Each profile shape is converted once to a closed polygon with a fixed number of points. This is done by sampling uniformly along the path length. This gives a common polygon representation for all subsequent operations such as interpolation, ray intersection, and point-in-polygon checks.



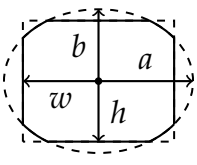
Circle. Radius r.



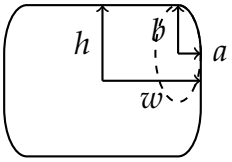
Rectangle. Half-width w and half-height h.



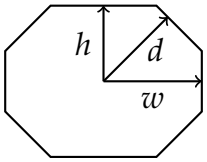
Ellipse. Half-major axis a and half-minor axis b.



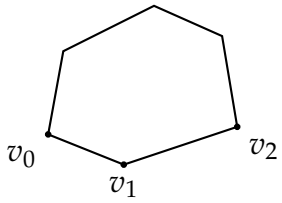
Rectellipse. Half-width w, half-height h, half-major axis a, and half-minor axis b.



Racetrack. Half-width w, half-height h, and ellipse-corner half-axes a, b.



Octagon. Half-width w, half-height h, and half-diagonal gap d.



Polygon. Arbitrary polygon given by an ordered list of vertices $(v_0, v_1, \ldots) = ((x_0, y_0), (x_1, y_1), \ldots)$.

12.1.4 Profiles

A *profile* comprises of any of the above-mentioned logical shapes. Tolerances can be specified on a profile installed in a pipe (a *profile position*) and on an installed pipe (a *pipe position*). At each position, three tolerances can be specified:

- `tol_r`: radial tolerance,
- `tol_x`: horizontal tolerance,
- `tol_y`: vertical tolerance.

For each installed aperture, the tolerances of its profile position and pipe position are added component by component to give the total `tol_r`, `tol_x`, and `tol_y`. These totals effectively form a tolerance racetrack with half-width of `tol_x` + `tol_r`, half-height `tol_y` + `tol_r`, and a circular radius of `tol_r`.

12.1.5 Beam envelope

The beam-envelope calculation uses:

- local optics and closed orbit values,
- beam and tolerance parameters specified by the user,
- summed aperture tolerances of the local profile position and pipe position.

In particular, `halo_params` define the following beam parameters:

- `nemitt_x` ($\varepsilon_{x,\mathrm{n}}$) and `nemitt_y` ($\varepsilon_{y,\mathrm{n}}$) – normalised emittances (in metres),
- `delta_rms` (δ_{rms}) – root-mean-square relative momentum spread (unitless),
- `tol_co` (r_{co}) – closed orbit error (in metres),
- `tol_disp` (f_D) – dispersion tolerance scaling factor (unitless),

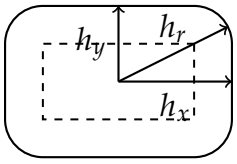
- `tol_disp_ref` (D_{ref}) – reference dispersion error (in metres),
- `tol_disp_ref_beta` ($\beta_{D,\text{ref}}$) – reference beta for dispersion scaling (in metres),
- `tol_beta_beating` (f_β) – beta beating tolerance scaling factor (unitless),
- $h_x := \frac{\texttt{halo_x}}{\texttt{halo_primary}}$, $h_y := \frac{\texttt{halo_y}}{\texttt{halo_primary}}$, and $h_r := \frac{\texttt{halo_r}}{\texttt{halo_primary}}$ – reference horizontal, vertical, and radial size of the beam in units of betatron sigma.

The optical beam sizes for a one-betatron sigma beam are given by

$$\sigma_x = \sqrt{\frac{\varepsilon_{x,\text{n}}}{\gamma_r \beta_r} \beta_x} \cdot f_\beta, \qquad \sigma_y = \sqrt{\frac{\varepsilon_{y,\text{n}}}{\gamma_r \beta_r} \beta_y} \cdot f_\beta.$$

We model the beam as a racetrack of shape determined by the parameters h_x, h_y, and h_r. To obtain the modelled n-sigma beam envelope in metres, the racetrack defined by the above parameters is scaled by $(n\sigma_x, n\sigma_y)$:

$$n \cdot \texttt{beam_racetrack} := n \begin{bmatrix} \sigma_x \\ \sigma_y \end{bmatrix} \cdot$$



Separately, we can build a tolerance racetrack which includes:

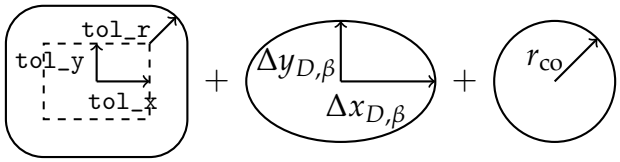
- the summed aperture tolerances `tol_x`, `tol_y`, `tol_r`,
- uncorrelated (also referred to as *spurious*) dispersion orbit shift:

$$\Delta x_{D,\beta} := f_\beta \cdot f_D \cdot D_{\text{ref}} \cdot \sqrt{\frac{\beta_x}{\beta_{D,\text{ref}}}} \cdot \delta_{\text{rms}}, \qquad \Delta y_{D,\beta} := f_\beta \cdot f_D \cdot D_{\text{ref}} \cdot \sqrt{\frac{\beta_y}{\beta_{D,\text{ref}}}} \cdot \delta_{\text{rms}},$$

- and the closed-orbit tolerance r_{co}.

This racetrack can be visualised as (where $+$ denotes convolution/Minkowski sum):

$$\texttt{halo_racetrack} :=$$



Since racetracks are closed under convolution, we can represent our beam envelope at n-sigmas (without including correlated dispersion orbit shift yet) as:

$$\texttt{envelope}(n) := \texttt{halo_racetrack} + n \cdot \texttt{beam_racetrack}.$$

Depending on the algorithm this representation will be converted to a polygon (beam envelope generation functions, bisection method for computing the max aperture sigma) or will be used directly for analytic calculations.

In aperture calculations we must further include the orbit shift error induced by correlated dispersion, also referred to as *model* dispersion. In the case of converting to a polygon, we can further include this orbit shift in the resulting shape by 'stretching' it. We can convolve `envelope`(n) with the line segment $[-\mathbf{v}_{D,\text{model}}, \mathbf{v}_{D,\text{model}}]$, where

$$\mathbf{v}_{D,\text{model}} := \begin{bmatrix} D_x \delta_{\text{rms}} \\ D_y \delta_{\text{rms}} \end{bmatrix},$$

to obtain an n-sigma beam envelope including the error related to correlated dispersion, as well as uncorrelated dispersion error, aperture tolerance, and closed-orbit tolerance errors. In the case of analytic methods, we will usually separately consider two envelopes shifted by $\pm\mathbf{v}_{D,\text{model}}$ instead.

12.2 Algorithms

12.2.1 Aperture bounds

For any installed profile let (where by pose we mean the position and orientation)

- M_S be the pose of the pipe's survey reference point in the survey frame,
- M_T be the pose of the pipe's origin $(x, y, s) = (0, 0, 0)$ relative to the survey reference point,
- M_P be the pose representing the installed profile's position within the pipe frame.

Then, $M_{P,\text{world}} = M_S\, M_T\, M_P$ represents the position and orientation of the installed profile in world coordinates (survey frame). In order to calculate the locations of the installed profiles in the survey frame, we perform the intersection of the profile plane (local $s = 0$ in the $M_{P,\text{world}}$ frame) with the survey curve. Each segment of the survey is defined as either a line segment or an arc segment, and we work our way outwards from the survey reference point testing for intersection, until a valid s is found. The bounds s_{start} and s_{end} are computed by projecting each 3D polygon point of a given installed profile onto the survey curve and taking the minimum and maximum values.
As mentioned in this chapter's introduction, aperture bounds are used for checking the validity of the model as well as for aperture interpolation. Validation checks that each installed pipe's survey reference is consistent and that the longitudinal intervals covered by different pipes' profile-centre positions do not overlap by more than `s_tol`. These intervals are distinct from the projected profile footprints, which can overlap. For rings, the validation accounts for pipes crossing the end of the survey.

12.2.2 Cross section interpolation

The module is capable of computing the aperture polygons in the plane orthogonal to an arbitrary s-position along the survey. Aperture bounds are used to find the correct

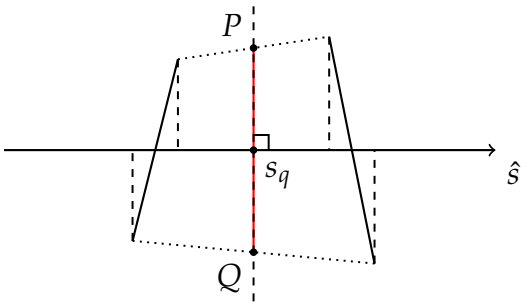


Figure 12.2: Visualisation of aperture interpolation at some s_q outside of any aperture bounds. The points P and Q are obtained by interpolating corresponding vertices of profiles on either side of s_q.

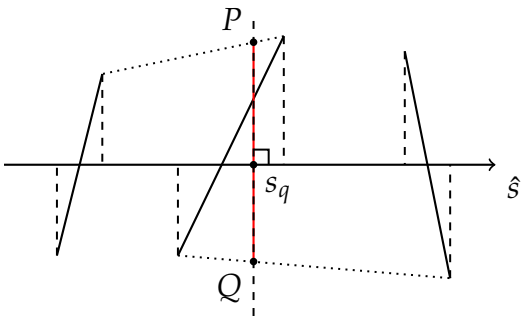


Figure 12.3: If s_q falls within bounds of an installed aperture, some of the vertices of the new cross section need to be interpolated with the aperture to the left, such as point P, while other ones with the aperture to the right, such as point Q.

installed apertures that need to be interpolated. If the s position for interpolation sits outside of any bounds, we interpolate the profiles on either side of s. However, if the s position sits within a bound of some aperture i, we need to partly interpolate $i-1$ with i, and partly interpolate i with $i+1$. This is illustrated in Figures 12.2 and 12.3. Profile-position tolerances are interpolated linearly in s between neighbouring profile centres within the same installed pipe, and the active pipe-position tolerances are added to the result. Across a pipe boundary, tolerances retain the active installed profile's summed values; they are not interpolated between pipes, although the aperture geometry is.

For a query at longitudinal position s, interpolation is performed in the cross-section plane defined by the resampled survey pose at that s. The active profile is selected from the bound containing s, or the immediately preceding bound when s lies between bounds. The target plane and neighbouring installed profiles are brought into the active profile's pipe frame. This is done to limit numerical noise that might otherwise be present when mixing small local quantities with world coordinates.

The profiles are uniformly discretised into the same number of points and the first step before actual interpolation is determining point correspondence between the profiles. This is done after projecting the neighbouring polygons into the target cross-section plane. The vertex order is reversed if the projected orientations differ, and a cyclic shift is chosen to minimise the sum of squared distances between corresponding

vertices. Interpolation then proceeds by connecting corresponding 3D vertices from the two neighbouring installed profiles and intersecting those line segments with the target plane.
Between profiles of different installed pipes, interpolation uses straight segments. Within a curved pipe, the following approximation is employed. Note that, for a curved pipe, M_P already includes the motion along the curved reference axis, i.e. the profile is first advanced by the pipe curvature to its local s-location and then given its local offsets/rotations. During interpolation, the segment-plane intersection is handled after 'straightening' the curvilinear frame. Given a Cartesian frame and a curvilinear frame with curvature h (or equivalently radius $R = h^{-1}$) whose origins coincide, a Cartesian point can be transformed into a curvilinear point as follows:

$$\begin{bmatrix} x \\ y \\ s \end{bmatrix} = \begin{bmatrix} \operatorname{sgn}(h)\sqrt{(X+R)^2+Z^2} - R \\ Y \\ R \cdot \operatorname{atan}_2\left(\operatorname{sgn}(h)Z,\, \operatorname{sgn}(h)(X+R)\right) \end{bmatrix}.$$

We can transform a plane, which is represented as a (Cartesian) normal (v_X, v_Y, v_Z) attached to a (curvilinear) point (x, y, s), like so:

$$\begin{bmatrix} v_x \\ v_y \\ v_s \end{bmatrix} = \begin{bmatrix} \cos(hs) & 0 & \sin(hs) \\ 0 & 1 & 0 \\ -\frac{\sin(hs)}{1+hx} & 0 & \frac{\cos(hs)}{1+hx} \end{bmatrix} \begin{bmatrix} v_X \\ v_Y \\ v_Z \end{bmatrix}.$$

Once the two polygon points together with the plane's point and normal are transformed, we can perform the intersection in the 'straightened' frame with the usual algorithm. The resulting point can be converted back to the Cartesian plane with:

$$\begin{bmatrix} X \\ Y \\ Z \end{bmatrix} = \begin{bmatrix} (R+x)\cos(hs) - R \\ y \\ (R+x)\sin(hs) \end{bmatrix}.$$

12.2.3 Maximum beam sigma

There are three methods currently implemented for computing the maximum number of sigmas for which the beam fits in a given cross section; this quantity is often referred to as n_1:

$$n_1 := \sup\left\{n \mid \texttt{total_envelope}(n) \subset \texttt{cross_section}\right\}. \tag{12.2.1}$$

The `total_envelope` corresponds to `envelope` with the correlated dispersion error applied; the precise method of the application of this error, and the computation of n_1 is what distinguishes the three different algorithms implemented in Xtrack. These algorithms are described below.

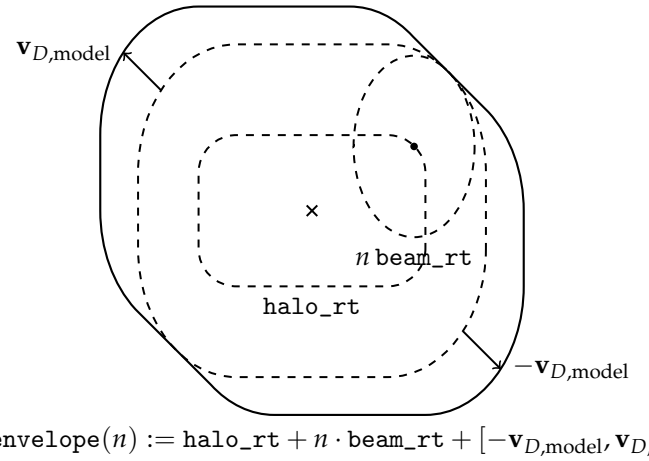


Figure 12.4: The construction of the `total_envelope` used in the *bisection* method. The $\times$ symbol marks the closed orbit. The envelope is repeatedly converted to a polygon for different n, until a limiting value for containment within the aperture is found through bisection.

12.2.3.1 'Bisection' method

The *bisection* method computes n_1 as the largest beam scale factor for which the full beam envelope polygon still fits inside the interpolated aperture polygon. In particular, the beam envelope is discretised to a polygon which includes the dispersive orbit error as a 'stretch' described in Section 12.1.5, and visualised in Fig. 12.4. At each s a trial envelope is repeatedly built, the algorithm checks polygon containment, and bisects until the limiting value is found. It is the most direct geometric implementation of Eq. 12.2.1, but also the most expensive at $O(EAK)$, where E is the number of envelope points, A is the number of aperture points, and $K = \log_2(\frac{\text{search space}}{\text{search tolerance}})$ is the number of bisection steps, currently $K \leq 25$.

12.2.3.2 'Rays' method

The *rays* method approximates the same limit by sampling a finite set of angles θ. For each ray direction θ, it computes the distances d_{halo}, d_{envelope}, and d_{aper} from the closed orbit to the `halo_racetrack`, `envelope`(1), and `aperture`, respectively, as visualised in Fig. 12.5. This calculation is analytical using a ray-at-θ–racetrack intersection formula. These are used to obtain a linear approximation of $n_1 \approx \frac{d_{\text{aper}} - d_{\text{halo}}}{d_{\text{envelope}} - d_{\text{halo}}}$, which is then used to refine the result using Newton's method. The dispersion-related orbit shift is included in the method by picking the more pessimistic of the two centroid options when calculating the distances. The *rays* method is much faster than bisection at $O(\text{number of rays})$, but its accuracy depends on the angular sampling density and can be inaccurate for very flat beams, due to the fact that the sampling is done along a single uniform direction θ.

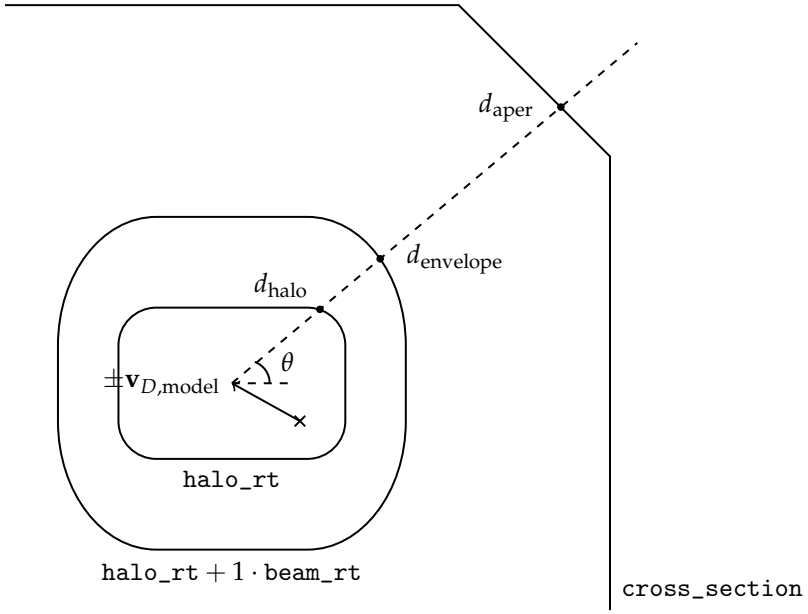


Figure 12.5: Let $t(\theta, n)$ be the length of the ray at angle θ intersecting `envelope`(n). The *rays* method finds the value of n_1 such that $t(\theta, n_1) - d_{\text{aper}} = 0$ for each θ. Solving this is a nonlinear problem (and in fact quartic), so we employ Newton's method with an initial linearly approximated guess $n_1 \approx \frac{d_{\text{aper}} - d_{\text{halo}}}{d_{\text{envelope}} - d_{\text{halo}}}$. For each θ, two centroids are considered for each of the $-\mathbf{v}_{D,\text{model}}$ and $\mathbf{v}_{D,\text{model}}$ (the $\times$ symbol marks the closed orbit), and the smaller of the two values is taken, to include the dispersion-related orbit shift error.

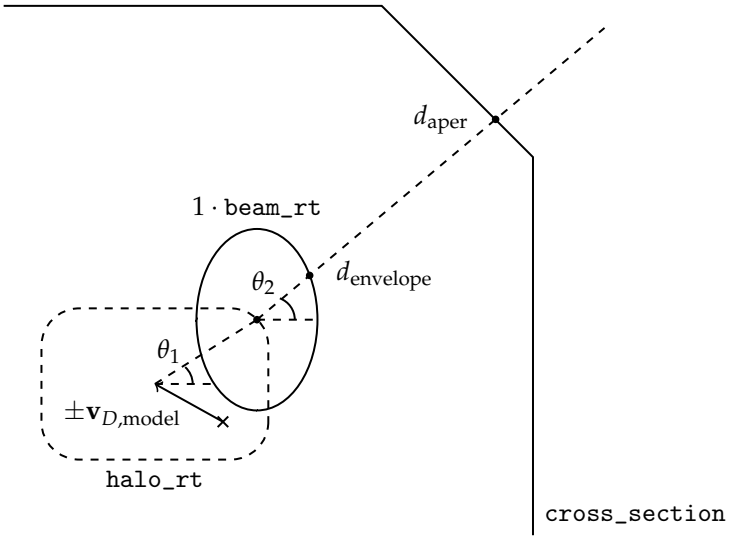


Figure 12.6: The *exact* method finds n_1 as the minimum value of $\frac{d_{\text{aper}}}{d_{\text{envelope}}}$ across all θ_1, θ_2, and considering both $-\mathbf{v}_{D,\text{model}}$ and $\mathbf{v}_{D,\text{model}}$ closed orbit shifts (the $\times$ symbol marks the closed orbit).

12.2.3.3 'Exact' method

The *exact* method is similar to *rays* in that it evaluates n_1 using analytically obtained distances. Instead of scanning a single set of rays, the search is performed along two sets of rays, as visualised in Fig. 12.6. First, the beam centroids are computed along one set of rays, using the `halo_racetrack` and including the dispersion-related orbit shift. Then, for each centroid position, another set of rays is emitted to calculate d_{aper}, the distance to the aperture from that point, and d_{envelope}, the distance to the boundary of the one-sigma `beam_racetrack` centred there. The halo tolerances are already included in the centroid position. Once the most pessimistic case is found, $n_1 := \frac{d_{\text{aper}}}{d_{\text{envelope}}}$. This method is slower than *rays*, as the complexity is $O((\text{number of rays})^2)$; it is nevertheless more performant than bisection.

Chapter 13

Modeling s-dependent magnetic fields

The `SplineBoris` and `BFieldExpansion` elements reconstruct three-dimensional static magnetic fields from longitudinal profiles of the field and its transverse derivatives on the reference axis. Applications include undulators, wigglers, combined-function magnets, fringe fields, and solenoids.
This chapter first develops the shared scalar-potential reconstruction in straight and curved reference frames, following Ref. [45], and derives a vector potential for canonical tracking. It then describes the two implementations. `SplineBoris` uses dimensional spline data in a straight frame and a second-order spatial Boris integrator. `BFieldExpansion` uses rigidity-normalized polynomial coefficients in a straight or curved frame and classical fourth-order Runge–Kutta integration. Their field conventions and integration properties are stated separately below.

13.1 Coordinates and field normalization

Let s be arc length along a planar reference trajectory of constant curvature h, and let x and y be the horizontal and vertical coordinates. Define $w(x) = 1 + hx$. The straight case has $h = 0$. The following expressions describe the regular coordinate region around the reference axis, with $w > 0$. The surface $w = 0$ is a coordinate singularity. Curvature specifies the reference frame, independently of the field; it does not set the dipole strength.

13.1.1 Line element and differential operators

Let $\boldsymbol{r}_0(s)$ be the reference trajectory and $(\boldsymbol{e}_x, \boldsymbol{e}_y, \boldsymbol{e}_s)$ its local orthonormal frame, with $\boldsymbol{e}_x$ pointing outward from a positive bend. A nearby point is

$$\boldsymbol{r}(x, y, s) = \boldsymbol{r}_0(s) + x\boldsymbol{e}_x(s) + y\boldsymbol{e}_y. \tag{13.1.1}$$

For a planar reference trajectory, the frame satisfies

$$\frac{\mathrm{d}\boldsymbol{r}_0}{\mathrm{d}s} = \boldsymbol{e}_s, \qquad \frac{\mathrm{d}\boldsymbol{e}_x}{\mathrm{d}s} = h\boldsymbol{e}_s, \qquad \frac{\mathrm{d}\boldsymbol{e}_y}{\mathrm{d}s} = 0. \tag{13.1.2}$$

Differentiating the position and taking its squared length gives

$$\mathrm{d}\boldsymbol{r} = \boldsymbol{e}_x\,\mathrm{d}x + \boldsymbol{e}_y\,\mathrm{d}y + w\boldsymbol{e}_s\,\mathrm{d}s, \tag{13.1.3}$$

$$\mathrm{d}\ell^2 = \mathrm{d}\boldsymbol{r}\cdot\mathrm{d}\boldsymbol{r} = \mathrm{d}x^2 + \mathrm{d}y^2 + w^2\mathrm{d}s^2. \tag{13.1.4}$$

The cross terms vanish because the frame is orthonormal. Equivalently, in a circular bend of radius $\rho = 1/h$, an angular increment $\mathrm{d}\theta$ spans $\mathrm{d}s = \rho\,\mathrm{d}\theta$ on the reference trajectory and $(\rho + x)\mathrm{d}\theta = w\,\mathrm{d}s$ at horizontal offset x.
For a scalar function f, the identity $\mathrm{d}f = \nabla f\cdot\mathrm{d}\boldsymbol{r}$ then gives

$$\nabla f = \boldsymbol{e}_x\,\partial_x f + \boldsymbol{e}_y\,\partial_y f + \boldsymbol{e}_s\,\frac{1}{w}\partial_s f. \tag{13.1.5}$$

Write a vector in physical components along the unit vectors as $\boldsymbol{V} = V_x\boldsymbol{e}_x + V_y\boldsymbol{e}_y + V_s\boldsymbol{e}_s$. A small coordinate cell has volume $w\,\mathrm{d}x\,\mathrm{d}y\,\mathrm{d}s$. Its face areas normal to x, y, and s are respectively $w\,\mathrm{d}y\,\mathrm{d}s$, $w\,\mathrm{d}x\,\mathrm{d}s$, and $\mathrm{d}x\,\mathrm{d}y$. Dividing the net outward flux by the volume gives

$$\nabla\cdot\boldsymbol{V} = \frac{1}{w}\left[\partial_x(wV_x) + \partial_y(wV_y) + \partial_s V_s\right] \tag{13.1.6}$$

$$= \partial_x V_x + \partial_y V_y + \frac{1}{w}\partial_s V_s + \frac{h}{w}V_x. \tag{13.1.7}$$

Similarly, circulation around the coordinate faces, divided by their areas, gives the curl. In the right-handed frame $\boldsymbol{e}_x\times\boldsymbol{e}_y = \boldsymbol{e}_s$, its physical components are

$$\begin{aligned}(\nabla\times\boldsymbol{V})_x &= \frac{1}{w}\left[\partial_y(wV_s) - \partial_s V_y\right],\\ (\nabla\times\boldsymbol{V})_y &= \frac{1}{w}\left[\partial_s V_x - \partial_x(wV_s)\right],\\ (\nabla\times\boldsymbol{V})_s &= \partial_x V_y - \partial_y V_x.\end{aligned} \tag{13.1.8}$$

Combining the gradient and divergence, for the constant curvature assumed here,

$$\nabla^2 f = \nabla\cdot\nabla f = \partial_x^2 f + \frac{h}{w}\partial_x f + \partial_y^2 f + \frac{1}{w^2}\partial_s^2 f. \tag{13.1.9}$$

13.1.2 Field normalization

We use the signed reference rigidity $B\rho = P_0/q_0$ and write

$$\boldsymbol{b} = \frac{\boldsymbol{B}}{B\rho}, \qquad \boldsymbol{a} = \frac{\boldsymbol{A}}{B\rho}, \qquad \boldsymbol{b} = -\nabla\phi. \tag{13.1.10}$$

Thus $\boldsymbol{b}$ has units of inverse metres, while $\boldsymbol{a}$ and the normalized scalar magnetic potential ϕ are dimensionless. This convention is used for the shared derivation and directly matches `BFieldExpansion`. The conversion to the dimensional field and the opposite scalar-potential sign used by `SplineBoris` is given in Sec. 13.4. The magnetic scalar potential is unrelated to the electric potential in the particle Hamiltonian.

13.2 Field profiles and scalar-potential reconstruction

Denote the total normal, skew, and longitudinal profiles by $N_n(s)$, $S_n(s)$, and $K_s(s)$. Their on-axis interpretation is

$$b_y(x,0,s) = \sum_{n\geq 0} N_n(s)\frac{x^n}{n!}, \quad b_x(x,0,s) = \sum_{n\geq 0} S_n(s)\frac{x^n}{n!}, \quad b_s(0,0,s) = K_s(s). \tag{13.2.1}$$

In particular, N_n and S_n are the n-th horizontal derivatives of b_y and b_x on the reference axis. The field representation is specified by these functions and K_s; their parametrization for each element is described below.
Inside a current-free aperture the magnetostatic Maxwell equations give $\nabla \times \boldsymbol{b} = 0$ and $\nabla \cdot \boldsymbol{b} = 0$. With Eqs. (13.1.10) and (13.1.9), the latter becomes

$$\nabla^2\phi = \partial_x^2\phi + \frac{h}{w}\partial_x\phi + \partial_y^2\phi + \frac{1}{w^2}\partial_s^2\phi = 0. \tag{13.2.2}$$

Expand the potential in the vertical coordinate,

$$\phi(x,y,s) = \sum_{i=0}^{\infty} \phi_i(x,s)\frac{y^i}{i!}. \tag{13.2.3}$$

13.2.1 Deriving the two seed functions

The first two Taylor coefficients are the potential and its first vertical derivative on the plane $y = 0$:

$$\phi_0(x,s) = \phi(x,0,s), \qquad \phi_1(x,s) = \partial_y\phi(x,y,s)\big|_{y=0}. \tag{13.2.4}$$

The physical field components in the local orthonormal frame are

$$b_x = -\partial_x\phi, \qquad b_y = -\partial_y\phi, \qquad b_s = -\frac{1}{w}\partial_s\phi. \tag{13.2.5}$$

The vertical field on $y = 0$ therefore determines ϕ_1 directly:

$$-\phi_1(x,s) = b_y(x,0,s) = \sum_{n\geq 0} N_n(s)\frac{x^n}{n!}. \tag{13.2.6}$$

Similarly, the horizontal field gives

$$-\partial_x\phi_0(x,s) = b_x(x,0,s) = \sum_{n\geq 0} S_n(s)\frac{x^n}{n!}. \tag{13.2.7}$$

Integrating with respect to x yields

$$\phi_0(x,s) = C(s) - \sum_{n\geq 0} S_n(s)\frac{x^{n+1}}{(n+1)!}. \tag{13.2.8}$$

The integration constant can depend on s, since the integration was only over x. The longitudinal field on the reference axis determines this function: at $x = y = 0$, $w = 1$ and $\phi = C(s)$, hence

$$K_s(s) = b_s(0,0,s) = -C'(s), \qquad C(s) = -\int^s K_s(u)\,\mathrm{d}u + C_0. \tag{13.2.9}$$

The constant C_0 has no effect on the field and can be set to zero. The input profiles thus determine the two seed functions:

$$\phi_0(x,s) = -\int^s K_s(u)\,\mathrm{d}u - \sum_{n\geq 0} S_n(s)\frac{x^{n+1}}{(n+1)!}, \tag{13.2.10}$$

$$\phi_1(x,s) = -\sum_{n\geq 0} N_n(s)\frac{x^n}{n!}. \tag{13.2.11}$$

13.2.2 Why two seeds determine the expansion

Laplace's equation is second order in y. It can be written as

$$\partial_y^2\phi = -\mathcal{D}_h\phi, \qquad \mathcal{D}_h = \partial_x^2 + \frac{h}{w}\partial_x + \frac{1}{w^2}\partial_s^2. \tag{13.2.12}$$

The operator $\mathcal{D}_h$ differentiates only in x and s, and its coefficients do not depend on y. Inserting the Taylor series (13.2.3) on both sides gives

$$\sum_{i=0}^{\infty}\phi_{i+2}(x,s)\frac{y^i}{i!} = \sum_{i=0}^{\infty}(-\mathcal{D}_h\phi_i(x,s))\frac{y^i}{i!}. \tag{13.2.13}$$

Differentiating twice in y shifts the coefficient index by two; equating coefficients of each power of y therefore gives

$$\boxed{\phi_{i+2} = -\mathcal{D}_h\phi_i.} \tag{13.2.14}$$

For example,

$$\phi_2 = -\mathcal{D}_h\phi_0, \qquad \phi_3 = -\mathcal{D}_h\phi_1, \tag{13.2.15}$$

$$\phi_4 = \mathcal{D}_h^2\phi_0, \qquad \phi_5 = \mathcal{D}_h^2\phi_1. \tag{13.2.16}$$

The potential consequently starts as

$$\phi = \phi_0 + y\phi_1 - \frac{y^2}{2!}\mathcal{D}_h\phi_0 - \frac{y^3}{3!}\mathcal{D}_h\phi_1 + \frac{y^4}{4!}\mathcal{D}_h^2\phi_0 + \cdots. \tag{13.2.17}$$

Thus ϕ_0 determines every even coefficient, and ϕ_1 every odd coefficient. The two independent inputs are functions of x and s, rather than two numbers. They determine the local field wherever the resulting series converges.
Longitudinal derivatives of the transverse profiles therefore generate longitudinal fringe fields and higher transverse orders automatically.

13.2.3 Coefficient recurrence in a curved frame

For $h = 0$, the operator in Eq. (13.2.14) is $-\mathcal{D}_0 = -\partial_x^2 - \partial_s^2$, and repeated differentiation of polynomial seeds eventually terminates. For $h \neq 0$, `BFieldExpansion` instead represents the coefficients using powers of $w = 1 + hx$:

$$\phi_i(x, s) = \sum_p c_{i,p}(s) w^p. \tag{13.2.18}$$

The seed polynomials in x can be expressed in this basis by substituting $x = (w - 1)/h$. The recurrence can then generate negative powers of w.
To derive the coefficient update, consider one term $c_{i,p}(s)w^p$. Since $\partial_x w = h$, the horizontal derivatives give

$$\partial_x^2 (c_{i,p} w^p) = h^2 p(p-1) c_{i,p} w^{p-2}, \tag{13.2.19}$$

$$\frac{h}{w} \partial_x (c_{i,p} w^p) = h^2 p \, c_{i,p} w^{p-2}. \tag{13.2.20}$$

Their sum contains $p(p-1) + p = p^2$. Also, w is independent of s for the constant curvature assumed here, so

$$\frac{1}{w^2} \partial_s^2 (c_{i,p} w^p) = c_{i,p}''(s) w^{p-2}. \tag{13.2.21}$$

Thus applying $\mathcal{D}_h$ lowers the power of w by two:

$$\mathcal{D}_h (c_{i,p} w^p) = \left[c_{i,p}''(s) + h^2 p^2 c_{i,p}(s) \right] w^{p-2}. \tag{13.2.22}$$

Substitution into $\phi_{i+2} = -\mathcal{D}_h \phi_i$ yields

$$\phi_{i+2}(x, s) = -\sum_p \left[c_{i,p}''(s) + h^2 p^2 c_{i,p}(s) \right] w^{p-2}. \tag{13.2.23}$$

To identify the coefficient of w^m, set $m = p - 2$, or $p = m + 2$. Equating coefficients then gives

$$c_{i+2,m}(s) = -\left[\frac{\mathrm{d}^2}{\mathrm{d}s^2} + h^2 (m+2)^2 \right] c_{i,m+2}(s). \tag{13.2.24}$$

This is the coefficient recurrence used to build the curved expansion. For example, a term proportional to w^1 with a nonzero constant coefficient generates a w^{-1} term, which in turn generates w^{-3}, and so on. The curved expansion therefore need not terminate, even when its seeds are polynomials.

13.3 Vector potential and gauge

Tracking in `BFieldExpansion` uses canonical momenta and therefore requires a vector potential as well as the magnetic field. Direct integration of the Lorentz force would

require only the magnetic field. The implementation chooses $a_y = 0$, $a_x(x, 0, s) = 0$, and $a_s(0, 0, s) = 0$. In this gauge a vector potential for the untruncated field is

$$a_x(x, y, s) = \frac{1}{w} \int_0^y \partial_s \phi(x, v, s)\, \mathrm{d}v, \tag{13.3.1}$$

$$a_y(x, y, s) = 0, \tag{13.3.2}$$

$$a_s(x, y, s) = \frac{1}{w} \int_0^x (1 + hu)\phi_1(u, s)\, \mathrm{d}u - \int_0^y \partial_x \phi(x, v, s)\, \mathrm{d}v. \tag{13.3.3}$$

Applying Eq. (13.1.8) to $\boldsymbol{a}$ with $a_y = 0$ gives

$$b_x = \partial_y a_s, \qquad b_y = \frac{\partial_s a_x - \partial_x (w a_s)}{w}, \qquad b_s = -\partial_y a_x. \tag{13.3.4}$$

These expressions follow by integrating the curl equations and fixing the integration constants with the stated gauge conditions.

13.3.1 Constructing the vector potential

First, equate the longitudinal field in Eq. (13.3.4) to that from the scalar potential:

$$-\partial_y a_x = -\frac{1}{w} \partial_s \phi. \tag{13.3.5}$$

Integrating in y, using $a_x(x, 0, s) = 0$, gives

$$a_x(x, y, s) = \frac{1}{w} \int_0^y \partial_s \phi(x, v, s)\, \mathrm{d}v. \tag{13.3.6}$$

The factor $1/w$ can be taken outside the integral because w does not depend on y. Next, the horizontal field requires

$$\partial_y a_s = -\partial_x \phi. \tag{13.3.7}$$

Integration in y gives

$$a_s(x, y, s) = C(x, s) - \int_0^y \partial_x \phi(x, v, s)\, \mathrm{d}v, \tag{13.3.8}$$

where $C(x, s) = a_s(x, 0, s)$ is still to be determined.
The vertical field on $y = 0$ fixes this function. Since $a_x(x, 0, s) = 0$ for every s, its longitudinal derivative is also zero on that plane. Equation (13.3.4) then gives

$$b_y(x, 0, s) = -\frac{1}{w} \partial_x (wC) = -\phi_1(x, s), \tag{13.3.9}$$

or $\partial_x (wC) = w\phi_1$. Integrating in x and imposing $C(0, s) = a_s(0, 0, s) = 0$ yields

$$C(x, s) = \frac{1}{w} \int_0^x (1 + hu)\phi_1(u, s)\, \mathrm{d}u. \tag{13.3.10}$$

Substitution gives the expression for a_s in Eq. (13.3.3).

13.3.2 Checking the vertical field away from the midplane

The construction already reproduces b_x and b_s everywhere, and b_y on $y = 0$. To check b_y away from that plane, substitute the potentials into the remaining curl component:

$$(\nabla \times \boldsymbol{a})_y = -\phi_1(x,s) + \int_0^y \mathcal{D}_h\phi(x,v,s)\,\mathrm{d}v. \tag{13.3.11}$$

Laplace's equation gives $\mathcal{D}_h\phi = -\partial_y^2\phi$, so

$$(\nabla \times \boldsymbol{a})_y = -\phi_1(x,s) - \big[\partial_y\phi(x,y,s) - \partial_y\phi(x,0,s)\big] \tag{13.3.12}$$

$$= -\partial_y\phi(x,y,s) = b_y(x,y,s), \tag{13.3.13}$$

where $\partial_y\phi(x,0,s) = \phi_1(x,s)$. Thus all three field components agree. This proof uses Laplace's equation exactly, which is why the expressions above refer to the untruncated field.

13.3.3 Evaluation and elementary examples

The code evaluates the series for the potentials and their derivatives analytically, rather than differentiating sampled field values numerically.
Two elementary cases fix the signs and normalization. A uniform vertical field $b_y = K$ has

$$\phi = -Ky, \qquad a_x = a_y = 0, \qquad a_s = -K\frac{x + hx^2/2}{1 + hx}. \tag{13.3.14}$$

In a straight frame this reduces to $a_s = -Kx$. A uniform straight solenoid, $b_s = K_s$, has $\phi = -K_s s$, $a_x = -K_s y$, and $a_y = a_s = 0$. Its nonzero transverse vector potential illustrates why canonical and kinetic momenta must be distinguished even in a uniform field.

13.4 Field representation in SplineBoris

The `SplineBoris` element uses the straight-frame specialization $h = 0$ of the reconstruction in Sec. 13.2. Its input field data are in SI units, and its symbolic field generator uses a dimensional scalar potential Φ with the convention

$$\boldsymbol{B} = \nabla\Phi, \qquad \Phi = -(B\rho)\phi. \tag{13.4.1}$$

The change of sign and normalization leaves the physical field unchanged. In the notation of the straight-frame generator, the independent longitudinal functions are

$$a_{n+1}(s) = \partial_x^n B_x\big|_{x=y=0} = (B\rho)S_n(s), \tag{13.4.2}$$

$$b_{n+1}(s) = \partial_x^n B_y\big|_{x=y=0} = (B\rho)N_n(s), \tag{13.4.3}$$

$$b_s(s) = B_s(0,0,s) = (B\rho)K_s(s). \tag{13.4.4}$$

Thus the common seed and recurrence formulas apply after this conversion; there is no separate field-reconstruction principle for the two elements.

Within each element, the longitudinal profiles are fourth-order polynomials supplied through `Spline4` objects. Each object specifies the value and longitudinal derivative at both ends of an interval, together with the mean value. Tuples of these objects describe successive horizontal derivatives of the transverse field. An extended field map is typically represented by several elements, one for each fitted longitudinal interval. The parameter `n_steps` sets the number of spatial Boris steps inside each element. The integrator uses the reconstructed magnetic field directly, without requiring the vector potential.

13.5 SplineBoris: spatial Boris integration

The spatial Boris-like method in `SplineBoris` builds on the original Boris pusher [46], the analyses in Refs. [47, 48], and spatial-stepping formulations in Refs. [49, 50]. It solves the relativistic Lorentz-force equations for a general magnetic field, with longitudinal coordinate z as the independent variable. Tracking is performed in a straight reference frame; curved reference frames are not supported. The algorithm has a symmetric drift–kick–rotation–kick–drift structure.
The magnetic-field representation supplied to the integrator is described in Sec. 13.4. The total momentum magnitude is preserved exactly. Phase-space volume is also preserved exactly in the reduced variables (x, y, P_x, P_y) and in the extended variables (x, y, P_x, P_y, t, E). For smooth magnetic fields away from $P_z = 0$, the fixed-length transfer map is reversible and second-order accurate in C^1. Under field-free entrance and exit conditions, its symplectic defect is of order $\mathcal{O}(\Delta z^2)$.

13.5.1 Lorentz-force equations in spatial form

For a charged particle in a static magnetic field $\boldsymbol{B}(\boldsymbol{r})$,

$$\frac{\mathrm{d}\boldsymbol{P}}{\mathrm{d}t} = q\,(\boldsymbol{v} \times \boldsymbol{B}), \qquad \frac{\mathrm{d}\boldsymbol{r}}{\mathrm{d}t} = \boldsymbol{v} = \frac{\boldsymbol{P}}{\gamma m},$$

with relativistic factor

$$\gamma = \sqrt{1 + \left(\frac{P}{mc}\right)^2}.$$

In the absence of electric fields, the total momentum magnitude

$$P = |\boldsymbol{P}| = \sqrt{P_x^2 + P_y^2 + P_z^2}$$

is constant in time.
Switching from time to the spatial coordinate z as the independent variable:

$$\frac{\mathrm{d}}{\mathrm{d}t} = v_z \frac{\mathrm{d}}{\mathrm{d}z} \quad \Longrightarrow \quad \frac{\mathrm{d}\boldsymbol{P}}{\mathrm{d}z} = \frac{q}{P_z}(\boldsymbol{P} \times \boldsymbol{B}), \qquad \frac{\mathrm{d}\boldsymbol{r}}{\mathrm{d}z} = \frac{\boldsymbol{P}}{P_z}.$$

This reformulation is meaningful only on intervals where P_z stays nonzero and does not change sign, so that z can be used as a valid independent variable. In what follows we restrict to the forward branch

$$P_z > 0,$$

so every occurrence of P_z is understood as the positive root

$$P_z = +\sqrt{P^2 - P_x^2 - P_y^2}.$$

For backward propagation one would instead keep the negative branch consistently throughout.

13.5.2 Integration algorithm

Since $v_z = P_z/(\gamma m)$, the infinitesimal relation between t and z is

$$\frac{\mathrm{d}t}{\mathrm{d}z} = \frac{1}{v_z} = \frac{\gamma m}{P_z} = \frac{E}{c^2 P_z}, \tag{13.5.1}$$

where $E = \gamma m c^2$ is constant in the magnetic-only case. For a finite step Δz, the elapsed time is approximated by a midpoint rule:

$$\Delta t \simeq \frac{\gamma m\, \Delta z}{P_{z,\mathrm{mid}}} = \frac{E\, \Delta z}{c^2 P_{z,\mathrm{mid}}}, \tag{13.5.2}$$

where $P_{z,\mathrm{mid}}$ is the longitudinal momentum evaluated at the midpoint of the step (after the first half-kick).
Writing $\boldsymbol{B} = (B_x, B_y, B_z)$, the equations of motion are

$$\frac{\mathrm{d}x}{\mathrm{d}z} = \frac{P_x}{P_z}, \tag{13.5.3}$$

$$\frac{\mathrm{d}y}{\mathrm{d}z} = \frac{P_y}{P_z}, \tag{13.5.4}$$

$$\frac{\mathrm{d}t}{\mathrm{d}z} = \frac{\gamma m}{P_z} = \frac{E}{c^2 P_z}, \tag{13.5.5}$$

$$\frac{\mathrm{d}P_x}{\mathrm{d}z} = \frac{q}{P_z}(P_y B_z - P_z B_y) = \frac{q}{P_z}(P_y B_z) - q B_y, \tag{13.5.6}$$

$$\frac{\mathrm{d}P_y}{\mathrm{d}z} = \frac{q}{P_z}(P_z B_x - P_x B_z) = q B_x - \frac{q}{P_z}(P_x B_z), \tag{13.5.7}$$

$$\frac{\mathrm{d}P_z}{\mathrm{d}z} = \frac{q}{P_z}(P_x B_y - P_y B_x). \tag{13.5.8}$$

The constant-magnitude constraint

$$P_z = +\sqrt{P^2 - P_x^2 - P_y^2}$$

is enforced algebraically at each substep on the forward branch.
The motion is advanced over a spatial step Δz by a symmetric Boris-type composition. More precisely, one first performs a half drift to the midpoint (x_h, y_h, z_h), evaluates the magnetic field there, and then keeps the resulting midpoint field $\boldsymbol{B}(x_h, y_h, z_h)$ fixed during the central kick–rotate–kick sequence. Thus, for general nonuniform $\boldsymbol{B}(x, y, z)$, the implemented step is not literally the exact Strang splitting of the full variable-coefficient operator $D + K + R$; rather, it is a symmetric midpoint-frozen approximation of that splitting. Here D denotes the drift in (x, y), K the transverse kicks from B_x, B_y, and R the rotation generated by B_z.

13.5.2.1 Step 1: Half drift in (x, y)

$$x_h = x + \frac{\Delta z}{2}\frac{P_x}{P_z}, \qquad y_h = y + \frac{\Delta z}{2}\frac{P_y}{P_z}, \qquad z_h = z + \frac{\Delta z}{2}.$$

The magnetic field is evaluated at (x_h, y_h, z_h).

13.5.2.2 Step 2: First half-kick from B_x, B_y

$$P_x^- = P_x - \frac{q\,\Delta z}{2}B_y, \qquad P_y^- = P_y + \frac{q\,\Delta z}{2}B_x.$$

At this midpoint, compute

$$P_{z,\text{mid}} = \sqrt{P^2 - (P_x^-)^2 - (P_y^-)^2}.$$

Using Eq. (13.5.2), the elapsed time increment is

$$\Delta t = \frac{\gamma m\,\Delta z}{P_{z,\text{mid}}}.$$

The total time is updated as $t' = t + \Delta t$.

13.5.2.3 Step 3: Rotation from B_z

During this substep, $B_x = B_y = 0$ and only B_z acts. The transverse equations become

$$\frac{\mathrm{d}P_x}{\mathrm{d}z} = \frac{qB_z}{P_z}P_y, \qquad \frac{\mathrm{d}P_y}{\mathrm{d}z} = -\frac{qB_z}{P_z}P_x. \tag{13.5.9}$$

The exact solution over one step Δz is a planar rotation with angle

$$\theta = \frac{qB_z\Delta z}{P_z}. \tag{13.5.10}$$

The Boris update replaces this with the Cayley-transform rotation

$$T = \frac{qB_z\Delta z}{2P_{z,\text{mid}}}, \qquad S = \frac{2T}{1+T^2}, \qquad C = \frac{1-T^2}{1+T^2},$$

so that

$$P_x^+ = C\,P_x^- + S\,P_y^-, \tag{13.5.11}$$
$$P_y^+ = -\,S\,P_x^- + C\,P_y^-. \tag{13.5.12}$$

Equivalently,

$$\boldsymbol{P}^* = \boldsymbol{P}^- + \boldsymbol{P}^- \times \boldsymbol{t}, \qquad \boldsymbol{P}^+ = \boldsymbol{P}^- + \boldsymbol{P}^* \times \boldsymbol{s},$$

with $\boldsymbol{t} = (0, 0, T)$ and $\boldsymbol{s} = (0, 0, S)$. This is a planar rotation by the angle $2\arctan T$, so it preserves $|\boldsymbol{P}_\perp|$ exactly while approximating the exact angle θ to second order in Δz.

13.5.2.4 Step 4: Second half-kick

Repeat the same transverse increments:

$$P'_x = P_x^+ - \frac{q\,\Delta z}{2} B_y, \qquad P'_y = P_y^+ + \frac{q\,\Delta z}{2} B_x.$$

13.5.2.5 Step 5: Recompute P_z and second half-drift

$$P'_z = \sqrt{P^2 - (P'_x)^2 - (P'_y)^2}.$$

Advance the positions by another half drift:

$$x' = x_h + \frac{\Delta z}{2}\frac{P'_x}{P'_z}, \qquad y' = y_h + \frac{\Delta z}{2}\frac{P'_y}{P'_z}, \qquad z' = z + \Delta z.$$

13.5.2.6 Complete algorithm summary

Given $(x, y, z, P_x, P_y, P, t)$:

(i) $P_z = \sqrt{P^2 - P_x^2 - P_y^2}$,

(ii) $x_h = x + \frac{\Delta z}{2}\frac{P_x}{P_z}$, $y_h = y + \frac{\Delta z}{2}\frac{P_y}{P_z}$, $z_h = z + \frac{\Delta z}{2}$,

(iii) $P_x^- = P_x - \frac{q\Delta z}{2} B_y$, $P_y^- = P_y + \frac{q\Delta z}{2} B_x$,

(iv) $P_{z,\text{mid}} = \sqrt{P^2 - (P_x^-)^2 - (P_y^-)^2}$, $\gamma = \sqrt{1 + \left(\frac{P}{mc}\right)^2}$, $\Delta t = \frac{\gamma m \Delta z}{P_{z,\text{mid}}}$,

(v) $t' = t + \Delta t$,

(vi) $T = \frac{q B_z \Delta z}{2 P_{z,\text{mid}}}$, $S = \frac{2T}{1+T^2}$, $C = \frac{1-T^2}{1+T^2}$,
$P_x^+ = C\,P_x^- + S\,P_y^-$, $P_y^+ = -S\,P_x^- + C\,P_y^-$,

(vii) $P'_x = P_x^+ - \frac{q\Delta z}{2} B_y$, $P'_y = P_y^+ + \frac{q\Delta z}{2} B_x$,

(viii) $P'_z = \sqrt{P^2 - (P'_x)^2 - (P'_y)^2}$,

(ix) $x' = x_h + \frac{\Delta z}{2}\frac{P'_x}{P'_z}$, $y' = y_h + \frac{\Delta z}{2}\frac{P'_y}{P'_z}$, $z' = z + \Delta z$.

13.5.3 Phase-space volume preservation

The spatial Boris step preserves volume exactly in both the reduced mechanical variables and the extended accelerator variables:

$$\boxed{\begin{array}{c} \det(D\Phi) = 1 \quad \text{for } (x, y, P_x, P_y), \\ \det(D\Psi) = 1 \quad \text{for } (x, y, P_x, P_y, t, E). \end{array}}$$

The proof is given in the following subsections by decomposing the method into its elementary substeps.
The continuous Lorentz flow in time preserves the six-dimensional Liouville volume element

$$dx\,dy\,dz\,dP_x\,dP_y\,dP_z.$$

The spatial Boris algorithm studied here is a different object: after fixing the momentum magnitude P and using z as the independent variable, the discrete dynamics is a reduced map in the variables (x, y, P_x, P_y), with

$$P_z = \sqrt{P^2 - P_x^2 - P_y^2}$$

reconstructed algebraically. We first show that this reduced four-dimensional map preserves the Euclidean volume element $dx\,dy\,dP_x\,dP_y$ exactly, and then extend the result to the accelerator variables (x, y, P_x, P_y, t, E).

13.5.3.1 Reduced four-dimensional map

Denote by $D_{\frac{1}{2}}$ the half drift in coordinates, by $K_{\frac{1}{2}}$ the half kick from the transverse field (B_x, B_y), and by R the rotation generated by B_z. The full step is their composition:

$$\Phi_{\Delta z} = D_{\frac{1}{2}} \circ K_{\frac{1}{2}} \circ R \circ K_{\frac{1}{2}} \circ D_{\frac{1}{2}}. \tag{13.5.13}$$

Since the determinant of the total Jacobian is the product of those of the individual substeps, it is enough to show that each one has determinant one.

- **(a) Half drift in (x, y):**

  $$x' = x + \frac{\Delta z}{2}\frac{P_x}{P_z}, \qquad y' = y + \frac{\Delta z}{2}\frac{P_y}{P_z}, \qquad P_x' = P_x, \quad P_y' = P_y.$$

  Since P_z depends only on (P_x, P_y), the Jacobian has block form

  $$D\Phi_{D_{\frac{1}{2}}} = \begin{pmatrix} I & * \\ 0 & I \end{pmatrix},$$

  and therefore

  $$\det(D\Phi_{D_{\frac{1}{2}}}) = 1.$$

- **(b) Half kick from (B_x, B_y):** During the kick the coordinates are fixed,

  $$P_x' = P_x - \frac{q\Delta z}{2}B_y(x, y, z_h), \qquad P_y' = P_y + \frac{q\Delta z}{2}B_x(x, y, z_h), \qquad x' = x,\ y' = y,$$

  so the Jacobian has block form

  $$D\Phi_{K_{\frac{1}{2}}} = \begin{pmatrix} I & 0 \\ * & I \end{pmatrix},$$

  and hence

  $$\det(D\Phi_{K_{\frac{1}{2}}}) = 1.$$

- **(c) Rotation from B_z:** During this substep the midpoint coordinates (x, y, z_h) are held fixed, so $B_z = B_z(x, y, z_h)$ is a frozen parameter of the rotation map. Write the transverse momentum in polar coordinates,

$$P_x = r\cos\phi, \qquad P_y = r\sin\phi, \qquad P_z = \sqrt{P^2 - r^2}.$$

The Boris rotation preserves the transverse norm exactly, so

$$r' = r, \qquad \phi' = \phi - \alpha(r; x, y, z_h),$$

where

$$\alpha(r; x, y, z_h) = 2\arctan\left(\frac{qB_z(x, y, z_h)\Delta z}{2P_z}\right).$$

For each fixed (x, y), the Jacobian in the momentum variables (r, ϕ) is

$$D_{(r,\phi)}\Phi_R = \begin{pmatrix} 1 & 0 \\ -\partial_r\alpha(r; x, y, z_h) & 1 \end{pmatrix},$$

whose determinant is 1. Since $dP_x\, dP_y = r\, dr\, d\phi$ and $r' = r$, the Cartesian area element is also preserved:

$$dP'_x\, dP'_y = dP_x\, dP_y.$$

Because the rotation leaves the coordinates unchanged,

$$x' = x, \qquad y' = y,$$

the full four-dimensional Jacobian has block lower-triangular form

$$D\Phi_R = \begin{pmatrix} I & 0 \\ * & \dfrac{\partial(P'_x, P'_y)}{\partial(P_x, P_y)} \end{pmatrix},$$

where the lower-right block has determinant 1. Therefore

$$\det(D\Phi_R) = 1.$$

13.5.3.2 Composition of the substeps

Combining the three determinants gives

$$\det(D\Phi_{\Delta z}) = \det(D\Phi_{D_{\frac{1}{2}}})\, \det(D\Phi_{K_{\frac{1}{2}}})\, \det(D\Phi_R)\, \det(D\Phi_{K_{\frac{1}{2}}})\, \det(D\Phi_{D_{\frac{1}{2}}}) = 1.$$

Therefore the full reduced map preserves the four-dimensional volume element exactly:

$$dx'\, dy'\, dP'_x\, dP'_y = dx\, dy\, dP_x\, dP_y.$$

13.5.3.3 Extension to accelerator variables

Introduce the extended variables

$$U = (x, y, P_x, P_y, t, E),$$

where $E = \gamma mc^2$ is constant in the magnetic-only problem. On the positive-energy shell one may write

$$P(E) = \frac{1}{c}\sqrt{E^2 - m^2c^4}, \qquad P_z = \sqrt{P(E)^2 - P_x^2 - P_y^2},$$

so the reduced map depends smoothly on E away from $P_z = 0$, and the arrival time is updated by

$$t' = t + g(x, y, P_x, P_y, E),$$

with g given by the midpoint rule in Eq. (13.5.2). The extended one-step map has the form

$$\Psi(U) = \big(\Phi_{\Delta z}(x, y, P_x, P_y; E),\ t + g,\ E\big).$$

Its Jacobian matrix is block triangular:

$$D\Psi = \begin{pmatrix} \dfrac{\partial \Phi_{\Delta z}}{\partial(x, y, P_x, P_y)} & 0 & \dfrac{\partial \Phi_{\Delta z}}{\partial E} \\ \dfrac{\partial g}{\partial(x, y, P_x, P_y)} & 1 & \dfrac{\partial g}{\partial E} \\ 0 & 0 & 1 \end{pmatrix}.$$

This matrix is not block diagonal: the row associated with the time update may be full, because the arrival-time increment g depends on (x, y, P_x, P_y, E). The determinant is nevertheless unaffected by this row. Indeed, writing

$$X = (x, y, P_x, P_y), \qquad A = \frac{\partial \Phi_{\Delta z}}{\partial X}, \quad b = \frac{\partial \Phi_{\Delta z}}{\partial E}, \quad c = \frac{\partial g}{\partial X}, \quad d = \frac{\partial g}{\partial E},$$

one has

$$D\Psi = \begin{pmatrix} A & 0 & b \\ c & 1 & d \\ 0 & 0 & 1 \end{pmatrix}.$$

Expanding the determinant along the column associated with t, which has only one nonzero entry, gives

$$\det(D\Psi) = \det \begin{pmatrix} A & b \\ 0 & 1 \end{pmatrix} = \det(A).$$

Therefore

$$\det(D\Psi) = \det\left(\frac{\partial \Phi_{\Delta z}}{\partial(x, y, P_x, P_y)} \right) = 1.$$

Hence the extended map preserves the six-dimensional Euclidean volume element

$$dx\, dy\, dP_x\, dP_y\, dt\, dE$$

exactly.

13.5.3.4 Interpretation

The precise statement proved here is a Jacobian statement:

$$\det(D\Phi_{\Delta z}) = 1 \quad \text{for the reduced map,} \qquad \det(D\Psi) = 1 \quad \text{for the extended map.}$$

This establishes exact volume preservation in the chosen reduced and extended variables. It should not be confused with a proof of symplecticity.

13.5.4 Reversibility and second-order accuracy

It is possible to prove that one step is reversible,

$$\boxed{\Phi_{-h} = \Phi_h^{-1}},$$

and that the full fixed-length transfer map is second-order accurate in C^1:

$$\boxed{\begin{aligned} \Phi_h^L - \varphi_L &= \mathcal{O}(h^2), \\ D\Phi_h^L - D\varphi_L &= \mathcal{O}(h^2). \end{aligned}}$$

Second-order accuracy in C^1 means that both:

- the tracked particle coordinates converge with error $\mathcal{O}(h^2)$; and
- the map's first derivatives with respect to the initial coordinates—its Jacobian or response matrix—also converge with error $\mathcal{O}(h^2)$.

The asymptotic notation is defined first, while the proof of the statements above is given in the following subsections.

13.5.4.1 Asymptotic notation

All order estimates in this section are meant uniformly on the compact region of phase space under consideration, for sufficiently small step size. For a family of maps $R_h(U)$, the notation

$$R_h(U) = \mathcal{O}(h^p)$$

means that there are constants $C > 0$ and $h_0 > 0$, independent of U in that compact region, such that

$$\|R_h(U)\| \le Ch^p \qquad \text{for } 0 < h < h_0.$$

The notation

$$R_h(U) = \mathcal{O}_{C^1}(h^p)$$

means that both the map and its derivative with respect to the initial condition U satisfy this bound:

$$\|R_h(U)\| \le Ch^p, \qquad \|DR_h(U)\| \le Ch^p.$$

Thus, if two maps differ by an $\mathcal{O}_{C^1}(h^p)$ remainder, then both the maps themselves and their Jacobians differ by $\mathcal{O}(h^p)$.

13.5.4.2 Extended mechanical system

Let

$$U = (x, y, P_x, P_y, t, E, z),$$

and let the exact spatial dynamics be the autonomous ODE

$$\frac{\mathrm{d}U}{\mathrm{d}z} = F(U),$$

with

$$F(U) = \left(\frac{P_x}{P_z}, \frac{P_y}{P_z}, q\frac{P_y}{P_z}B_z - qB_y, qB_x - q\frac{P_x}{P_z}B_z, \frac{E}{c^2 P_z}, 0, 1 \right),$$

where

$$P(E) = \frac{1}{c}\sqrt{E^2 - m^2c^4}, \qquad P_z = \sqrt{P(E)^2 - P_x^2 - P_y^2},$$

and the magnetic field is evaluated at (x, y, z). On compact sets where $E \geq E_0 > mc^2$ and $P_z \geq c_0 > 0$, this vector field is smooth whenever $\boldsymbol{B}$ is smooth.

13.5.4.3 Smoothness of one step

Each substep of the algorithm is obtained from finitely many additions, multiplications, evaluations of $\boldsymbol{B}$, the square root

$$P_z = \sqrt{P(E)^2 - P_x^2 - P_y^2},$$

and the rational functions defining the Cayley rotation. Since $P_z \geq c_0 > 0$, all denominators stay uniformly away from zero, so for $|h|$ small enough the one-step map Φ_h is C^1 in U, and in fact C^2 in U and C^3 in h, uniformly on the compact region.

13.5.4.4 Proof of reversibility

For every step for which the construction is well defined, the spatial Boris step is reversible:

$$\Phi_{-h} = \Phi_h^{-1}. \tag{13.5.14}$$

The step is the symmetric composition

$$\Phi_h = D_{\frac{h}{2}} \circ K_{\frac{h}{2}} \circ R_h \circ K_{\frac{h}{2}} \circ D_{\frac{h}{2}}.$$

Starting from the final state and applying the same construction with step $-h$, the first backward half drift returns exactly to the same midpoint (x_h, y_h, z_h), so the same magnetic field is used. The backward half kick undoes the last forward half kick, the Cayley rotation with parameter $-T$ is the inverse of the forward rotation, the second backward half kick undoes the first forward half kick, and the final backward half drift returns to the initial position. □

13.5.4.5 Proof of second-order accuracy

Assume $\boldsymbol{B} \in C^3$ on a neighborhood of the compact region visited by the exact and numerical trajectories, and assume $P_z \geq c_0 > 0$ there. Then, for h sufficiently small, one Boris step is a C^1 map of U. Moreover, if $h = L/N$ with $N \in \mathbb{N}$, the projected full map over fixed length L in the six variables (x, y, P_x, P_y, t, E) is second-order accurate in C^1:

$$\Phi_h^L - \varphi_L = \mathcal{O}(h^2), \qquad D\Phi_h^L - D\varphi_L = \mathcal{O}(h^2), \tag{13.5.15}$$

uniformly on the region of interest, where φ_L denotes the exact transfer map of the spatial Lorentz system over length L.

First-order consistency Write

$$d(U) = \left(\frac{P_x}{P_z}, \frac{P_y}{P_z}\right), \qquad k(U) = (-qB_y, qB_x), \qquad \omega(U) = \frac{qB_z}{P_z}.$$

The first half drift gives

$$x_h = x + \frac{h}{2} d_x(U), \qquad y_h = y + \frac{h}{2} d_y(U), \qquad z_h = z + \frac{h}{2},$$

and therefore, by smoothness of $\boldsymbol{B}$,

$$\boldsymbol{B}(x_h, y_h, z_h) = \boldsymbol{B}(x, y, z) + \mathcal{O}(h).$$

Equivalently,

$$k(x_h, y_h, z_h) = k(U) + \mathcal{O}(h),$$

where the $\mathcal{O}(h)$ term denotes the difference between the midpoint-evaluated kick field and the kick field at the initial state. The first half kick gives

$$\begin{pmatrix} P_x^- \\ P_y^- \end{pmatrix} = \begin{pmatrix} P_x \\ P_y \end{pmatrix} + \frac{h}{2} k(x_h, y_h, z_h) = \begin{pmatrix} P_x \\ P_y \end{pmatrix} + \frac{h}{2} k(U) + \mathcal{O}(h^2),$$

and smoothness of P_z on the region $P_z \geq c_0$ gives

$$P_{z,\mathrm{mid}} = P_z + \mathcal{O}(h), \qquad \frac{1}{P_{z,\mathrm{mid}}} = \frac{1}{P_z} + \mathcal{O}(h).$$

Thus

$$T = \frac{h}{2} \frac{qB_z(x_h, y_h, z_h)}{P_{z,\mathrm{mid}}} = \frac{h}{2} \omega(U) + \mathcal{O}(h^2),$$

and the Cayley coefficients satisfy

$$C = 1 + \mathcal{O}(h^2), \qquad S = h\,\omega(U) + \mathcal{O}(h^2).$$

The rotation step therefore yields

$$\begin{pmatrix} P_x^+ \\ P_y^+ \end{pmatrix} = \begin{pmatrix} P_x^- \\ P_y^- \end{pmatrix} + h\,\omega(U) \begin{pmatrix} P_y \\ -P_x \end{pmatrix} + \mathcal{O}(h^2).$$

After the second half kick,

$$\begin{pmatrix} P_x' \\ P_y' \end{pmatrix} = \begin{pmatrix} P_x \\ P_y \end{pmatrix} + h \begin{pmatrix} q\frac{P_y}{P_z}B_z - qB_y \\ qB_x - q\frac{P_x}{P_z}B_z \end{pmatrix} + \mathcal{O}(h^2).$$

Since $P_x' - P_x = \mathcal{O}(h)$ and $P_y' - P_y = \mathcal{O}(h)$, the second half drift gives

$$x' = x + h\frac{P_x}{P_z} + \mathcal{O}(h^2), \qquad y' = y + h\frac{P_y}{P_z} + \mathcal{O}(h^2).$$

Similarly,

$$t' = t + h\frac{E}{c^2 P_z} + \mathcal{O}(h^2), \qquad E' = E, \qquad z' = z + h.$$

Collecting all components,

$$\Phi_h(U) = U + hF(U) + \mathcal{O}(h^2), \tag{13.5.16}$$

uniformly on the compact region.

Second-order local defect Because Φ_h is C^2 in U and C^3 in h, consistency gives an expansion

$$\Phi_h(U) = U + hF(U) + h^2 A(U) + \mathcal{O}_{C^1}(h^3)$$

for some C^1 function $A(U)$. Using the same expansion for Φ_{-h}, inserting

$$V = \Phi_h(U) = U + hF(U) + \mathcal{O}(h^2),$$

and expanding $F(V)$ and $A(V)$ around U, one obtains

$$\Phi_{-h}(V) = U + h^2\big(2A(U) - F'(U)F(U)\big) + \mathcal{O}_{C^1}(h^3).$$

By reversibility, Eq. (13.5.14), this must equal U. Hence

$$A(U) = \frac{1}{2}F'(U)F(U),$$

and therefore

$$\Phi_h(U) = U + hF(U) + \frac{h^2}{2}F'(U)F(U) + \mathcal{O}_{C^1}(h^3). \tag{13.5.17}$$

The exact flow φ_h of the ODE has the same Taylor expansion, as shown in Sec. 13.5.9, so the difference between Eqs. (13.5.17) and (13.5.24) is an $\mathcal{O}_{C^1}(h^3)$ remainder. In particular, both the maps and their Jacobians differ by order h^3:

$$\Phi_h(U) - \varphi_h(U) = \mathcal{O}(h^3), \qquad D\Phi_h(U) - D\varphi_h(U) = \mathcal{O}(h^3), \tag{13.5.18}$$

uniformly on the compact region.

Global state error over fixed length L Let $U_n = \Phi_h^n(U_0)$ and $V_n = \varphi_{nh}(U_0)$, with $nh \le L$, and let $e_n = U_n - V_n$. The next-step error is

$$e_{n+1} = U_{n+1} - V_{n+1} = \Phi_h(U_n) - \varphi_h(V_n).$$

Add and subtract $\Phi_h(V_n)$:

$$e_{n+1} = \big(\Phi_h(U_n) - \Phi_h(V_n)\big) + \big(\Phi_h(V_n) - \varphi_h(V_n)\big).$$

Taking norms gives

$$\|e_{n+1}\| \le \|\Phi_h(U_n) - \Phi_h(V_n)\| + \|\Phi_h(V_n) - \varphi_h(V_n)\|.$$

The second term is the one-step local defect. By Eq. (13.5.18),

$$\|\Phi_h(V_n) - \varphi_h(V_n)\| \le Ch^3.$$

For the first term, Eq. (13.5.16) implies

$$D\Phi_h(U) = I + hF'(U) + \mathcal{O}(h^2),$$

uniformly on the compact region. Since F' is bounded on the compact region, this gives the operator-norm bound

$$\|D\Phi_h(U)\| \le 1 + Ch$$

for all U in the region and all sufficiently small h. To compare $\Phi_h(U_n)$ and $\Phi_h(V_n)$, write

$$\Phi_h(U_n) - \Phi_h(V_n) = \int_0^1 D\Phi_h(V_n + s(U_n - V_n))\,(U_n - V_n)\,ds.$$

Taking norms and using the uniform bound on $D\Phi_h$ gives

$$\|\Phi_h(U_n) - \Phi_h(V_n)\| \le (1 + Ch)\|U_n - V_n\| = (1 + Ch)\|e_n\|.$$

Combining the two bounds yields the recurrence

$$\|e_{n+1}\| \le (1 + Ch)\|e_n\| + Ch^3.$$

Since $e_0 = 0$, the discrete Gronwall lemma in Sec. 13.5.10 gives

$$\|e_n\| \le Ch^2 \qquad \text{for } 0 \le nh \le L. \tag{13.5.19}$$

Global tangent-map error Let

$$A_n = D\Phi_h^n(U_0), \qquad B_n = D\varphi_{nh}(U_0).$$

Thus A_n is the Jacobian, with respect to the initial condition U_0, of the numerical transfer map after n steps, while B_n is the corresponding Jacobian of the exact transfer map over the same distance nh. For the numerical map,

$$U_{n+1} = \Phi_h^{n+1}(U_0) = \Phi_h(\Phi_h^n(U_0))\,.$$

Differentiating with respect to the initial condition U_0 and applying the chain rule gives

$$D\Phi_h^{n+1}(U_0) = D\Phi_h(\Phi_h^n(U_0))\; D\Phi_h^n(U_0).$$

Since $\Phi_h^n(U_0) = U_n$ and $A_n = D\Phi_h^n(U_0)$, this becomes

$$A_{n+1} = D\Phi_h(U_n)\, A_n.$$

Similarly, for the exact flow,

$$V_{n+1} = \varphi_{(n+1)h}(U_0) = \varphi_h(\varphi_{nh}(U_0))\,.$$

Differentiating gives

$$D\varphi_{(n+1)h}(U_0) = D\varphi_h(\varphi_{nh}(U_0))\; D\varphi_{nh}(U_0).$$

Since $\varphi_{nh}(U_0) = V_n$ and $B_n = D\varphi_{nh}(U_0)$, we obtain

$$B_{n+1} = D\varphi_h(V_n)\, B_n.$$

We next compare the one-step tangent maps evaluated at U_n and V_n. By the triangle inequality,

$$\begin{aligned}\|D\Phi_h(U_n) - D\varphi_h(V_n)\| \le{}& \|D\Phi_h(U_n) - D\varphi_h(U_n)\| \\ &+ \|D\varphi_h(U_n) - D\varphi_h(V_n)\|.\end{aligned}$$

The first term is bounded by Eq. (13.5.18):

$$\|D\Phi_h(U_n) - D\varphi_h(U_n)\| \le Ch^3.$$

For the second term, set $G_h(U) = D\varphi_h(U)$. The mean-value theorem, applied now to the map G_h, gives

$$\|G_h(U_n) - G_h(V_n)\| \le \sup_{0\le s\le 1} \|DG_h(V_n + s(U_n - V_n))\|\, \|U_n - V_n\|.$$

Here $DG_h = D^2\varphi_h$. From the Taylor expansion of the exact flow,

$$\varphi_h(U) = U + hF(U) + \mathcal{O}(h^2),$$

we obtain, after differentiating twice with respect to U,

$$D^2\varphi_h(U) = hF''(U) + \mathcal{O}(h^2).$$

Since F'' is bounded on the compact region under consideration, it follows that

$$\|D^2\varphi_h(U)\| \le Ch.$$

Therefore

$$\|D\varphi_h(U_n) - D\varphi_h(V_n)\| \le Ch\, \|U_n - V_n\|.$$

Using the state-error estimate (13.5.19), this gives

$$\|D\varphi_h(U_n) - D\varphi_h(V_n)\| \le Ch\, Ch^2 \le Ch^3.$$

Combining the two bounds, we obtain

$$\|D\Phi_h(U_n) - D\varphi_h(V_n)\| \le Ch^3.$$

Since $\|D\Phi_h(U_n)\| \le 1 + Ch$ and $\|B_n\| \le C$ uniformly on $0 \le nh \le L$,

$$\|A_{n+1} - B_{n+1}\| \le (1 + Ch)\|A_n - B_n\| + Ch^3.$$

With $A_0 = B_0 = I$, another application of Sec. 13.5.10 yields

$$\|A_n - B_n\| \le Ch^2 \qquad \text{for } 0 \le nh \le L. \tag{13.5.20}$$

Equations (13.5.19) and (13.5.20) prove Eq. (13.5.15) in the autonomous variables $U = (x, y, P_x, P_y, t, E, z)$. Because both the numerical and exact updates advance z exactly by h, projecting after $N = L/h$ steps onto the six variables (x, y, P_x, P_y, t, E) preserves the same C^1 error order. □

13.5.5 Global symplectic defect at field-free boundaries

The reduced mechanical variables used inside the algorithm are not canonical variables in the presence of a magnetic field, so there is no reason to expect the interior slice-to-slice map to be exactly symplectic with respect to the constant canonical matrix S. However, a different statement becomes available for the *full* transfer map from entrance to exit when the two ends of the region are field-free. The statement in this section is formulated entirely in the canonical entrance/exit variables and does not rely on interpreting the interior slice-to-slice Boris map as symplectic. Under the field-free boundary assumptions made precise below, the Jacobian M of the full numerical entrance-to-exit map satisfies

$$\boxed{M^\top S M - S = \mathcal{O}(h^2)}$$

over any fixed propagation length L. The mechanism behind the scaling is simple. In canonical boundary coordinates, the exact full transfer map is symplectic. If the numerical full transfer map and its tangent map both approximate the exact ones with global error $\mathcal{O}(h^2)$, then inserting $M = T + \mathcal{O}(h^2)$ into $M^\top S M - S$ immediately yields an $\mathcal{O}(h^2)$ symplectic defect for the full map. This is a statement about the entrance-to-exit transfer map only; it does not assert symplecticity, or a canonical symplectic-defect estimate, for the interior slice-to-slice Boris updates. The proof is given in the following subsections by combining exact symplecticity of the continuous boundary map with the C^1 accuracy estimate from Sec. 13.5.4.

13.5.5.1 Additional boundary assumptions

In addition to the regularity and $P_z \ge c_0 > 0$ assumptions of Sec. 13.5.4, assume that the entrance and exit lie in field-free neighborhoods and choose a gauge such that $A = 0$ in those neighborhoods. Then canonical and mechanical transverse momenta coincide at the entrance and exit:

$$p_x = P_x, \qquad p_y = P_y.$$

13.5.5.2 Boundary variables and symplectic matrix

Let

$$\xi = (x, p_x, y, p_y, t, -E)$$

be the canonical boundary state vector. At the entrance and exit, this is equivalently

$$\xi = (x, P_x, y, P_y, t, -E).$$

In this ordering, the canonical symplectic matrix is

$$S = \begin{pmatrix} 0 & 1 & 0 & 0 & 0 & 0 \\ -1 & 0 & 0 & 0 & 0 & 0 \\ 0 & 0 & 0 & 1 & 0 & 0 \\ 0 & 0 & -1 & 0 & 0 & 0 \\ 0 & 0 & 0 & 0 & 0 & 1 \\ 0 & 0 & 0 & 0 & -1 & 0 \end{pmatrix}.$$

To justify the exact symplecticity of the entrance-to-exit map, recall the standard spatial Hamiltonian reduction for a static magnetic field. Let $\boldsymbol{A}(x, y, z)$ be a vector potential with $\nabla \times \boldsymbol{A} = \boldsymbol{B}$ and $\phi = 0$. The relativistic energy relation in canonical variables is

$$E^2 = m^2c^4 + c^2\Big[(p_x - qA_x)^2 + (p_y - qA_y)^2 + (p_z - qA_z)^2\Big].$$

On the forward branch $P_z > 0$, solving for p_z gives

$$p_z = qA_z + \sqrt{\frac{E^2}{c^2} - m^2c^2 - (p_x - qA_x)^2 - (p_y - qA_y)^2}.$$

Using z as the independent variable, the associated spatial Hamiltonian is

$$\mathcal{K}(x, y, z, p_x, p_y, E) = -\,p_z.$$

Then the exact dynamics of $\xi = (x, p_x, y, p_y, t, -E)$ is governed by the canonical Hamilton equations

$$\frac{\mathrm{d}\xi}{\mathrm{d}z} = S\,\nabla_{\xi}\mathcal{K}(\xi, z).$$

Therefore, for every fixed propagation length L, the exact transfer map in the boundary variables is symplectic.

13.5.5.3 Exact and numerical maps

Let Ψ^L be the exact transfer map over a fixed length L, and let

$$T = D\Psi^L$$

be its Jacobian matrix in the boundary variables ξ. Since Ψ^L is the exact flow of the spatial Hamiltonian system in canonical variables, its Jacobian satisfies

$$T^{\top} S T = S. \tag{13.5.21}$$

Let Φ_h^L be the full numerical map over the same fixed length $L = Nh$, and let

$$M = D\Phi_h^L$$

be its Jacobian matrix in the boundary variables. By Eq. (13.5.15), and because canonical and mechanical momenta coincide at the field-free boundaries,

$$M - T = \mathcal{O}(h^2). \tag{13.5.22}$$

13.5.5.4 Proof of the main result

Under the assumptions stated above, for any fixed propagation length L,

$$M^\top S M - S = \mathcal{O}(h^2) \qquad \text{as } h \to 0. \tag{13.5.23}$$

Write

$$M = T + E, \qquad E = \mathcal{O}(h^2).$$

Then

$$M^\top S M - S = (T+E)^\top S (T+E) - S.$$

Expanding gives

$$M^\top S M - S = T^\top S T - S + T^\top S E + E^\top S T + E^\top S E.$$

By Eq. (13.5.21), the first term vanishes. Since $T = \mathcal{O}(1)$ and $E = \mathcal{O}(h^2)$, the remaining terms are $\mathcal{O}(h^2)$, $\mathcal{O}(h^2)$, and $\mathcal{O}(h^4)$, respectively. This proves Eq. (13.5.23). □

13.5.6 Volume preservation of the exact spatial flow

The volume-preservation result proved in Sec. 13.5.3 is a property of the discrete spatial Boris map. The corresponding exact magnetic-only dynamics has the same volume-preservation property, away from the singular set $P_z = 0$. We use the standard implication recalled in Sec. 13.5.7: a smooth vector field with zero divergence has a flow with unit Jacobian determinant.

First, in the original time-parametrized Cartesian variables, the Lorentz equations preserve the six-dimensional Liouville volume element

$$dx\, dy\, dz\, dP_x\, dP_y\, dP_z.$$

Indeed, writing

$$\frac{\mathrm{d}\boldsymbol{r}}{\mathrm{d}t} = \frac{\boldsymbol{P}}{\gamma m}, \qquad \frac{\mathrm{d}\boldsymbol{P}}{\mathrm{d}t} = q\,\frac{\boldsymbol{P}}{\gamma m} \times \boldsymbol{B}(\boldsymbol{r}),$$

the position part has zero divergence with respect to $\boldsymbol{r}$, since $\boldsymbol{P}/(\gamma m)$ is independent of position. The momentum part also has zero divergence. Explicitly, since $\boldsymbol{B}$ is independent of $\boldsymbol{P}$,

$$\nabla_{\boldsymbol{P}} \cdot \left(q\,\frac{\boldsymbol{P}}{\gamma m} \times \boldsymbol{B} \right) = \frac{q}{m}\, \nabla_{\boldsymbol{P}} \cdot \left(\frac{1}{\gamma}\, \boldsymbol{P} \times \boldsymbol{B} \right)$$

$$= \frac{q}{m}\left[\nabla_{\boldsymbol{P}}\left(\frac{1}{\gamma}\right)\cdot(\boldsymbol{P}\times\boldsymbol{B}) + \frac{1}{\gamma}\nabla_{\boldsymbol{P}}\cdot(\boldsymbol{P}\times\boldsymbol{B})\right].$$

The first term is zero because

$$\nabla_{\boldsymbol{P}}\left(\frac{1}{\gamma}\right) = -\frac{\boldsymbol{P}}{\gamma^3 m^2 c^2},$$

which is parallel to $\boldsymbol{P}$, and hence orthogonal to $\boldsymbol{P}\times\boldsymbol{B}$. The second term is also zero, since

$$\nabla_{\boldsymbol{P}}\cdot(\boldsymbol{P}\times\boldsymbol{B}) = \partial_{P_x}(P_yB_z - P_zB_y) + \partial_{P_y}(P_zB_x - P_xB_z) + \partial_{P_z}(P_xB_y - P_yB_x) = 0.$$

This is consistent with the usual Hamiltonian statement in canonical variables. Let $\boldsymbol{A}(\boldsymbol{r})$ be a vector potential, $\boldsymbol{B} = \nabla\times\boldsymbol{A}$, and define the canonical momentum

$$\boldsymbol{p} = \boldsymbol{P} + q\boldsymbol{A}(\boldsymbol{r}).$$

In the canonical variables $(\boldsymbol{r},\boldsymbol{p})$, the magnetic-only motion is Hamiltonian, and therefore preserves the canonical phase-space volume element

$$dx\,dy\,dz\,dp_x\,dp_y\,dp_z.$$

The change of variables from mechanical to canonical momentum has Jacobian

$$\frac{\partial(\boldsymbol{r},\boldsymbol{p})}{\partial(\boldsymbol{r},\boldsymbol{P})} = \begin{pmatrix} I & 0 \\ q\,\partial_{\boldsymbol{r}}\boldsymbol{A} & I \end{pmatrix},$$

whose determinant is one. Hence

$$dx\,dy\,dz\,dp_x\,dp_y\,dp_z = dx\,dy\,dz\,dP_x\,dP_y\,dP_z.$$

Thus the canonical and mechanical coordinates give the same volume element.
Now fix the energy, equivalently the momentum magnitude P, and use z as the independent variable on the branch $P_z > 0$. The exact reduced spatial system in $X = (x, y, P_x, P_y)$ is

$$\frac{\mathrm{d}x}{\mathrm{d}z} = \frac{P_x}{P_z}, \qquad \frac{\mathrm{d}y}{\mathrm{d}z} = \frac{P_y}{P_z},$$

$$\frac{\mathrm{d}P_x}{\mathrm{d}z} = q\frac{P_y}{P_z}B_z - qB_y, \qquad \frac{\mathrm{d}P_y}{\mathrm{d}z} = qB_x - q\frac{P_x}{P_z}B_z,$$

where

$$P_z = \sqrt{P^2 - P_x^2 - P_y^2},$$

and the magnetic field is evaluated at (x, y, z). Since P_z depends only on (P_x, P_y), and $\boldsymbol{B}$ depends only on position, the divergence with respect to X is

$$\nabla_X\cdot F = \partial_x\left(\frac{P_x}{P_z}\right) + \partial_y\left(\frac{P_y}{P_z}\right)$$

$$+\partial_{P_x}\left(q\frac{P_y}{P_z}B_z - qB_y\right) + \partial_{P_y}\left(qB_x - q\frac{P_x}{P_z}B_z\right)$$
$$= qB_zP_y\,\partial_{P_x}\left(\frac{1}{P_z}\right) - qB_zP_x\,\partial_{P_y}\left(\frac{1}{P_z}\right).$$

Using

$$\partial_{P_x}\left(\frac{1}{P_z}\right) = \frac{P_x}{P_z^3}, \qquad \partial_{P_y}\left(\frac{1}{P_z}\right) = \frac{P_y}{P_z^3},$$

the two remaining terms cancel, and therefore

$$\nabla_X \cdot F = 0.$$

By Sec. 13.5.7, the exact reduced spatial flow therefore preserves

$$dx\,dy\,dP_x\,dP_y.$$

Equivalently, at fixed z, one may introduce transverse canonical momenta

$$p_x = P_x + qA_x(x,y,z), \qquad p_y = P_y + qA_y(x,y,z).$$

The transverse change of variables

$$(x,y,P_x,P_y) \mapsto (x,y,p_x,p_y)$$

again has triangular Jacobian

$$\frac{\partial(x,y,p_x,p_y)}{\partial(x,y,P_x,P_y)} = \begin{pmatrix} I & 0 \\ * & I \end{pmatrix},$$

and determinant one. Therefore

$$dx\,dy\,dp_x\,dp_y = dx\,dy\,dP_x\,dP_y.$$

The reduced mechanical volume preserved by the spatial flow is therefore the same volume as the corresponding transverse canonical volume.
The extended accelerator variables add

$$\frac{\mathrm{d}t}{\mathrm{d}z} = \frac{E}{c^2P_z}, \qquad \frac{\mathrm{d}E}{\mathrm{d}z} = 0.$$

The corresponding vector field in (x,y,P_x,P_y,t,E) has divergence

$$\nabla_X \cdot F + \partial_t\left(\frac{E}{c^2P_z}\right) + \partial_E(0) = 0.$$

Again by Sec. 13.5.7, the exact magnetic-only spatial flow also preserves the extended Euclidean volume element

$$dx\,dy\,dP_x\,dP_y\,dt\,dE.$$

Since the change from (P_x,P_y) to (p_x,p_y) has unit Jacobian and leaves t and E unchanged, this is equivalently the preservation of

$$dx\,dy\,dp_x\,dp_y\,dt\,dE.$$

The discrete result in Sec. 13.5.3 may therefore be viewed as exact preservation, by the algorithm, of the same reduced and extended volume elements preserved by the continuous spatial dynamics.

13.5.7 Divergence-free vector fields and volume preservation

For completeness we recall the standard argument connecting zero divergence with volume preservation. Let

$$\frac{\mathrm{d}U}{\mathrm{d}z} = F(U)$$

be a smooth autonomous system in $\mathbb{R}^n$, and let $\varphi_z(U_0)$ be its flow. Define the Jacobian matrix of the flow with respect to the initial condition,

$$J(z) = D\varphi_z(U_0).$$

Differentiating the flow with respect to U_0 gives the variational equation

$$\frac{\mathrm{d}J}{\mathrm{d}z} = DF(\varphi_z(U_0))\,J, \qquad J(0) = I.$$

By Jacobi's formula for the derivative of a determinant,

$$\frac{\mathrm{d}}{\mathrm{d}z}\det J = \det J\ \mathrm{tr}\left(J^{-1}\frac{\mathrm{d}J}{\mathrm{d}z}\right).$$

Substituting the variational equation gives

$$\frac{\mathrm{d}}{\mathrm{d}z}\det J = \det J\ \mathrm{tr}\Big(J^{-1}DF(\varphi_z(U_0))J\Big).$$

Using cyclic invariance of the trace,

$$\mathrm{tr}\Big(J^{-1}DFJ\Big) = \mathrm{tr}(DF) = \nabla\cdot F.$$

Therefore

$$\frac{\mathrm{d}}{\mathrm{d}z}\det D\varphi_z(U_0) = \big(\nabla\cdot F\big)(\varphi_z(U_0))\ \det D\varphi_z(U_0).$$

If $\nabla\cdot F = 0$, then

$$\frac{\mathrm{d}}{\mathrm{d}z}\det D\varphi_z(U_0) = 0.$$

Since $D\varphi_0(U_0) = I$, one obtains

$$\det D\varphi_z(U_0) = 1$$

for all z for which the flow is defined. Thus the Euclidean volume element is preserved by the flow.

13.5.8 Consistency check for the parallel case

To verify the accuracy when the true Lorentz force vanishes, consider a uniform magnetic field $\boldsymbol{B} = (B_x, B_y, B_z)$ and an initial momentum exactly parallel to it, $\boldsymbol{P}^0 = \alpha\,\boldsymbol{B}$ with constant $\alpha > 0$. Physically, $\boldsymbol{P}$ must remain constant:

$$\frac{d\boldsymbol{P}}{dz} = \frac{q}{P_z}(\boldsymbol{P}\times\boldsymbol{B}) = 0, \qquad \boldsymbol{P}(z) = \boldsymbol{P}^0.$$

13.5.8.1 Step 1: Half-kick

$$P_x^- = \alpha B_x - \frac{q\Delta z}{2} B_y, \qquad P_y^- = \alpha B_y + \frac{q\Delta z}{2} B_x.$$

13.5.8.2 Step 2: Rotation expanded

Let $B_\perp^2 := B_x^2 + B_y^2$. From the half-kick we have

$$P_x^- = \alpha B_x - \frac{q\Delta z}{2} B_y, \qquad P_y^- = \alpha B_y + \frac{q\Delta z}{2} B_x.$$

Compute the transverse magnitude:

$$(P_x^-)^2 + (P_y^-)^2 = \alpha^2 B_\perp^2 + \frac{q^2\Delta z^2}{4} B_\perp^2.$$

Hence

$$P_{z,\mathrm{mid}}^2 = P^2 - (P_x^-)^2 - (P_y^-)^2 = \alpha^2 B_z^2 - \frac{q^2\Delta z^2}{4} B_\perp^2.$$

Expanding the square root,

$$P_{z,\mathrm{mid}} = \alpha B_z \left(1 - \frac{q^2\Delta z^2}{8\alpha^2} \frac{B_\perp^2}{B_z^2}\right) + O(\Delta z^4).$$

Therefore

$$\frac{1}{P_{z,\mathrm{mid}}} = \frac{1}{\alpha B_z} \left(1 + \frac{q^2\Delta z^2}{8\alpha^2} \frac{B_\perp^2}{B_z^2}\right) + O(\Delta z^4).$$

The exact spatial rotation angle is

$$\theta = \frac{qB_z\Delta z}{P_{z,\mathrm{mid}}} = \frac{q}{\alpha}\,\Delta z + O(\Delta z^3),$$

whereas the Boris map rotates by

$$\theta_B = 2\arctan\left(\frac{qB_z\Delta z}{2P_{z,\mathrm{mid}}}\right) = \theta + O(\Delta z^3).$$

Using $\sin\theta_B = \theta_B + O(\Delta z^3)$ and $\cos\theta_B = 1 - \frac{1}{2}\theta_B^2 + O(\Delta z^4)$, we obtain

$$P_x^+ = (1 - \tfrac{1}{2}\theta_B^2) P_x^- + \theta_B P_y^- = \alpha B_x + \frac{q\Delta z}{2} B_y + O(\Delta z^3),$$

$$P_y^+ = -\theta_B P_x^- + (1 - \tfrac{1}{2}\theta_B^2) P_y^- = \alpha B_y - \frac{q\Delta z}{2} B_x + O(\Delta z^3).$$

13.5.8.3 Step 3: Second half-kick

$$P_x' = P_x^+ - \frac{q\Delta z}{2} B_y = \alpha B_x + O(\Delta z^3), \qquad P_y' = P_y^+ + \frac{q\Delta z}{2} B_x = \alpha B_y + O(\Delta z^3).$$

All $O(\Delta z)$ and $O(\Delta z^2)$ terms cancel exactly. Therefore

$$\boldsymbol{P}' = \boldsymbol{P}^0 + O(\Delta z^3).$$

The local truncation error per step is $O(\Delta z^3)$, leading to a global error $O(\Delta z^2)$ over a fixed distance. Hence even when $\boldsymbol{P} \parallel \boldsymbol{B}$, the algorithm preserves the momentum direction up to second order in Δz, and any residual spurious kick decreases quadratically with step size.

13.5.9 Taylor expansion of the exact flow

Let $\varphi_h(U)$ be the exact flow of

$$\frac{\mathrm{d}U}{\mathrm{d}z} = F(U).$$

Writing $U(z) = \varphi_z(U)$, Taylor's theorem gives

$$U(h) = U(0) + hU'(0) + \frac{h^2}{2} U''(0) + \mathcal{O}(h^3).$$

Since

$$U'(z) = F(U(z)),$$

we have

$$U'(0) = F(U).$$

Differentiating once more gives

$$U''(z) = F'(U(z))\, U'(z) = F'(U(z))F(U(z)),$$

and therefore

$$U''(0) = F'(U)F(U).$$

Thus the exact flow satisfies

$$\varphi_h(U) = U + hF(U) + \frac{h^2}{2} F'(U)F(U) + \mathcal{O}_{C^1}(h^3). \tag{13.5.24}$$

Here $\mathcal{O}_{C^1}(h^3)$ means that both the remainder and its derivative with respect to the initial condition U are bounded by Ch^3, uniformly on the compact region under consideration. This C^1 version is the expansion used in Sec. 13.5.4.

13.5.10 Discrete Gronwall lemma

For completeness we record the elementary discrete estimate used in the proof of the C^1 global error bounds.

13.5.10.1 Lemma

Let $h > 0$, let $\alpha, \beta \geq 0$, let $p \geq 1$, and let $\{a_n\}_{n\geq 0}$ be a nonnegative sequence satisfying

$$a_{n+1} \leq (1 + \alpha h)a_n + \beta h^p \qquad \text{for all } n \geq 0. \tag{13.5.25}$$

Then for every $n \geq 0$,

$$a_n \leq (1 + \alpha h)^n a_0 + \beta h^p \sum_{j=0}^{n-1} (1 + \alpha h)^j. \tag{13.5.26}$$

In particular, if $nh \leq L$, then

$$a_n \leq e^{\alpha L} a_0 + \frac{\beta}{\alpha}\big(e^{\alpha L} - 1\big)h^{p-1} \qquad (\alpha > 0), \tag{13.5.27}$$

while for $\alpha = 0$ one has

$$a_n \leq a_0 + \beta L h^{p-1}. \tag{13.5.28}$$

13.5.10.2 Proof

Iterating Eq. (13.5.25) gives

$$a_n \leq (1 + \alpha h)^n a_0 + \beta h^p \sum_{k=0}^{n-1} (1 + \alpha h)^k,$$

which is Eq. (13.5.26). If $\alpha > 0$, then

$$\sum_{k=0}^{n-1} (1 + \alpha h)^k = \frac{(1 + \alpha h)^n - 1}{\alpha h} \leq \frac{e^{\alpha n h} - 1}{\alpha h} \leq \frac{e^{\alpha L} - 1}{\alpha h},$$

which proves Eq. (13.5.27). If $\alpha = 0$, Eq. (13.5.26) reduces to

$$a_n \leq a_0 + n\beta h^p \leq a_0 + \beta L h^{p-1},$$

which proves Eq. (13.5.28). □

13.5.10.3 Corollary used in the main text

If $a_0 = 0$, $p = 3$, and $nh \leq L$, then the lemma gives

$$a_n \leq C h^2,$$

where C depends only on α, β, and L, but not on h or n.

13.6 BFieldExpansion: RK4 tracking

The `BFieldExpansion` element implements the field and vector-potential construction in Secs. 13.2 and 13.3, with polynomial longitudinal profiles. It advances canonical coordinates using classical RK4, which is not an exactly symplectic integrator.

13.6.1 Polynomial profiles and additional strengths

The current implementation selects straight geometry for $h = 0$ and supports curved geometry for $h > 10^{-4}\,\mathrm{m}^{-1}$. The quantities returned as `Bx`, `By`, `Bs`, `Ax`, `Ay`, `As`, and `phi` by `get_field` use the normalization in Eq. (13.1.10).
The polynomial coordinate runs from `s_start` to `s_start` $+ L$, where L is the element length. It need not coincide with the accumulated particle coordinate `s` in a line. The field-evaluation argument `s_local` is entrance-relative, so that the profiles are evaluated at $s =$ `s_start` $+$ `s_local`.
With only polynomial input coefficients and unit scale,

$$N_n(s) = \sum_{j=0}^{d_n} \mathtt{knc}_{nj} s^j, \qquad S_n(s) = \sum_{j=0}^{d_s} \mathtt{ksc}_{nj} s^j, \qquad K_s(s) = \sum_{j=0}^{d_\ell} \mathtt{ksolc}_j s^j. \tag{13.6.1}$$

The transverse factorial is included in Eq. (13.2.1); there is no longitudinal factorial in Eq. (13.6.1). The suffix `c` denotes coefficients. The three polynomial degrees d_n, d_s, and d_ℓ are independent. Transverse rows of different lengths are padded within their own matrix at construction; omitted profiles remain empty and contribute zero. Every supplied `ksolc` coefficient is used. Its scalar-potential seed is

$$\phi_0^{\mathrm{sol}}(s) = -\int_0^s K_s(u)\,\mathrm{d}u = -\sum_{j=0}^{d_\ell} \frac{\mathtt{ksolc}_j}{j+1} s^{j+1}. \tag{13.6.2}$$

The additional degree is reserved internally, so users do not pad the longitudinal profile or the transverse matrices for this integral. In particular, a constant longitudinal field needs only `ksolc=[ks]`. The read-only array `ksoll` contains its longitudinal integral over the element interval, including `kscale`.
Uniform scalar strengths and integrated strengths are incorporated before constructing the potential. For example,

$$N_n(s) = \mathtt{kscale}\left[\sum_j \mathtt{knc}_{nj} s^j + k_n + \frac{\mathtt{knl}_n}{L}\right], \tag{13.6.3}$$

with the analogous expression for the skew profile. The independent k_n and skew scalar strengths exist through octupole order; missing entries contribute zero. The factor `kscale` also multiplies K_s, all reconstructed fields, and both potentials. Nonzero integrated strengths require $L \neq 0$.

13.6.2 Expansion order and convergence

The parameter `num_phi` specifies the maximum retained power of y in field evaluation. An additional scalar-potential coefficient is stored to obtain b_y by differentiation; vector potentials are evaluated through the requested order. For a nonterminating expansion, the infinite-series identities above hold only to the orders retained by the corresponding series. Finite truncation is an approximation to the three-dimensional Maxwell field.

The default `num_phi='auto'` retains the complete polynomial reconstruction, including the vector potential, in straight geometry. Its choice accounts for allocated polynomial degrees and transverse orders, as well as the independent scalar strengths, including coefficients that are initially zero. In curved geometry it adds two vertical orders, retaining the full expansion through first order in h. Higher powers of h are generally incomplete: the curved recurrence need not terminate. Increasing an explicit `num_phi` and checking convergence over the aperture of interest is therefore necessary when higher curvature terms matter. The allocated shapes and truncation order remain fixed after construction, including capacity for explicitly supplied zero coefficients. Evaluation skips unused orders and degrees, with the populated bounds recomputed after input updates.
There are three separate approximations to control: the input profile fit, the transverse expansion order, and the integration step size. Higher longitudinal derivatives enter Eq. (13.2.14), so agreement of an on-axis fit alone does not establish off-axis accuracy. Increasing the number of tracking steps cannot restore fringe terms absent from the field model. For piecewise profiles, derivatives and vector-potential matching at the joins also need to be checked.

13.6.3 Hamiltonian and equations of motion

We use the canonical variables $z = (x, p_x, y, p_y, \tau, p_\tau)$ defined in Eqs. (1.6.2)–(1.6.3), with $\tau = \zeta/\beta_0 = s/\beta_0 - ct$, and the species factor $\chi = (q/q_0)(m_0/m)$. Let

$$\begin{aligned} D &= 1 + \delta = \sqrt{1 + 2p_\tau/\beta_0 + p_\tau^2}, & \pi_s &= \sqrt{D^2 - \pi_x^2 - \pi_y^2}, \\ \pi_x &= p_x - \chi a_x, & \pi_y &= p_y - \chi a_y. \end{aligned} \tag{13.6.4}$$

Here $\boldsymbol{\pi}$ is the normalized kinetic momentum. The forward branch $\pi_s > 0$ is used, away from longitudinal turning points. Specializing the accelerator Hamiltonian (1.7.2) to a static magnetic field gives

$$H = \frac{p_\tau}{\beta_0} - w(\pi_s + \chi a_s). \tag{13.6.5}$$

The Hamiltonian formalism and canonical normalization are discussed in Ref. [12]. No paraxial expansion of the square root is made here.
In the implemented gauge $a_y = 0$, Hamilton's equations are

$$\frac{\mathrm{d}x}{\mathrm{d}s} = w\frac{\pi_x}{\pi_s}, \qquad \frac{\mathrm{d}y}{\mathrm{d}s} = w\frac{\pi_y}{\pi_s}, \tag{13.6.6}$$

$$\frac{\mathrm{d}p_x}{\mathrm{d}s} = h(\pi_s + \chi a_s) + w\chi\left(\frac{\pi_x}{\pi_s}\partial_x a_x + \partial_x a_s\right), \quad \frac{\mathrm{d}p_y}{\mathrm{d}s} = w\chi\left(\frac{\pi_x}{\pi_s}\partial_y a_x + \partial_y a_s\right), \tag{13.6.7}$$

$$\frac{\mathrm{d}\tau}{\mathrm{d}s} = \frac{1}{\beta_0} - w\frac{p_\tau + 1/\beta_0}{\pi_s}, \qquad \frac{\mathrm{d}p_\tau}{\mathrm{d}s} = 0. \tag{13.6.8}$$

Energy, and hence D, is constant because there is no electric field. The spatial Hamiltonian itself can depend explicitly on s and need not be constant along the trajectory.

13.6.4 Numerical integration

Both geometries use classical RK4 [51]. For $\mathrm{d}z/\mathrm{d}s = f(s,z)$, a step of length $\Delta s = L/\texttt{num_integration_steps}$ is

$$k_1 = f(s_n, z_n), \tag{13.6.9}$$
$$k_2 = f(s_n + \Delta s/2, z_n + \Delta s\, k_1/2), \tag{13.6.10}$$
$$k_3 = f(s_n + \Delta s/2, z_n + \Delta s\, k_2/2), \tag{13.6.11}$$
$$k_4 = f(s_n + \Delta s, z_n + \Delta s\, k_3), \tag{13.6.12}$$
$$z_{n+1} = z_n + \frac{\Delta s}{6}(k_1 + 2k_2 + 2k_3 + k_4). \tag{13.6.13}$$

The potential and its derivatives are reevaluated at every stage. For a fixed smooth field and a trajectory bounded away from $\pi_s = 0$, the local integration error is $\mathcal{O}(\Delta s^5)$, and the global error over a fixed length is $\mathcal{O}(\Delta s^4)$. This statement concerns integration error, separately from field truncation and fitting.
Classical RK4 does not preserve the symplectic form exactly, even when applied to Hamilton's equations. Nor does it generally preserve phase-space volume exactly. The distinction between Hamiltonian flow and a symplectic discrete map is discussed in Ref. [52]. Here p_τ remains constant because its right-hand side is identically zero; this fact alone does not imply symplecticity. Backtracking reverses Δs and the integration interval, but RK4 is not exactly reversible at finite step size.

13.6.5 Canonical and kinetic momenta at boundaries

The flag `pkin_const` selects how transverse momenta are transferred between vector-potential conventions at the entrance and exit. It does not change RK4 or its order of accuracy. Let $\alpha_{x,y} = \chi a_{x,y}$; the particle attributes `ax` and `ay` store these species-scaled quantities. Then $\pi_{x,y} = p_{x,y} - \alpha_{x,y}$, as exposed by `kin_px` and `kin_py`.
With `pkin_const=False`, the default, the entrance canonical momenta are used without conversion. At the exit, the element leaves the momenta in its gauge and stores the exit α_x, α_y. Consequently, keeping p_x, p_y fixed while changing the transverse vector potential at a join changes the kinetic momenta. To initialize a particle with prescribed kinetic momenta inside a nonzero field, use

$$p_x = \pi_x + \chi a_x(x, y, s_{\mathrm{in}}), \qquad p_y = \pi_y + \chi a_y(x, y, s_{\mathrm{in}}), \tag{13.6.14}$$

and set the stored `ax`, `ay` consistently.
With `pkin_const=True`, the entrance conversion is

$$p_{x,y}^{\mathrm{in}} = p_{x,y}^{\mathrm{old}} + \chi a_{x,y}^{\mathrm{in}} - \alpha_{x,y}^{\mathrm{old}}. \tag{13.6.15}$$

At the exit the element subtracts $\chi a_{x,y}^{\mathrm{out}}$ and sets the stored transverse vector potential to zero. These conversions preserve kinetic momenta across the changes of potential convention. They do not supply missing physical fringe fields or make the finite-step map symplectic. For a smooth piecewise magnetic model, the field profiles, their derivatives, and the choice of boundary convention must describe a consistent physical join.

Chapter 14

Space charge and beam-beam forces

14.1 Fields generated by a bunch of particles

We assume that the bunch travels rigidly along s with velocity $\beta_0 c$:

$$\rho\left(x,y,s,t\right) = \rho_0\left(x,y,s-\beta_0 ct\right) \tag{14.1.1}$$
$$\mathbf{J}\left(x,y,s,t\right) = \beta_0 c\,\rho_0\left(x,y,s-\beta_0 ct\right)\hat{\mathbf{i}}_s \tag{14.1.2}$$

We define an auxiliary variable ζ as the position along the bunch:

$$\zeta = s - \beta_0 ct\,. \tag{14.1.3}$$

We call K the lab reference frame in which we have defined all equations above, and we introduce a boosted frame K' moving rigidly with the reference particle. The coordinates in the two systems are related by a Lorentz transformation [53]:

$$ct' = \gamma_0\left(ct - \beta_0 s\right) \tag{14.1.4}$$
$$x' = x \tag{14.1.5}$$
$$y' = y \tag{14.1.6}$$
$$s' = \gamma_0\left(s - \beta_0 ct\right) = \gamma_0\zeta \tag{14.1.7}$$

The corresponding inverse transformation is:

$$ct = \gamma_0\left(ct' + \beta_0 s'\right) \tag{14.1.8}$$
$$x = x' \tag{14.1.9}$$
$$y = y' \tag{14.1.10}$$
$$s = \gamma_0\left(s' + \beta_0 ct'\right) \tag{14.1.11}$$

The quantities $\left(c\rho, J_x, J_y, J_s\right)$ form a Lorentz 4-vector and therefore they are transformed between K and K' by relationships similar to Eqs. 14.1.4-14.1.6 [53]:

$$c\rho'\left(\mathbf{r'},t'\right) = \gamma_0\left[c\rho\left(\mathbf{r}\left(\mathbf{r'},t'\right),t\left(\mathbf{r'},t'\right)\right) - \beta_0 J_s\left(\mathbf{r}\left(\mathbf{r'},t'\right),t\left(\mathbf{r'},t'\right)\right)\right] \tag{14.1.12}$$
$$J_s'\left(\mathbf{r'},t'\right) = \gamma_0\left[J_s\left(\mathbf{r}\left(\mathbf{r'},t'\right),t\left(\mathbf{r'},t'\right)\right) - \beta_0 c\rho\left(\mathbf{r}\left(\mathbf{r'},t'\right),t\left(\mathbf{r'},t'\right)\right)\right] \tag{14.1.13}$$

where the transformations $\mathbf{r}\left(\mathbf{r'}, t'\right)$ and $t\left(\mathbf{r'}, t'\right)$ are defined by Eqs. 14.1.8 and 14.1.11 respectively. The transverse components J_x and J_y of the current vector are invariant for our transformation, and are anyhow zero in our case.
Using Eq. 14.1.2 these become:

$$\rho'\left(\mathbf{r'}, t'\right) = \frac{1}{\gamma_0}\rho\left(\mathbf{r}\left(\mathbf{r'}, t'\right), t\left(\mathbf{r'}, t'\right)\right) \tag{14.1.14}$$

$$J'_s\left(\mathbf{r'}, t'\right) = 0 \tag{14.1.15}$$

Using Eqs. 14.1.1 and 14.1.8-14.1.10, we obtain:

$$\rho\left(x', y', s(s', t'), t(s', t')\right) = \rho_0\left(x', y', s(s', t') - \beta_0 c\, t(s', t')\right) \tag{14.1.16}$$

From Eq. 14.1.7 we get:

$$s(s', t') - \beta_0 c\, t(s', t') = \frac{s'}{\gamma_0} \tag{14.1.17}$$

where the coordinate t' has disappeared.
We can therefore write:

$$\rho'\left(x', y', s', t'\right) = \frac{1}{\gamma_0}\rho_0\left(x', y', \frac{s'}{\gamma_0}\right) \tag{14.1.18}$$

The electric potential in the bunch frame is the solution of Poisson's equation:

$$\frac{\partial^2\phi'}{\partial x'^2} + \frac{\partial^2\phi'}{\partial y'^2} + \frac{\partial^2\phi'}{\partial s'^2} = -\frac{\rho'(x', y', s')}{\varepsilon_0} \tag{14.1.19}$$

From Eq. 14.1.18 we can write:

$$\frac{\partial^2\phi'}{\partial x'^2} + \frac{\partial^2\phi'}{\partial y'^2} + \frac{\partial^2\phi'}{\partial s'^2} = -\frac{1}{\gamma_0\varepsilon_0}\rho_0\left(x', y', \frac{s'}{\gamma_0}\right) \tag{14.1.20}$$

We now make the substitution:

$$\zeta = \frac{s'}{\gamma_0} \tag{14.1.21}$$

obtained from Eq. 14.1.7, which allows us to rewrite Eq. 14.1.20 as:

$$\frac{\partial^2\phi'}{\partial x^2} + \frac{\partial^2\phi'}{\partial y^2} + \frac{1}{\gamma_0^2}\frac{\partial^2\phi'}{\partial \zeta^2} = -\frac{1}{\gamma_0\varepsilon_0}\rho_0\left(x, y, \zeta\right) \tag{14.1.22}$$

Here we have dropped the "′" sign from x and y as these coordinates are unaffected by the Lorentz boost.
The quantities $\left(\frac{\phi}{c}, A_x, A_y, A_s\right)$ form a Lorentz 4-vector, so we can write:

$$\phi = \gamma_0\left(\phi' + \beta_0 c A'_s\right) \tag{14.1.23}$$

$$A_s = \gamma_0\left(A'_s + \beta_0\frac{\phi'}{c}\right) \tag{14.1.24}$$

In the bunch frame the charges are at rest, therefore $A'_x = A'_y = A'_s = 0$ and:

$$\phi = \gamma_0 \phi' \tag{14.1.25}$$

$$A_s = \gamma_0 \beta_0 \frac{\phi'}{c} = \frac{\beta_0}{c} \phi \tag{14.1.26}$$

Combining Eq. 14.1.25 with Eq. 14.1.22 we obtain the equation in ϕ:

$$\boxed{\frac{\partial^2 \phi}{\partial x^2} + \frac{\partial^2 \phi}{\partial y^2} + \frac{1}{\gamma_0^2} \frac{\partial^2 \phi}{\partial \zeta^2} = -\frac{1}{\varepsilon_0} \rho_0 \left(x, y, \zeta\right)} \tag{14.1.27}$$

14.1.1 2.5D approximation

For large enough values of γ_0, Eq. 14.1.22 can be approximated by:

$$\boxed{\frac{\partial^2 \phi}{\partial x^2} + \frac{\partial^2 \phi}{\partial y^2} = -\frac{1}{\varepsilon_0} \rho_0 \left(x, y, \zeta\right)} \tag{14.1.28}$$

which means that we can solve a simple 2D problem for each beam slice (identified by its coordinate ζ).

14.1.2 Modulated 2D

Often the beam distribution can be factorized as:

$$\rho_0(x, y, \zeta) = q_0 \lambda_0(\zeta) \rho_\perp(x, y) \tag{14.1.29}$$

where:

$$\int \rho_\perp(x, y)\, dx\, dy = 1 \tag{14.1.30}$$

and $\lambda_0(z)$ is therefore the bunch line density.
For a bunched beam:

$$\int \lambda_0(z)\, dz = N \tag{14.1.31}$$

where N is the bunch population.
In this case the potential can be factorized as:

$$\phi(x, y, \zeta) = q_0 \lambda(\zeta) \phi_\perp(x, y) \tag{14.1.32}$$

where $\phi_\perp(x, y)$ is the solution of the following 2D Poisson equation:

$$\frac{\partial^2 \phi_\perp}{\partial x^2} + \frac{\partial^2 \phi_\perp}{\partial y^2} = -\frac{1}{\varepsilon_0} \rho_\perp \left(x, y\right) \tag{14.1.33}$$

14.2 Lorentz force

We now compute the Lorentz force on the particles moving in the longitudinal direction, including particles of the bunch itself (space charge forces) and particles of a colliding bunch moving in the opposite direction (beam-beam forces). The angles of such test particles are neglected as done in the usual thin-lens approximation. Therefore the velocity of a test particle can be written as:

$$\mathbf{v} = \beta c\, \hat{\mathbf{i}}_s \tag{14.2.1}$$

The Lorentz force can be written as:

$$\begin{aligned} \mathbf{F} &= q\left(-\nabla\phi - \frac{\partial \mathbf{A}}{\partial t} + \beta c\, \hat{\mathbf{i}}_s \times (\nabla \times \mathbf{A})\right) \\ &= q\left(-\nabla\phi - \frac{\beta_0}{\gamma_0 c}\frac{\partial \phi}{\partial t}\hat{\mathbf{i}}_s + \beta c\, \hat{\mathbf{i}}_s \times (\nabla \times \mathbf{A})\right) \end{aligned} \tag{14.2.2}$$

We compute the vector product:

$$\begin{aligned} \hat{\mathbf{i}}_s \times (\nabla \times \mathbf{A}) &= \left(\frac{\partial A_s}{\partial x} - \frac{\partial A_x}{\partial s}\right)\hat{\mathbf{i}}_x + \left(\frac{\partial A_s}{\partial y} - \frac{\partial A_y}{\partial s}\right)\hat{\mathbf{i}}_y \\ &= \left(\frac{\partial A_s}{\partial x} - \frac{\partial A_x}{\partial s}\right)\hat{\mathbf{i}}_x + \left(\frac{\partial A_s}{\partial y} - \frac{\partial A_y}{\partial s}\right)\hat{\mathbf{i}}_y + \underbrace{\left(\frac{\partial A_s}{\partial s} - \frac{\partial A_s}{\partial s}\right)}_{=0}\hat{\mathbf{i}}_s \\ &= \nabla A_s - \frac{\partial \mathbf{A}}{\partial s} \end{aligned} \tag{14.2.3}$$

We replace:

$$\mathbf{F} = q\left(-\nabla\phi - \frac{\beta_0}{\gamma_0 c}\frac{\partial \phi}{\partial t}\hat{\mathbf{i}}_s + \beta\beta_0\nabla\phi - \frac{\beta\beta_0}{\gamma_0}\frac{\partial \phi}{\partial s}\hat{\mathbf{i}}_s\right) \tag{14.2.4}$$

The potentials will have the same form as the sources (this can be shown explicitly using the Lorentz transformations):

$$\phi(x, y, s, t) = \phi\left(x, y, t - \frac{s}{\beta_0 c}\right) \tag{14.2.5}$$

For a function in this form we can write:

$$\frac{\partial \phi}{\partial s} = \frac{\partial}{\partial \zeta} = -\frac{1}{\beta_0 c}\frac{\partial \phi}{\partial t} \tag{14.2.6}$$

obtaining:

$$\mathbf{F} = q\left(-\nabla\phi + \frac{\beta_0^2}{\gamma_0}\frac{\partial \phi}{\partial \zeta}\hat{\mathbf{i}}_s + \beta\beta_0\nabla\phi - \frac{\beta\beta_0}{\gamma_0}\frac{\partial \phi}{\partial \zeta}\hat{\mathbf{i}}_s\right) \tag{14.2.7}$$

Reorganizing:

$$\mathbf{F} = -q(1 - \beta\beta_0)\nabla\phi - \frac{\beta_0(\beta - \beta_0)}{\gamma_0}\frac{\partial \phi}{\partial \zeta}\hat{\mathbf{i}}_s \tag{14.2.8}$$

Writing the dependencies explicitly:

$$F_x(x,y,\zeta(t)) = -q(1-\beta\beta_0)\frac{\partial\phi}{\partial x}(x,y,\zeta(t)) \tag{14.2.9}$$

$$F_y(x,y,\zeta(t)) = -q(1-\beta\beta_0)\frac{\partial\phi}{\partial y}(x,y,\zeta(t)) \tag{14.2.10}$$

$$F_z(x,y,\zeta(t)) = -q\left(1-\beta\beta_0-\frac{\beta_0(\beta-\beta_0)}{\gamma_0}\right)\frac{\partial\phi}{\partial\zeta}(x,y,\zeta(t)) \tag{14.2.11}$$

where $\zeta(t)$ is the position of the particle within the bunch.

14.3 Space charge

Over the single interaction we neglect the particle slippage[1]:

$$\beta = \beta_0 \tag{14.3.1}$$

$$\zeta(t) = \zeta \tag{14.3.2}$$

This gives the following simplification of Eqs. (14.2.9) - (14.2.11):

$$F_x(x,y,\zeta) = -q(1-\beta_0^2)\frac{\partial\phi}{\partial x}(x,y,\zeta) \tag{14.3.3}$$

$$F_y(x,y,\zeta) = -q(1-\beta_0^2)\frac{\partial\phi}{\partial y}(x,y,\zeta) \tag{14.3.4}$$

$$F_z(x,y,\zeta) = -q(1-\beta_0^2)\frac{\partial\phi}{\partial\zeta}(x,y,\zeta) \tag{14.3.5}$$

In this way the force over the single interaction becomes independent of time and therefore we can compute the kicks simply as:

$$\Delta\mathbf{P} = \frac{L}{\beta_0 c}\mathbf{F} \tag{14.3.6}$$

where L is the portion of the machine on which we want to compute the e-cloud interaction.
The kicks on the normalized momenta can be expressed as (recalling that $P_0 = m_0\beta_0\gamma_0 c$):

$$\boxed{\Delta p_x = \frac{m_0}{m}\frac{\Delta P_x}{P_0} = -\frac{qL(1-\beta_0^2)}{m\gamma_0\beta_0^2c^2}\frac{\partial\phi}{\partial x}(x,y,\zeta)} \tag{14.3.7}$$

$$\boxed{\Delta p_y = \frac{m_0}{m}\frac{\Delta P_y}{P_0} = -\frac{qL(1-\beta_0^2)}{m\gamma_0\beta_0^2c^2}\frac{\partial\phi}{\partial y}(x,y,\zeta)} \tag{14.3.8}$$

[1] In any case one would need to take into account also the dispersion in order to have the right slippage.

$$\boxed{\Delta\delta \simeq \Delta p_z = \frac{m_0}{m}\frac{\Delta P_z}{P_0} = -\frac{qL(1-\beta_0^2)}{m\gamma_0\beta_0^2c^2}\frac{\partial\phi}{\partial\zeta}(x,y,\zeta)} \tag{14.3.9}$$

If the beam includes particles of different species (tracking of fragments), note that here q and m refer to the individual particle while m_0 is the mass of the reference particle.
In the modulated 2D case (see Sec. 14.1.2 and in particular Eq. 14.1.32), the kick can be expressed as:

$$\boxed{\Delta p_x = \frac{m_0}{m}\frac{\Delta P_x}{P_0} = -\frac{qq_0L(1-\beta_0^2)}{m\gamma_0\beta_0^2c^2}\lambda_0(\zeta)\frac{\partial\phi_\perp}{\partial x}(x,y)} \tag{14.3.10}$$

$$\boxed{\Delta p_y = \frac{m_0}{m}\frac{\Delta P_y}{P_0} = -\frac{qq_0L(1-\beta_0^2)}{m\gamma_0\beta_0^2c^2}\lambda_0(\zeta)\frac{\partial\phi_\perp}{\partial y}(x,y)} \tag{14.3.11}$$

$$\boxed{\Delta\delta \simeq \Delta p_z = \frac{m_0}{m}\frac{\Delta P_z}{P_0} = -\frac{qq_0L(1-\beta_0^2)}{m\gamma_0\beta_0^2c^2}\frac{d\lambda_0}{d\zeta}(\zeta)\,\phi_\perp(x,y)} \tag{14.3.12}$$

In some cases, for example in the case of transversely Gaussian beams, an analytic closed form exists for the quantities $\frac{\partial\phi_\perp}{\partial x}$ and $\frac{\partial\phi_\perp}{\partial y}$ but not for the potential $\phi_\perp$ itself. In those cases, in order to compute the longitudinal kick, it is possible to obtain a function $\phi_\perp(x,y)$ generating the same transverse kicks by computing numerically the integral:

$$\phi_\perp(x,y) = \int_{(0,0)}^{(x,y)}\left(\frac{\partial\phi_\perp}{\partial x}\hat{\mathbf{i}}_x + \frac{\partial\phi_\perp}{\partial y}\hat{\mathbf{i}}_y\right)\cdot d\mathbf{r}' \tag{14.3.13}$$

14.4 Beam-beam interaction (4D model)

We consider a test particle moving in the opposite direction with velocity:

$$\mathbf{v}_W = -\beta_{0W}c\,\hat{\mathbf{i}}_s \tag{14.4.1}$$
$$s_W(t) = -\beta_{0W}ct \tag{14.4.2}$$

Equations (14.2.9) - (14.2.11) become:

$$F_x(x,y,\zeta_W(t)) = -q(1+\beta_{0W}\beta_{0S})\frac{\partial\phi}{\partial x}(x,y,\zeta_W(t)) \tag{14.4.3}$$
$$F_y(x,y,\zeta_W(t)) = -q(1+\beta_{0W}\beta_{0S})\frac{\partial\phi}{\partial y}(x,y,\zeta_W(t)) \tag{14.4.4}$$
$$F_z(x,y,\zeta_W(t)) = -q\left(1+\beta_{0W}\beta_{0S}-\frac{\beta_{0S}(\beta_{0W}+\beta_{0S})}{\gamma_0}\right)\frac{\partial\phi}{\partial\zeta}(x,y,\zeta_W(t)) \tag{14.4.5}$$

where we have used the subscript S (strong) for the bunch generating the fields, and the subscript W (weak) for the test particle.

$\zeta_W(t)$ is the position of the test particle within the bunch generating the fields:

$$\zeta_W(t) = s_W(t) - \beta_{0S} ct = -(\beta_{0W} + \beta_{0S})ct \tag{14.4.6}$$

In the modulated-2D case (Eq. 14.1.32), Eqs. (14.4.3) - (14.4.4) become:

$$F_x(x, y, \zeta_W(t)) = -qq_{0S}(1 + \beta_{0W}\beta_{0S})\lambda_{0S}(\zeta_W(t))\frac{\partial \phi_\perp}{\partial x}(x, y) \tag{14.4.7}$$

$$F_y(x, y, \zeta_W(t)) = -qq_{0S}(1 + \beta_{0W}\beta_{0S})\lambda_{0S}(\zeta_W(t))\frac{\partial \phi_\perp}{\partial y}(x, y) \tag{14.4.8}$$

$$F_z(x, y, \zeta_W(t)) = -qq_{0S}\left(1 + \beta_{0W}\beta_{0S} - \frac{\beta_{0S}(\beta_{0W} + \beta_{0S})}{\gamma_0}\right)\frac{d\lambda_{0S}}{d\zeta}(\zeta_W(t))\phi_\perp(x, y) \tag{14.4.9}$$

The change in momentum for the test particle is given by:

$$\Delta \mathbf{P} = \int_{-\infty}^{+\infty} \mathbf{F}(t)\, dt \tag{14.4.10}$$

Therefore:

$$\Delta P_x(x, y, \zeta_W(t)) = -qq_{0S}N_S(1 + \beta_{0W}\beta_{0s})\frac{\partial \phi_\perp}{\partial x}(x, y)\int_{-\infty}^{+\infty} \lambda_{0S}(\zeta_W(t))\, dt \tag{14.4.11}$$

$$\Delta P_y(x, y, \zeta_W(t)) = -qq_{0S}N_S(1 + \beta_{0W}\beta_{0s})\frac{\partial \phi_\perp}{\partial y}(x, y)\int_{-\infty}^{+\infty} \lambda_{0S}(\zeta_W(t))\, dt \tag{14.4.12}$$

$$\Delta P_z(x, y, \zeta_W(t)) = -qq_{0S}\left(1 + \beta_{0W}\beta_{0S} - \frac{\beta_{0S}(\beta_{0W} + \beta_{0S})}{\gamma_0}\right)\phi_\perp(x, y)\int_{-\infty}^{+\infty} \frac{d\lambda_{0S}}{d\zeta}(\zeta_W(t))\, dt \tag{14.4.13}$$

Using Eq. (14.4.6) and Eq. (14.1.31) we can write:

$$\int_{-\infty}^{+\infty} \lambda_{0S}(\zeta_W(t))\, dt = \frac{1}{(\beta_{0W} + \beta_{0S})c}\int_{-\infty}^{+\infty} \lambda_{0S}(\zeta)\, d\zeta = \frac{N_S}{(\beta_{0W} + \beta_{0S})c} \tag{14.4.14}$$

Similarly, for a bunched beam:

$$\int_{-\infty}^{+\infty} \frac{d\lambda_{0S}}{d\zeta}(\zeta_W(t))\, dt = \frac{1}{(\beta_{0W} + \beta_{0S})c}\int_{-\infty}^{+\infty} \frac{d\lambda_{0S}}{d\zeta}\, d\zeta = \frac{\lambda_{0S}(+\infty) - \lambda_{0S}(-\infty)}{(\beta_{0W} + \beta_{0S})c} = 0 \tag{14.4.15}$$

From which we can write:

$$\boxed{\Delta p_x = \frac{m_0}{m}\frac{\Delta P_x}{P_0} = -\frac{qq_{0S}N_S}{m\beta_{0W}\gamma_{0W}c^2}\frac{(1 + \beta_{0W}\beta_{0s})}{(\beta_{0W} + \beta_{0S})}\frac{\partial \phi_\perp}{\partial x}(x, y)} \tag{14.4.16}$$

$$\boxed{\Delta p_y = \frac{m_0}{m}\frac{\Delta P_y}{P_0} = -\frac{qq_{0S}N_S}{m\beta_{0W}\gamma_{0W}c^2}\frac{(1 + \beta_{0W}\beta_{0s})}{(\beta_{0W} + \beta_{0S})}\frac{\partial \phi_\perp}{\partial y}(x, y)} \tag{14.4.17}$$

$$\boxed{\Delta p_z = \frac{m_0}{m}\frac{\Delta P_z}{P_0} = 0} \tag{14.4.18}$$

14.5 Longitudinal profiles

14.5.1 Gaussian profile

The profile is in the form:

$$\lambda_0(z) = \frac{N}{\sqrt{2\pi}\sigma} e^{-\frac{(z-z_0)^2}{2\sigma^2}} \tag{14.5.1}$$

14.5.2 q-Gaussian

The profile is in the form:

$$\lambda_0(z) = \frac{N\sqrt{\beta}}{C_q} e_q\left(-\beta(z-z_0)^2\right) \tag{14.5.2}$$

where e_q is the q-exponential function:

$$e_q(x) = [1+(1-q)x]_+^{\frac{1}{1-q}} \tag{14.5.3}$$

C_q is a normalization factor dependent on q alone:

$$C_q = \frac{\sqrt{\pi}\Gamma\left(\frac{3-q}{2(q-1)}\right)}{\sqrt{q-1}\Gamma\left(\frac{1}{q-1}\right)} \tag{14.5.4}$$

The parameter beta defines the standard deviation of the distribution:

$$\sigma = \sqrt{\frac{1}{\beta(5-3q)}} \iff \beta = \frac{1}{\sigma^2(5-3q)} \tag{14.5.5}$$

These expressions are valid for values of the parameter q in the range of interest:

$$1 < q < \frac{5}{3} \tag{14.5.6}$$

In general the q-Gaussian is defined outside this range, but for smaller values it has limited support (not of interest) and for larger values it has an undefined standard deviation.

14.6 Beam-beam interaction (6D model, Hirata method)

This section describes in detail the numerical method used for the simulation of beam-beam interactions in the weak-strong framework using the "Synchro Beam Mapping" approach [54, 55]. This allows correctly modeling the coupling introduced by beam-beam between the longitudinal and transverse planes. The goal of this section is in particular to provide in a compact, complete and self-consistent manner, the set of

equations that are needed for the implementation in a numerical code. Complementary information can be found in [56], including graphical representations of the procedure presented in this section and several validation tests.
The effect of a "crossing angle" in an arbitrary "crossing plane" with respect to the assigned reference frame is taken into account with a suitable coordinate transformation following the approach described in [54, 9]. The employed description of the strong beam allows the correct inclusion of the hour-glass effect as well as the linear coupling at the interaction point, following the treatment presented in [9].
If not differently stated in an explicit way in the following, all coordinates are given in the reference system defined by the closed orbit of the weak beam, which is traveling with positive speed along the s direction. The Interaction Point (IP) is located at s=0 and the crossing plane is defined by the angle that the strong beam forms with the s-axis. In the presence of an offset between the beams (separation), the orientation of the reference system is defined by the closed orbit of the weak beam and the system is centered at the IP location as defined for the strong beam. Therefore the strong beam always passes through the origin of the reference frame.

14.6.1 Direct Lorentz boost (for the weak beam)

We want to transform the coordinates by moving to a Lorentz boosted frame in which the collision is head-on (i.e. $p_x = p_y = 0$ for the strong beam and for the reference particle of the weak beam). We call ϕ the half crossing angle and α the angle that the crossing plane makes with respect to the $x - z$ plane. For this purpose, we perform a transformation which actually includes four operations (more details can be found in Appendix 14.6.6.1 and in [56, 9]):

- Transform the accelerator positions and momenta into Cartesian coordinates (which can then be Lorentz boosted);
- Rotate particle coordinates to the "barycentric" reference frame;
- Perform the Lorentz boost;
- Drift all the particles back to $s = 0$ (as not all particles with $s = 0$ are fixed points of the transformation, and we are tracking with respect to s and not with respect to time).

We name the original accelerator coordinates (as defined in the SixTrack Physics Manual [57]):

$$\left(x, p_x, y, p_y, \sigma, \delta\right) \tag{14.6.1}$$

and the transformed coordinates:

$$\left(x^*, p_x^*, y^*, p_y^*, \sigma^*, \delta^*\right) \tag{14.6.2}$$

We start by computing the drift Hamiltonian in the original coordinates (we are doing a Lorentz transformation, therefore constants matter as we are assuming that h is the total energy of the particle):

$$h = \delta + 1 - \sqrt{(1+\delta)^2 - p_x^2 - p_y^2} \tag{14.6.3}$$

We transform the momenta:

$$p_x^* = \frac{p_x}{\cos\phi} - h\cos\alpha\frac{\tan\phi}{\cos\phi} \tag{14.6.4}$$

$$p_y^* = \frac{p_y}{\cos\phi} - h\sin\alpha\frac{\tan\phi}{\cos\phi} \tag{14.6.5}$$

$$\delta^* = \delta - p_x\cos\alpha\tan\phi - p_y\sin\alpha\tan\phi + h\tan^2\phi \tag{14.6.6}$$

In order to calculate the angles in the transformed frame, we evaluate:

$$p_z^* = \sqrt{(1+\delta^*)^2 - p_x^{*2} - p_y^{*2}} \tag{14.6.7}$$

We can now evaluate the following derivatives of the transformed Hamiltonian (from Hamilton's equations it can be easily seen that these are the angles in the boosted frame):

$$h_x^* = \frac{\partial h^*}{\partial p_x^*} = \frac{p_x^*}{p_z^*} \tag{14.6.8}$$

$$h_y^* = \frac{\partial h^*}{\partial p_y^*} = \frac{p_y^*}{p_z^*} \tag{14.6.9}$$

$$h_\sigma^* = \frac{\partial h^*}{\partial \delta} = 1 - \frac{\delta^*+1}{p_z^*} \tag{14.6.10}$$

These can be used to build the following matrix:

$$L = \begin{pmatrix} (1+h_x^*\cos\alpha\sin\phi) & h_x^*\sin\alpha\sin\phi & \cos\alpha\tan\phi \\ h_y^*\cos\alpha\sin\phi & \left(1+h_y^*\sin\alpha\sin\phi\right) & \sin\alpha\tan\phi \\ h_\sigma^*\cos\alpha\sin\phi & h_\sigma^*\sin\alpha\sin\phi & \frac{1}{\cos\phi} \end{pmatrix} \tag{14.6.11}$$

which can then be used to transform the test-particle positions:

$$\begin{pmatrix} x^* \\ y^* \\ \sigma^* \end{pmatrix} = L \begin{pmatrix} x \\ y \\ \sigma \end{pmatrix} \tag{14.6.12}$$

14.6.2 Synchro-beam mapping

Following the approach introduced in [54], the strong beam is sliced along z. A common approach is to use constant-charge slices (see Appendix 14.6.6.2). For each particle in the weak beam and for each slice in the strong beam we perform the following.

We identify the position of the Collision Point (CP):

$$S = \frac{\sigma^* - \sigma_{\mathrm{sl}}^*}{2} \tag{14.6.13}$$

Here σ^* is defined in the reference system of the weak beam ($\sigma^* > 0$ for particles at the head of the weak bunch) while $\sigma^*_{\rm sl}$ is defined in the reference system of the strong beam ($\sigma^*_{\rm sl} > 0$ for particles at the head of the strong bunch). S is the coordinate of the collision point in the reference system of the weak beam (from Eq. 14.6.13, we can see that particles at the head of the weak bunch collide with particles at the tail of the strong bunch at $S > 0$).

N.B. Here we are making an approximation since we are assuming that particles are moving at the speed of light along z independently of their angles. This means that the presented approach works only for small particle angles. It is for this reason that we need to Lorentz boost to get rid of the crossing angle and we cannot just move to the reference of the strong beam using a rotation (in this case the weak beam would have large angles).
We now evaluate the transverse position of the particle at the CP, with respect to the centroid of the slice, taking into account the particle angles:

$$\overline{x}^* = x^* + p^*_x S - (x^*_{\rm sl} - p^*_{x,\rm sl} S) \tag{14.6.14}$$
$$\overline{y}^* = y^* + p^*_y S - (y^*_{\rm sl} - p^*_{y,\rm sl} S) \tag{14.6.15}$$

Here $x^*_{\rm sl}$, $y^*_{\rm sl}$, $p^*_{x,\rm sl}$ and $p^*_{y,\rm sl}$ are defined in the coordinate system of the weak beam. The momenta of the strong slice appear with a negative sign since in the weak frame the strong slice is travelling "backwards".

14.6.3 Propagation of the strong beam to the collision point

The distribution of the strong beam in the transverse phase-space can be written using the Σ-matrix [12]:

$$f(\eta) = f_0 e^{-\eta^{\rm T}\Sigma^{-1}\eta} \tag{14.6.16}$$

where:

$$\eta = \begin{pmatrix} x \\ p_x \\ y \\ p_y \end{pmatrix} \tag{14.6.17}$$

Points having the same phase space density lie on hyper-elliptic manifolds defined by the equation:

$$\eta^{\rm T}\Sigma^{-1}\eta = \text{const.} \tag{14.6.18}$$

Further considerations on the Σ-matrix can be found in Appendix 14.6.6.3.
We transform the Σ-matrix at the Interaction Point to take into account the Lorentz Boost:

$$\Sigma^{*0}_{11} = \Sigma^0_{11} \tag{14.6.19}$$
$$\Sigma^{*0}_{12} = \Sigma^0_{12}/\cos\phi \tag{14.6.20}$$
$$\Sigma^{*0}_{13} = \Sigma^0_{13} \tag{14.6.21}$$
$$\Sigma^{*0}_{14} = \Sigma^0_{14}/\cos\phi \tag{14.6.22}$$

$$\Sigma_{22}^{*0} = \Sigma_{22}^{0} / \cos^2\phi \tag{14.6.23}$$
$$\Sigma_{23}^{*0} = \Sigma_{23}^{0} / \cos\phi \tag{14.6.24}$$
$$\Sigma_{24}^{*0} = \Sigma_{24}^{0} / \cos^2\phi \tag{14.6.25}$$
$$\Sigma_{33}^{*0} = \Sigma_{33}^{0} \tag{14.6.26}$$
$$\Sigma_{34}^{*0} = \Sigma_{34}^{0} / \cos\phi \tag{14.6.27}$$
$$\Sigma_{44}^{*0} = \Sigma_{44}^{0} / \cos^2\phi \tag{14.6.28}$$
$$\tag{14.6.29}$$

We transport the position part of the boosted Σ-matrix to the CP (here we are taking into account the hourglass effect, assuming that we are in a drift space):

$$\Sigma_{11}^{*} = \Sigma_{11}^{*0} + 2\Sigma_{12}^{*0} S + \Sigma_{22}^{*0} S^2 \tag{14.6.30}$$
$$\Sigma_{33}^{*} = \Sigma_{33}^{*0} + 2\Sigma_{34}^{*0} S + \Sigma_{44}^{*0} S^2 \tag{14.6.31}$$
$$\Sigma_{13}^{*} = \Sigma_{13}^{*0} + \left(\Sigma_{14}^{*0} + \Sigma_{23}^{*0}\right) S + \Sigma_{24}^{*0} S^2 \tag{14.6.32}$$

The Σ-matrix is given in the reference system of the weak beam.
For singular cases we will also need to transport the other terms:

$$\Sigma_{12}^{*} = \Sigma_{12}^{*0} + \Sigma_{22}^{*0} S \tag{14.6.33}$$
$$\Sigma_{14}^{*} = \Sigma_{14}^{*0} + \Sigma_{24}^{*0} S \tag{14.6.34}$$
$$\Sigma_{22}^{*} = \Sigma_{22}^{*0} \tag{14.6.35}$$
$$\Sigma_{23}^{*} = \Sigma_{23}^{*0} + \Sigma_{24}^{*0} S \tag{14.6.36}$$
$$\Sigma_{24}^{*} = \Sigma_{24}^{*0} \tag{14.6.37}$$
$$\Sigma_{34}^{*} = \Sigma_{34}^{*0} + \Sigma_{44}^{*0} S \tag{14.6.38}$$
$$\Sigma_{44}^{*} = \Sigma_{44}^{*0} \tag{14.6.39}$$

We introduce the following three auxiliary quantities:

$$R(S) = \Sigma_{11}^{*} - \Sigma_{33}^{*} \tag{14.6.40}$$
$$W(S) = \Sigma_{11}^{*} + \Sigma_{33}^{*} \tag{14.6.41}$$
$$T(S) = R^2 + 4{\Sigma_{13}^{*}}^2 \tag{14.6.42}$$

The following derivatives will be needed later:

$$\frac{\partial R}{\partial S} = 2\left(\Sigma_{12}^{0} - \Sigma_{34}^{0}\right) + 2S\left(\Sigma_{22}^{0} - \Sigma_{44}^{0}\right) \tag{14.6.43}$$
$$\frac{\partial W}{\partial S} = 2\left(\Sigma_{12}^{0} + \Sigma_{34}^{0}\right) + 2S\left(\Sigma_{22}^{0} + \Sigma_{44}^{0}\right) \tag{14.6.44}$$
$$\frac{\partial \Sigma_{13}^{*}}{\partial S} = \Sigma_{14}^{0} + \Sigma_{23}^{0} + 2\Sigma_{24}^{0} S \tag{14.6.45}$$
$$\frac{\partial T}{\partial S} = 2R\frac{\partial R}{\partial S} + 8\Sigma_{13}^{*}\frac{\partial \Sigma_{13}^{*}}{\partial S} \tag{14.6.46}$$

We will now compute, at the location of the CP, the coupling angle θ, defining a reference frame in which the beam is decoupled. We will call $\hat{x}$ and $\hat{y}$ the coordinates in the decoupled frame and $\hat{\Sigma}^*_{11}$, $\hat{\Sigma}^*_{33}$ the corresponding squared beam sizes. The angle θ is defined as the angle between the $\hat{x}$-axis and the x-axis.
These quantities can be found by diagonalizing the $x-y$ block of the Σ-matrix. We will make determination choices (Eqs. 14.6.49, 14.6.52 and 14.6.56) so that the set $(\theta, \hat{\Sigma}^*_{11}, \hat{\Sigma}^*_{33})$ is uniquely defined and the coupling angle θ lies in the interval:

$$-\frac{\pi}{4} < \theta < \frac{\pi}{4} \tag{14.6.47}$$

Different cases need to be treated separately:

Case T>0, $\left|\Sigma^*_{13}\right|$>0

We evaluate the coupling angle at the position of the CP in the boosted frame:

$$\cos 2\theta = \mathrm{sgn}\left(\Sigma^*_{11} - \Sigma^*_{33}\right) \frac{\Sigma^*_{11} - \Sigma^*_{33}}{\sqrt{\left(\Sigma^*_{11} - \Sigma^*_{33}\right)^2 + 4{\Sigma^*_{13}}^2}} \tag{14.6.48}$$

Or more synthetically:

$$\cos 2\theta = \mathrm{sgn}(R)\frac{R}{\sqrt{T}} \tag{14.6.49}$$

In the following we will also need the derivative of this quantity:

$$\frac{\partial}{\partial S}\left[\cos 2\theta\right] = \mathrm{sgn}(R)\left(\frac{\partial R}{\partial S}\frac{1}{\sqrt{T}} - \frac{R}{2\left(\sqrt{T}\right)^3}\frac{\partial T}{\partial S}\right) \tag{14.6.50}$$

It can be proved that [9]:

$$\cos\theta = \sqrt{\frac{1}{2}\left(1+\cos 2\theta\right)} \tag{14.6.51}$$

$$\sin\theta = \mathrm{sgn}(R)\mathrm{sgn}(\Sigma^*_{13})\sqrt{\frac{1}{2}\left(1-\cos 2\theta\right)} \tag{14.6.52}$$

The corresponding derivatives are given by:

$$\frac{\partial}{\partial S}\cos\theta = \frac{1}{4\cos\theta}\frac{\partial}{\partial S}\cos 2\theta \tag{14.6.53}$$

$$\frac{\partial}{\partial S}\sin\theta = -\frac{1}{4\sin\theta}\frac{\partial}{\partial S}\cos 2\theta \tag{14.6.54}$$

The squared beam sizes in the rotated (uncoupled) boosted frame are given by:

$$\hat{\Sigma}^*_{11} = \frac{1}{2}\left[\left(\Sigma^*_{11} + \Sigma^*_{33}\right) + \mathrm{sgn}\left(\Sigma^*_{11} - \Sigma^*_{33}\right)\sqrt{\left(\Sigma^*_{11} - \Sigma^*_{33}\right)^2 + 4{\Sigma^*_{13}}^2}\right] \tag{14.6.55}$$

$$\hat{\Sigma}^*_{33} = \frac{1}{2}\left[(\Sigma^*_{11} + \Sigma^*_{33}) - \mathrm{sgn}\,(\Sigma^*_{11} - \Sigma^*_{33})\sqrt{(\Sigma^*_{11} - \Sigma^*_{33})^2 + 4{\Sigma^*_{13}}^2}\right] \tag{14.6.56}$$

Equation 14.6.56 can be written in a compact form as:

$$\hat{\Sigma}^*_{11} = \frac{1}{2}\left(W + \mathrm{sgn}(R)\sqrt{T}\right) \tag{14.6.57}$$

$$\hat{\Sigma}^*_{33} = \frac{1}{2}\left(W - \mathrm{sgn}(R)\sqrt{T}\right) \tag{14.6.58}$$

The corresponding derivatives, which will be needed in the following, are given by:

$$\frac{\partial}{\partial S}\left[\hat{\Sigma}^*_{11}\right] = \frac{1}{2}\left(\frac{\partial W}{\partial S} + \mathrm{sgn}(R)\frac{1}{2\sqrt{T}}\frac{\partial T}{\partial S}\right) \tag{14.6.59}$$

$$\frac{\partial}{\partial S}\left[\hat{\Sigma}^*_{33}\right] = \frac{1}{2}\left(\frac{\partial W}{\partial S} - \mathrm{sgn}(R)\frac{1}{2\sqrt{T}}\frac{\partial T}{\partial S}\right) \tag{14.6.60}$$

Case T>0, $\left|\Sigma^*_{13}\right|$=0:

The treatment of the previous case is still applicable with the exception of Eq. 14.6.54 in which the denominator becomes zero. This happens when Σ^*_{13}=0, which implies $\sqrt{T} = |R|$ and therefore $\cos 2\theta = 1$. The case $T = 0$ will be treated separately later, therefore here we can assume $|R| > 0$. We can expand with respect to Σ^*_{13}/R obtaining:

$$\cos 2\theta = \frac{|R|}{\sqrt{R^2 + 4{\Sigma^*_{13}}^2}} = \frac{1}{\sqrt{1 + 4\frac{{\Sigma^*_{13}}^2}{R^2}}} \simeq \frac{1}{1 + 2\frac{{\Sigma^*_{13}}^2}{R^2}} \simeq 1 - 2\frac{{\Sigma^*_{13}}^2}{R^2} \tag{14.6.61}$$

Replacing this result in Eq. 14.6.52 we obtain:

$$\sin\theta = \mathrm{sgn}(R)\mathrm{sgn}(\Sigma^*_{13})\frac{\left|\Sigma^*_{13}\right|}{|R|} = \frac{\Sigma^*_{13}}{R} \tag{14.6.62}$$

We call S_0 the location at which $\Sigma^*_{13} = 0$. At this location we define the auxiliary quantities:

$$c = \Sigma^*_{14} + \Sigma^*_{23} \tag{14.6.63}$$

$$d = \Sigma^*_{24} \tag{14.6.64}$$

We introduce $\Delta S = S - S_0$ and we can write using Eqs. 14.6.30–14.6.32:

$$\Sigma^*_{13} = c\Delta S + d\Delta S^2 \tag{14.6.65}$$

By taking the derivative of Eq. 14.6.62 and using Eq. 14.6.65 we obtain:

$$\frac{\partial}{\partial S}\sin\theta = \frac{1}{R^2}\left[(c + 2d\Delta S)\,R\; - \frac{\partial R}{\partial S}\left(c\Delta S + d\Delta S^2\right)\right] \tag{14.6.66}$$

In the implementation we need only the value for ΔS=0, which is simply given by:

$$\frac{\partial}{\partial S}\sin\theta = \frac{c}{R} \tag{14.6.67}$$

Case T=0, $|c|$>0

Special care has to be taken at sections S_0 at which $\Sigma^*_{11} = \Sigma^*_{33}$ and $\Sigma^*_{13} = 0$ as Eqs. 14.6.49 and 14.6.60 cannot be evaluated directly. Also in this case we define:

$$\Delta S = S - S_0 \tag{14.6.68}$$

At the location of the apparent singularity (ΔS=0) we define the auxiliary quantities:

$$a = \Sigma^*_{12} - \Sigma^*_{34} \tag{14.6.69}$$
$$b = \Sigma^*_{22} - \Sigma^*_{44} \tag{14.6.70}$$
$$c = \Sigma^*_{14} + \Sigma^*_{23} \tag{14.6.71}$$
$$d = \Sigma^*_{24} \tag{14.6.72}$$

and therefore, using Eqs. 14.6.30–14.6.32, we can write:

$$R = 2a\Delta S + b\Delta S^2 \tag{14.6.73}$$
$$\Sigma^*_{13} = c\Delta S + d\Delta S^2 \tag{14.6.74}$$

With these definitions the function T (defined by Eq. 14.6.42) can be expanded around $\Delta S = 0$ (using the Eqs. 14.6.30, 14.6.31, 14.6.32):

$$T = \Delta S^2\left[(2a + b\Delta S)^2 + 4\,(c + d\Delta S)^2\right] \tag{14.6.75}$$

Replacing Eq. 14.6.75 in Eq. 14.6.49 allows removing the apparent singularity:

$$\cos 2\theta = \frac{|2a + b\Delta S|}{\sqrt{(2a + b\Delta S)^2 + 4\,(c + d\Delta S)^2}} \tag{14.6.76}$$

This can be differentiated, obtaining:

$$\frac{\partial}{\partial S}\left[\cos 2\theta\right] = \mathrm{sgn}(2a + b\Delta S)\left[\frac{b}{\sqrt{(2a + b\Delta S)^2 + 4\,(c + d\Delta S)^2}} - \frac{(2a + b\Delta S)(2ab + b^2\Delta s + 4cd + 4d^2\Delta S)}{\left(\sqrt{(2a + b\Delta S)^2 + 4\,(c + d\Delta S)^2}\right)^3}\right] \tag{14.6.77}$$

Similarly, replacing Eq. 14.6.75 in Eq. 14.6.58 we obtain:

$$\hat{\Sigma}^*_{11} = \frac{W}{2} + \frac{1}{2}\mathrm{sgn}\left(2a\Delta S + b\Delta S^2\right)|\Delta S|\sqrt{(2a + b\Delta S)^2 + 4\,(c + d\Delta S)^2} \tag{14.6.78}$$

$$\hat{\Sigma}^*_{33} = \frac{W}{2} - \frac{1}{2}\mathrm{sgn}\left(2a\Delta S + b\Delta S^2\right)|\Delta S|\sqrt{(2a+b\Delta S)^2 + 4\,(c+d\Delta S)^2} \tag{14.6.79}$$

This can be differentiated, obtaining:

$$\frac{\partial}{\partial S}\left[\hat{\Sigma}^*_{11}\right] = \frac{1}{2}\frac{\partial W}{\partial S} + \frac{1}{2}\mathrm{sgn}\left(2a\Delta S + b\Delta S^2\right)\mathrm{sgn}(\Delta S)\left[\sqrt{(2a+b\Delta S)^2 + 4\,(c+d\Delta S)^2} + \frac{\Delta S\left(2ab + b^2\Delta s + 4cd + 4d^2\Delta S\right)}{\sqrt{(2a+b\Delta S)^2 + 4\,(c+d\Delta S)^2}}\right] \tag{14.6.80}$$

$$\frac{\partial}{\partial S}\left[\hat{\Sigma}^*_{33}\right] = \frac{1}{2}\frac{\partial W}{\partial S} - \frac{1}{2}\mathrm{sgn}\left(2a\Delta S + b\Delta S^2\right)\mathrm{sgn}(\Delta S)\left[\sqrt{(2a+b\Delta S)^2 + 4\,(c+d\Delta S)^2} + \frac{\Delta S\left(2ab + b^2\Delta s + 4cd + 4d^2\Delta S\right)}{\sqrt{(2a+b\Delta S)^2 + 4\,(c+d\Delta S)^2}}\right] \tag{14.6.81}$$

In the implementation only the values at ΔS=0 are needed. For this case the results obtained above can be simplified as:

$$\cos 2\theta = \frac{|2a|}{2\sqrt{a^2+c^2}} \tag{14.6.82}$$

$$\frac{\partial}{\partial S}\left[\cos 2\theta\right] = \mathrm{sgn}(2a)\left[\frac{b}{2\sqrt{a^2+c^2}} - \frac{a(ab+2cd)}{2\left(\sqrt{a^2+c^2}\right)^3}\right] \tag{14.6.83}$$

$$\hat{\Sigma}^*_{11} = \frac{W}{2} \tag{14.6.84}$$

$$\hat{\Sigma}^*_{33} = \frac{W}{2} \tag{14.6.85}$$

$$\frac{\partial}{\partial S}\left[\hat{\Sigma}^*_{11}\right] = \frac{1}{2}\frac{\partial W}{\partial S} + \mathrm{sgn}(2a)\sqrt{a^2+c^2} \tag{14.6.86}$$

$$\frac{\partial}{\partial S}\left[\hat{\Sigma}^*_{33}\right] = \frac{1}{2}\frac{\partial W}{\partial S} - \mathrm{sgn}(2a)\sqrt{a^2+c^2} \tag{14.6.87}$$

Eqs. 14.6.52 and 14.6.54 can still be used to evaluate $\sin\theta$ and $\cos\theta$ and the corresponding derivatives, once we assume that $\mathrm{sgn}(0) = 1$ and notice from Eqs. 14.6.73 and 14.6.74 that for small ΔS:

$$\mathrm{sgn}(R)\mathrm{sgn}(\Sigma^*_{13}) = \mathrm{sgn}(a)\mathrm{sgn}(c) \tag{14.6.88}$$

Case T=0, c=0, $|a|$>0

The treatment of the previous case is still applicable with the exception of Eq. 14.6.54 in which the denominator becomes zero.
For this case we can write (from Eq. 14.6.76) around the point where this condition is verified:

$$\cos 2\theta = \frac{1}{\sqrt{1+\frac{4d^2\Delta S^2}{(2a+b\Delta S)^2}}} \simeq 1 - \frac{2d^2\Delta S^2}{(2a+b\Delta S)^2} \tag{14.6.89}$$

We notice from Eqs. 14.6.73 and 14.6.74 that for small ΔS:

$$\mathrm{sgn}(R)\mathrm{sgn}(\Sigma_{13}^*) = \mathrm{sgn}(a)\mathrm{sgn}(d)\mathrm{sgn}(\Delta S) \tag{14.6.90}$$

Replacing Eq. 14.6.89 and 14.6.90 into Eq. 14.6.52 we obtain:

$$\sin\theta = \frac{d\Delta S}{2a}\left|1 - \frac{b\Delta S}{2a}\right| \tag{14.6.91}$$

which can be differentiated at $\Delta S = 0$, obtaining:

$$\frac{\partial}{\partial S}\sin\theta = \frac{d}{2a} \tag{14.6.92}$$

The case in which also $d = 0$ is (or is equivalent to) the uncoupled case as Σ_{13}^* is zero for all S.

Case T=0, c=0, a=0

Around the apparently singular point we can write:

$$R = b\Delta S^2 \tag{14.6.93}$$

$$\Sigma_{13}^* = d\Delta S^2 \tag{14.6.94}$$

Therefore:

$$T = S^4\left(b^2 + 4d^2\right) \tag{14.6.95}$$

and:

$$\cos 2\theta = \frac{|b|}{\sqrt{b^2+4d^2}} \tag{14.6.96}$$

which is a constant. Eqs. 14.6.52 and 14.6.54 can still be used to evaluate $\sin\theta$ and $\cos\theta$ while the corresponding derivatives vanish:
This can be differentiated, obtaining:

$$\frac{\partial}{\partial S}\cos\theta = 0 \tag{14.6.97}$$

$$\frac{\partial}{\partial S}\sin\theta = 0 \tag{14.6.98}$$

Replacing $a = c = 0$ into Eq 14.6.79 we obtain:

$$\hat{\Sigma}_{11}^* = \frac{W}{2} + \frac{1}{2}\mathrm{sgn}(b)\Delta S^2\sqrt{b^2+4d^2} \tag{14.6.99}$$

$$\hat{\Sigma}^*_{33} = \frac{W}{2} - \frac{1}{2}\mathrm{sgn}(b)\Delta S^2\sqrt{b^2+4d^2} \tag{14.6.100}$$

and:

$$\frac{\partial}{\partial S}\left[\hat{\Sigma}^*_{11}\right] = \frac{1}{2}\frac{\partial W}{\partial S} \tag{14.6.101}$$

$$\frac{\partial}{\partial S}\left[\hat{\Sigma}^*_{33}\right] = \frac{1}{2}\frac{\partial W}{\partial S} \tag{14.6.102}$$

The case in which also $d = 0$ is (or is equivalent to) the uncoupled case as Σ^*_{13} is zero for all S.

14.6.4 Forces and kicks on weak beam particles

The positions of the weak beam particle in the uncoupled boosted frame are given by:

$$\hat{\bar{x}}^* = \bar{x}^*\cos\theta + \bar{y}^*\sin\theta \tag{14.6.103}$$

$$\hat{\bar{y}}^* = -\bar{x}^*\sin\theta + \bar{y}^*\cos\theta \tag{14.6.104}$$

In the following we will also need to evaluate:

$$\frac{\partial}{\partial S}\left[\hat{\bar{x}}^*\left(\theta(S)\right)\right] = \frac{\partial \bar{x}^*}{\partial S}\cos\theta + \bar{x}^*\frac{\partial}{\partial S}\left[\cos\theta\right] + \frac{\partial \bar{y}^*}{\partial S}\sin\theta + \bar{y}^*\frac{\partial}{\partial S}\left[\sin\theta\right] \tag{14.6.105}$$

$$\frac{\partial}{\partial S}\left[\hat{\bar{y}}^*\left(\theta(S)\right)\right] = -\frac{\partial \bar{x}^*}{\partial S}\sin\theta - \bar{x}^*\frac{\partial}{\partial S}\left[\sin\theta\right] + \frac{\partial \bar{y}^*}{\partial S}\cos\theta + \bar{y}^*\frac{\partial}{\partial S}\left[\cos\theta\right] \tag{14.6.106}$$

In this boosted, rotated and re-centered frame, closed formulas exist to evaluate the following quantities:

$$\hat{F}^*_x = -K_{sl}\frac{\partial \hat{U}^*}{\partial \hat{\bar{x}}^*}\left(\hat{\bar{x}}^*, \hat{\bar{y}}^*, \hat{\Sigma}^*_{11}, \hat{\Sigma}^*_{33}\right) \tag{14.6.107}$$

$$\hat{F}^*_y = -K_{sl}\frac{\partial \hat{U}^*}{\partial \hat{\bar{y}}^*}\left(\hat{\bar{x}}^*, \hat{\bar{y}}^*, \hat{\Sigma}^*_{11}, \hat{\Sigma}^*_{33}\right) \tag{14.6.108}$$

$$\hat{G}^*_x = -K_{sl}\frac{\partial \hat{U}^*}{\partial \hat{\Sigma}^*_{11}}\left(\hat{\bar{x}}^*, \hat{\bar{y}}^*, \hat{\Sigma}^*_{11}, \hat{\Sigma}^*_{33}\right) \tag{14.6.109}$$

$$\hat{G}^*_y = -K_{sl}\frac{\partial \hat{U}^*}{\partial \hat{\Sigma}^*_{33}}\left(\hat{\bar{x}}^*, \hat{\bar{y}}^*, \hat{\Sigma}^*_{33}, \hat{\Sigma}^*_{33}\right) \tag{14.6.110}$$

where $\hat{U}^*$ is the electric potential associated with the normalized transverse distribution and:

$$K_{sl} = \frac{N_{sl}q_{sl}q_0}{P_0 c} \tag{14.6.111}$$

where N_{sl} is the number of particles in the strong-beam slice, q_{sl} and q_0 are the particle charges for the strong and weak beam respectively, and P_0 is the reference momentum of the weak beam.

The minus sign in Eqs. 14.6.107-14.6.110 comes from the definition of electric potential, i.e. $E = -\nabla U$.
For a bi-Gaussian beam (elliptic) [54]:

$$\hat{f}_x^* = -\frac{\partial \hat{U}^*}{\partial \hat{\bar{x}}^*} = \frac{1}{2\epsilon_0\sqrt{2\pi\left(\hat{\Sigma}_{11}^* - \hat{\Sigma}_{33}^*\right)}}\mathrm{Im}\left[w\left(\frac{\hat{\bar{x}}^* + i\hat{\bar{y}}^*}{\sqrt{2\left(\hat{\Sigma}_{11}^* - \hat{\Sigma}_{33}^*\right)}}\right) - \exp\left(-\frac{(\hat{\bar{x}}^*)^2}{2\hat{\Sigma}_{11}^*} - \frac{(\hat{\bar{y}}^*)^2}{2\hat{\Sigma}_{33}^*}\right) w\left(\frac{\hat{\bar{x}}^*\sqrt{\frac{\hat{\Sigma}_{33}^*}{\hat{\Sigma}_{11}^*}} + i\hat{\bar{y}}^*\sqrt{\frac{\hat{\Sigma}_{11}^*}{\hat{\Sigma}_{33}^*}}}{\sqrt{2\left(\hat{\Sigma}_{11}^* - \hat{\Sigma}_{33}^*\right)}}\right)\right] \tag{14.6.112}$$

$$\hat{f}_y^* = -\frac{\partial \hat{U}^*}{\partial \hat{\bar{x}}^*} = \frac{1}{2\epsilon_0\sqrt{2\pi\left(\hat{\Sigma}_{11}^* - \hat{\Sigma}_{33}^*\right)}}\mathrm{Re}\left[w\left(\frac{\hat{\bar{x}}^* + i\hat{\bar{y}}^*}{\sqrt{2\left(\hat{\Sigma}_{11}^* - \hat{\Sigma}_{33}^*\right)}}\right) - \exp\left(-\frac{(\hat{\bar{x}}^*)^2}{2\hat{\Sigma}_{11}^*} - \frac{(\hat{\bar{y}}^*)^2}{2\hat{\Sigma}_{33}^*}\right) w\left(\frac{\hat{\bar{x}}^*\sqrt{\frac{\hat{\Sigma}_{33}^*}{\hat{\Sigma}_{11}^*}} + i\hat{\bar{y}}^*\sqrt{\frac{\hat{\Sigma}_{11}^*}{\hat{\Sigma}_{33}^*}}}{\sqrt{2\left(\hat{\Sigma}_{11}^* - \hat{\Sigma}_{33}^*\right)}}\right)\right] \tag{14.6.113}$$

$$\hat{g}_x^* = -\frac{\partial \hat{U}^*}{\partial \hat{\Sigma}_{11}^*} = -\frac{1}{2\left(\hat{\Sigma}_{11}^* - \hat{\Sigma}_{33}^*\right)}\left\{\hat{\bar{x}}^*\hat{E}_x^* + \hat{\bar{y}}^*\hat{E}_y^* + \frac{1}{2\pi\epsilon_0}\left[\sqrt{\frac{\hat{\Sigma}_{33}^*}{\hat{\Sigma}_{11}^*}}\exp\left(-\frac{(\hat{\bar{x}}^*)^2}{2\hat{\Sigma}_{11}^*} - \frac{(\hat{\bar{y}}^*)^2}{2\hat{\Sigma}_{33}^*}\right) - 1\right]\right\} \tag{14.6.114}$$

$$\hat{g}_y^* = -\frac{\partial \hat{U}^*}{\partial \hat{\Sigma}_{33}^*} = \frac{1}{2\left(\hat{\Sigma}_{11}^* - \hat{\Sigma}_{33}^*\right)}\left\{\hat{\bar{x}}^*\hat{E}_x^* + \hat{\bar{y}}^*\hat{E}_y^* + \frac{1}{2\pi\epsilon_0}\left[\sqrt{\frac{\hat{\Sigma}_{11}^*}{\hat{\Sigma}_{33}^*}}\exp\left(-\frac{(\hat{\bar{x}}^*)^2}{2\hat{\Sigma}_{11}^*} - \frac{(\hat{\bar{y}}^*)^2}{2\hat{\Sigma}_{33}^*}\right) - 1\right]\right\} \tag{14.6.115}$$

where w is the Faddeeva function.
For a round beam, i.e. $\hat{\Sigma}_{11}^* = \hat{\Sigma}_{33}^* = \hat{\Sigma}^*$:

$$\hat{f}_x^* = -\frac{\partial \hat{U}^*}{\partial \hat{\bar{x}}^*} = \frac{1}{2\pi\epsilon_0}\left[1 - \exp\left(-\frac{(\hat{\bar{x}}^*)^2 + (\hat{\bar{y}}^*)^2}{2\hat{\Sigma}^*}\right)\right]\frac{x}{(\hat{\bar{x}}^*)^2 + (\hat{\bar{y}}^*)^2} \tag{14.6.116}$$

$$\hat{f}_y^* = -\frac{\partial \hat{U}^*}{\partial \hat{\bar{x}}^*} = \frac{1}{2\pi\epsilon_0}\left[1 - \exp\left(-\frac{(\hat{\bar{x}}^*)^2 + (\hat{\bar{y}}^*)^2}{2\hat{\Sigma}^*}\right)\right]\frac{y}{(\hat{\bar{x}}^*)^2 + (\hat{\bar{y}}^*)^2} \tag{14.6.117}$$

$$\hat{g}_x^* = -\frac{\partial \hat{U}^*}{\partial \hat{\Sigma}_{11}^*} = \frac{1}{2\left[(\hat{\bar{x}}^*)^2 + (\hat{\bar{y}}^*)^2\right]}\left[\hat{\bar{y}}^*\hat{E}_y^* - \hat{\bar{x}}^*\hat{E}_x^* + \frac{1}{2\pi\epsilon_0}\frac{\left(\hat{\bar{x}}^*\right)^2}{\hat{\Sigma}^*}\exp\left(-\frac{(\hat{\bar{x}}^*)^2 + (\hat{\bar{y}}^*)^2}{2\hat{\Sigma}^*}\right)\right] \tag{14.6.118}$$

$$\hat{g}_y^* = -\frac{\partial \hat{U}^*}{\partial \hat{\Sigma}_{33}^*} = \frac{1}{2\left[(\hat{\bar{x}}^*)^2 + (\hat{\bar{y}}^*)^2\right]}\left[\hat{\bar{x}}^*\hat{E}_x^* - \hat{\bar{y}}^*\hat{E}_y^* + \frac{1}{2\pi\epsilon_0}\frac{\left(\hat{\bar{y}}^*\right)^2}{\hat{\Sigma}^*}\exp\left(-\frac{(\hat{\bar{x}}^*)^2 + (\hat{\bar{y}}^*)^2}{2\hat{\Sigma}^*}\right)\right] \tag{14.6.119}$$

We have used lower-case symbols to indicate that the factor given by Eq. 14.6.111 is not yet applied.

The transverse kicks in the coupled (but still boosted) reference frame are given by:

$$F_x^* = \hat{F}_x^* \cos\theta - \hat{F}_y^* \sin\theta \tag{14.6.120}$$

$$F_y^* = \hat{F}_x^* \sin\theta + \hat{F}_y^* \cos\theta \tag{14.6.121}$$

To compute the longitudinal kick we notice from Eq. 14.6.13 that:

$$\frac{\partial}{\partial z} = \frac{1}{2}\frac{\partial}{\partial S} \tag{14.6.122}$$

Therefore:

$$F_z^* = \frac{1}{2}\frac{\partial}{\partial S}\left[\hat{U}^*\left(\hat{\bar{x}}^*\left(\theta(S)\right), \hat{\bar{y}}^*\left(\theta(S)\right), \hat{\Sigma}_{11}^*(S), \hat{\Sigma}_{33}^*(S)\right)\right] \tag{14.6.123}$$

This can be rewritten as:

$$F_z^* = \frac{1}{2}\left(\hat{F}_x^*\frac{\partial}{\partial S}\left[\hat{\bar{x}}^*\left(\theta(S)\right)\right] + \hat{F}_y^*\frac{\partial}{\partial S}\left[\hat{\bar{y}}^*\left(\theta(S)\right)\right] + \hat{G}_x^*\frac{\partial}{\partial S}\left[\hat{\Sigma}_{11}^*(S)\right] + \hat{G}_y^*\frac{\partial}{\partial S}\left[\hat{\Sigma}_{33}^*(S)\right]\right) \tag{14.6.124}$$

where all the terms have been evaluated before.
The quantities evaluated so far can be used to compute the effect of the beam-beam interaction on the particle coordinates and momenta [54]:

$$x_{new}^* = x^* - SF_x^* \tag{14.6.125}$$

$$p_{x,new}^* = p_x^* + F_x^* \tag{14.6.126}$$

$$y_{new}^* = y^* - SF_y^* \tag{14.6.127}$$

$$p_{y,new}^* = p_y^* + F_y^* \tag{14.6.128}$$

$$z_{new}^* = z^* \tag{14.6.129}$$

$$\delta_{new}^* = \delta^* + F_z^* + \frac{1}{2}\left[F_x^*\left(p_x^* + \frac{1}{2}F_x^* + p_{x,\mathrm{sl}}^*\right) + F_y^*\left(p_y^* + \frac{1}{2}F_y^* + p_{y,\mathrm{sl}}^*\right)\right] \tag{14.6.130}$$

The physical meaning of the different terms in these equations is illustrated in [56].

14.6.5 Inverse Lorentz boost (for the weak beam)

Now we need to go back to the accelerator coordinates by undoing the transformation described in Sec. 14.6.1.
As before we evaluate:

$$p_z^* = \sqrt{(1+\delta^*)^2 - p_x^{*2} - p_y^{*2}} \tag{14.6.131}$$

and then:

$$h_x^* = \frac{p_x^*}{p_z^*} \tag{14.6.132}$$

$$h_y^* = \frac{p_y^*}{p_z^*} \tag{14.6.133}$$

$$h_\sigma^* = 1 - \frac{\delta^* + 1}{p_z^*} \tag{14.6.134}$$

We invert the matrix (14.6.11) using Cramer's rule:

$$\mathrm{Det}\,(L) = \frac{1}{\cos\phi} + \left(h_x^* \cos\alpha + h_y^* \sin\alpha - h_\sigma^* \sin\phi\right) \tan\phi \tag{14.6.135}$$

$$L^{\mathrm{inv}} = \frac{1}{\mathrm{Det}\,(L)} \times \begin{pmatrix} \left(\frac{1}{\cos\phi} + \sin\alpha\tan\phi\left(h_y^* - h_\sigma^*\sin\alpha\sin\phi\right)\right) & \sin\alpha\tan\phi\left(h_\sigma^*\cos\alpha\sin\phi - h_x^*\right) & -\tan\phi\left(\cos\alpha - h_x^*\sin^2\alpha\sin\phi + h_y^*\cos\alpha\sin\alpha\sin\phi\right) \\ \cos\alpha\tan\phi\left(-h_y^* + h_\sigma^*\sin\alpha\sin\phi\right) & \left(\frac{1}{\cos\phi} + \cos\alpha\tan\phi\left(h_x^* - h_\sigma^*\cos\alpha\sin\phi\right)\right) & -\tan\phi\left(\sin\alpha - h_y^*\cos^2\alpha\sin\phi + h_x^*\cos\alpha\sin\alpha\sin\phi\right) \\ -h_\sigma^*\cos\alpha\sin\phi & -h_\sigma^*\sin\alpha\sin\phi & \left(1 + h_x^*\cos\alpha\sin\phi + h_y^*\sin\alpha\sin\phi\right) \end{pmatrix} \tag{14.6.136}$$

This can be used to transform the positions:

$$\begin{pmatrix} x \\ y \\ \sigma \end{pmatrix} = L^{\mathrm{inv}} \begin{pmatrix} x^* \\ y^* \\ \sigma^* \end{pmatrix} \tag{14.6.137}$$

The Hamiltonian can be transformed with a re-scaling:

$$h = h^* \cos^2\phi = \left(\delta^* + 1 - \sqrt{(1+\delta^*)^2 - p_x^{*2} - p_y^{*2}}\right)\cos^2\phi \tag{14.6.138}$$

This can be used to transform the transverse momenta (inverting Eqs. 14.6.4 and following):

$$p_x = p_x^* \cos\phi + h\cos\alpha\tan\phi \tag{14.6.139}$$

$$p_y = p_y^* \cos\phi + h\sin\alpha\tan\phi \tag{14.6.140}$$

The longitudinal momentum can be calculated directly using Eq. 14.6.6:

$$\delta = \delta^* + p_x\cos\alpha\tan\phi + p_y\sin\alpha\tan\phi - h\tan^2\phi \tag{14.6.141}$$

14.6.6 Additional material

14.6.6.1 Detailed explanation of "the boost" transformation

The reference frame transformation used in Sec. 14.6.1 can be written as [54, 9]:

$$\begin{pmatrix} \sigma^* \\ x^* \\ s^* \\ y^* \end{pmatrix} = A^{-1} {R_{\mathrm{CP}}}^{-1} L_{\mathrm{boost}} R_{\mathrm{CA}} R_{\mathrm{CP}} A \begin{pmatrix} \sigma \\ x \\ s \\ y \end{pmatrix} \tag{14.6.142}$$

Here A is the matrix transforming the accelerator coordinates (Courant-Snyder) to Cartesian coordinates:

$$\begin{pmatrix} ct \\ X \\ Z \\ Y \end{pmatrix} = A \begin{pmatrix} \sigma \\ x \\ s \\ y \end{pmatrix} = \begin{pmatrix} -1 & 0 & 1 & 0 \\ 0 & 1 & 0 & 0 \\ 0 & 0 & 1 & 0 \\ 0 & 0 & 0 & 1 \end{pmatrix} \begin{pmatrix} \sigma \\ x \\ s \\ y \end{pmatrix} \tag{14.6.143}$$

R_{CP} is a rotation matrix bringing the crossing plane to the $X-Z$ plane:

$$R_{\mathrm{CP}} = \begin{pmatrix} 1 & 0 & 1 & 0 \\ 0 & \cos\alpha & 0 & \sin\alpha \\ 0 & 0 & 1 & 0 \\ 0 & -\sin\alpha & 0 & \cos\alpha \end{pmatrix} \tag{14.6.144}$$

R_{CA} is a rotation matrix moving to the barycentric reference frame (in which the two beams are symmetric with respect to the s-axis):

$$R_{\mathrm{CA}} = \begin{pmatrix} 1 & 0 & 0 & 0 \\ 0 & \cos\phi & \sin\phi & 0 \\ 0 & -\sin\phi & \cos\phi & 0 \\ 0 & 0 & 0 & 1 \end{pmatrix} \tag{14.6.145}$$

L_{boost} is the matrix defining a Lorentz boost in the direction of the rotated X-axis:

$$L_{\mathrm{boost}} = \begin{pmatrix} 1/\cos\phi & -\tan\phi & 0 & 0 \\ -\tan\phi & 1/\cos\phi & 0 & 0 \\ 0 & 0 & 1 & 0 \\ 0 & 0 & 0 & 1 \end{pmatrix} \tag{14.6.146}$$

The momenta are transformed similarly [9]:

$$\begin{pmatrix} \delta^* \\ p_x^* \\ h^* \\ p_y^* \end{pmatrix} = B^{-1} {R_{\mathrm{CP}}}^{-1} L_{\mathrm{boost}} R_{\mathrm{CA}} R_{\mathrm{CP}} B \begin{pmatrix} \delta \\ p_x \\ h \\ p_y \end{pmatrix} \tag{14.6.147}$$

where the transformation from accelerator to Cartesian coordinates is given by:

$$\begin{pmatrix} E/c - p_0 \\ P_x \\ P_z - p_0 \\ P_y \end{pmatrix} = p_0 \begin{pmatrix} 1 & 0 & 0 & 0 \\ 0 & 1 & 0 & 0 \\ 0 & 0 & -1 & 0 \\ 0 & 0 & 0 & 1 \end{pmatrix} \begin{pmatrix} \delta \\ p_x \\ h \\ p_y \end{pmatrix} \tag{14.6.148}$$

As explained in Sec.14.6.1 not all particles with $s = 0$ are fixed points of the transformation, therefore a drift back to s=0 needs to be performed as we are tracking w.r.t. s and not w.r.t. time. The net effect of the transformation is to move from the reference frame of the weak beam to the boosted barycentric frame.

14.6.6.2 Constant charge slicing

We consider a Gaussian longitudinal bunch distribution:

$$\lambda(z) = \frac{1}{\sigma_z\sqrt{2\pi}} e^{-\frac{z^2}{2\sigma_z^2}} \tag{14.6.149}$$

We introduce the cumulative distribution function:

$$Q(z) = \int_{-\infty}^{z} \lambda(z')dz' = \frac{1}{2} + \frac{1}{2}\text{erf}\left(\frac{z}{\sqrt{2}\sigma_z}\right) \tag{14.6.150}$$

We define longitudinal cuts z_n^{cut} such that the bunch is sliced in N sections having the same charge:

$$Q(z_n^{\text{cut}}) = \frac{n}{N} \tag{14.6.151}$$

Replacing 14.6.151 in 14.6.150 we obtain:

$$z_n^{\text{cut}} = \sqrt{2}\sigma_z \text{erf}^{-1}\left(\frac{2n}{N} - 1\right) \tag{14.6.152}$$

For each slice we need to find the longitudinal centroid position. For a generic slice having edges z_1 and z_2 the centroid position can be written as:

$$z^{centroid} = \frac{1}{Q(z_2) - Q(z_1)} \int_{z_1}^{z_2} z\lambda(z)dz = \frac{\sigma_z}{\sqrt{2\pi}\left(Q(z_2) - Q(z_1)\right)} \left(e^{-\frac{z_1^2}{2\sigma_z^2}} - e^{-\frac{z_2^2}{2\sigma_z^2}}\right) \tag{14.6.153}$$

14.6.6.3 Considerations on the Σ-matrix description

Given the reduced Σ-matrix of the beam (including only position terms, no momenta):

$$\Sigma = \begin{pmatrix} \Sigma_{11} & \Sigma_{13} \\ \Sigma_{13} & \Sigma_{33} \end{pmatrix} \tag{14.6.154}$$

the distribution for a Gaussian beam can be written as:

$$\rho(\mathbf{x}) = \rho_0 e^{-\mathbf{x}^{\text{T}}\Sigma^{-1}\mathbf{x}} \tag{14.6.155}$$

Points having the same density lie on ellipses defined by the equation:

$$\mathbf{x}^{\text{T}}\Sigma^{-1}\mathbf{x} = \text{const.} \tag{14.6.156}$$

As Σ is symmetric, it can be diagonalized:

$$\Sigma = \mathbf{V}\mathbf{W}\mathbf{V}^T \tag{14.6.157}$$

where the matrix $\mathbf{V}$ has in its columns the eigenvectors of Σ and $\mathbf{W}$ is a diagonal matrix with the corresponding eigenvalues:

$$W = \begin{pmatrix} \hat{\Sigma}_{11} & 0 \\ 0 & \hat{\Sigma}_{33} \end{pmatrix} \tag{14.6.158}$$

$\mathbf{V}$ is a unitary matrix (eigenvectors are orthonormal):

$$\mathbf{V}\mathbf{V}^T = \mathbf{I} \Rightarrow \mathbf{V}^{-1} = \mathbf{V}^T \tag{14.6.159}$$

$\mathbf{V}$ can be used to transform coordinates from the initial frame to the decoupled frame: where $\hat{\mathbf{x}}$ are the coordinates in the decoupled frame, i.e. the projections of $\mathbf{x}$ on the eigenvectors:

$$\hat{\mathbf{x}} = \mathbf{V}^T\mathbf{x} \tag{14.6.160}$$

Combining Eqs. 14.6.157 and 14.6.159 we can write:

$$\Sigma^{-1} = \mathbf{V}\mathbf{W}^{-1}\mathbf{V}^T \tag{14.6.161}$$

This can be replaced in Eq. 14.6.156, re-writing the equation of the ellipse as:

$$\mathbf{x}^{\mathrm{T}}\mathbf{V}\mathbf{W}^{-1}\mathbf{V}^T\mathbf{x} = \text{const.} \tag{14.6.162}$$

Using Eq. 14.6.160 we obtain the equation of the ellipse in the reference system of the eigenvectors:

$$\hat{\mathbf{x}}^{\mathrm{T}}\mathbf{W}^{-1}\hat{\mathbf{x}} = \text{const.} \tag{14.6.163}$$

which can be rewritten in the familiar form:

$$\frac{\hat{x}^2}{\hat{\Sigma}_{11}} + \frac{\hat{y}^2}{\hat{\Sigma}_{33}} = \text{const.} \tag{14.6.164}$$

Once the Σ-matrix is assigned, the one-sigma ellipse can be drawn by the following procedure:

- We diagonalize Σ and we generate an auxiliary matrix defined as:

$$\mathbf{A} = \mathbf{V}\sqrt{\mathbf{W}}\mathbf{V}^T \tag{14.6.165}$$

- We generate a set of points on the unit circle

$$\mathbf{z} = \begin{bmatrix} \cos t \\ \sin t \end{bmatrix} \tag{14.6.166}$$

- We apply $\mathbf{A}$ to t to generate points on the one-sigma ellipse:

$$\mathbf{x}_{1\sigma} = \mathbf{A}\mathbf{z} \tag{14.6.167}$$

This can be verified as follows:

$$\begin{aligned} {\mathbf{x}_{1\sigma}}^{\mathrm{T}}\Sigma^{-1}\mathbf{x}_{1\sigma} &= \mathbf{z}^{\mathrm{T}}\mathbf{A}^{\mathrm{T}}\Sigma^{-1}\mathbf{A}\mathbf{z} = \mathbf{z}^{\mathrm{T}}(\mathbf{V}\sqrt{\mathbf{W}}\mathbf{V})(\mathbf{V}^T\mathbf{W}^{-1}\mathbf{V}^T)(\mathbf{V}\sqrt{\mathbf{W}}\mathbf{V}^T)\mathbf{z} \\ &= \mathbf{z}^{\mathrm{T}}\mathbf{V}\sqrt{\mathbf{W}}\mathbf{W}^{-1}\sqrt{\mathbf{W}}\mathbf{V}^T\mathbf{z} = \mathbf{z}^{\mathrm{T}}\mathbf{V}\mathbf{V}^T\mathbf{z} = \mathbf{z}^{\mathrm{T}}\mathbf{z} = 1 \end{aligned} \tag{14.6.168}$$

14.7 Beam-beam interaction (6d model, Particle In Cell)

To simulate self-consistently the interaction between two bunches of particles, it is possible to use the Particle In Cell method. The computation is done in a boosted reference frame in which the bunches move mainly along s as illustrated in the previous section.
For this purpose, as for space charge simulations, we define a uniform 3D grid with grid sizes Δx, Δy, $\Delta\zeta$. We note that each value of ζ corresponds to a different time of arrival at the Interaction Point (IP):

$$\zeta = s_{\mathrm{IP}} - \beta_0 c t \;\Leftrightarrow\; t = \frac{s_{\mathrm{IP}} - \zeta}{\beta_0 c} \tag{14.7.1}$$

We simulate the interaction in discrete time intervals corresponding to the passage of the different slices. The duration of each interval is

$$\Delta t = \frac{\Delta\zeta}{\beta_0 c} \tag{14.7.2}$$

We call t_i the time at which the i-th slice is passing at the IP. This is related to the ζ_i coordinate of the slice by the relation

$$t_i = \frac{s_{\mathrm{IP}} - \zeta_i}{\beta_0 c} \tag{14.7.3}$$

14.7.1 Propagation of particles during the interaction

From the conventional tracking using s as the independent variable we get for all particles the coordinates at the IP, which we call x_{IP}, $p_{\mathrm{x\,IP}}$, y_{IP}, $p_{\mathrm{y\,IP}}$, $zeta_{\mathrm{IP}} = s_{\mathrm{y\,IP}} - \beta_0 c t_{\mathrm{IP}}$, where t_{IP} is the time of arrival of the particle at the IP. Assuming the motion is in a drift space, for each time step, we propagate the particles from the IP to their positions at the time t_i:

$$x\left(t_i\right) = x_{\mathrm{IP}} + \beta_x c\left(t_i - t_{\mathrm{IP}}\right) = x_{\mathrm{IP}} + \beta_x c\left(\frac{s_{\mathrm{IP}} - \zeta_i}{\beta_0 c} - \frac{s_{\mathrm{IP}} - \zeta_{\mathrm{IP}}}{\beta_0 c}\right) \tag{14.7.4}$$

Using the fact that:

$$p_x = \frac{P_x}{P_0} = \frac{m_0 \gamma \beta_x c}{m_0 \gamma_0 \beta_0 c} = \frac{\gamma \beta_x}{\gamma_0 \beta_0} \tag{14.7.5}$$

we can write:

$$x\left(t_i\right) = x_{\mathrm{IP}} + p_x \frac{\gamma_0}{\gamma}\left(\zeta_{\mathrm{IP}} - \zeta_i\right) \tag{14.7.6}$$

With the coordinates of the propagated particles we can solve a Poisson problem having as source the 3D particle distribution at time t_i. Using the fact that the bunches are elongated and relativistic, we can solve the 2D Poisson equation instead of the full 3D problem. This procedure needs to be performed for the two colliding bunches.

14.7.2 Time relation between the two beams

For a particle of beam 1 having longitudinal coordinate $\zeta_{\mathrm{IP}}^{\mathrm{B1}}$ we want to know the longitudinal coordinate $\zeta_{\mathrm{IP}}^{\mathrm{B2}}$ corresponding to the section of beam 2 crossing the particle at time t_i.
We assume that the reference systems of the two beams are antiparallel and coincident in the transverse plane:

$$s^{\mathrm{B2}} - s_{\mathrm{IP}}^{\mathrm{B2}} = -\left(s^{\mathrm{B1}} - s_{\mathrm{IP}}^{\mathrm{B1}}\right) \tag{14.7.7}$$

$$x^{\mathrm{B2}} = -x^{\mathrm{B1}} \tag{14.7.8}$$

$$y^{\mathrm{B2}} = +x^{\mathrm{B1}} \tag{14.7.9}$$

Similarly to what is done in Sec. 14.7.1, we can write the s position at the time t_i for the particles of beam 1 and beam 2:

$$s^{\mathrm{B1}}(t_i) = s_{\mathrm{IP}}^{\mathrm{B1}} + \frac{\beta_s^{\mathrm{B1}}}{\beta_0^{\mathrm{B1}}}\left(\zeta_{\mathrm{IP}}^{\mathrm{B1}} - \zeta_i^{\mathrm{B1}}\right) \tag{14.7.10}$$

$$s^{\mathrm{B2}}(t_i) = s_{\mathrm{IP}}^{\mathrm{B2}} + \frac{\beta_s^{\mathrm{B2}}}{\beta_0^{\mathrm{B2}}}\left(\zeta_{\mathrm{IP}}^{\mathrm{B2}} - \zeta_i^{\mathrm{B2}}\right) \tag{14.7.11}$$

To find particles that are at the same s at time t_i we replace Eqs. 14.7.10-14.7.11 in Eq. 14.7.7, obtaining:

$$\zeta_{\mathrm{IP}}^{\mathrm{B2}} = \zeta_i^{\mathrm{B2}} - \frac{\beta_s^{\mathrm{B1}}}{\beta_0^{\mathrm{B1}}}\frac{\beta_0^{\mathrm{B2}}}{\beta_s^{\mathrm{B2}}}\left(\zeta_{\mathrm{IP}}^{\mathrm{B1}} - \zeta_i^{\mathrm{B1}}\right) \tag{14.7.12}$$

This relation can be used to probe the field map generated by the other bunch at the position of each particle.

14.7.3 Computation of the kick

The transverse kick at each time step can be written as:

$$\Delta p_x^{\mathrm{B1}} = \frac{\Delta P_x^{\mathrm{B1}}}{P_0^{\mathrm{B1}}} = \frac{F_x \Delta t}{P_0^{\mathrm{B1}}} \tag{14.7.13}$$

Using Eqs. 14.2.9 and 14.7.2, taking into account that the beams move in opposite directions, we obtain:

$$\Delta p_x^{\mathrm{B1}} = -\frac{q\Delta\zeta^{\mathrm{B1}}}{m_0^{\mathrm{B1}}\gamma_0^{\mathrm{B1}}(\beta_0^{\mathrm{B1}})^2 c^2}\left(1 + \beta^{\mathrm{B1}}\beta^{\mathrm{B2}}\right)\frac{\partial\phi^{\mathrm{B2}}}{\partial x}(x, y, \zeta^{\mathrm{B2}}) \tag{14.7.14}$$

14.8 Configuration of beam-beam lenses for tracking simulations (weak-strong)

The effects of the non-linear forces introduced by beam-beam interactions in the Large Hadron Collider (LHC) are studied with tracking simulations using, for example, the

SixTrack and sixtracklib codes [57, 58]. In these simulations the beam-beam interactions are modeled by a set of "thin" non-linear lenses around the collision points. "6D beam-beam lenses" based on Hirata's synchro-beam method [54, 59, 56] are used to model the Head-On (HO) interactions at the four interaction points (IPs) while simpler "4D lenses" are used to model parasitic Long-Range encounters [60].
This section describes a method to configure the beam-beam lenses in tracking simulations based on the model of the accelerator, which has been recently developed as an evolution of existing tools in the MAD-X scripting language [61][2]
In particular, in Sec. 14.8.1, we discuss how to reconstruct the absolute position of the two beams with respect to the lab frame using the twiss and survey tables; in Sec. 14.8.2 we discuss how to compute the separation between the two beams; in Sec. 14.8.3 we describe how to identify the crossing plane and crossing angle; in Sec. 14.8.6 we describe how to configure the anticlockwise beam (conventionally called beam 4) from the MAD-X model based on two clockwise-oriented sequences; in Sec. 14.8.7 we introduce the effect of crab cavities on the beam-beam configuration.

14.8.1 Identification of the beam position and direction

The position and orientation of the beams at a certain machine element can be obtained from MAD-X combining the information from the survey and twiss tables.
We assume that:

- The sequences start from an element at which the reference trajectories of the two beams are known to be parallel;
- Both beams (B1 and B2) have the same orientation (clockwise);
- Markers or beam-beam lenses are installed at the s-locations of the beam-beam interactions.

The survey provides the coordinates in the lab frame of the two beams:

$$\mathbf{P}^{\mathrm{su}} = \begin{pmatrix} x^{\mathrm{su}} \\ y^{\mathrm{su}} \\ s^{\mathrm{su}} \end{pmatrix} \tag{14.8.1}$$

and the corresponding set of angles $(\theta^{\mathrm{su}}, \phi^{\mathrm{su}}, \psi^{\mathrm{su}})$ defining the orientation of the local reference system used by the twiss [1]. The origin and the orientation of the lab frame are defined by the first element in the sequence.
The components of the unit vectors defining the local reference frame with respect to the lab frame can be obtained from the following relationship:

[2]The authors would like to acknowledge all the colleagues who have contributed to the development of the MAD-X tools for the configuration of tracking simulations, on which the present work is largely based, and have provided important input and support, in particular G. Arduini, J. Barranco Garcia, R. De Maria, S. Fartoukh, M. Giovannozzi, S. Kostoglou, E. Métral, Y. Papaphippou, D. Pellegrini, T. Pieloni and F. Van Der Veken.

$$(\hat{\mathbf{e}}_x, \hat{\mathbf{e}}_y, \hat{\mathbf{e}}_s) = \begin{pmatrix} \cos\theta^{\mathrm{su}} & 0 & \sin\theta^{\mathrm{su}} \\ 0 & 1 & 0 \\ -\sin\theta^{\mathrm{su}} & 0 & \cos\theta^{\mathrm{su}} \end{pmatrix} \times \begin{pmatrix} 1 & 0 & 0 \\ 0 & \cos\phi^{\mathrm{su}} & \sin\phi^{\mathrm{su}} \\ 0 & -\sin\phi^{\mathrm{su}} & \cos\phi^{\mathrm{su}} \end{pmatrix} \times \begin{pmatrix} \cos\psi^{\mathrm{su}} & -\sin\psi^{\mathrm{su}} & 0 \\ \sin\psi^{\mathrm{su}} & \cos\psi^{\mathrm{su}} & 0 \\ 0 & 0 & 1 \end{pmatrix} . \tag{14.8.2}$$

The MAD-X twiss provides the transverse position of the beam in the local reference frame $(x^{\mathrm{tw}}, y^{\mathrm{tw}})$, so that the absolute position of the beam in the lab frame can be written as

$$\mathbf{P} = \mathbf{P}^{\mathrm{su}} + x^{\mathrm{tw}}\hat{\mathbf{e}}_x + y^{\mathrm{tw}}\hat{\mathbf{e}}_y \,. \tag{14.8.3}$$

At the beam-beam locations the local reference frames for the two beams are assumed to be aligned. This is not strictly the case in the regions between the separation-recombination magnets (D1 and D2), but also in that case the existing small divergence can be considered negligible. The beam-beam module of pymask checks the conditions:

$$||\hat{\mathbf{e}}_x^{\mathrm{b1}} - \hat{\mathbf{e}}_x^{\mathrm{b2}}|| \ll 1 \,, \tag{14.8.4}$$

$$||\hat{\mathbf{e}}_y^{\mathrm{b1}} - \hat{\mathbf{e}}_y^{\mathrm{b2}}|| \ll 1 \,. \tag{14.8.5}$$

Therefore we will simply define:

$$\hat{\mathbf{e}}_x = \hat{\mathbf{e}}_x^{\mathrm{b1}} = \hat{\mathbf{e}}_x^{\mathrm{b2}} \,, \tag{14.8.6}$$

$$\hat{\mathbf{e}}_y = \hat{\mathbf{e}}_y^{\mathrm{b1}} = \hat{\mathbf{e}}_y^{\mathrm{b2}} \,. \tag{14.8.7}$$

14.8.2 Computation of beam-beam separations

The beam-beam separations are defined as the transverse coordinates of the strong beam with respect to the weak beam. They can be computed as:

$$\Delta x = \hat{\mathbf{e}}_x \cdot \left(\mathbf{P}^S - \mathbf{P}^W\right) \,, \tag{14.8.8}$$

$$\Delta y = \hat{\mathbf{e}}_y \cdot \left(\mathbf{P}^S - \mathbf{P}^W\right) \,, \tag{14.8.9}$$

where the superscripts identify the weak (W) and the strong (S) beam.
Typically the accuracy of the survey table is insufficient to compute the separations correctly, especially for elements that are too far from the first element in the sequence, due to accumulation of errors along the sequence. A correction can be computed looking at the apparent displacement of the closest Interaction Point (IP) between the two surveys, as the IPs are supposed to coincide.

14.8.3 Crossing plane and crossing angle

At the beam-beam encounters the local reference frames for the two beams share the same orientation. Therefore the elevation angle α of the crossing plane and the crossing angle θ can be computed in the local reference frame, as will be illustrated in the following.

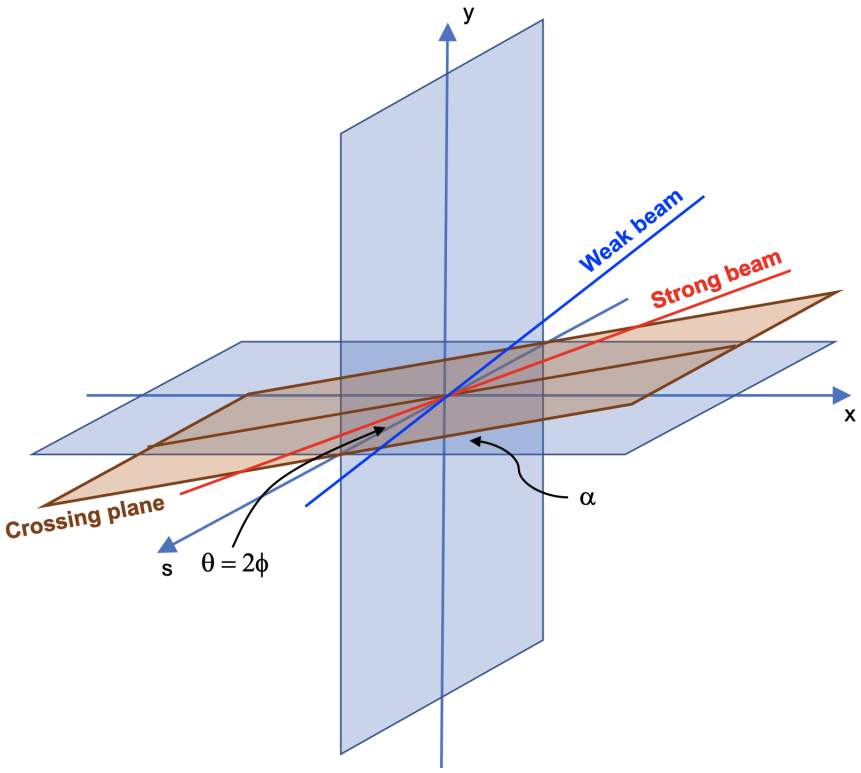


Figure 14.1: Schematic illustration of the crossing plane.

14.8.4 The crossing plane

The directions defined by the local trajectories of the two beams are identified by the unit vectors

$$\hat{\mathbf{p}}^W = \left(p_x^W, p_y^W, p_s^W\right) , \tag{14.8.10}$$

$$\hat{\mathbf{p}}^S = \left(p_x^S, p_y^S, p_s^S\right) , \tag{14.8.11}$$

containing the angles of the closed orbit obtained from the twiss of the two beams. The plane defined by these two directions is called Crossing Plane (XP), as illustrated in Fig. 14.1, and its equation is given by:

$$\mathbf{v}_{\mathrm{XP}}(w_1, w_2) = w_1 \hat{\mathbf{p}}^W + w_2 \hat{\mathbf{p}}^S . \tag{14.8.12}$$

The line defined by the intersection of the crossing plane and the transverse plane identified by the unit vectors $\hat{\mathbf{e}}_x$ and $\hat{\mathbf{e}}_y$ is given by the condition:

$$\mathbf{v}_{\mathrm{XP}}(w_1, w_2) \cdot \hat{\mathbf{e}}_s = 0 . \tag{14.8.13}$$

Replacing Eq. (14.8.12) into Eq. (14.8.13) we obtain:

$$w_1 p_s^W + w_2 p_s^S = 0 , \tag{14.8.14}$$

and replacing this condition in Eq. (14.8.12) we obtain the equation of the intersection line

$$\mathbf{v}_{\mathrm{T}}(w_1) = w_1 \left(\hat{\mathbf{p}}^W - \frac{p_s^W}{p_s^S}\hat{\mathbf{p}}^S\right) . \tag{14.8.15}$$

The elevation angle α of the intersection line with respect to the local x-direction ($\hat{\mathbf{e}}_x$) can be written as:

$$\alpha = \arctan \frac{\mathbf{v}_\mathrm{T} \cdot \hat{\mathbf{e}}_y}{\mathbf{v}_\mathrm{T} \cdot \hat{\mathbf{e}}_x} \,. \tag{14.8.16}$$

Using Eq. (14.8.15) we obtain:

$$\alpha = \arctan \frac{\left(p_y^W - \frac{p_s^W}{p_s^S} p_y^S \right)}{\left(p_x^W - \frac{p_s^W}{p_s^S} p_x^S \right)} . \tag{14.8.17}$$

In the paraxial approximation ($p_s^S \simeq p_s^W \simeq 1$) this simply becomes:

$$\alpha = \arctan \frac{\Delta p_y}{\Delta p_x} , \tag{14.8.18}$$

where we have defined:

$$\Delta p_x = p_x^W - p_x^S \,, \tag{14.8.19}$$

$$\Delta p_y = p_y^W - p_y^S \,. \tag{14.8.20}$$

In the legacy beam-beam macros as well as in the configuration pymask tool, the following logic is implemented

$$\alpha = \begin{cases} \arctan\left(\dfrac{\Delta p_y}{\Delta p_x}\right) & \text{if } |\Delta p_x| \geq |\Delta p_y| \\ \dfrac{\pi}{2} - \arctan\left(\dfrac{\Delta p_x}{\Delta p_y}\right) & \text{if } |\Delta p_x| < |\Delta p_y| \end{cases} , \tag{14.8.21}$$

for which α is limited to the range:

$$-\frac{\pi}{4} \leq \alpha \leq \frac{3}{4}\pi \,. \tag{14.8.22}$$

In particular, for a purely horizontal crossing we have $\alpha = 0$ and for a purely vertical crossing we have $\alpha = \frac{\pi}{2}$.

14.8.5 The crossing angle

The crossing angle θ between the two beams can be found from the relation:

$$\cos\theta = \hat{\mathbf{p}}^W \cdot \hat{\mathbf{p}}^S \,. \tag{14.8.23}$$

The half crossing angle

$$\phi = \frac{\theta}{2} \tag{14.8.24}$$

is often used instead of θ.
In the paraxial approximation

$$p_x \ll 1\,, \tag{14.8.25}$$
$$p_y \ll 1\,, \tag{14.8.26}$$
$$\tag{14.8.27}$$

the scalar product in Eq. (14.8.23) can be rewritten as

$$\begin{aligned}
\hat{\mathbf{p}}^W \cdot \hat{\mathbf{p}}^S &= p_x^W p_x^S + p_y^W p_y^S + p_s^W p_s^S \\
&= p_x^W p_x^S + p_y^W p_y^S + \sqrt{1-\left(p_x^W\right)^2 - \left(p_y^W\right)^2}\sqrt{1-\left(p_x^S\right)^2 - \left(p_y^S\right)^2} \\
&\simeq p_x^W p_x^S + p_y^W p_y^S + \left(1 - \frac{\left(p_x^W\right)^2}{2} - \frac{\left(p_y^W\right)^2}{2}\right)\left(1 - \frac{\left(p_x^S\right)^2}{2} - \frac{\left(p_y^S\right)^2}{2}\right) \\
&\simeq p_x^W p_x^S + p_y^W p_y^S + 1 - \frac{\left(p_x^W\right)^2}{2} - \frac{\left(p_y^W\right)^2}{2} - \frac{\left(p_x^S\right)^2}{2} - \frac{\left(p_y^S\right)^2}{2},
\end{aligned} \tag{14.8.28}$$

which can be written in compact form as:

$$\hat{\mathbf{p}}^W \cdot \hat{\mathbf{p}}^S \simeq 1 - \frac{\left(p_x^W - p_x^S\right)^2 + \left(p_y^W - p_y^S\right)^2}{2}. \tag{14.8.29}$$

For small crossing angle we can write:

$$\cos\theta \simeq 1 - \frac{\theta^2}{2}. \tag{14.8.30}$$

Replacing Eqs. (14.8.29) and (14.8.30) into Eq. (14.8.23) we obtain

$$|\theta| = \sqrt{\Delta p_x^2 + \Delta p_y^2}\,. \tag{14.8.31}$$

The sign of θ is defined positive when the weak beam needs to rotate in the clockwise sense in the crossing plane in order to be brought on the strong beam. This corresponds to the following sign choices:

	$\lvert\Delta p_x\rvert > \lvert\Delta p_y\rvert$	$\lvert\Delta p_x\rvert < \lvert\Delta p_y\rvert$
$\Delta p_x \geq 0,\ \Delta p_y \geq 0$	$\theta > 0$	$\theta > 0$
$\Delta p_x < 0,\ \Delta p_y \geq 0$	$\theta < 0$	$\theta > 0$
$\Delta p_x < 0,\ \Delta p_y < 0$	$\theta < 0$	$\theta < 0$
$\Delta p_x \geq 0,\ \Delta p_y < 0$	$\theta > 0$	$\theta < 0$

which are consistent with the sign convention used in LHC operation.

14.8.6 Transformations for the anticlockwise beam (B4)

The typically used MAD-X model of the LHC consists of two sequences both having clockwise (CW) orientation, conventionally called Beam 1 and Beam 2. To perform tracking simulations of the anticlockwise (ACW) beam, an anticlockwise sequence needs to be generated, which is conventionally called Beam 4. The beam-beam lenses in the Beam 4 sequence can be configured based on the beam-beam lenses defined in Beam 2, taking into account that the two are related by the following change of coordinates:

$$x^{\mathrm{ACW}} = -x^{\mathrm{CW}}, \tag{14.8.32}$$
$$y^{\mathrm{ACW}} = +y^{\mathrm{CW}}, \tag{14.8.33}$$
$$s^{\mathrm{ACW}} = -s^{\mathrm{CW}}. \tag{14.8.34}$$

The corresponding transformation for the transverse momenta is:

$$p_x^{\mathrm{ACW}} = +p_x^{\mathrm{CW}}, \tag{14.8.35}$$
$$p_y^{\mathrm{ACW}} = -p_y^{\mathrm{CW}}. \tag{14.8.36}$$

This can be easily seen from the fact that:

$$p_x \simeq \frac{dx}{ds}, \tag{14.8.37}$$
$$p_y \simeq \frac{dy}{ds}. \tag{14.8.38}$$

Additionally, from Eqs. (14.8.32) - (14.8.36) it is possible to derive the following relations to transform the Σ-matrix [59] of the strong beam:

$$\Sigma_{11}^{\mathrm{ACW}} = +\Sigma_{11}^{\mathrm{CW}}, \tag{14.8.39}$$
$$\Sigma_{12}^{\mathrm{ACW}} = -\Sigma_{12}^{\mathrm{CW}}, \tag{14.8.40}$$
$$\Sigma_{13}^{\mathrm{ACW}} = -\Sigma_{13}^{\mathrm{CW}}, \tag{14.8.41}$$
$$\Sigma_{14}^{\mathrm{ACW}} = +\Sigma_{14}^{\mathrm{CW}}, \tag{14.8.42}$$
$$\Sigma_{22}^{\mathrm{ACW}} = +\Sigma_{22}^{\mathrm{CW}}, \tag{14.8.43}$$
$$\Sigma_{23}^{\mathrm{ACW}} = +\Sigma_{23}^{\mathrm{CW}}, \tag{14.8.44}$$
$$\Sigma_{24}^{\mathrm{ACW}} = -\Sigma_{24}^{\mathrm{CW}}, \tag{14.8.45}$$
$$\Sigma_{33}^{\mathrm{ACW}} = +\Sigma_{33}^{\mathrm{CW}}, \tag{14.8.46}$$
$$\Sigma_{34}^{\mathrm{ACW}} = -\Sigma_{34}^{\mathrm{CW}}, \tag{14.8.47}$$
$$\Sigma_{44}^{\mathrm{ACW}} = +\Sigma_{44}^{\mathrm{CW}}. \tag{14.8.48}$$
$$\tag{14.8.49}$$

14.8.7 Crab crossing

To discuss the effect of crab cavities, we define along the bunches of Beam 1 and Beam 2 (sharing the same s coordinate as in the MAD-X model), the longitudinal coordinates z_1 and z_2, oriented like s.

Assuming that the slices with $z_1 = z_2 = 0$ collide at s=0, the collision point (CP) for two generic slices z_1 and z_2 is at the location:

$$s_{\mathrm{CP}} = \frac{z_1 + z_2}{2}\,. \tag{14.8.50}$$

In the absence of crab crossing, the transverse position of the two beams is independent of z:

$$x_1 = +\phi s\,, \tag{14.8.51}$$
$$x_2 = -\phi s\,. \tag{14.8.52}$$

Ideal crab cavities, in the linear approximation, introduce a z-dependent orbit correction such that:

$$x_1(s) = +\phi s + \phi_c z_1\,, \tag{14.8.53}$$
$$x_2(s) = -\phi s - \phi_c z_2\,, \tag{14.8.54}$$

where ϕ_c is the crabbing angle and we assume, without loss of generality, a horizontal crabbing plane.
The separation of the two slices at their collision point is obtained by replacing (14.8.50) into (14.8.53) and (14.8.54):

$$\Delta x(s_{\mathrm{CP}}) = x_2(s_{\mathrm{CP}}) - x_1(s_{\mathrm{CP}}) = -(\phi + \phi_c)(z_1 + z_2)\,. \tag{14.8.55}$$

If $\phi_c = -\phi$, the separation is zero independently of z_1 and z_2 (perfect crabbing).
The crab crossing in the IPs of the HL-LHC for the clockwise and anticlockwise beams is illustrated with the relevant sign conventions in Figs. 14.2 - 14.5.

14.8.7.1 Configuration of beam-beam lenses for beam 1

In order to model the HO interaction for a crab crossing, the "strong bunch" is sliced longitudinally using the constant charge method, and one beam-beam lens for each slice is installed in the sequence.
In particular, in the sequence of beam 1, the lens corresponding to a slice of the strong beam (beam 2) having longitudinal coordinate $z_2 = Z_2$ is installed at the location where the slice encounters the synchronous particle of the weak beam (see Eq. (14.8.50) with $z_1 = 0$):

$$s_{\mathrm{lens}} = +\frac{Z_2}{2}\,. \tag{14.8.56}$$

The position of the strong beam at the lens can be found by replacing Eq. (14.8.56) into Eq. (14.8.54):

$$X_2 = -s_{\mathrm{lens}}(\phi + 2\phi_c)\,. \tag{14.8.57}$$

The effect of the crab bump alone is given by:

$$X_2^{\mathrm{crab}} = -2\phi_c s_{\mathrm{lens}} = -\phi_c Z_2\,. \tag{14.8.58}$$

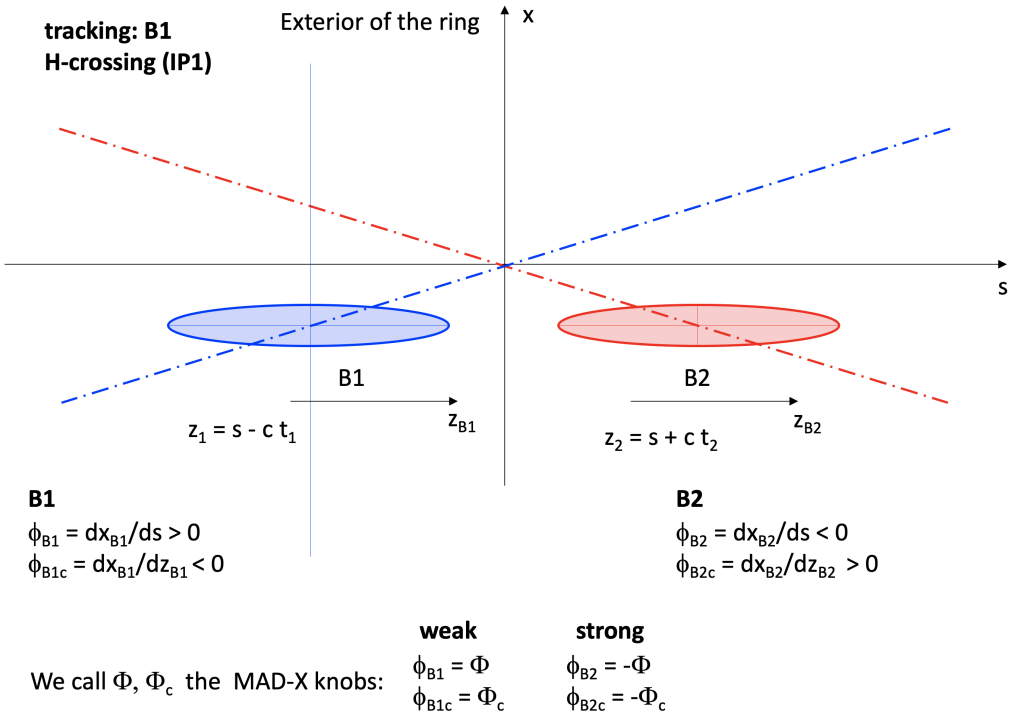


Figure 14.2: Crab crossing in the IP1 of the HL-LHC modeled for the tracking of the clockwise beam (beam 1).

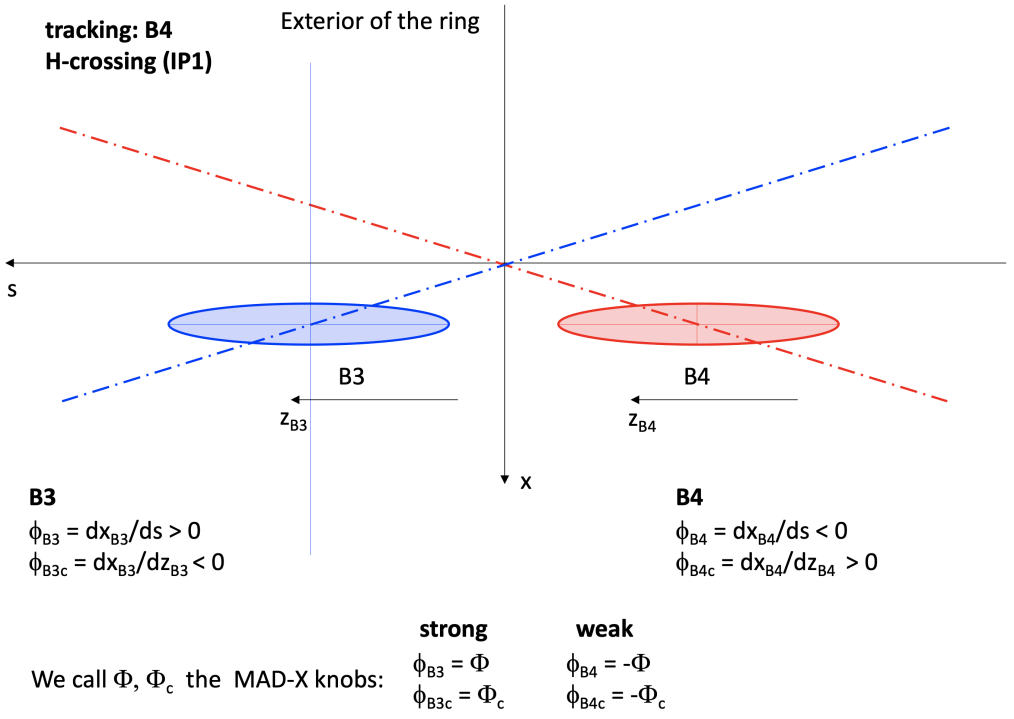


Figure 14.3: Crab crossing in the IP1 of the HL-LHC modeled for the tracking of the anti-clockwise beam (beam 4).

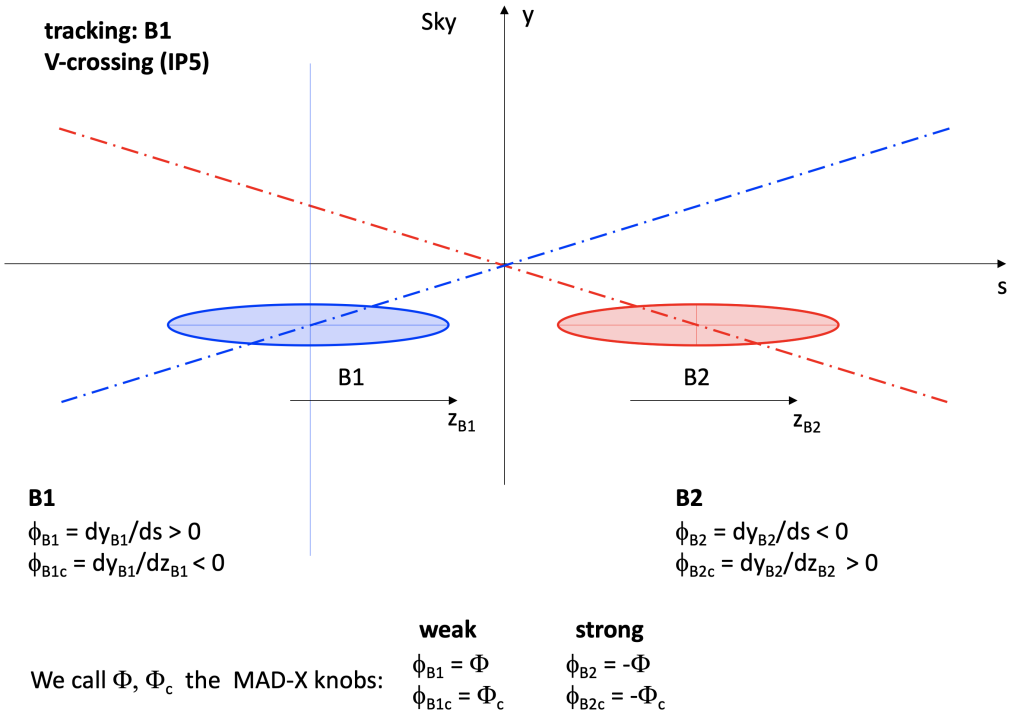


Figure 14.4: Crab crossing in the IP5 of the HL-LHC modeled for the tracking of the clockwise beam (beam 1).

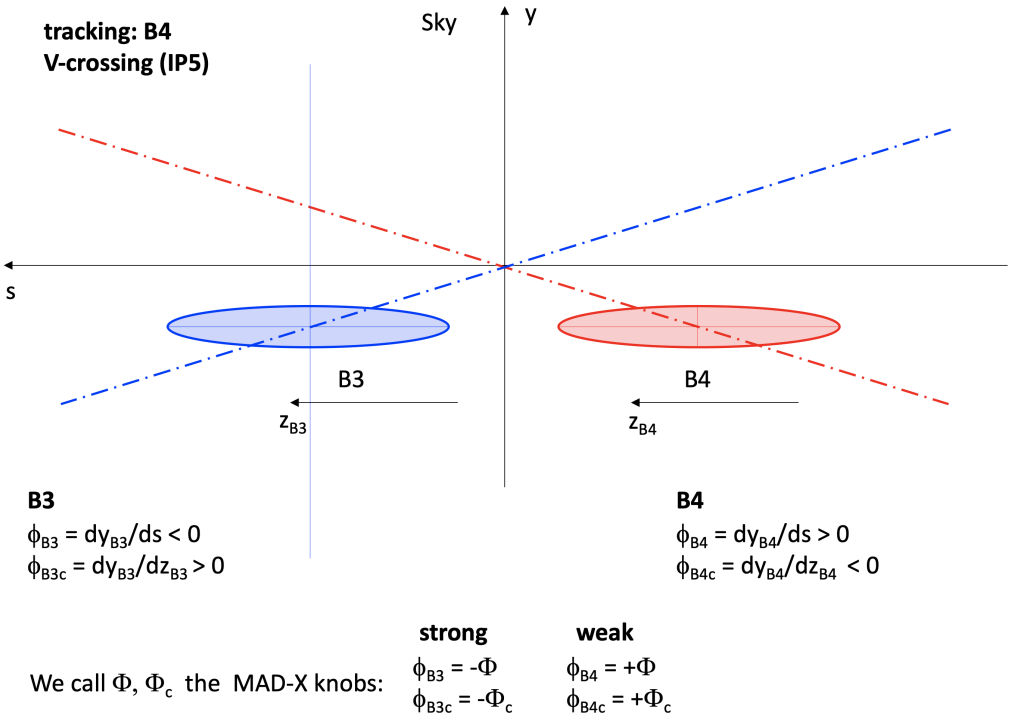


Figure 14.5: Crab crossing in the IP5 of the HL-LHC modeled for the tracking of the anti-clockwise beam (beam 4).

Taking into account the RF curvature coming from the crab cavity frequency, the position of the slice at the beam-beam lens can be written as:

$$X_2^{\text{crab}} = -\phi_c \frac{L_{\text{ring}}}{2\pi h_{\text{CC}}} \sin\left(\frac{2\pi h_{\text{CC}}}{L_{\text{ring}}} Z_2\right) = -\phi_c \frac{L_{\text{ring}}}{2\pi h_{\text{CC}}} \sin\left(\frac{2\pi h_{\text{CC}}}{L_{\text{ring}}} 2s_{\text{lens}}\right), \quad (14.8.59)$$

where h_{CC} is the harmonic number of the crab cavity and L_{ring} is the circumference of the ring.

14.8.8 Configuration of beam-beam lenses for beam 2

In the sequence of beam 2, we install the beam-beam lens for a slice of the strong beam (beam 1) having longitudinal coordinate $z_1 = Z_1$ at the location where the slice encounters the synchronous particle of the weak beam (see Eq. (14.8.50) with $z_2 = 0$):

$$s_{\text{lens}} = \frac{Z_1}{2}. \quad (14.8.60)$$

The position of the strong beam at the lens can be found by replacing Eq. (14.8.60) into Eq. (14.8.53):

$$X_1 = s_{\text{lens}}(\phi + 2\phi_c). \quad (14.8.61)$$

The effect of the crab bump alone is given by:

$$X_1^{\text{crab}} = 2\phi_c s_{\text{lens}} = \phi_c Z_1. \quad (14.8.62)$$

Taking into account the RF curvature coming from the crab cavity frequency, the position of the slice at the beam-beam lens can be written as:

$$X_1^{\text{crab}} = \phi_c \frac{L_{\text{ring}}}{2\pi h_{\text{CC}}} \sin\left(\frac{2\pi h_{\text{CC}}}{L_{\text{ring}}} Z_1\right) = \phi_c \frac{L_{\text{ring}}}{2\pi h_{\text{CC}}} \sin\left(\frac{2\pi h_{\text{CC}}}{L_{\text{ring}}} 2s_{\text{lens}}\right). \quad (14.8.63)$$

From Eqs. (14.8.59) and (14.8.63), we find that for lenses at the same longitudinal position s_{lens} the corresponding slices of the two beams $Z_1 = Z_2 = 2s_{\text{lens}}$ have opposite transverse coordinates:

$$X_1^{\text{crab}} = -X_2^{\text{crab}}. \quad (14.8.64)$$

14.8.8.1 Crab bump from twiss table

For a non-ideal crabbing, for example in the presence of a non-closure of the crab-bump, the realistic z-dependent orbit distortion introduced by the crab cavities can be characterized using the twiss, by installing orbit correctors at the position of the crab cavities that introduce the crab cavity deflection as seen at a certain reference position along the bunch z_{ref}. To obtain the effect on particles at different positions along the bunch it is possible to apply the following scaling:

$$x(z) = x(z_{\text{ref}}) \frac{\sin\left(\frac{2\pi h_{\text{CC}}}{L_{\text{ring}}} z\right)}{\sin\left(\frac{2\pi h_{\text{CC}}}{L_{\text{ring}}} z_{\text{ref}}\right)}. \quad (14.8.65)$$

14.8.9 Step-by-step configuration procedure

Based on the method introduced in the previous sections, the following procedure has been implemented in pymask to configure the beam-beam lenses in the SixTrack and sixtracklib tracking model:

1. Inactive beam-beam lenses (not configured) are installed in both clockwise sequences (Beam 1 and Beam 2) at the locations of the HO and LR beam-beam encounters. As discussed in Sec. 14.8.7, at each IP a set of lenses is installed to model the HO, one corresponding to each bunch slice.

2. The MAD-X twiss and survey tables are computed for both clockwise sequences.

3. The transverse beam shapes (Σ-matrix) are extracted from the twiss table for all beam-beam lenses.

4. The positions of the beams at the beam-beam lenses in the lab frame are computed combining the information from the survey and twiss tables, as discussed in Sec. 14.8.1.

5. The beam-beam separations are computed, as discussed in Sec. 14.8.2.

6. For all HO interactions, the crossing plane and the crossing angle are identified, as discussed in Sec. 14.8.3.

7. The relevant quantities for the beam-beam lenses in the anticlockwise sequences (Beam 3 and Beam 4) are obtained from the data computed for the lenses in the clockwise sequences (Beam 1 and Beam 2), using the transformations described in Sec. 14.8.6.

8. The effect of the crab cavities is introduced by using the shape of the crab bumps obtained from twiss tables computed with orbit correctors at the locations of the cavities, as discussed in Sec. 14.8.7.

9. The information computed before is used to configure the beam-beam lenses in the MAD-X model of the sequence for which the tracking simulation will be performed, typically either Beam 1 or Beam 4.

10. The SixTrack input and the pysixtrack/sixtracklib input files are generated using the MAD-X model and the additional information computed as described above.

11. The closed orbit as computed from the MAD-X sequences is saved on file, for the generation of matched beam distributions and for the computation of the beam-beam dipolar kicks on the closed orbit, which are usually subtracted in weak-strong tracking simulations.

Chapter 15

Bhabha scattering and beamstrahlung

15.1 Bhabha scattering

In quantum electrodynamics (QED), the Coulomb attraction of two opposite charges (e.g. an electron and a positron) is called Bhabha scattering [62]. The mathematical treatment of Bhabha scattering can be done using the method of equivalent photons (Weizsäcker-Williams approach) [63, 64]. The essence of this method lies in the fact that the electromagnetic field of a relativistic charged particle, say the positron, is almost transversal and can therefore accurately be substituted by an appropriately chosen equivalent radiation field of photons. Thus, the cross section for the scattering of an electron with this positron (Bhabha scattering) can be approximated by that of the electron and an "equivalent" photon (Compton scattering). In this case, the equivalent photon corresponds to the exchanged virtual photon between the scattering primaries. The whole process, including the subsequent emission of bremsstrahlung photons, can be treated in a numerical simulation as an inverse Compton scattering process [65]. In this, the virtual photons emitted by the positron will collide with the electron. Due to the relativistic dynamics of the participating leptons, the virtual photons have an energy which is often negligible compared to that of the leptons, thus we can treat them as real. The process is called inverse since here the electron will lose energy while the photons will gain energy, contrary to standard Compton scattering. The scattered photons are real and typically end up with an energy E'_γ comparable to the initial lepton energy E_e [66].

The generation of photons from radiative Bhabha scattering in Xsuite can be divided into 3 steps. First, the charge density of the opposite bunch slice at the location of the macroparticle in the soft-Gaussian approximation is computed [67]. From this one computes the integrated luminosity of the collision of the macroparticle with the virtual photons represented by the slice, integrated over the time of passing through the slice. Second, a set of virtual photons is generated corresponding to the total energy of the opposite slice. Third, the code iterates over these virtual photons and simulates the bremsstrahlung process as a series of inverse Compton scattering events between the macroparticle and each virtual photon.

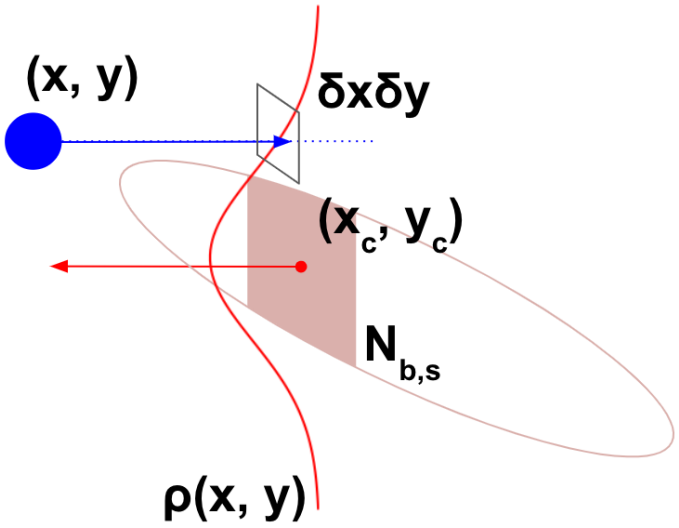


Figure 15.1: Schematic illustration of a single macroparticle from bunch 1 (blue) colliding with a single longitudinal slice of the opposing bunch 2 (red).

15.1.1 Luminosity Computation

Figure 15.1 illustrates how `Xfields` computes the integrated luminosity in a collision of a single macroparticle from one beam with a single slice of the opposing beam[1]. In the figure x, y denote the transverse coordinates of a macroparticle in the boosted and uncoupled frame, at the collision point with a slice of the opposing bunch, corresponding to the notation $\hat{\hat{x}}^*, \hat{\hat{y}}^*$ in the previous sections. The centroid (mean) coordinate of the opposing slice, with a bunch intensity of $N_{b,s}$, is denoted by x_c, y_c, in the boosted, uncoupled, transported reference frame of its own bunch. `Xfields` models the charge density of a longitudinal slice as a 2D Gaussian distribution $\rho(x, y)$. Considering an infinitesimal area $\delta x \delta y$ around the transverse position x, y of a given macroparticle at the collision point with the slice, one can write the number of charges with which this macroparticle will interact:

$$N_e(x, y) = N_{b,s} \rho(x, y) \delta x \delta y, \tag{15.1.1}$$

and the integrated luminosity of the macroparticle-slice collision:

$$L = \frac{N_{b,m} \cdot N_e(x, y)}{\delta x \delta y} = N_{b,m} N_{b,s} \rho(x, y), \tag{15.1.2}$$

where $N_{b,m}$ denotes the number of elementary charges per macroparticle.

[1]Note that this luminosity can be recorded in a table with the **flag_luminosity** flag of the `BeamBeamGaussian3D` element and **lumitable** keyword in the `Xline` internal log. The recorded entries must be summed up to get the total integrated luminosity of the collision. This method has an uncertainty of $\pm 10\%$ compared to the analytical formula.

15.1.2 Virtual Photon Generation

Equation (15.1.2) describes the integrated luminosity of primary-primary collisions. In order to simulate the collision of the primaries with virtual photons instead, `Xfields` uses the assumption that the virtual photon distribution $N_\gamma(x, y)$ is proportional to that of the primary charges:

$$N_\gamma(x, y) = nN_e(x, y), \tag{15.1.3}$$

where n is a proportionality factor denoting the number of virtual photons corresponding to one elementary charge. The number density spectrum of virtual photons is given by:

$$\frac{dn}{dxdQ^2} = \frac{\alpha}{2\pi}\frac{1+(1-x)^2}{x}\frac{1}{Q^2}, \tag{15.1.4}$$

where $x = \dfrac{\hbar\omega}{E_e} = \dfrac{E_\gamma}{E_e}$ is the total energy of the virtual photon normalized to the primary energy and Q^2 is the squared virtuality of the virtual photon [68].
The virtual photon energies and virtualities can be drawn using the method of inverse CDF (Cumulative Distribution Function) sampling. The sampling algorithm in `Xsuite` has been adapted from `GUINEA-PIG` [69], a Particle In Cell (PIC) based single beam-beam collision simulation software. For each macroparticle in the beam, we first compute the total number of equivalent photons using the energy of the opposite bunch slice. Subsequently, the energy and virtuality of each photon will be sampled. In the current implementation all virtual photons inherit the dynamical variables of the strong bunch slice centroid. Note that the virtual photons sampled this way will also be "macroparticles" in the sense that they represent the dynamics of all virtual photons generated by all charges in a primary macroparticle.

15.1.3 Inverse Compton Scattering of Virtual Photons

We account for the proportionality of the primary charge and virtual photon distributions described by Eq. (15.1.3) by resampling the virtual photons for each macroparticle. With each photon, we simulate the bremsstrahlung process in the form of a set of inverse Compton scattering events. The number of Compton events can be described as:

$$R = \sigma_{C,tot}(s)L = \sigma_{C,tot}(s)N_{b,m}N_{b,s}\rho(x, y), \tag{15.1.5}$$

where $s \approx \dfrac{4E_\gamma E_e}{m_e^2c^4}$ is the center of mass energy squared of the photon-primary Compton interaction, normalized to the rest mass of the primary [70], and $\sigma_{C,tot}(s)$ denotes the total Compton scattering cross section, given by:

$$\sigma_{C,tot}(s) = \frac{2\pi r_e^2}{s}\left[\ln(s+1)\left(1-\frac{4}{s}-\frac{8}{s^2}\right).+\frac{1}{2}+\frac{8}{s}-\frac{1}{2(s+1)^2}\right], \tag{15.1.6}$$

with r_e being the classical electron radius. For each event, we sample the scattered photon energy from the differential cross section:

$$\frac{d\sigma_C}{dy} = \frac{2\pi r_e^2}{s}\left[\frac{1}{1-y} + 1 - y - \frac{4y}{s(1-y)} + \frac{4y^2}{s^2(1-y)^2}\right], \tag{15.1.7}$$

which describes the scattering of a beam of unpolarized photons on the primary charge [65]. Here $y = \frac{\hbar\omega'}{E_e} = \frac{E'_\gamma}{E_e}$ is the energy of the scattered photon in units of the total energy of the colliding primary. Given the energy E'_γ, we can compute the scattering angle of the primary and the photon as well as their momenta, using the constraints given by energy and momentum conservation. While the emitted photon spectrum corresponds to the sum of all charges represented by a macroparticle, a given macroparticle should represent the dynamics of a single primary charge. Thus, the dynamical variables of the macroparticles are updated according to energy and momentum conservation accounting for the emission of only a fraction of the photons. The latter are picked randomly based on a probability corresponding to the inverse of the number of charges per macroparticle.

15.2 Beamstrahlung

The implementation of beamstrahlung in `Xfields` is based on `GUINEA-PIG` [69]. In this section a high level summary of the modeling is presented. Further details can be found in [71].
`Xfields` samples the quantum theoretical synchrotron radiation spectrum $G(v, \xi)$:

$$G(v,\xi) = \frac{v^2}{(1-(1-\xi)v^3)^2}\left(G_1(y) + \frac{\xi^2 y^2}{1+\xi y}G_2(y)\right), \tag{15.2.1}$$

which is normalized such that $G(v=0,\xi) = 1$ and $G(v,\xi) \leq 1$ for all v and ξ. The variable ξ is defined as:

$$\xi = \frac{E_{crit}}{E} \tag{15.2.2}$$

and denotes the magnitude of the quantum correction, i.e. the critical energy normalized to the energy E of the primary particle in GeV undergoing the beamstrahlung process. The critical beamstrahlung energy is defined in the classical way as:

$$E_{crit} = \frac{3\hbar c\gamma^3}{2\rho} \tag{15.2.3}$$

The unitless variable y is related to the energy of the emitted beamstrahlung photon E_γ:

$$y = \frac{E_\gamma}{E_{crit}}\frac{1}{1-\frac{E_\gamma}{E}}. \tag{15.2.4}$$

Equation 15.2.4 can be expressed with the help of a uniform random variable v as follows:

$$y = \frac{v^3}{1 - v^3};\ v \in U[0,1]. \tag{15.2.5}$$

With these the number of beamstrahlung photons emitted in the interval $[v,\ v + \Delta v]$ during a time interval δ_t can be given as:

$$\Delta N_\gamma = p_0 G(v, \xi) \Delta v, \tag{15.2.6}$$

where

$$p_0 = \frac{2^{\frac{2}{3}}}{\Gamma(\frac{4}{3})} \frac{\alpha \gamma \delta_t}{\rho} \approx 25.4 \cdot \frac{E \delta_t}{\rho} \tag{15.2.7}$$

is a scaling factor dependent on the relativistic γ of the primary, the instantaneous bending radius ρ and the fine structure constant α. The bending radius of each macroparticle in the electromagnetic field of a given longitudinal slice of the opposite bunch is obtained from the radial kick:

$$F_r^* = r_{pp} \sqrt{F_x^{*2} + F_y^{*2}}, \tag{15.2.8}$$

$$\rho = \frac{1}{F_r^*}, \tag{15.2.9}$$

with $r_{pp} = \frac{1}{1+\delta} = \frac{p}{p_0}$. In the `Xfields` `BeamBeamGaussian3D` element the time interval δ_t is expressed as a longitudinal distance Δz, which is the distance the macroparticle travels between two consecutive longitudinal slices and it corresponds to the bin width of the longitudinal slicing.
Figure 15.2 shows the beamstrahlung photon number density $p_0 G(v, \xi)$ for a fixed value of p_0 and ξ. The area in the region C is the mean number of beamstrahlung photons emitted during an interval δ_t, i.e. a passage through one longitudinal slice of width Δz.
The functions $G_1(y)$ and $G_2(y)$ are defined as follows:

$$\begin{aligned} G_1(y) &= \frac{\sqrt{3}\Gamma(\frac{1}{3})}{2^{\frac{5}{3}}\pi} \int_y^\infty K_{\frac{5}{3}}(x) dx, \\ G_2(y) &= \frac{\sqrt{3}\Gamma(\frac{1}{3})}{2^{\frac{5}{3}}\pi} K_{\frac{2}{3}}(y). \end{aligned} \tag{15.2.10}$$

Equations 15.2.10 are evaluated numerically with the below approximate formulas:

$$\begin{aligned} &0 \le y \le 1.54 \\ &\quad G_1(y) = y^{-\frac{2}{3}}(1 - 0.8432885317 \cdot y^{\frac{2}{3}} + 0.1835132767 \cdot y^2 \\ &\qquad - 0.0527949659 \cdot y^{\frac{10}{3}} + 0.0156489316 \cdot y^4) \\ &\quad G_2(y) = y^{-\frac{2}{3}}(0.4999456517 - 0.5853467515 \cdot y^{\frac{4}{3}} \\ &\qquad + 0.3657833336 \cdot y^2 - 0.0695055284 \cdot y^{\frac{10}{3}} + 0.0191803860 \cdot y^4) \end{aligned} \tag{15.2.11}$$

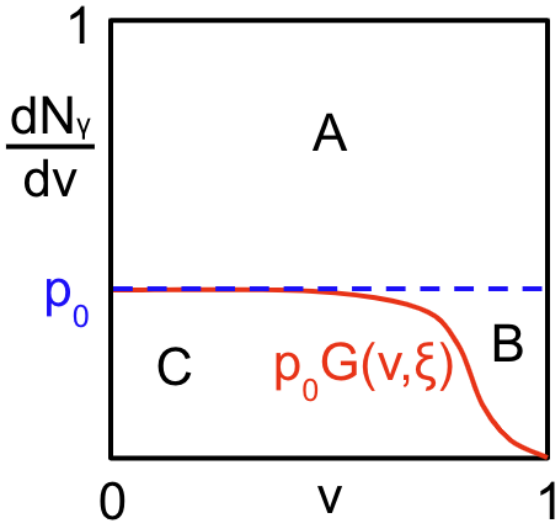


Figure 15.2: Schematic illustration of the number density function of beamstrahlung photons $p_0 G(v, \xi)$ (red curve) for a given p_0 (blue dashed line) and ξ, as a function of v.

$$1.54 < y \leq 4.48$$

$$G_1(y) = \frac{2.066603927 - 0.5718025331 \cdot y + 0.04243170587 \cdot y^2}{-0.9691386396 + 5.651947051 \cdot y - 0.6903991322 \cdot y^2 + y^3}$$
$$G_2(y) = \frac{1.8852203645 - 0.5176616313 \cdot y + 0.03812218492 \cdot y^2}{-0.4915880600 + 6.1800441958 \cdot y - 0.6524469236 \cdot y^2 + y^3} \tag{15.2.12}$$

$$4.48 < y \leq 165.0$$

$$G_1(y) = \frac{e^{-y}}{\sqrt{y}} \cdot \frac{1.0174394594 + 0.5831679349 \cdot y}{0.9949036186 + y} \tag{15.2.13}$$
$$G_2(y) = \frac{e^{-y}}{\sqrt{y}} \cdot \frac{0.2847316689 + 0.5830684600 \cdot y}{0.3915531539 + y}.$$

For $y > 165$ the model assumes no radiation. With these one can simulate beamstrahlung emission by first drawing a random uniform number p. The condition $p > p_0$ corresponds to region A in Fig. 15.2, therefore no photons are emitted. In the other case a second random uniform number v is drawn, and Eq. 15.2.1 is computed. If $p < p_0 G(v, \xi)$ is satisfied (region C) a photon is emitted with an energy

$$\frac{E_\gamma}{E} = \frac{\xi v^3}{1 - (1 - \xi) v^3}, \tag{15.2.14}$$

otherwise no photon is emitted (region B). The generated beamstrahlung photons are themselves macroparticles in the sense that they represent the dynamics of all photons generated by all charges in a primary macroparticle.

Chapter 16

Wakefields and impedances

16.1 Transverse wakefields

Transverse wakefields are defined such that the corresponding transverse kicks can be written as:

$$\Delta p_x = \frac{q^2 e^2}{m_0 \gamma \beta_0^2 c^2} \sum_{i,j,k,l \geq 0} x^k y^l \int_{-\infty}^{\infty} \bar{x}^i(z') \bar{y}^j(z') \lambda(z') W_x^{i,j,k,l}(z - z')\, dz' \tag{16.1.1}$$

$$\Delta p_y = \frac{q^2 e^2}{m_0 \gamma \beta_0^2 c^2} \sum_{i,j,k,l \geq 0} x^k y^l \int_{-\infty}^{\infty} \bar{x}^i(z') \bar{y}^j(z') \lambda(z') W_y^{i,j,k,l}(z - z')\, dz' \tag{16.1.2}$$

where $\bar{x}(z)$ and $\bar{y}(z)$ are the transverse centroid positions along the beam.
The convolution can be obtained numerically using the method of Section 19.2.
The lower order terms of the summation are often referred to as:

- $W_x^{0,0,0,0}$ constant x
- $W_y^{0,0,0,0}$ constant y
- $W_x^{1,0,0,0}$ dipolar x, or driving x
- $W_y^{0,1,0,0}$ dipolar y, or driving y
- $W_x^{0,1,0,0}$ dipolar xy, or driving xy
- $W_y^{1,0,0,0}$ dipolar yx, or driving yx
- $W_x^{0,0,1,0}$ quadrupolar x, or detuning x
- $W_y^{0,0,0,1}$ quadrupolar y, or detuning y
- $W_x^{0,0,0,1}$ quadrupolar xy, or detuning xy
- $W_y^{0,0,1,0}$ quadrupolar yx, or detuning yx

The z variable can be written as a function of time in the lab frame as:

$$z = -\beta_0 ct, \tag{16.1.3}$$

We call $\widehat{W}_{x,y}$ the wakefield defined as a function of time t:

$$\widehat{W}_{x,y}(t) = W_{x,y}\left(-\beta_0 ct\right) \tag{16.1.4}$$

$$W_{x,y}(z) = \widehat{W}_{x,y}\left(-\frac{z}{\beta_0 c}\right) \tag{16.1.5}$$

For ultrarelativistic beams we have:

$$\widehat{W}_{x,y}(t) = 0 \qquad \text{for } t < 0 \tag{16.1.6}$$

$$W_{x,y}(z) = 0 \qquad \text{for } z > 0 \tag{16.1.7}$$

The coefficient $1/\gamma\beta_0^2$ in Eqs. 16.1.1 and 16.1.2 comes from the fact that, if we have a force F_x acting on a length Δs, we can derive the corresponding kick as follows:

$$\Delta P_x = F_x \Delta t, \tag{16.1.8}$$

and substituting the P_x with the normalized one $p_x = \frac{P_x}{P_0}$ we find

$$\Delta p_x = \frac{F_x}{P_0}\Delta t = \frac{F_x}{P_0}\frac{\Delta s}{\beta_0 c}, \tag{16.1.9}$$

hence substituting $P_0 = m_0\gamma\beta_0 c$ we find

$$\Delta p_x = \frac{F_x}{m_0\gamma\beta_0^2 c^2}\Delta s. \tag{16.1.10}$$

16.2 Transverse impedances

The transverse beam coupling impedances $Z_{x,y}(\omega)$ are related to the wakefields through a Fourier transform (see [72, Eq. 1.216]):

$$\widehat{W}_{x,y}(t) = -\frac{j}{2\pi}\int_{-\infty}^{+\infty} d\omega\, e^{j\omega t} Z_{x,y}(\omega)\,, \tag{16.2.1}$$

$$Z_{x,y}(\omega) = j\int_{-\infty}^{+\infty} dt\, e^{-j\omega t}\widehat{W}_{x,y}(t)\,. \tag{16.2.2}$$

The equivalence between the two equations can be seen multiplying both sides of Eq. 16.2.1 by $e^{-j\omega' t}$ and integrating over t

$$\int_{-\infty}^{\infty} dt\, e^{-j\omega' t}\widehat{W}_{x,y}(t) = -\frac{j}{2\pi}\int_{-\infty}^{\infty} dt \int_{-\infty}^{+\infty} d\omega Z_{x,y}(\omega) e^{j(\omega-\omega')t} \tag{16.2.3}$$

$$= -\frac{j}{2\pi}\int_{-\infty}^{+\infty} d\omega\, Z_{x,y}(\omega)\int_{-\infty}^{\infty} dt\, e^{j(\omega-\omega')t}. \tag{16.2.4}$$

We now apply the following property of the Dirac δ function

$$\delta(\omega - \omega') = \frac{j}{2\pi} \int_{-\infty}^{\infty} dt\, e^{j(\omega-\omega')t}, \tag{16.2.5}$$

and we find

$$\int_{-\infty}^{\infty} dt\, e^{-j\omega' t} \widehat{W}_{x,y}(t) = -j \int_{-\infty}^{+\infty} d\omega\, Z_{x,y}(\omega)\delta(\omega - \omega') = -jZ_{x,y}(\omega'). \tag{16.2.6}$$

We can write the impedances also in terms of the wakefield expressed as a function of $z = -\beta_0 ct$ (using Eqs. 16.1.4 and 16.1.5):

$$W_{x,y}(z) = -\frac{j}{2\pi} \int_{-\infty}^{+\infty} d\omega\, e^{-j\omega \frac{z}{\beta_0 c}} Z_{x,y}(\omega)\,, \tag{16.2.7}$$

$$Z_{x,y}(\omega) = \frac{j}{\beta_0 c} \int_{-\infty}^{+\infty} dz e^{j\omega \frac{z}{\beta_0 c}} W_{x,y}(z)\,. \tag{16.2.8}$$

As the transverse wakes are real functions, the impedances satisfy the following symmetry properties:

$$\mathrm{Re}\left\{Z_{x,y}(-\omega)\right\} = -\,\mathrm{Re}\left\{Z_{x,y}(\omega)\right\} \tag{16.2.9}$$

$$\mathrm{Im}\left\{Z_{x,y}(-\omega)\right\} = \mathrm{Im}\left\{Z_{x,y}(\omega)\right\} \tag{16.2.10}$$

16.3 Longitudinal wakefield

Longitudinal wakefields are defined such that the corresponding kicks can be written as:

$$\Delta\delta = -\frac{q^2 e^2}{m_0 \gamma \beta_0^2 c^2} \int_{-\infty}^{+\infty} dz' \lambda(z') W_s(z - z')\,. \tag{16.3.1}$$

The minus sign is introduced such that a positive wake causes the particles to lose energy. The convolution can be obtained numerically using the method of Section 19.2.
Also in this case, we call $\widehat{W}_s$ the wakefield defined as a function of time t:

$$\widehat{W}_s(t) = W_s\left(\beta_0 ct\right) \tag{16.3.2}$$

$$W_s(z) = \widehat{W}_s\left(-\frac{z}{\beta_0 c}\right) \tag{16.3.3}$$

16.4 Longitudinal impedance

The longitudinal beam coupling impedances $Z_s(\omega)$ are related to the wakefields through a Fourier transform (see [72, Eq. 1.216]):

$$\widehat{W}_s(t) = \frac{1}{2\pi} \int_{-\infty}^{+\infty} d\omega\, e^{j\omega t} Z_s(\omega)\,, \tag{16.4.1}$$

$$Z_s(\omega) = \int_{-\infty}^{+\infty} dt\, e^{-j\omega t} \widehat{W}_s(t)\,. \tag{16.4.2}$$

We can write the impedances also in terms of the wakefield expressed as a function of $z = -\beta_0 ct$ (using Eqs. 16.3.2 and 16.3.3):

$$W_s(z) = \frac{1}{2\pi} \int_{-\infty}^{+\infty} d\omega\, e^{-j\omega \frac{z}{\beta_0 c}} Z_s(\omega)\,, \tag{16.4.3}$$

$$Z_s(\omega) = \frac{1}{\beta_0 c} \int_{-\infty}^{+\infty} dz e^{j\omega \frac{z}{\beta_0 c}} W_s(z)\,. \tag{16.4.4}$$

As the longitudinal wake is a real function, the corresponding impedance satisfies the following symmetry properties:

$$\mathrm{Re}\,\{Z_s(-\omega)\} = \mathrm{Re}\,\{Z_s(\omega)\} \tag{16.4.5}$$

$$\mathrm{Im}\,\{Z_s(-\omega)\} = -\,\mathrm{Im}\,\{Z_s(\omega)\} \tag{16.4.6}$$

16.5 Integrated wakefields

We consider the horizontal dipolar wake term. The corresponding contribution to the horizontal kick is:

$$\Delta p_x^{\mathrm{dip}}(z) = \frac{q^2 e^2}{m_0 \gamma \beta_0^2 c^2} \int_{-\infty}^{+\infty} \lambda(z') \bar{x}(z') W_x^{1,0,0,0}(z - z')\, dz'. \tag{16.5.1}$$

In the following we keep the normalization factor outside the discretization and define:

$$K_x^{\mathrm{dip}}(z) = \int_{-\infty}^{+\infty} \lambda(z') \bar{x}(z') W_x^{1,0,0,0}(z - z')\, dz'. \tag{16.5.2}$$

We sample the bunch on a uniform grid:

$$z_n = n\Delta z. \tag{16.5.3}$$

Splitting the integral into bins centered on z_j, the convolution evaluated at the grid point z_i can be written as:

$$K_{x,i}^{\mathrm{dip}} = \sum_j \int_{z_j - \frac{\Delta z}{2}}^{z_j + \frac{\Delta z}{2}} \lambda(z') \bar{x}(z') W_x^{1,0,0,0}(z_i - z')\, dz', \tag{16.5.4}$$

where $K_{x,i}^{\mathrm{dip}} = K_x^{\mathrm{dip}}(z_i)$.

Conventional discretization

If both the source term $\lambda(z)\bar{x}(z)$ and the wakefield $W_x^{1,0,0,0}(z)$ are sufficiently smooth over a bin of size Δz, they can both be replaced by their values at the bin centers:

$$\lambda(z')\bar{x}(z') \simeq \lambda_j \bar{x}_j, \qquad W_x^{1,0,0,0}(z_i - z') \simeq W_x^{1,0,0,0}(z_i - z_j). \tag{16.5.5}$$

Equation (16.5.4) then becomes:

$$K_{x,i}^{\text{dip}} \simeq \Delta z \sum_j \lambda_j \bar{x}_j W_x^{1,0,0,0}(z_i - z_j) = \Delta z \sum_j \lambda_j \bar{x}_j W_{x,i-j}^{1,0,0,0,\text{sample}}, \tag{16.5.6}$$

where:

$$W_{x,k}^{1,0,0,0,\text{sample}} = W_x^{1,0,0,0}(z_k). \tag{16.5.7}$$

With this approach the bin size has to be small enough to resolve both the variation of the source term $\lambda(z)\bar{x}(z)$ and the variation of the wakefield $W_x^{1,0,0,0}(z)$. For short-range wakes this approximation may require a very small bin size, even when the bunch density and the horizontal centroid are slowly varying.

Integrated wakefield

When the wakefield varies much faster than the bunch density and centroid, one can keep only the source term constant within each bin:

$$\lambda(z')\bar{x}(z') \simeq \lambda_j \bar{x}_j, \tag{16.5.8}$$

while retaining the variation of the wakefield inside the bin. Equation (16.5.4) becomes:

$$K_{x,i}^{\text{dip}} \simeq \sum_j \lambda_j \bar{x}_j \int_{z_j - \frac{\Delta z}{2}}^{z_j + \frac{\Delta z}{2}} W_x^{1,0,0,0}(z_i - z')\, dz'. \tag{16.5.9}$$

We now work on the integral that remains. With the change of variable:

$$u = z_i - z', \tag{16.5.10}$$

we have $dz' = -du$. The lower and upper limits in z' become:

$$z' = z_j - \frac{\Delta z}{2} \quad \Rightarrow \quad u = \left(i - j + \frac{1}{2}\right)\Delta z, \tag{16.5.11}$$

$$z' = z_j + \frac{\Delta z}{2} \quad \Rightarrow \quad u = \left(i - j - \frac{1}{2}\right)\Delta z. \tag{16.5.12}$$

The minus sign from $dz' = -du$ reverses these limits, giving:

$$\int_{z_j - \frac{\Delta z}{2}}^{z_j + \frac{\Delta z}{2}} W_x^{1,0,0,0}(z_i - z')\, dz' = \int_{\left(i-j-\frac{1}{2}\right)\Delta z}^{\left(i-j+\frac{1}{2}\right)\Delta z} W_x^{1,0,0,0}(u)\, du. \tag{16.5.13}$$

We define the integrated horizontal dipolar wakefield as:

$$W_{x,k}^{1,0,0,0,\text{int}} = \frac{1}{\Delta z} \int_{\left(k-\frac{1}{2}\right)\Delta z}^{\left(k+\frac{1}{2}\right)\Delta z} W_x^{1,0,0,0}(u)\, du, \tag{16.5.14}$$

or, equivalently:

$$\int_{\left(k-\frac{1}{2}\right)\Delta z}^{\left(k+\frac{1}{2}\right)\Delta z} W_x^{1,0,0,0}(u)\, du = \Delta z\, W_{x,k}^{1,0,0,0,\text{int}}. \tag{16.5.15}$$

Therefore the sampled kick is again a discrete convolution:

$$K_{x,i}^{\mathrm{dip}} \simeq \Delta z \sum_j \lambda_j \bar{x}_j W_{x,i-j}^{1,0,0,0,\mathrm{int}}. \tag{16.5.16}$$

With the integrated wakefield approach the bin size Δz needs only to resolve the variation of the source term $\lambda(z)\bar{x}(z)$. The possibly much faster variation of the wakefield is accounted for by the bin integral in Eq. (16.5.14).
The same derivation can be used for the other wake components by replacing the source term and wakefield with the ones corresponding to the term being discretized.

16.6 Analytical wakes

Resonator

Ultra-relativistic resonator with shunt impedance R, quality factor $Q > 1$ and resonant frequency f_r

- Longitudinal:

$$W_s(t) = \frac{\omega_r R}{Q} e^{-\alpha t} \left(\cos(\widehat{\omega}_r t) - \frac{\alpha}{\widehat{\omega}_r} \sin(\widehat{\omega}_r t) \right) , \tag{16.6.1}$$

$$Z_s(\omega) = \frac{R}{1 - jQ\left(\frac{\omega_r}{\omega} - \frac{\omega}{\omega_r}\right)} . \tag{16.6.2}$$

- Transverse:

$$W_{x,y}(t) = \frac{\omega_r^2 R}{Q\widehat{\omega}_r} e^{-\alpha t} \sin(\widehat{\omega}_r t) , \tag{16.6.3}$$

$$Z_{x,y}(\omega) = \frac{\omega_r}{\omega} \frac{R}{1 - jQ\left(\frac{\omega_r}{\omega} - \frac{\omega}{\omega_r}\right)} . \tag{16.6.4}$$

where $\omega_r = 2\pi f_r$, $\widehat{\omega}_r = \omega_r \sqrt{1 - \frac{1}{4Q^2}}$, $\alpha = \frac{\omega_r}{2Q}$. Ref: [72, Section 2.2]

Cylindrical thick wall

Cylindrical resistive wall wake, based on the "classic thick wall formula" (see e.g. [73, Chapter 2]) with resistivity ρ, permeability μ, radius r and length L:

- Longitudinal:

$$W_s(t) = -L \frac{1}{4\pi r} \sqrt{\frac{Z_0 \rho}{\pi c}} t^{-\frac{3}{2}} , \tag{16.6.5}$$

$$Z_s(\omega) = L\,(1 + j\,\mathrm{sign}(\omega))\,\frac{\rho}{2\pi r}\frac{1}{\delta_s(\omega)} , \tag{16.6.6}$$

where $\delta_s(\omega) = \sqrt{\frac{2\rho}{|\omega|}}$ is the frequency-dependent skin depth.
Note: the longitudinal resistive wall wake is negative for any value of t, while, with the adopted sign convention, longitudinal wakes should be positive for $t \to 0+$. This happens because the thick wall approximation is not valid for small t. Computing the wake numerically with IW2D shows that the resistive wall wake is actually positive close to zero and performs a few oscillations after which it agrees very well with the formula above. For applications where short range effects are relevant this model should not be used.

- Transverse:

$$W_{x,y}(t) = L\frac{1}{\pi r^3}\sqrt{\frac{cZ_0\rho}{\pi}}t^{-\frac{1}{2}}\,, \tag{16.6.7}$$

$$Z_{x,y}(\omega) = L(1 + j\,\mathrm{sign}(\omega))\frac{\rho}{\pi r^3}\frac{1}{\omega\sqrt{\varepsilon_0\mu_0}}\frac{1}{\delta_s(\omega)}\,. \tag{16.6.8}$$

Chapter 17

Intra-Beam Scattering

Intra-beam scattering (IBS) is the process of small angle, multiple Coulomb scattering of charged particles within the beam. It leads to a redistribution of the particle momenta in six-dimensional phase space.

17.1 Analytical Growth Rates

Theoretical models commonly characterize the effect of intra-beam scattering through growth rates, or growth times. The former is expressed in $\left[s^{-1}\right]$ and the latter in $[s]$. These govern the evolution of the rms beam sizes or rms emittances of the beam, depending on the convention used.

Growth rates (and growth times) can be expressed in either amplitude or emittance convention. The former governs the evolution of rms beam sizes while the latter governs that of rms emittances. The two conventions are equivalent by a factor 2 and conversion can be done as:

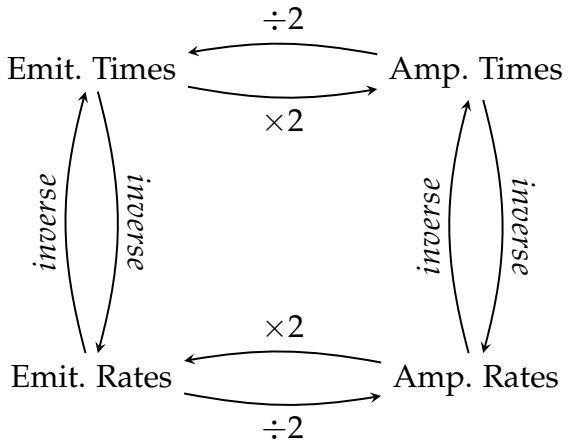


Figure 17.1: Illustration of the conversions between IBS growth rates and times, across emittance and amplitude conventions.

The growth rates themselves are expressed from the lattice optics as well as the beam properties.

In Xsuite, for consistency with synchrotron radiation damping times (see section 9.1), **the amplitude growth rates are computed**. The horizontal (K_x), vertical (K_y) and longitudinal (K_z) amplitude growth rates are defined as:

$$\begin{aligned} K_x &= \frac{1}{\tau_x} = \frac{1}{\varepsilon_x^{1/2}} \frac{d\varepsilon_x^{1/2}}{dt}, \\ K_y &= \frac{1}{\tau_y} = \frac{1}{\varepsilon_y^{1/2}} \frac{d\varepsilon_y^{1/2}}{dt}, \\ K_z &= \frac{1}{\tau_z} = \frac{1}{\varepsilon_z^{1/2}} \frac{d\varepsilon_z^{1/2}}{dt}, \end{aligned} \tag{17.1.1}$$

where (τ_x), (τ_y) and (τ_z) are the amplitude growth times.

Currently two different formalisms are available to compute these growth rates. Both assume transverse and longitudinal Gaussian bunch profiles. Both rely on the computation of the Coulomb logarithm L_C, which in *Xfields* is computed according to the expression in the Physics Vade Mecum [74]:

$$L_C = \ln\left(\frac{r_{max}}{r_{min}}\right) . \tag{17.1.2}$$

In Eq (17.1.2) r_{max} is taken as the smaller of σ_x and the Debye length, while r_{min} is taken as the larger of the classical distance of closest approach and the quantum diffraction limit from the nuclear radius.

17.1.1 Nagaitsev Formalism

One available formalism follows the approach introduced by S. Nagaitsev in [75]. It provides a fast computation method through symmetric elliptic integrals of the second kind, $R_D(x, y, z)$, defined as:

$$R_D(x, y, z) = \frac{3}{2} \int_0^\infty \frac{dt}{\sqrt{(t+x)(t+y)(t+z)^3}} . \tag{17.1.3}$$

Interestingly, this elliptic integral has the following special properties:

$$R_D(x, x, x) = x^{-3/2}, \tag{17.1.4}$$

$$R_D(x, y, z) + R_D(y, z, x) + R_D(z, x, y) = \frac{3}{\sqrt{xyz}} . \tag{17.1.5}$$

Thanks to Eq (17.1.5) only two evaluations of this integral are needed to obtain various simple terms from which one can compute the growth rates. Importantly, the computation time of this integral in Nagaitsev's approach does not scale with the size of the lattice.

First the a_x, a_y, a_s, a_1 and a_2 terms are computed:

$$\begin{aligned} a_x &= \frac{\beta_x}{\varepsilon_x}, a_y = \frac{\beta_y}{\varepsilon_y}, a_s = a_x \left(\frac{D_x^2}{\beta_x^2} + \Phi_x^2 \right) + \frac{1}{\sigma_p^2}, \\ a_1 &= \frac{1}{2}(a_x + \gamma^2 a_s), a_2 = \frac{1}{2}(a_x - \gamma^2 a_s) \, , \end{aligned} \tag{17.1.6}$$

where the $\Phi_{x,y}$ term is defined as:

$$\Phi_{x,y} = D'_{x,y} - \frac{\beta'_{x,y} D_{x,y}}{2\beta_{x,y}} \, . \tag{17.1.7}$$

Then the λ_1, λ_2 and λ_3 terms are computed:

$$\lambda_1 = a_y \, , \lambda_2 = a_1 + \sqrt{a_2^2 + \gamma^2 a_x^2 \Phi_x^2} \, , \lambda_3 = a_1 - \sqrt{a_2^2 + \gamma^2 a_x^2 \Phi_x^2} \, . \tag{17.1.8}$$

and used to compute three integrals R_1, R_2 and R_3 (though with Eq (17.1.5) only two need to be computed):

$$\begin{aligned} R1 &= \frac{1}{\lambda_1} R_D(\frac{1}{\lambda_2}, \frac{1}{\lambda_3}, \frac{1}{\lambda_1}) \, , \\ R2 &= \frac{1}{\lambda_2} R_D(\frac{1}{\lambda_3}, \frac{1}{\lambda_1}, \frac{1}{\lambda_2}) \, , \\ R3 &= \frac{1}{\lambda_3} R_D(\frac{1}{\lambda_1}, \frac{1}{\lambda_2}, \frac{1}{\lambda_3}) \, . \end{aligned} \tag{17.1.9}$$

Using all the above the S_p, S_x and S_{xp} terms are computed according to Eq (17.1.10):

$$\begin{aligned} S_p &= \frac{\gamma^2}{2} \left[2R_1 - R_2 \left(1 - \frac{3a_2}{\sqrt{a_2^2 + \gamma^2 a_x^2 \Phi_x^2}} \right) - R_3 \left(1 + \frac{3a_2}{\sqrt{a_2^2 + \gamma^2 a_x^2 \Phi_x^2}} \right) \right] \, , \\ S_x &= \frac{1}{2} \left[2R_1 - R_2 \left(1 + \frac{3a_2}{\sqrt{a_2^2 + \gamma^2 a_x^2 \Phi_x^2}} \right) - R_3 \left(1 - \frac{3a_2}{\sqrt{a_2^2 + \gamma^2 a_x^2 \Phi_x^2}} \right) \right] \, , \\ S_{xp} &= \frac{3\gamma^2 \Phi_x^2 a_x}{\sqrt{a_2^2 + \gamma^2 a_x^2 \Phi_x^2}} \left(R_3 - R_2 \right) \, . \end{aligned} \tag{17.1.10}$$

From these, one computes the integrals - called the *Nagaitsev integrals* in the *Xfields* code base - I_x, I_y and I_z:

$$\begin{aligned} I_x &= \int_0^C \frac{\beta_x ds}{L\sigma_x\sigma_y} \left[S_x + \left(\frac{D_x^2}{\beta_x^2} + \Phi_x^2 \right) S_p + S_{xp} \right] \, , \\ I_y &= \int_0^C \frac{\beta_y ds}{L\sigma_x\sigma_y} \left(R_2 + R_3 - 2R_1 \right) \, , \\ I_z &= \int_0^C \frac{ds}{L\sigma_x\sigma_y} S_p \, . \end{aligned} \tag{17.1.11}$$

with C the circumference (or length) of the machine. Finally, the *emittance growth rates* in the horizontal, vertical and longitudinal planes are computed as:

$$\boxed{\frac{1}{\varepsilon_x}\frac{d\varepsilon_x}{dt} = \frac{1}{\varepsilon_x}\frac{Nr_0^2 cL_C}{12\pi\beta^3\gamma^5\sigma_z}I_x} \tag{17.1.12}$$

$$\boxed{\frac{1}{\varepsilon_y}\frac{d\varepsilon_y}{dt} = \frac{1}{\varepsilon_y}\frac{Nr_0^2 cL_C}{12\pi\beta^3\gamma^5\sigma_z}I_y} \tag{17.1.13}$$

$$\boxed{\frac{1}{\varepsilon_z}\frac{d\varepsilon_z}{dt} = \frac{1}{\sigma_p^2}\frac{Nr_0^2 cL_C}{12\pi\beta^3\gamma^5\sigma_z}I_z} \tag{17.1.14}$$

In the above N is the total beam intensity, r_0 the classical particle radius, c the speed of light in vacuum, L_C the Coulomb logarithm from Eq (17.1.2), β and γ the relativistic parameters of the beam and σ_z the bunch length.

Please note: Nagaitsev's computations yield emittance growth rates. In Xsuite these are computed as exposed above, and converted to amplitude growth rates before being returned to the user, as shown in Fig. 17.1.

Importantly, this formalism does not take into account vertical dispersion, and in the presence of D_y will yield an erroneous vertical growth rate. For machines with vertical dispersion, the Bjorken-Mtingwa formalism presented below is recommended.

17.1.2 Bjorken-Mtingwa Formalism

The IBS growth rates can also be computed according to the theory by Bjorken and Mtingwa [76]. The specific implementation follows that of the MAD-X code, for which modifications to the terms of B&M's theory have been made by Antoniou and Zimmermann to account for vertical dispersion and non-ultrarelativistic beams [77].

In this formalism, growth rates are computed at every element in the lattice and averaged over the machine. For a given plane u (horizontal, vertical or longitudinal), the *emittance growth rate* is computed as:

$$T_u = \frac{Nr_0^2 cm^3 L_C \pi^2}{\gamma\Gamma}\left\langle \int_0^\infty \frac{d\lambda\lambda^{1/2}}{[\det(L+\lambda I)]^{1/2}}\left\{\mathrm{Tr}\,L^{(u)}\,\mathrm{Tr}\left(\frac{1}{L+\lambda I}\right) - 3\,\mathrm{Tr}\,L^{(u)}\left(\frac{1}{L+\lambda I}\right)\right\}\right\rangle \tag{17.1.15}$$

in which N is the total beam intensity, r_0 the classical particle radius, c the speed of light in vacuum, m the mass of the considered particle, L_C the Coulomb logarithm from Eq (17.1.2), γ the relativistic parameter of the beam, and Γ the six-dimensional phase space volume of the beam, defined as:

$$\Gamma = (2\pi)^3\,(\beta\gamma)^3\,m^3\varepsilon_x\varepsilon_y\sigma_\delta\sigma_z \tag{17.1.16}$$

with σ_δ the relative momentum spread and σ_z the bunch length. One should note the expression for Γ is corrected by a factor $\sqrt{2}$ for coasting beams.
In Eq (17.1.15) λ is simply the integration variable, I is the 3x3 identity matrix, and L is a 3x3 matrix; the matrix L is defined as:

$$L = L^{(x)} + L^{(y)} + L^{(z)} \,, \tag{17.1.17}$$

where the plane-dependent matrices $L^{(x)}, L^{(y)}$ and $L^{(z)}$ are defined as:

$$L^{(x)} = \frac{\beta_x}{\epsilon_x} \begin{pmatrix} 1 & -\gamma\phi_x & 0 \\ -\gamma\phi_x & \gamma^2 H_x/\beta_x & 0 \\ 0 & 0 & 0 \end{pmatrix} \,, \tag{17.1.18}$$

$$L^{(y)} = \frac{\beta_y}{\epsilon_y} \begin{pmatrix} 0 & 0 & 0 \\ 0 & \gamma^2 H_y/\beta_y & -\gamma\phi_y \\ 0 & -\gamma\phi_y & 1 \end{pmatrix} \,, \tag{17.1.19}$$

$$L^{(z)} = \frac{\gamma^2}{\sigma_\delta^2} \begin{pmatrix} 0 & 0 & 0 \\ 0 & 1 & 0 \\ 0 & 0 & 0 \end{pmatrix} \,. \tag{17.1.20}$$

The $\Phi_{x,y}$ and $H_{x,y}$ terms are defined as:

$$\phi_{x,y} = D'_{x,y} - \frac{\beta'_{x,y} D_{x,y}}{2\beta_{x,y}} \,, \tag{17.1.21}$$

and

$$H_{x,y} = \frac{D_{x,y}^2 + \beta_{x,y}^2 \phi_{x,y}^2}{\beta_{x,y}} \,. \tag{17.1.22}$$

In [77] a new expression was derived for each growth rate, which is the implemented approach. In *Xfields*, the computation of the growth rates takes the following steps. First the $a, b, c, a_x, b_x, a_y, b_y, a_z$ and b_z terms are computed as defined below:

$$a = \gamma^2 \left(\frac{H_x}{\varepsilon_x} + \frac{H_y}{\varepsilon_y} \right) + \frac{\gamma^2}{\sigma_\delta^2} + \left(\frac{\beta_x}{\varepsilon_x} + \frac{\beta_y}{\varepsilon_y} \right) \,, \tag{17.1.23}$$

$$b = \left(\frac{\beta_x}{\varepsilon_x} + \frac{\beta_y}{\varepsilon_y} \right) \left(\frac{\gamma^2 D_x^2}{\varepsilon_x \beta_x} + \frac{\gamma^2 D_y^2}{\varepsilon_y \beta_y} + \frac{\gamma^2}{\sigma_\delta^2} \right) + \frac{\beta_x \beta_y}{\varepsilon_x \varepsilon_y} \gamma^2 \left(\Phi_x^2 + \Phi_y^2 \right) + \frac{\beta_x \beta_y}{\varepsilon_x \varepsilon_y} \,, \tag{17.1.24}$$

$$c = \frac{\beta_x \beta_y}{\varepsilon_x \varepsilon_y} \left(\frac{\gamma^2 D_x^2}{\varepsilon_x \beta_x} + \frac{\gamma^2 D_y^2}{\varepsilon_y \beta_y} + \frac{\gamma^2}{\sigma_\delta^2} \right) \,, \tag{17.1.25}$$

$$\begin{aligned} a_x =& 2\gamma^2 \left(\frac{H_x}{\varepsilon_x} + \frac{H_y}{\varepsilon_y} + \frac{1}{\sigma_\delta^2} \right) - \frac{\beta_x H_y}{H_x \varepsilon_y} + \frac{\beta_x}{H_x \gamma^2} \left(\frac{2\beta_x}{\varepsilon_y} - \frac{\beta_y}{\varepsilon_y} - \frac{\gamma^2}{\sigma_\delta^2} \right) \\ & - 2\frac{\beta_x}{\varepsilon_x}\frac{\beta_y}{\varepsilon_y} + \frac{\beta_x}{\gamma^2 H_x} \left(\frac{6\beta_x}{\varepsilon_x} \gamma^2 \Phi_x^2 \right) , \end{aligned} \tag{17.1.26}$$

$$\begin{aligned} b_x =& \left(\frac{\beta_x}{\varepsilon_x} + \frac{\beta_y}{\varepsilon_y} \right) \left(\frac{\gamma^2 H_x}{\varepsilon_x} + \frac{\gamma^2 H_y}{\varepsilon_y} + \frac{\gamma^2}{\sigma_\delta^2} \right) - \gamma^2 \left(\frac{\beta_x^2}{\varepsilon_x^2} \Phi_x^2 + \frac{\beta_y^2}{\varepsilon_y^2} \Phi_y^2 \right) + \left(\frac{\beta_x}{\varepsilon_x} - \frac{4\beta_y}{\varepsilon_y} \right) \frac{\beta_x}{\varepsilon_x} \\ & + \frac{\beta_x}{\gamma^2 H_x} \left(\frac{\gamma^2}{\sigma_\delta^2} \left(\frac{\beta_x}{\varepsilon_x} - \frac{2\beta_y}{\varepsilon_y} \right) + \frac{\beta_x \beta_y}{\varepsilon_x \varepsilon_y} + \frac{6\beta_x \beta_y}{\varepsilon_x \varepsilon_y} \gamma^2 \Phi_x^2 + \gamma^2 \left(\frac{2\beta_y^2 \Phi_y^2}{\varepsilon_y^2} - \frac{\beta_x^2 \Phi_x^2}{\varepsilon_x^2} \right) \right) \\ & + \frac{\beta_x H_y}{\varepsilon_y H_x} \left(\frac{\beta_x}{\varepsilon_x} - \frac{2\beta_y}{\varepsilon_y} \right) \end{aligned} \tag{17.1.27}$$

$$\begin{aligned} a_y =& -\gamma^2 \left(\frac{H_x}{\varepsilon_x} + \frac{2H_y}{\varepsilon_y} + \frac{\beta_x}{\beta_y}\frac{H_y}{\varepsilon_x} + \frac{1}{\sigma_\delta^2} \right) + 2\gamma^4 \frac{H_y}{\beta_y} \left(\frac{H_y}{\varepsilon_y} + \frac{H_x}{\varepsilon_x} \right) \\ & + \frac{2\gamma^4 H_y}{\beta_y \sigma_\delta^2} - \left(\frac{\beta_x}{\varepsilon_x} - \frac{2\beta_y}{\varepsilon_y} \right) + \left(\frac{6\beta_y}{\varepsilon_y} \gamma^2 \Phi_y^2 \right) \end{aligned} \tag{17.1.28}$$

$$\begin{aligned} b_y =& \gamma^2 \left(\frac{\beta_y}{\varepsilon_y} - \frac{2\beta_x}{\varepsilon_x} \right) \left(\frac{H_x}{\varepsilon_x} + \frac{1}{\sigma_\delta^2} \right) + \left(\frac{\beta_y}{\varepsilon_y} - \frac{4\beta_x}{\varepsilon_x} \right) \frac{\gamma^2 H_y}{\varepsilon_y} + \frac{\beta_x \beta_y}{\varepsilon_x \varepsilon_y} \\ & + \gamma^2 \left(\frac{2\beta_x^2 \Phi_x^2}{\varepsilon_x^2} - \frac{\beta_y^2 \Phi_y^2}{\varepsilon_y^2} \right) + \frac{\gamma^4 H_y}{\beta_y} \left(\frac{\beta_x}{\varepsilon_x} + \frac{\beta_y}{\varepsilon_y} \right) \left(\frac{H_y}{\varepsilon_y} + \frac{1}{\sigma_\delta^2} \right) \\ & + \left(\frac{\beta_x}{\varepsilon_x} + \frac{\beta_y}{\varepsilon_y} \right) \gamma^4 \frac{H_x H_y}{\beta_y \varepsilon_x} - \gamma^4 \frac{H_y}{\beta_y} \left(\frac{\beta_x^2}{\varepsilon_x^2} \Phi_x^2 + \frac{\beta_y^2}{\varepsilon_y^2} \Phi_y^2 \right) + \frac{6\beta_x \beta_y}{\varepsilon_x \varepsilon_y} \gamma^2 \Phi_y^2 \end{aligned} \tag{17.1.29}$$

$$a_z = 2\gamma^2 \left(\frac{H_x}{\varepsilon_x} + \frac{H_y}{\varepsilon_y} + \frac{1}{\sigma_\delta^2} \right) - \frac{\beta_x}{\varepsilon_x} - \frac{\beta_y}{\varepsilon_y} \tag{17.1.30}$$

$$b_z = \left(\frac{\beta_x}{\varepsilon_x} + \frac{\beta_y}{\varepsilon_y} \right) \gamma^2 \left(\frac{H_x}{\varepsilon_x} + \frac{H_y}{\varepsilon_y} + \frac{1}{\sigma_\delta^2} \right) - 2\frac{\beta_x \beta_y}{\varepsilon_x \varepsilon_y} - \gamma^2 \left(\frac{\beta_x^2 \Phi_x^2}{\varepsilon_x^2} + \frac{\beta_y^2 \Phi_y^2}{\varepsilon_y^2} \right) \tag{17.1.31}$$

Finally, the *emittance growth rates* in the horizontal, vertical and longitudinal planes are computed as:

$$\boxed{\frac{1}{\varepsilon_x}\frac{d\varepsilon_x}{dt} = \frac{N r_0^2 c m^3 L_C \pi^2}{\gamma \Gamma} \left\langle \left[\frac{\gamma^2 H_x}{\varepsilon_x} \right] \int_0^\infty \frac{\lambda^{1/2} \left[a_x \lambda + b_x \right]}{(\lambda^3 + a\lambda^2 + b\lambda + c)} d\lambda \right\rangle} \tag{17.1.32}$$

$$\boxed{\frac{1}{\varepsilon_y}\frac{d\varepsilon_y}{dt} = \frac{N r_0^2 c m^3 L_C \pi^2}{\gamma \Gamma} \left\langle \left[\frac{\beta_y}{\varepsilon_y} \right] \int_0^\infty \frac{\lambda^{1/2} \left[a_y \lambda + b_y \right]}{(\lambda^3 + a\lambda^2 + b\lambda + c)} d\lambda \right\rangle} \tag{17.1.33}$$

$$\boxed{\frac{1}{\varepsilon_z}\frac{d\varepsilon_z}{dt} = \frac{Nr_0^2 cm^3 L_C \pi^2}{\gamma\Gamma}\left\langle\left[\frac{\gamma^2}{\sigma_\delta^2}\right]\int_0^\infty \frac{\lambda^{1/2}\left[a_z\lambda + b_z\right]}{\left(\lambda^3 + a\lambda^2 + b\lambda + c\right)}d\lambda\right\rangle} \tag{17.1.34}$$

where the constants in the common fraction term are the same as for Eq (17.1.15), λ is an integration variable and the angled brackets signify the averaging over the lattice, given the terms contained inside are arrays with one value per element.

Please note: Bjorken and Mtingwa's computations yield emittance growth rates. In Xsuite these are computed as exposed above, and converted to amplitude growth rates before being returned to the user, as shown in Fig. 17.1.

17.2 Steady-state emittances

The steady-state emittances in the presence of Synchrotron Radiation (SR), Quantum Excitation (QE), and Intra-Beam Scattering (IBS) emerge from a dynamic equilibrium, where these three phenomena balance each other out. More specifically, the QE and SR are accounted for through the natural emittances and SR damping constants, the IBS is described by its growth rates. Each of these effects depends on the optical functions along the storage ring. All the following equations remain valid independently of which formalism (Nagaitsev or Bjorken-Mtingwa) is used when computing the IBS growth rates. In addition, the SR damping constants and IBS growth rates follow the amplitude convention as defined in Eq. (9.1.6).

17.2.1 Steady-state emittances with QE, SR, and IBS

The steady-state emittances are solutions to a system of three ordinary differential equations describing the dynamic interplay of the QE, SR, and IBS. The system of differential equations can be solved numerically by computing the emittance evolution for a succession of infinitesimal time steps. The equations are as follows:

$$\frac{d\varepsilon_u}{dt} = -2\alpha_u^{SR}\left(\varepsilon_u - \varepsilon_{u,0}\right) + 2\alpha_u^{IBS}\varepsilon_u, \quad u = x, y, z \tag{17.2.1}$$

$\varepsilon_{u,0}$ is the natural emittance, ε_u the emittance, α_u^{SR} the SR damping constant and α_u^{IBS} the IBS growth rate. It can be noted that the IBS growth rates are a function of all three emittances ($\alpha_u^{IBS}(\varepsilon_x, \varepsilon_y, \varepsilon_z)$).
The steady-state emittance is reached when the emittance evolution reaches zero and leads to:

$$\varepsilon_u = \frac{\varepsilon_{u,0}}{1 - \alpha_u^{IBS}/\alpha_u^{SR}}, \quad u = x, y, z \tag{17.2.2}$$

Although mathematically correct, the equation assumes a finite vertical emittance. In the case of lepton storage rings, the vertical emittance is often negligible in the absence of vertical dispersion or betatron coupling. As a result, the IBS growth rates would reach extremely large values when a near zero vertical emittance is considered. A finite vertical emittance is introduced through betatron coupling or an external excitation to overcome this limitation.

17.2.2 Steady-state emittances due to betatron coupling

In the presence of betatron coupling, emittance sharing occurs between the two transverse planes. The treatment of betatron coupling can be simplified by expressing it through the emittance coupling factor $\kappa = \tilde{\varepsilon}_y/\tilde{\varepsilon}_x$, the ratio of the perturbed vertical emittance to the horizontal one.
Based on the natural emittance, defined in Eq. (9.2.24) but written in a form [78] so that the horizontal damping partition number j_x appears:

$$\varepsilon_0 = C_q \frac{\gamma^2}{j_x} \frac{I_5}{I_2},$$

where $C_q = \frac{55}{32\sqrt{3}} \frac{\hbar}{m_e c} \approx 3.84 \times 10^{-13}$ m for electrons, γ the relativistic gamma and I_2, I_5 respectively the second and fifth radiation integrals.

$$\tilde{\varepsilon_0} = C_q \frac{\gamma^2}{\tilde{j_x}} \frac{\langle K^3 \mathcal{H} \rangle}{K^2}, \qquad \text{where} \quad \tilde{j_x} = \frac{j_x}{1+\kappa} + \frac{\kappa j_y}{1+\kappa} \tag{17.2.3}$$

Here, j_y represents the vertical damping partition number. After some simplifications and remembering $\tilde{\varepsilon}_0 = \tilde{\varepsilon}_x + \tilde{\varepsilon}_y$ we finally obtain:

$$\tilde{\varepsilon}_{x,0} = \frac{\tilde{\varepsilon}_0}{1+\kappa} = \frac{\tilde{\varepsilon}_0}{1+\kappa\frac{j_y}{j_x}}, \qquad \tilde{\varepsilon}_{y,0} = \frac{\kappa\tilde{\varepsilon}_0}{1+\kappa} = \frac{\kappa\tilde{\varepsilon}_0}{1+\kappa\frac{j_y}{j_x}} \tag{17.2.4}$$

Furthermore, the perturbed horizontal and vertical emittances can be expressed as a function of the ones without betatron coupling:

$$\tilde{\varepsilon}_x = \frac{\varepsilon}{1+\kappa\frac{j_y}{j_x}}, \quad \tilde{\varepsilon}_y = \frac{\kappa\varepsilon}{1+\kappa\frac{j_y}{j_x}}$$

It can be noted that total transverse emittance conservation occurs solely if $j_x = j_y$.
As a result, the transverse emittance evolution can be rewritten as:

$$\frac{d\tilde{\varepsilon}_u}{dt} = -2\alpha_u^{SR}\left(\tilde{\varepsilon}_u - \tilde{\varepsilon}_{u,0}\right) + 2\alpha_u^{IBS}\tilde{\varepsilon}_u, \quad u = x, y \tag{17.2.5}$$

And the steady-state transverse emittances become:

$$\tilde{\varepsilon}_u = \frac{\tilde{\varepsilon}_{u,0}}{1 - \frac{\alpha_u^{IBS}}{\alpha_u^{SR}\left(1+\kappa j_y/j_x\right)}}, \quad u = x, y \tag{17.2.6}$$

17.2.3 Steady-state emittances due to an external excitation

Alternatively, a finite vertical emittance can also be obtained by exciting the beam using the Pulse-Picking by Resonant Excitation (PPRE) method [79] in the vertical plane. In this situation, the horizontal and vertical planes are left uncoupled while the vertical emittance can be controlled. Nonetheless, the emittance coupling factor can still be employed. In this scenario, the emittance evolution follows Eq. (17.2.5) and the final emittance Eq. (17.2.2). Compared to the previous case, the total transverse emittance is not conserved even if $j_x = j_y$.

17.3 IBS Kicks

The approach of using analytical growth rates does not provide a way to study the interplay of IBS with arbitrary effects, such as space charge, electron clouds, beam-beam, etc. To do so, it is necessary to include IBS effects in tracking simulations together with other desired effects. In *Xfields* two elements are available to model IBS effects in tracking simulations, both providing momentum kicks to tracked particles according to a specific formalism.

17.3.1 Analytical Kicks

A first element is available to provide momentum kicks based on analytical growth rates, according to the approach introduced by R. Bruce [80]. In *Xfields* the computation of the kick is done as follows.

First, the beam intensity N, bunch length σ_z, momentum deviation σ_δ, and geometric emittances $\varepsilon_{x,y}$ are inferred from the tracked particles object. These are used to compute the analytical IBS growth rates. From these, each particle is given a momentum kick in each dimension according to:

$$\boxed{\Delta p_u = R\sigma_{p_u}\sqrt{2T_{IBS,u}T_{rev}\sigma_z\sqrt{\pi}\rho(z)}\ ;\ u = x, y, z} \tag{17.3.1}$$

Here R is a random number from the standard normal distribution; σ_{p_u} is the standard deviation of the momentum in plane u; $T_{IBS,u}$ is the *emittance growth rate* for plane u; T_{rev} is the revolution frequency and $\rho(z)$ is the longitudinal line density.

Note from the form of Eq (17.3.1) that only zero or strictly positive growth rates are valid, and as such this formalism is traditionally available above transition energy.

The longitudinal line density $\rho(z)$ is used as a weighting factor to provide a stronger kick to particles in the denser regions of the bunch. It is obtained by binning the longitudinal plane of the particle distribution and normalizing the values.

17.3.2 Kinetic Kicks

A second element is available to provide momentum kicks based on diffusion and friction terms from the kinetic theory of gases, as introduced by P. Zenkevich [81]. The momentum kick has a form similar to the Langevin equation:

$$\Delta p_u = -K_u p_u \sigma_z\sqrt{\pi}\rho(z)\Delta t + R\sigma_{p_u}\sqrt{2C_u\sigma_z\sqrt{\pi}\rho(z)\Delta t}\ ;\ u = x, y, z \tag{17.3.2}$$

where K_u and C_u are functions of the friction and diffusion terms, respectively.

In *Xfields* the exact implementation makes use of terms from the Nagaitsev formalism (see Sec. 17.1.1) as derived by M. Zampetakis [82]. First the a_x, a_y, a_s, a_1 and a_2 terms are computed according to Eq (17.1.6). Then the λ_1, λ_2 and λ_3 terms are computed according to Eq (17.1.8), to obtain the R_1, R_2 and R_3 elliptic integrals according

to Eq (17.1.9).

New forms equivalent to the original diffusion and friction terms of the Approximate Model can be expressed from these. By first defining

$$q = \sqrt{a_2^2 + \gamma^2 a_x^2 \Phi_x^2}\,, \tag{17.3.3}$$

one can first compute:

$$\begin{aligned} D_{x,x} &= \frac{1}{2}\left[2R_1 + R2\left(1 - \frac{a_2}{q}\right) + R_3\left(1 + \frac{a_2}{q}\right)\right], \\ D_{x,z} &= \frac{3\gamma^2\Phi_x^2 a_x}{q}\left(R_3 - R_2\right), \\ D_{y,y} &= R_2 + R_3, \\ D_{z,z} &= \frac{\gamma^2}{2}\left[2R_1 + R_2\left(1 + \frac{a_2}{q}\right) + R_3\left(1 - \frac{a_2}{q}\right)\right], \end{aligned} \tag{17.3.4}$$

and then:

$$\begin{aligned} K_x &= R_2\left(1 + \frac{a_2}{q}\right) + R_3\left(1 - \frac{a_2}{q}\right), \\ K_y &= 2R_1, \\ K_z &= \gamma^2\left[R_2\left(1 - \frac{a_2}{q}\right) + R_3\left(1 + \frac{a_2}{q}\right)\right]. \end{aligned} \tag{17.3.5}$$

The following integrals are computed from the above:

$$\begin{aligned} D_{xi} &= \int_0^C \frac{\beta_x ds}{C\sigma_x\sigma_y}\left[D_{x,x} + \left(\frac{D_x^2}{\beta_x^2} + \Phi_x^2\right)D_{z,z} + D_{x,z}\right], \\ D_{yi} &= \int_0^C \frac{\beta_y ds}{C\sigma_x\sigma_y} D_{y,y}, \\ D_{zi} &= \int_0^C \frac{ds}{C\sigma_x\sigma_y} D_{z,z}\,. \end{aligned} \tag{17.3.6}$$

$$\begin{aligned} F_{xi} &= \int_0^C \frac{\beta_x ds}{C\sigma_x\sigma_y}\left[K_x + \left(\frac{D_x^2}{\beta_x^2} + \Phi_x^2\right)K_z\right], \\ F_{yi} &= \int_0^C \frac{\beta_y ds}{C\sigma_x\sigma_y} K_x, \\ F_{zi} &= \int_0^C \frac{ds}{C\sigma_x\sigma_y} K_z\,. \end{aligned} \tag{17.3.7}$$

with C the circumference of the machine. Finally, the new diffusion coefficients are computed according to:

$$\boxed{G_x = \frac{1}{\varepsilon_x}\frac{N r_0^2 c L_C}{12\pi\beta^3\gamma^5\sigma_z} D_{xi}} \tag{17.3.8}$$

$$\boxed{G_y = \frac{1}{\varepsilon_y} \frac{N r_0^2 c L_C}{12\pi\beta^3\gamma^5\sigma_z} D_{yi}} \tag{17.3.9}$$

$$\boxed{G_z = \frac{1}{\sigma_\delta^2} \frac{N r_0^2 c L_C}{12\pi\beta^3\gamma^5\sigma_z} D_{zi}} \tag{17.3.10}$$

and the friction coefficients according to:

$$\boxed{F_x = \frac{1}{\varepsilon_x} \frac{N r_0^2 c L_C}{12\pi\beta^3\gamma^5\sigma_z} F_{xi}} \tag{17.3.11}$$

$$\boxed{F_y = \frac{1}{\varepsilon_y} \frac{N r_0^2 c L_C}{12\pi\beta^3\gamma^5\sigma_z} F_{yi}} \tag{17.3.12}$$

$$\boxed{F_z = \frac{1}{\sigma_\delta^2} \frac{N r_0^2 c L_C}{12\pi\beta^3\gamma^5\sigma_z} F_{zi}} \tag{17.3.13}$$

In the above N is the total beam intensity, r_0 the classical particle radius, c the speed of light in vacuum, L_C the Coulomb logarithm from Eq (17.1.2). β and γ are the relativistic parameters of the beam and σ_z the bunch length.

From these coefficients, each particle is given a momentum kick in each dimension according to:

$$\boxed{\Delta p_u = -F_u p_u T_{rev} 2\sqrt{\pi}\sigma_z \rho(z) + R\sigma_{p_u}\sqrt{T_{rev} G_u 2\sqrt{\pi}\sigma_z \rho(z)}\ ;\ u = x, y, z} \tag{17.3.14}$$

Here R is a random number from the standard normal distribution; p_u and σ_{p_u} are the momentum and its standard deviation in plane u; T_{rev} is the revolution frequency and $\rho(z)$ is the longitudinal line density as defined previously (see Sec. 17.3.1).

Chapter 18

Touschek scattering

Touschek scattering originates from single Coulomb scattering events between two relativistic leptons belonging to the same bunch [83]. If the resulting momentum deviation exceeds the momentum acceptance of the machine, or if the induced closed-orbit and betatron oscillations exceed the physical or dynamic aperture, the particles are lost from the beam. In modern low-emittance $e^{\pm}$ storage rings the Touschek effect is typically the dominant limitation to the beam lifetime.
Unlike intra-beam scattering, which describes the cumulative effect of many small-angle Coulomb collisions on the beam emittances, the Touschek effect is a *single-event*, large-momentum-transfer process.
The model described in this chapter follows the approach of Xiao and Borland [84], originally developed for `elegant` [85], and is described in more detail in Ref. [86].

18.1 Touschek scattering rate

In the c.m. frame the probability that one of the two interacting particles is scattered into the element of solid angle $d\Omega^*$ is given by the Møller differential cross-section [87, 84]

$$\frac{d\sigma^*}{d\Omega^*}(\theta^*) = \frac{r_e^2}{4\gamma^{*2}}\left[\left(1+\frac{1}{\beta^{*2}}\right)^2 \frac{4-3\sin^2\theta^*}{\sin^4\theta^*} + \frac{4}{\sin^2\theta^*} + 1\right], \tag{18.1.1}$$

where r_e is the classical electron radius, γ^* and β^* are the relativistic factors in the c.m. frame, θ^* is the c.m. polar scattering angle, ϕ^* the azimuthal angle, and $d\Omega^* = \sin\theta^*\, d\theta^*\, d\phi^*$.
The total Touschek scattering rate is obtained by integrating over all scattering angles and over all particles in the bunch [84]. In the c.m. frame,

$$R^* = 2\int |v^*|\, \sigma^*\, \rho(\mathbf{x}_1^*)\, \rho(\mathbf{x}_2^*)\, dV^*, \tag{18.1.2}$$

where $|v^*|$ is the relative velocity of the two particles and $\rho(\mathbf{x}_i^*)$ the beam phase-space density. The volume element dV^* spans the phase space of both particles, and σ^* is the total Møller cross-section

$$\sigma^* = \int_0^{2\pi}\int_0^{\pi/2} \frac{d\sigma^*}{d\Omega^*}\, \sin\theta^*\, d\theta^*\, d\phi^*. \tag{18.1.3}$$

Transforming to the laboratory frame [84],

$$|v|\,\sigma = \frac{|v^*|}{\gamma}\,\frac{\sigma^*}{\gamma}, \qquad R = 2\int |v|\,\sigma\,\rho(\mathbf{x}_1)\,\rho(\mathbf{x}_2)\,dV, \tag{18.1.4}$$

with

$$dV = dx_\beta\,dy_\beta\,dz\,dx'_{\beta1}\,dx'_{\beta2}\,dy'_{\beta1}\,dy'_{\beta2}\,d\delta_1\,d\delta_2,$$

where (x_β, x'_β) and (y_β, y'_β) denote the betatron coordinates (i.e. with the dispersive contribution removed) and $\delta_i = \Delta p_i/p_0$ the relative momentum deviations. Combining Eqs. (18.1.3) and (18.1.4), the Touschek scattering rate in the laboratory frame can be written in the expanded form

$$R = 2\int\!\!\int_0^{2\pi}\int_0^{\pi/2} \frac{|v^*|}{\gamma^2}\,\frac{d\sigma^*}{d\Omega^*}\,\sin\theta^*\,\rho(\mathbf{x}_1)\,\rho(\mathbf{x}_2)\,d\theta^*\,d\phi^*\,dV. \tag{18.1.5}$$

18.2 Piwinski formula

For a Gaussian bunch, Piwinski [88] evaluated Eq. (18.1.5) in closed form, obtaining an expression for the Touschek scattering rate in terms of the linear optics functions and the beam parameters:

$$\begin{aligned} R_P = {} & \frac{r_e^2 c N_b^2}{8\pi\gamma^2\sigma_z\sqrt{\sigma_x^2\sigma_y^2 - \sigma_\delta^4 D_x^2 D_y^2}}\,\sqrt{\pi(B_1^2 - B_2^2)} \\ & \times \int_{\tau_m}^{\infty}\left[\left(2+\frac{1}{\tau}\right)^2\left(\frac{\tau/\tau_m}{1+\tau}-1\right)+1-\frac{\sqrt{1+\tau}}{\sqrt{\tau/\tau_m}}\right. \\ & \left. -\frac{1}{2\tau}\left(4+\frac{1}{\tau}\right)\ln\frac{\tau/\tau_m}{1+\tau}\right] e^{-B_1\tau} I_0(B_2\tau)\,\frac{\sqrt{\tau}\,d\tau}{\sqrt{1+\tau}}. \end{aligned} \tag{18.2.1}$$

Here N_b is the bunch intensity, c the speed of light in vacuum, γ the Lorentz factor, σ_z the RMS bunch length, σ_δ the RMS relative momentum spread, and I_0 the modified Bessel function of the first kind of order zero. In the implementation the integral is evaluated with the change of variable $\tau = \tan^2 k$, so that $d\tau = 2\tan k(1+\tan^2 k)\,dk$. This maps the semi-infinite interval $\tau \in [\tau_m, \infty)$ to the finite interval $k \in [\arctan\sqrt{\tau_m}, \pi/2)$, which is more convenient for numerical quadrature of the logarithmic, exponential, and Bessel-function terms appearing in the integrand. The Jacobian is included in the numerical integrand: the factor

$$\frac{\sqrt{\tau}}{\sqrt{1+\tau}}\,d\tau = 2\tau\sqrt{1+\tau}\,dk$$

is obtained after the substitution. The RMS transverse beam sizes are

$$\sigma_x = \sqrt{\varepsilon_x\beta_x + D_x^2\sigma_\delta^2}, \qquad \sigma_y = \sqrt{\varepsilon_y\beta_y + D_y^2\sigma_\delta^2}, \tag{18.2.2}$$

while $\sigma_{x\beta} = \sqrt{\varepsilon_x\beta_x}$ and $\sigma_{y\beta} = \sqrt{\varepsilon_y\beta_y}$ denote the betatron beam sizes, with $\varepsilon_{x,y}$ the geometric emittances and $D_{x,y}$ the dispersion functions.

The lower integration limit is related to the local momentum acceptance δ_a through

$$\tau_m = \beta^2 \delta_a^2, \tag{18.2.3}$$

where $\beta = v/c$. The local momentum acceptance (LMA) is the largest momentum deviation that a particle can sustain at a given longitudinal position without being lost. It is in general not symmetric, and is therefore described by a negative and a positive limit, $\delta_N < 0$ and $\delta_P > 0$. In the implementation, Eq. (18.2.1) is evaluated separately for $\delta_a = |\delta_N|$ and $\delta_a = \delta_P$, and the two contributions are averaged to obtain the local Piwinski rate.
The auxiliary quantities B_1 and B_2 are defined as

$$B_1 = \frac{\beta_x^2}{2\beta^2\gamma^2\sigma_{x\beta}^2}\left(1 - \frac{\sigma_h^2 \widetilde{D}_x^2}{\sigma_{x\beta}^2}\right) + \frac{\beta_y^2}{2\beta^2\gamma^2\sigma_{y\beta}^2}\left(1 - \frac{\sigma_h^2 \widetilde{D}_y^2}{\sigma_{y\beta}^2}\right), \tag{18.2.4}$$

$$B_2^2 = B_1^2 - \frac{\beta_x^2\beta_y^2\sigma_h^2}{\beta^4\gamma^4\sigma_{x\beta}^4\sigma_{y\beta}^4\sigma_\delta^2}\left(\sigma_x^2\sigma_y^2 - \sigma_\delta^4 D_x^2 D_y^2\right), \tag{18.2.5}$$

with

$$\widetilde{D}_x = \alpha_x D_x + \beta_x D_x', \qquad \widetilde{D}_y = \alpha_y D_y + \beta_y D_y', \tag{18.2.6}$$

and

$$\frac{1}{\sigma_h^2} = \frac{1}{\sigma_\delta^2} + \frac{D_x^2 + \widetilde{D}_x^2}{\sigma_{x\beta}^2} + \frac{D_y^2 + \widetilde{D}_y^2}{\sigma_{y\beta}^2}. \tag{18.2.7}$$

18.3 Monte Carlo evaluation of the scattering rate

The Piwinski formula gives the local scattering rate, but not the phase-space distribution of the scattered particles, which is what is needed in a particle tracking code to evaluate the beam loss distribution from Touschek scattering. In Xsuite the distribution of scattered particles is obtained by Monte Carlo integration of Eq. (18.1.5).
Using the general Monte Carlo approximation of an integral,

$$\int_V f(\mathbf{x})\, d\mathbf{x} \approx \frac{V}{N}\sum_{i=1}^{N} f(\mathbf{x}_i), \tag{18.3.1}$$

the Touschek scattering rate for particles ending up outside the local momentum acceptance can be written as

$$R_{\mathrm{MC}} = \frac{V}{N}\sum_{i=1}^{M}\left[\frac{|v^*|}{\gamma^2}\frac{d\sigma^*}{d\Omega^*}\sin\theta^*\,\rho(\mathbf{x}_1)\rho(\mathbf{x}_2)\right]_i = \sum_{i=1}^{M} r_i, \tag{18.3.2}$$

where V is the sampled phase-space volume, N the total number of simulated scattering events, and M the number of scattered particles falling outside the acceptance.[1] The term r_i is the contribution of the i-th selected particle to the total rate. For sufficiently large N, R_{MC} converges to the true rate.

[1] A single scattering event can produce one or two such particles; each is counted individually in Eq. (18.3.2).

18.3.1 Sampling of the scattering pair

The sampling is performed in normalized phase space, assuming a Gaussian bunch and no x–y coupling. The longitudinal plane is treated on the same footing as the transverse ones by defining

$$\varepsilon_z = \sigma_z \sigma_\delta, \qquad \beta_z = \frac{\sigma_z}{\sigma_\delta}, \qquad \alpha_z = 0. \tag{18.3.3}$$

Eleven uniformly distributed random numbers are drawn per scattering event. Six of them define the normalized coordinates $(X_1, X_1', Y_1, Y_1', Z_1, \Delta_1)$ of the first particle, drawn uniformly in

$$\left[-n_u\sqrt{\varepsilon_u},\ +n_u\sqrt{\varepsilon_u}\right], \qquad u = x, y, z, \tag{18.3.4}$$

where n_x, n_y and n_z are user-defined truncation parameters (default $n_x = n_y = n_z = 3$, i.e. sampling up to three beam sigmas). Three further random numbers define the normalized slopes and momentum deviation of the second particle, (X_2', Y_2', Δ_2); the two particles are assumed to collide at the same point, so their spatial coordinates coincide,

$$x_2 = x_1, \qquad y_2 = y_1, \qquad z_2 = z_1. \tag{18.3.5}$$

The last two random numbers define the scattering angles, as described in Section 18.3.2. The physical longitudinal coordinates follow from the normalized ones as $z_1 = \sqrt{\beta_z}\, Z_1$ and $\delta_i = \Delta_i / \sqrt{\beta_z}$, so that z_1 and δ_i are sampled uniformly within $\pm n_z\sigma_z$ and $\pm n_z\sigma_\delta$, respectively.
Applying the transformation from normalized to physical coordinates and adding the dispersive contribution gives, for the first particle,

$$\begin{cases} x_1 = \sqrt{\beta_x}\, X_1 + \delta_1 D_x, \\ x_1' = \dfrac{X_1' - \alpha_x X_1}{\sqrt{\beta_x}} + \delta_1 D_x', \\ y_1 = \sqrt{\beta_y}\, Y_1 + \delta_1 D_y, \\ y_1' = \dfrac{Y_1' - \alpha_y Y_1}{\sqrt{\beta_y}} + \delta_1 D_y', \end{cases} \tag{18.3.6}$$

and, for the second particle, whose physical position is imposed by Eq. (18.3.5),

$$\begin{cases} X_2 = \dfrac{x_1 - \delta_2 D_x}{\sqrt{\beta_x}}, \\ x_2' = \dfrac{X_2' - \alpha_x X_2}{\sqrt{\beta_x}} + \delta_2 D_x', \\ Y_2 = \dfrac{y_1 - \delta_2 D_y}{\sqrt{\beta_y}}, \\ y_2' = \dfrac{Y_2' - \alpha_y Y_2}{\sqrt{\beta_y}} + \delta_2 D_y'. \end{cases} \tag{18.3.7}$$

The Gaussian phase-space density at the particles' coordinates is

$$\rho = \frac{N_b}{8\pi^3 \varepsilon_x \varepsilon_y \varepsilon_z} \exp\left(-\frac{z^2}{2\sigma_z^2} - \frac{\delta^2}{2\sigma_\delta^2}\right) \times \exp\left(-\frac{x_\beta^2 + (\alpha_x x_\beta + \beta_x x'_\beta)^2}{2\sigma_{x\beta}^2} - \frac{y_\beta^2 + (\alpha_y y_\beta + \beta_y y'_\beta)^2}{2\sigma_{y\beta}^2}\right), \quad (18.3.8)$$

where the subscript β again denotes betatron coordinates.
The sampled phase-space volume appearing in Eq. (18.3.2) is

$$V = \frac{\pi^2}{\sqrt{\beta_x \beta_y \beta_z}} \left(2n_x\sqrt{\varepsilon_x}\right)^3 \left(2n_y\sqrt{\varepsilon_y}\right)^3 \left(2n_z\sqrt{\varepsilon_z}\right)^3. \quad (18.3.9)$$

18.3.2 Scattering kinematics

Each sampled pair is boosted from the laboratory frame to its center-of-mass frame. The two remaining random numbers define the polar scattering angle θ^*, drawn uniformly in $[\theta_{\min}, \theta_{\max}]$, with $\theta_{\min} = 0.00005\pi$ and $\theta_{\max} = 0.99995\pi$, and the azimuthal angle ϕ^*, drawn uniformly in $[0, \pi]$. The small exclusion around 0 and π avoids the forward/backward divergence of the Møller cross-section.
The momenta are then rotated by (θ^*, ϕ^*) in the c.m. frame and boosted back to the laboratory frame.
The weight of the event is finally computed as the integrand of Eq. (18.3.2), i.e. the product of the two densities, $\sin\theta^*$, the Møller cross-section evaluated at θ^*, and the kinematic factor β^*/γ^2.

18.3.3 Selection of the particles to be tracked

After the boost back to the laboratory frame the pair is ordered so that particle 1 carries the smaller momentum deviation. A particle is retained as a candidate for tracking only if its momentum deviation falls outside the local momentum acceptance,

$$\delta_1 < \delta_N \qquad \text{or} \qquad \delta_2 > \delta_P. \quad (18.3.10)$$

Particles that remain inside the acceptance cannot be lost and are discarded.
The acceptance used in Eq. (18.3.10) is the LMA scaled by a safety factor smaller than one. This accounts for the fact that particles with non-zero betatron amplitude can be lost at momentum deviations smaller than the on-orbit acceptance, and therefore prevents potentially lost particles from being missed.

18.3.4 Weighting of the scattered macroparticles

A lumped-element approach is used to model the losses: the lattice is divided into a series of sections by placing scattering elements at different locations, chosen such that the optics functions vary slowly between adjacent elements. Evaluating the local scattering rate by Monte Carlo integration everywhere in the machine would be computationally expensive. Instead, the Piwinski formula is used to estimate rapidly the

total Touschek scattering rate over each lattice section, and this is used to normalize the Monte Carlo distribution.
The Piwinski rate $R_P(s)$ is evaluated at each scattering element and integrated with the trapezoidal rule over the lattice section between the current and the preceding scattering element. Normalizing to the machine circumference C gives the contribution of that section to the ring-averaged scattering rate,

$$\overline{R}_P = \frac{1}{C} \int_{s_{k-1}}^{s_k} R_P(s)\, ds. \tag{18.3.11}$$

Each scattered macroparticle generated at the element, carrying the local contribution r_i of Eq. (18.3.2), is then assigned the weight

$$w_i = \frac{r_i}{\sum_{j \in S} r_j}\, \overline{R}_P, \tag{18.3.12}$$

where S is the full set of particles selected by Eq. (18.3.10). By default, only the highest-weight subset $S_{\mathrm{tr}} \subseteq S$ is returned for tracking: the retained particles are chosen such that their cumulative contribution is approximately $f_{\mathrm{ret}} \sum_{j \in S} r_j$, where f_{ret} is the `weight_retention_fraction` parameter. For particles in S_{tr} the weights are still normalized with the denominator in Eq. (18.3.12), i.e. with the full selected set S rather than with the retained subset. Therefore, for $f_{\mathrm{ret}} = 1$ the returned ensemble reproduces the total scattering rate from the corresponding section, while for $f_{\mathrm{ret}} < 1$ it reproduces the retained fraction of that rate. Summed over all sections, Eq. (18.3.11) reproduces by construction the ring-averaged Piwinski rate of Eq. (18.3.14) when no particles are discarded.
The full beam-loss profile is obtained by tracking the scattered macroparticles from the location of their scattering element and histogramming the loss positions weighted by w_i. The total Touschek loss rate is the sum of the weights of the lost particles, from which the Touschek lifetime follows as

$$\tau_T = \frac{N_b}{\sum_i w_i}. \tag{18.3.13}$$

For reference, the corresponding analytical estimate from the Piwinski formula is obtained by averaging the local rate over the machine circumference [88],

$$\frac{1}{\tau_T} = \left\langle \frac{R_P}{N_b} \right\rangle = \frac{1}{C} \oint_C \frac{R_P(s)}{N_b}\, ds. \tag{18.3.14}$$

Chapter 19

FFT solvers and convolutions

19.1 Notation for Discrete Fourier Transform

We will use the following notation for the Discrete Fourier Transform of a sequence of length M:

$$\hat{a}_k = \mathrm{DFT}_M(a_m) = \sum_{m=0}^{M-1} a_m \, e^{-j2\pi \frac{km}{M}} \quad \text{for } k \in 0, ..., M \tag{19.1.1}$$

The corresponding inverse transform is defined as:

$$a_m = \mathrm{DFT}_M^{-1}(\hat{a}_k) = \frac{1}{M} \sum_{k=0}^{M-1} \hat{a}_k \, e^{j2\pi \frac{km}{M}} \quad \text{for } m \in 0, ..., M \tag{19.1.2}$$

Multidimensional Discrete Fourier Transforms are obtained by applying 1D DFTs sequentially. For example, in two dimensions:

$$\begin{aligned} \hat{a}_{k_x k_y} &= \mathrm{DFT}_{M_x M_y} \left\{ a_{m_x m_y} \right\} = \mathrm{DFT}_{M_y} \left\{ \mathrm{DFT}_{M_x} \left\{ a_{m_x m_y} \right\} \right\} \\ &= \sum_{m_x=0}^{M_x-1} e^{-j2\pi \frac{k_x m_x}{M_x}} \sum_{m_y=0}^{M_y-1} e^{-j2\pi \frac{k_y m_y}{M_y}} a_{m_x m_y} \end{aligned} \tag{19.1.3}$$

$$\begin{aligned} a_{m_x m_y} &= \mathrm{DFT}^{-1}_{M_x M_y} \left\{ a_{k_x k_y} \right\} = \mathrm{DFT}^{-1}_{M_y} \left\{ \mathrm{DFT}^{-1}_{M_x} \left\{ \hat{a}_{k_x k_y} \right\} \right\} \\ &= \frac{1}{M_x M_y} \sum_{k_x=0}^{M_x-1} e^{j2\pi \frac{k_x m_x}{M_x}} \sum_{k_y=0}^{M_y-1} e^{j2\pi \frac{k_y m_y}{M_y}} \hat{a}_{k_x k_y} \end{aligned} \tag{19.1.4}$$

19.2 FFT convolution - 1D case

The potential can be written as the convolution of a Green function with the charge distribution:

$$\phi(x) = \int_{-\infty}^{+\infty} \rho(x') \, G(x - x') dx' \tag{19.2.1}$$

We assume that the source is limited to the region $[0, L]$:

$$\rho(x) = \rho(x)\,\Pi_{[0,L]}\,(x) \tag{19.2.2}$$

where $\Pi_{[a,b]}(x)$ is a rectangular window function defined as:

$$\Pi_{[a,b]}(x) = \begin{cases} 1 & \text{for } x \in [a,b] \\ 0 & \text{elsewhere} \end{cases} \tag{19.2.3}$$

We are interested in the electric potential only in the region occupied by the sources, so we can compute:

$$\phi_L(x) = \phi(x)\Pi_{[0,L]}\,(x) \tag{19.2.4}$$

We replace Eq. (19.2.2) and Eq. (19.2.4) into Eq.(19.2.1), obtaining:

$$\phi_L(x) = \Pi_{[0,L]}\,(x) \int_{-\infty}^{+\infty} \Pi_{[0,L]}\,(x')\,\rho(x')\,G(x-x')dx' \tag{19.2.5}$$

We apply the change of variable $x'' = x - x'$:

$$\phi_L(x) = \int_{-\infty}^{+\infty} \Pi_{[0,L]}\,(x)\,\Pi_{[0,L]}\,(x-x'')\,\rho(x-x'')\,G(x'')\,dx'' \tag{19.2.6}$$

The integrand vanishes outside the set of the (x, x'') defined by:

$$\begin{cases} 0 < x < L \\ 0 < (x - x'') < L \end{cases} \tag{19.2.7}$$

We flip the signs in the second equation, obtaining:

$$\begin{cases} 0 < x < L \\ -L < (x'' - x) < 0 \end{cases} \tag{19.2.8}$$

Combining the two equations we obtain:

$$-L < -L + x < x'' < x < L \tag{19.2.9}$$

i.e. the integrand is zero for $-L < x'' < L$. Therefore in Eq. (19.2.6) we can replace $G(x'')$ with its truncated version:

$$G_{2L}(x'') = G(x'')\,\Pi_{[-L,L]}\,(x'') \tag{19.2.10}$$

obtaining:

$$\phi_L(x) = \int_{-\infty}^{+\infty} \Pi_{[0,L]}\,(x)\,\Pi_{[0,L]}\,(x-x'')\,\rho(x-x'')\,G_{2L}(x'')dx'' \tag{19.2.11}$$

Since the two window functions force the integrand to zero outside the region $|x''| < L$ we can replace $G_{2L}(x'')$ with its replicated version:

$$G_{2LR}(x'') = \sum_{n=-\infty}^{+\infty} G_{2L}(x'' - 2nL) = \sum_{n=-\infty}^{+\infty} G(x'' - 2nL)\,\Pi_{[-L,L]}\,(x'' - 2nL) \tag{19.2.12}$$

obtaining:

$$\phi_L(x) = \int_{-\infty}^{+\infty} \Pi_{[0,L]}(x)\, \Pi_{[0,L]}\left(x - x''\right) \rho(x - x'')\, G_{2LR}(x'')dx'' \tag{19.2.13}$$

We can go back to the initial coordinate by substituting $x'' = x - x'$:

$$\phi_L(x) = \Pi_{[0,L]}(x) \int_{-\infty}^{+\infty} \rho(x')\, G_{2LR}(x - x')dx' \tag{19.2.14}$$

This is a cyclic convolution, so we can proceed as follows. We split the integral:

$$\phi_L(x) = \Pi_{[0,L]}(x) \sum_{n=-\infty}^{+\infty} \int_{2nL}^{2(n+1)L} \rho(x')\, G_{2LR}(x - x')\, dx' \tag{19.2.15}$$

In each term we replace $x''' = x' + 2nL$:

$$\phi_L(x) = \Pi_{[0,L]}(x) \sum_{n=-\infty}^{+\infty} \int_{0}^{2L} \rho(x''' - 2nL)\, G_{2LR}(x - x''' - 2nL)\, dx''' \tag{19.2.16}$$

We use the fact that $G_{2LR}(x)$ is periodic:

$$\begin{aligned} \phi_L(x) &= \Pi_{[0,L]}(x) \sum_{n=-\infty}^{+\infty} \int_{0}^{2L} \rho(x''' - 2nL)\, G_{2LR}(x - x''')dx''' \\ &= \Pi_{[0,L]}(x) \int_{0}^{2L} \sum_{n=-\infty}^{+\infty} \rho(x''' - 2nL)\, G_{2LR}(x - x''')dx''' \end{aligned} \tag{19.2.17}$$

We can define a replicated version of $\rho(x)$:

$$\rho_{2LR}(x) = \sum_{n=-\infty}^{+\infty} \rho(x - 2nL) \tag{19.2.18}$$

noting that this implies:

$$\rho_{2LR}(x) = 0 \quad \text{for } x \in [L, 2L] \tag{19.2.19}$$

We obtain:

$$\phi_L(x) = \Pi_{[0,L]}(x) \int_{0}^{2L} \rho_{2LR}(x')\, G_{2LR}(x - x')dx' \tag{19.2.20}$$

The function:

$$\phi_{2LR}(x) = \int_{0}^{2L} \rho_{2LR}(x')\, G_{2LR}(x - x')dx' \tag{19.2.21}$$

is periodic with period $2L$. From it the potential of interest can be simply calculated by selecting the first half period $[0, L]$:

$$\phi_L(x) = \Pi_{[0,L]}(x)\, \phi_{2LR}(x) \tag{19.2.22}$$

To compute the convolution in Eq. 19.2.21 we expand $\phi_{2LR}(x)$ in Fourier series:

$$\phi_{2LR}(x) = \sum_{k=-\infty}^{+\infty} \tilde{\phi}_k \, e^{j2\pi k \frac{x}{2L}} \tag{19.2.23}$$

where the Fourier coefficients are given by:

$$\tilde{\phi}_k = \frac{1}{2L} \int_0^{2L} \phi_{2LR}(x) \, e^{-j2\pi k \frac{x}{2L}} \, dx \tag{19.2.24}$$

We replace Eq. (19.2.21) into Eq. (19.2.24) obtaining:

$$\hat{\phi}_k = \frac{1}{2L} \int_0^{2L} \int_0^{2L} \rho_{2LR}(x') \, G_{2LR}(x - x') \, e^{-j2\pi k \frac{x}{2L}} \, dx' \, dx \tag{19.2.25}$$

With the change of variable $x'' = x - x'$ we obtain:

$$\tilde{\phi}_k = \frac{1}{2L} \int_0^{2L} \rho_{2LR}(x') e^{-j2\pi k \frac{x'}{2L}} dx' \int_0^{2L} G_{2LR}(x'') e^{-j2\pi k \frac{x''}{2L}} \, dx'' \tag{19.2.26}$$

where we recognize the Fourier coefficients of $\rho_{2LR}(x)$ and $G_{2LR}(x)$:

$$\tilde{\rho}_k = \frac{1}{2L} \int_0^{2L} \rho_{2LR}(x) \, e^{-j2\pi k \frac{x}{2L}} \, dx \tag{19.2.27}$$

$$\tilde{G}_k = \frac{1}{2L} \int_0^{2L} G_{2LR}(x) \, e^{-j2\pi k \frac{x}{2L}} \, dx \tag{19.2.28}$$

obtaining simply:

$$\hat{\phi}_k = 2L \, \hat{G}_k \, \hat{\rho}_k \tag{19.2.29}$$

We assume that the functions $\rho_{2LR}(x)$ and $G_{2LR}(x)$ are sampled (or averaged) with step:

$$h_x = \frac{2L}{M} = \frac{L}{N} \tag{19.2.30}$$

We can approximate the integrals in Eqs. (19.2.27) and (19.2.28) as:

$$\tilde{\rho}_k = \frac{1}{M} \sum_{n=0}^{M-1} \rho_{2LR}(x_n) \, e^{-j2\pi \frac{kn}{M}} = \frac{1}{M} \hat{\rho}_k \tag{19.2.31}$$

$$\tilde{G}_k = \frac{1}{M} \sum_{n=0}^{M-1} G_{2LR}(x_n) \, e^{-j2\pi \frac{kn}{M}} = \frac{1}{M} \hat{G}_k \tag{19.2.32}$$

where we recognize the Discrete Fourier Transforms:

$$\hat{\rho}_k = \mathrm{DFT}_M \left\{ \rho_{2LR}(x_n) \right\} \tag{19.2.33}$$

$$\hat{G}_k = \mathrm{DFT}_M \left\{ G_{2LR}(x_n) \right\} \tag{19.2.34}$$

Using Eq. (19.2.23) we can obtain a sampled version of $\phi(x)$:

$$\phi_{2LR}(x_n) = \sum_{n=0}^{M-1} \tilde{\phi}_k \, e^{j2\pi \frac{kn}{M}} \tag{19.2.35}$$

where we have assumed that $\phi(x)$ is sufficiently smooth to allow truncating the sum. Using Eqs. (19.2.29), (19.2.31) and (19.2.32) we obtain:

$$\phi_{2LR}(x_n) = 2L \sum_{n=0}^{M-1} \tilde{G}_k \, \tilde{\rho}_k \, e^{j2\pi \frac{kn}{M}} = \frac{2L}{M^2} \sum_{n=0}^{M-1} \hat{G}_k \, \hat{\rho}_k \, e^{j2\pi \frac{kn}{M}} \tag{19.2.36}$$

This can be rewritten as:

$$\phi_{2LR}(x_n) = \frac{1}{M} \sum_{n=0}^{M-1} (h_x \hat{G}_k) \, \hat{\rho}_k \, e^{j2\pi \frac{kn}{M}} = \text{DFT}_M^{-1} \{\phi_k\} \tag{19.2.37}$$

where

$$\hat{\phi}_k = h_x \hat{G}_k \, \hat{\rho}_k \tag{19.2.38}$$

We call "Integrated Green Function" the quantity:

$$G_{2LR}(x_n) = h_x G_{2LR}(x_n) \tag{19.2.39}$$

We introduce the corresponding Fourier transform:

$$\hat{G}_k^{\text{int}} = \text{DFT}_M \left\{ G_{2LR}^{\text{int}}(x_n) \right\} \tag{19.2.40}$$

Eq. (19.2.38) can be rewritten as:

$$\boxed{\hat{\phi}_k = \hat{G}_k^{\text{int}} \, \hat{\rho}_k} \tag{19.2.41}$$

In summary the potential at the grid nodes can be computed as follows:

1. We compute the Integrated Green function at the grid points in the range $[0, L]$:

$$G_{2LR}^{\text{int}}(x_n) = \int_{x_n - \frac{h_x}{2}}^{x_n + \frac{h_x}{2}} G(x) dx \tag{19.2.42}$$

2. We extend to the interval $[L, 2L]$ using the fact that in this interval:

$$G_{2LR}^{\text{int}}(x_n) = G_{2LR}^{\text{int}}(x_n - 2L) = G_{2LR}^{\text{int}}(2L - x_n) \tag{19.2.43}$$

   where the first equality comes from the periodicity of $G_{2LR}^{\text{int}}(x)$ and the second from the fact that $G(x)$ is an even function (i.e. $G(x) = G(-x)$). Note that for $x_n \in [L, 2L]$ we have that $2L - x_n \in [0, L]$ so we can reuse the values computed at the previous step.

3. We transform it:

$$\hat{G}_k^{\text{int}} = \text{DFT}_{2N} \{G_{2LR}(x_n)\} \tag{19.2.44}$$

4. We assume that we are given $\rho(x_n)$ in the interval $[0, L]$. From this we can obtain $\rho_{2LR}(x_n)$ over the interval $[0, 2L]$ simply extending the sequence with zeros (see Eq. (19.2.19)).

5. We transform it:
$$\hat{\rho}_k = \mathrm{DFT}_{2N}\left\{\rho_{2LR}(x_n)\right\} \tag{19.2.45}$$

6. We compute the potential in the transformed domain:
$$\hat{\phi}_k = \hat{G}^{\mathrm{int}}_k \hat{\rho}_k \quad \text{for } k \in [0, 2N] \tag{19.2.46}$$

7. We inverse-transform:
$$\phi_{2LR}(x_n) = \mathrm{DFT}^{-1}_{2N}\left\{\hat{\phi}_k\right\} \tag{19.2.47}$$
which provides the physical potential in the range $[0, L]$:
$$\phi(x_n) = \phi_{2LR}(x_n) \quad \text{for } x_n \in [0, L] \tag{19.2.48}$$

19.3 Extension to multiple dimensions

The procedure described above can be extended to multiple dimensions by applying the same reasoning for all coordinates. This gives the following procedure:

1. We compute the Integrated Green function at the grid points in the volume $[0, L_x] \times [0, L_y] \times [0, L_z]$:
$$G^{\mathrm{int}}_{2LR}(x_{n_x}, y_{n_y}, z_{n_z}) = \int_{x_{n_x}-\frac{h_x}{2}}^{x_{n_x}+\frac{h_x}{2}} dx \int_{y_{n_y}-\frac{h_y}{2}}^{y_{n_y}+\frac{h_y}{2}} dy \int_{z_{n_z}-\frac{h_z}{2}}^{z_{n_z}+\frac{h_z}{2}} dz\, G(x, y, z) \tag{19.3.1}$$

2. We extend to the region $[0, 2L_x] \times [0, 2L_y] \times [0, 2L_z]$ using the fact that:
$$G^{\mathrm{int}}_{2LR}(x_n, y_n, z_n) = G^{\mathrm{int}}_{2LR}(x_n - 2L_x, y_n, z_n) = G^{\mathrm{int}}_{2LR}(2L_x - x_n, y_n, z_n)$$
$$\text{for } x_n \in [L_x, 2L_x], y_n \in [0, 2L_y], z_n \in [0, 2L_z] \tag{19.3.2}$$

$$G^{\mathrm{int}}_{2LR}(x_n, y_n, z_n) = G^{\mathrm{int}}_{2LR}(x_n, y_n - 2L_y, z_n) = G^{\mathrm{int}}_{2LR}(x_n, 2L_y - y_n, z_n)$$
$$\text{for } y_n \in [L_y, 2L_y], x_n \in [0, 2L_x], z_n \in [0, 2L_z] \tag{19.3.3}$$

$$G^{\mathrm{int}}_{2LR}(x_n, y_n, z_n) = G^{\mathrm{int}}_{2LR}(x_n, y_n, z_n - 2L_z) = G^{\mathrm{int}}_{2LR}(x_n, y_n, 2L_z - z_n)$$
$$\text{for } z_n \in [L_z, 2L_z], x_n \in [0, 2L_x], y_n \in [0, 2L_y] \tag{19.3.4}$$

   This allows reusing the values computed at the previous step.

3. We transform it:
$$\hat{G}^{\mathrm{int}}_{k_x k_y k_z} = \mathrm{DFT}_{2N_x 2N_y 2N_z}\left\{G_{2LR}(x_n, y_n, z_n)\right\} \tag{19.3.5}$$

4. We assume that we are given $\rho(x_n, y_n, z_n)$ in the region $[0, L_x] \times [0, L_y] \times [0, L_z]$. From this we can obtain $\rho_{2LR}(x_n)$ over the region $[0, 2L_x] \times [0, 2L_y] \times [0, 2L_z]$ simply extending the matrix with zeros (see Eq. (19.2.19)).

5. We transform it:

$$\hat{\rho}^{\text{int}}_{k_x k_y k_z} = \text{DFT}_{2N_x 2N_y 2N_z} \{\rho_{2LR}(x_n, y_n, z_n)\} \tag{19.3.6}$$

6. We compute the potential in the transformed domain:

$$\hat{\phi}_{k_x k_y k_z} = \hat{G}^{\text{int}}_{k_x k_y k_z} \hat{\rho}_{k_x k_y k_z} \quad \text{for } k_{x/y/z} \in [0, 2N_{x/y/z}] \tag{19.3.7}$$

7. We inverse-transform:

$$\phi_{2LR}(x_n, y_n, z_n) = \text{DFT}^{-1}_{2N_x 2N_y 2N_z} \left\{ \hat{\phi}_{k_x k_y k_z} \right\} \tag{19.3.8}$$

which provides the physical potential in the region $[0, L_x] \times [0, L_y] \times [0, L_z]$:

$$\phi(x_n, y_n, z_n) \;=\; \phi_{2LR}(x_n, y_n, z_n) \text{ for } (x_n, y_n, z_n) \;\in\; [0, L_x] \times [0, L_y] \times [0, L_z] \tag{19.3.9}$$

19.4 Green functions for 2D and 3D Poisson problems

3D Poisson problem, free space boundary conditions

For the equation:

$$\nabla^2 \phi(x, y, z) = -\frac{1}{\varepsilon_0} \rho(x, y, z) \tag{19.4.1}$$

where:

$$\nabla = \left(\frac{\partial}{\partial x}, \frac{\partial}{\partial y}, \frac{\partial}{\partial z} \right) \tag{19.4.2}$$

the solution can be written as

$$\phi(x, y, z) = \iiint_{-\infty}^{+\infty} \rho(x', y', z')\, G(x - x', y - y', z - z')\, dx'\, dy'\, dz' \tag{19.4.3}$$

where:

$$G(x, y, z) = \frac{1}{4\pi\varepsilon_0} \frac{1}{\sqrt{x^2 + y^2 + z^2}} \tag{19.4.4}$$

The corresponding integrated Green function [89] can be written as:

$$G^{\text{int}}_{2LR}(x_{n_x}, y_{n_y}, z_{n_z}) = \int_{x_{n_x} - \frac{h_x}{2}}^{x_{n_x} + \frac{h_x}{2}} dx \int_{y_{n_y} - \frac{h_y}{2}}^{y_{n_y} + \frac{h_y}{2}} dy \int_{z_{n_z} - \frac{h_z}{2}}^{x_{n_z} + \frac{h_z}{2}} dz\, G(x, y, z) \tag{19.4.5}$$

$$= + F\left(x_{n_x} + \frac{h_x}{2}, y_{n_x} + \frac{h_y}{2}, z_{n_x} + \frac{h_z}{2} \right) \tag{19.4.6}$$

$$- F\left(x_{n_x} + \frac{h_x}{2}, y_{n_x} + \frac{h_y}{2}, z_{n_x} - \frac{h_z}{2} \right) \tag{19.4.7}$$

$$- F\left(x_{n_x} + \frac{h_x}{2}, y_{n_x} - \frac{h_y}{2}, z_{n_x} + \frac{h_z}{2} \right) \tag{19.4.8}$$

$$+F\left(x_{n_x}+\frac{h_x}{2},y_{n_x}-\frac{h_y}{2},z_{n_x}-\frac{h_z}{2}\right) \tag{19.4.9}$$

$$-F\left(x_{n_x}-\frac{h_x}{2},y_{n_x}+\frac{h_y}{2},z_{n_x}+\frac{h_z}{2}\right) \tag{19.4.10}$$

$$+F\left(x_{n_x}-\frac{h_x}{2},y_{n_x}+\frac{h_y}{2},z_{n_x}-\frac{h_z}{2}\right) \tag{19.4.11}$$

$$+F\left(x_{n_x}-\frac{h_x}{2},y_{n_x}-\frac{h_y}{2},z_{n_x}+\frac{h_z}{2}\right) \tag{19.4.12}$$

$$-F\left(x_{n_x}-\frac{h_x}{2},y_{n_x}-\frac{h_y}{2},z_{n_x}-\frac{h_z}{2}\right) \tag{19.4.13}$$

where $F(x,y,z)$ is a primitive of $G(x,y,z)$, which can be obtained as:

$$F(x,y,z)=\int_{x_0}^{x}dx\int_{y_0}^{y}dy\int_{z_0}^{x}dz\,G(x,y,z) \tag{19.4.14}$$

with (x_0,y_0,z_0) being an arbitrary starting point.
An expression for $F(x,y,z)$ is the following

$$F(x,y,z)=\frac{1}{4\pi\varepsilon_0}\iiint\frac{1}{\sqrt{x^2+y^2+z^2}}dxdydz \tag{19.4.15}$$

$$=\frac{1}{4\pi\varepsilon_0}\left[-\frac{z^2}{2}\arctan\left(\frac{xy}{z\sqrt{x^2+y^2+z^2}}\right)-\frac{y^2}{2}\arctan\left(\frac{xz}{y\sqrt{x^2+y^2+z^2}}\right)\right. \tag{19.4.16}$$

$$-\frac{x^2}{2}\arctan\left(\frac{yz}{x\sqrt{x^2+y^2+z^2}}\right)+yz\ln\left(x+\sqrt{x^2+y^2+z^2}\right) \tag{19.4.17}$$

$$\left.+xz\ln\left(y+\sqrt{x^2+y^2+z^2}\right)+xy\ln\left(z+\sqrt{x^2+y^2+z^2}\right)\right] \tag{19.4.18}$$

Note that we need to choose the first cell center to be in (0,0,0) for evaluation of the integrated Green function. Therefore the cell edges have non zero coordinates and the denominators in the formula will always be non-vanishing.

2D Poisson problem, free space boundary conditions

For the equation:

$$\nabla_\perp^2\phi(x,y)=-\frac{1}{\varepsilon_0}\rho(x,y) \tag{19.4.19}$$

where:

$$\nabla=\left(\frac{\partial}{\partial x},\frac{\partial}{\partial y}\right) \tag{19.4.20}$$

the solution can be written as

$$\phi(x,y)=\iint_{-\infty}^{+\infty}\rho(x',y')\,G(x-x',y-y')\,dx'\,dy' \tag{19.4.21}$$

where:

$$G(x,y) = -\frac{1}{4\pi\varepsilon_0}\log\left(\frac{x^2+y^2}{r_0^2}\right) \tag{19.4.22}$$

where r_0 is an arbitrary constant which has no effect on the evaluated fields (changes the potential by an additive constant).
The corresponding integrated Green function can be written as:

$$G_{2LR}^{\text{int}}(x_{n_x}, y_{n_y}) = \int_{x_{n_x}-\frac{h_x}{2}}^{x_{n_x}+\frac{h_x}{2}} dx \int_{y_{n_y}-\frac{h_y}{2}}^{y_{n_y}+\frac{h_y}{2}} dy\, G(x,y,z) \tag{19.4.23}$$

$$= +F\left(x_{n_x}+\frac{h_x}{2}, y_{n_x}+\frac{h_y}{2}\right) \tag{19.4.24}$$

$$-F\left(x_{n_x}+\frac{h_x}{2}, y_{n_x}-\frac{h_y}{2}\right) \tag{19.4.25}$$

$$-F\left(x_{n_x}-\frac{h_x}{2}, y_{n_x}+\frac{h_y}{2}\right) \tag{19.4.26}$$

$$+F\left(x_{n_x}-\frac{h_x}{2}, y_{n_x}-\frac{h_y}{2}\right) \tag{19.4.27}$$

where $F(x,y)$ is a primitive of $G(x,y)$, which can be obtained as:

$$F(x,y) = \int_{x_0}^{x} dx \int_{y_0}^{y} dy\, G(x,y) \tag{19.4.28}$$

where (x_0, y_0) is an arbitrary starting point.
An expression for $F(x,y)$ is the following (where we have chosen $r_0 = 1$):

$$F(x,y) = -\frac{1}{4\pi\varepsilon_0}\iint \ln\left(x^2+y^2\right) dx/,dy \tag{19.4.29}$$

$$= \frac{1}{4\pi\varepsilon_0}\left[3xy - x^2\arctan(y/x) - y^2\arctan(x/y) - xy\ln\left(x^2+y^2\right)\right] \tag{19.4.30}$$

Note that we need to choose the first cell center to be in (0,0) for evaluation of the integrated Green function. Therefore the cell edges have non zero coordinates and the denominators in the formula will always be non-vanishing.

19.5 Generalization to observation interval different from source interval

The potential generated by a source $\rho(x)$ can be written as the convolution of a Green function with the charge distribution:

$$\phi(x) = \int_{-\infty}^{+\infty} \rho(x')\, G(x-x')dx' \tag{19.5.1}$$

We assume that the source is limited to the region $[a,b]$:

$$\rho(x) = \rho(x)\,\Pi_{[a,b]}(x) \tag{19.5.2}$$

where $\Pi_{[a,b]}(x)$ is a rectangular window function defined as:

$$\Pi_{[a,b]}(x) = \begin{cases} 1 & \text{for } x \in [a,b] \\ 0 & \text{elsewhere} \end{cases} \tag{19.5.3}$$

We are interested in the electric potential in a given region $[c,d]$, so we can compute:

$$\phi_{cd}(x) = \phi(x)\Pi_{[c,d]}(x) \tag{19.5.4}$$

We combine Eqs. (19.5.2), (19.5.4) and (19.5.1), obtaining:

$$\phi_{cd}(x) = \Pi_{[c,d]}(x) \int_{-\infty}^{+\infty} \Pi_{[a,b]}(x') \, \rho(x') \, G(x-x') dx' \tag{19.5.5}$$

We apply the change of variable $x'' = x - x'$:

$$\phi_{cd}(x) = \int_{-\infty}^{+\infty} \Pi_{[c,d]}(x) \, \Pi_{[a,b]}(x - x'') \, \rho(x - x'') \, G(x'') \, dx'' \tag{19.5.6}$$

The integrand vanishes outside the set of the (x, x'') defined by the two window functions:

$$\begin{cases} c < x < d \\ a < (x - x'') < b \end{cases} \tag{19.5.7}$$

We flip the signs in the second equation, obtaining:

$$\begin{cases} c < x < d \\ -b < (x'' - x) < -a \end{cases} \tag{19.5.8}$$

Combining the two equations we obtain:

$$c - b < -b + x < x'' < -a + x < d - a \tag{19.5.9}$$

i.e. the integrand is not zero for $c - b < x'' < d - a$. Therefore in Eq. (19.5.6) we can replace $G(x'')$ with its truncated version:

$$G_{\text{tr}}(x'') = G(x'') \, \Pi_{[c-b,\, d-a]}(x'') \tag{19.5.10}$$

obtaining:

$$\phi_{cd}(x) = \int_{-\infty}^{+\infty} \Pi_{[c,d]}(x) \, \Pi_{[a,b]}(x - x'') \, \rho(x - x'') \, G_{\text{tr}}(x'') dx'' \tag{19.5.11}$$

We can go back to the initial coordinate by substituting $x'' = x - x'$:

$$\phi_{cd}(x) = \Pi_{[c,d]}(x) \int_{-\infty}^{+\infty} \rho(x') \, G_{\text{tr}}(x - x') dx' \tag{19.5.12}$$

We call:

$$L_1 = b - a \tag{19.5.13}$$

$$L_2 = d - c \tag{19.5.14}$$

The measure of the set on which $G_{\text{tr}}(x'')$ is non zero is

$$(d-a) - (c-b) = L_1 + L_2 \tag{19.5.15}$$

We define L such that:

$$L_1 + L_2 = 2L \tag{19.5.16}$$

Since the two window functions in Eq. 19.5.11 force the integrand to zero outside the region $c - b < x'' < d - a$ of measure $2L$, we can replace $G_{\text{tr}}(x'')$ with its replicated version:

$$G_R(x'') = \sum_{n=-\infty}^{+\infty} G_{\text{tr}}(x'' - 2nL) = \sum_{n=-\infty}^{+\infty} G(x'' - 2nL)\, \Pi_{[c-b,\, d-a]}\left(x'' - 2nL\right) \tag{19.5.17}$$

obtaining:

$$\phi_{cd}(x) = \int_{-\infty}^{+\infty} \Pi_{[c,d]}\left(x\right) \Pi_{[a,b]}\left(x - x''\right) \rho(x - x'')\, G_R(x'') dx'' \tag{19.5.18}$$

We can go back to the initial coordinate by substituting $x'' = x - x'$:

$$\phi_{cd}(x) = \Pi_{[c,d]}\left(x\right) \int_{-\infty}^{+\infty} \rho(x')\, G_R(x - x') dx' \tag{19.5.19}$$

This is a cyclic convolution, so we can proceed as follows. We split the integral:

$$\phi_{cd}(x) = \Pi_{[c,d]}\left(x\right) \sum_{n=-\infty}^{+\infty} \int_{2nL}^{2(n+1)L} \rho(x')\, G_R(x - x')\, dx' \tag{19.5.20}$$

In each term we replace $x''' = x' + 2nL$:

$$\phi_{cd}(x) = \Pi_{[c,d]}\left(x\right) \sum_{n=-\infty}^{+\infty} \int_{0}^{2L} \rho(x''' - 2nL)\, G_R(x - x''' - 2nL)\, dx''' \tag{19.5.21}$$

We use the fact that $G_R(x)$ is periodic:

$$\begin{aligned} \phi_{cd}(x) &= \Pi_{[c,d]}\left(x\right) \sum_{n=-\infty}^{+\infty} \int_{0}^{2L} \rho(x''' - 2nL)\, G_R(x - x''') dx''' \\ &= \Pi_{[c,d]}\left(x\right) \int_{0}^{2L} G_R(x - x''') \sum_{n=-\infty}^{+\infty} \rho(x''' - 2nL)\, dx''' \end{aligned} \tag{19.5.22}$$

We can define a replicated version of $\rho(x)$:

$$\rho_R(x) = \sum_{n=-\infty}^{+\infty} \rho(x - 2nL) \tag{19.5.23}$$

We obtain:

$$\phi_{cd}(x) = \Pi_{[c,d]}(x) \int_0^{2L} \rho_R(x')\, G_R(x - x')dx' \tag{19.5.24}$$

The function:

$$\phi_R(x) = \int_0^{2L} \rho_R(x')\, G_R(x - x')dx' \tag{19.5.25}$$

is periodic with period $2L$. Replacing in Eq. 19.5.24 we see that the potential of interest can be simply calculated by selecting the right interval $[c, d]$:

$$\phi_{cd}(x) = \Pi_{[c,d]}(x)\, \phi_R(x) \tag{19.5.26}$$

To compute the convolution in Eq. 19.5.25 we expand $\phi_R(x)$ in a Fourier series starting from $x = c$:

$$\phi_R(x) = \sum_{k=-\infty}^{+\infty} \tilde{\phi}_k\, e^{j2\pi k \frac{x}{2L}} \tag{19.5.27}$$

where the Fourier coefficients are given by:

$$\tilde{\phi}_k = \frac{1}{2L} \int_0^{2L} \phi_R(x)\, e^{-j2\pi k \frac{x}{2L}}\, dx \tag{19.5.28}$$

We replace Eq. (19.5.25) into Eq. (19.5.28) obtaining:

$$\tilde{\phi}_k = \frac{1}{2L} \int_0^{2L} \int_0^{2L} \rho_R(x')\, G_R(x - x')\, e^{-j2\pi k \frac{x}{2L}}\, dx'\, dx \tag{19.5.29}$$

With the change of variable $x'' = x - x'$ we obtain:

$$\tilde{\phi}_k = \frac{1}{2L} \int_0^{2L} \rho_R(x') e^{-j2\pi k \frac{x'}{2L}} dx' \int_0^{2L} G_R(x'') e^{-j2\pi k \frac{x''}{2L}}\, dx'' \tag{19.5.30}$$

where we recognize the Fourier coefficients of $\rho_R(x)$ and $G_R(x)$:

$$\tilde{\rho}_k = \frac{1}{2L} \int_0^{2L} \rho_R(x)\, e^{-j2\pi k \frac{x}{2L}}\, dx \tag{19.5.31}$$

$$\tilde{G}_k = \frac{1}{2L} \int_0^{2L} G_R(x)\, e^{-j2\pi k \frac{x}{2L}}\, dx \tag{19.5.32}$$

obtaining simply:

$$\tilde{\phi}_k = 2L\, \tilde{G}_k\, \tilde{\rho}_k \tag{19.5.33}$$

We assume that the functions $\rho_R(x)$ and $G_R(x)$ are sampled (or averaged) with step:

$$h_x = \frac{2L}{M} \tag{19.5.34}$$

We assume that all intervals have a size multiple of h_x. So we can define:

$$N_1 = L_1/h_x \tag{19.5.35}$$

$$N_2 = L_2/h_x \tag{19.5.36}$$

We call:

$$\rho_{Rn} = \rho_R\left(a + nh_x\right) \tag{19.5.37}$$
$$\phi_{Rn} = \phi_R\left(c + nh_x\right) \tag{19.5.38}$$
$$G_{Rn} = G_R\left(c - b + nh_x\right) \tag{19.5.39}$$

By construction in the range $0 \leq n < M$:

$$\rho_{Rn} \equiv \rho_n = \begin{cases} \rho\left(a + nh_x\right) & \text{for } 0 \leq n < N_1 \\ 0 & \text{for } N_1 \leq n < M \end{cases} \tag{19.5.40}$$

$$G_{Rn} \equiv G_n = G\left(c - b + nh_x\right) \text{ for } 0 \leq n < M \tag{19.5.41}$$

We can approximate the integral as follows:

$$\tilde{\rho}_k = \frac{1}{2L}\int_0^{2L} \rho_R(x)\, e^{-j2\pi k\frac{x}{2L}}\, dx = \frac{1}{2L}\int_a^{a+2L} \rho_R(x)\, e^{-j2\pi k\frac{x}{2L}}\, dx \tag{19.5.42}$$
$$\simeq \frac{h_x}{2L}\sum_{n=0}^{M-1} \rho_R(a + nh_x)\, e^{-j2\pi k\frac{a+nh_x}{2L}} = e^{-j2\pi k\frac{a}{2L}}\frac{1}{M}\sum_{n=0}^{M-1} \rho_{Rn} e^{-j2\pi\frac{kn}{M}} \tag{19.5.43}$$

We recognize the Discrete Fourier Transform:

$$\tilde{\rho}_k = e^{-j2\pi k\frac{a}{2L}}\frac{1}{M}\text{DFT}_M\left\{\rho_{Rn}\right\} = e^{-j2\pi k\frac{a}{2L}}\frac{1}{M}\hat{\rho}_k \tag{19.5.44}$$

and similarly we can obtain

$$\tilde{\phi}_k = e^{-j2\pi k\frac{c}{2L}}\frac{1}{M}\text{DFT}_M\left\{\phi_{Rn}\right\} = e^{-j2\pi k\frac{c}{2L}}\frac{1}{M}\hat{\phi}_k \tag{19.5.45}$$

$$\tilde{G}_k = e^{-j2\pi k\frac{c-b}{2L}}\frac{1}{M}\text{DFT}_M\left\{G_{Rn}\right\} = e^{-j2\pi k\frac{c-b}{2L}}\frac{1}{M}\hat{G}_k \tag{19.5.46}$$

Replacing in Eq. 19.5.33 we obtain

$$\hat{\phi}_k = h_x e^{j2\pi k\frac{b-a}{2L}}\hat{\rho}_k\hat{G}_k = h_x e^{j2\pi k\frac{N_1}{M}}\hat{\rho}_k\hat{G}_k \tag{19.5.47}$$

19.6 Compressed FFT convolution

We assume that the source has the form

$$\rho(x) = \sum_{j=A}^{B-1} \rho_j^{\text{loc}}(x - jP) \tag{19.6.1}$$

where $\rho_j^{\text{loc}}(x)$ is limited to the interval $[a, b]$.
We are interested in the potential in a set of intervals given by:

$$[c + iP,\ d + iP] \quad \text{for } i = C, ..., D - 1 \tag{19.6.2}$$

The contribution of the j-th term of ρ to ϕ in the i-th interval is:

$$\phi_{ij}(x) = \int_{-\infty}^{+\infty} \rho_j^{\text{loc}}(x' - jP)\, G_{i-j}^{\text{tr}}(x - x')dx' \tag{19.6.3}$$

where:

$$G_l^{\text{tr}}(x'') = G(x'')\, \Pi_{[c-b+lP,\, d-a+lP]}\left(x''\right) \tag{19.6.4}$$

We define a local version of G^{tr} as

$$G_l^{\text{tr, loc}}(x) = G_l^{\text{tr}}(x + lP) = G(x + lP)\, \Pi_{[c-b,\, d-a]}\left(x\right) \tag{19.6.5}$$

obtaining:

$$\phi_{ij}(x) = \int_{-\infty}^{+\infty} \rho_j^{\text{loc}}(x' - jP)\, G_{i-j}^{\text{tr, loc}}(x - x' - (i-j)P)dx' \tag{19.6.6}$$

We replace $x' = x' - jP$:

$$\phi_{ij}(x) = \int_{-\infty}^{+\infty} \rho_j^{\text{loc}}(x')\, G_{i-j}^{\text{tr, loc}}(x - x' - iP)dx' \tag{19.6.7}$$

We define a local version of ϕ:

$$\phi_{ij}^{\text{loc}}(x) = \phi_{ij}(x + iP) \tag{19.6.8}$$

obtaining:

$$\phi_{ij}^{\text{loc}}(x) = \int_{-\infty}^{+\infty} \rho_j^{\text{loc}}(x')\, G_{i-j}^{\text{tr, loc}}(x - x')dx' \tag{19.6.9}$$

We write all the window functions explicitly:

$$\phi_{ij}^{\text{loc}}(x) = \int_{-\infty}^{+\infty} \Pi_{[a,b]}(x')\Pi_{[c-b,\, d-a]}(x - x')\rho_j^{\text{loc}}(x')\, G_{i-j}^{\text{tr, loc}}(x - x')dx' \tag{19.6.10}$$

Again, we want to find the region in x where this is non-zero:

$$a < x' < b \tag{19.6.11}$$
$$c - b < x - x' < d - a \tag{19.6.12}$$

from which:

$$c - b + x' < x < d - a + x' \tag{19.6.13}$$
$$c - b + a < x < d - a + b \tag{19.6.14}$$

So we find that $\phi_{ij}^{\text{loc}}(x)$ is non-zero in the region:

$$c - L_1 < x < d + L_1 \tag{19.6.15}$$

The total potential in the i-th interval of interest:

$$\phi_i^{\text{loc}}(x) = \sum_{j=A}^{B-1} \phi_{ij}^{\text{loc}}(x) = \sum_{j=A}^{B-1} \int_{-\infty}^{+\infty} \rho_j^{\text{loc}}(x')\, G_{i-j}^{\text{tr, loc}}(x - x')dx' \tag{19.6.16}$$

Since all terms in the sum are zero outside the region defined by Eq. 19.6.15 also $\phi_i^{\text{loc}}(x)$ is zero outside the same interval, which is larger by $2L_1$ compared to the set of interest $[c,d]$.
We build:

$$G^{\text{aux}}(x) = \sum_{l=C-B+1}^{D-A-1} G_l^{\text{tr, loc}}(x - lL_{\text{aux}}) \tag{19.6.17}$$

where:

$$L_{\text{aux}} = L_1 + L_2 \tag{19.6.18}$$

and

$$\rho^{\text{aux}}(x) = \sum_{j=A}^{B-1} \rho_j^{\text{loc}}(x - jL_{\text{aux}}) \tag{19.6.19}$$

and we define

$$\phi^{\text{aux}}(x) = \int_{-\infty}^{+\infty} \rho^{\text{aux}}(x')\, G^{\text{aux}}(x - x')dx' \tag{19.6.20}$$

We extract a segment of it:

$$\phi_i^{\text{aux, loc}}(x) = \phi^{\text{aux}}(x + iL_{\text{aux}})\Pi_{[c,d]}(x) \tag{19.6.21}$$

We replace Eq. 19.6.17:

$$\phi_i^{\text{aux, loc}}(x) = \Pi_{[c,d]}(x) \int_{-\infty}^{+\infty} \rho^{\text{aux}}(x')\, G^{\text{aux}}(x - x' + iL_{\text{aux}})dx' \tag{19.6.22}$$

We replace Eq. 19.6.19 and Eq. 19.6.17:

$$\phi_i^{\text{aux, loc}}(x) = \Pi_{[c,d]}(x) \int_{-\infty}^{+\infty} \sum_{j=A}^{B-1} \rho_j^{\text{loc}}(x' - jL_{\text{aux}}) \sum_{l=C-B+1}^{D-A-1} G_l^{\text{tr, loc}}(x - x' + (i-l)L_{\text{aux}})dx' \tag{19.6.23}$$

$$= \Pi_{[c,d]}(x) \sum_{l=C-B+1}^{D-A-1} \sum_{j=A}^{B-1} \int_{-\infty}^{+\infty} \rho_j^{\text{loc}}(x' - jL_{\text{aux}})\, G_l^{\text{tr, loc}}(x - x' + (i-l)L_{\text{aux}})dx' \tag{19.6.24}$$

We change variable $x'' = x' - (i-l)L_{\text{aux}}$

$$\phi_i^{\text{aux, loc}}(x) = \sum_{l=C-B+1}^{D-A-1} \sum_{j=A}^{B-1} \int_{-\infty}^{+\infty} \Pi_{[c,d]}(x)\rho_j^{\text{loc}}(x'' + (i-l-j)L_{\text{aux}})\, G_l^{\text{tr, loc}}(x - x'')dx'' \tag{19.6.25}$$

The integrand is nonzero for:

$$c < x < d \tag{19.6.26}$$

$$a < x'' + (i-l-j)L_{\text{aux}}) < b \tag{19.6.27}$$

$$c - b < x - x'' < d - a \tag{19.6.28}$$

We subtract the first and the last:

$$a < x'' + (i - l - j)L_{\text{aux}}) < b \tag{19.6.29}$$
$$-b < -x'' < -a \tag{19.6.30}$$

We flip the last:

$$a < x'' + (i - l - j)L_{\text{aux}}) < b \tag{19.6.31}$$
$$a < x'' < b \tag{19.6.32}$$

The two are compatible only if

$$l = i - j \tag{19.6.33}$$

This means that in the double sum only the terms satisfying Eq. 19.6.33 are nonzero, hence:

$$\phi_i^{\text{aux, loc}}(x) = \Pi_{[c,d]}(x) \sum_{j=A}^{B-1} \int_{-\infty}^{+\infty} \rho_j^{\text{loc}}(x''+)\, G_{i-j}^{\text{tr, loc}}(x - x'')dx'' \tag{19.6.34}$$

Comparing against Eq. 19.6.16 we find:

$$\Pi_{[c,d]}(x)\phi_i^{\text{aux, loc}}(x) = \Pi_{[c,d]}(x)\phi_i^{\text{loc}}(x) \tag{19.6.35}$$

Using Eq. 19.6.21 we obtain:

$$\Pi_{[c,d]}(x)\phi_i^{\text{loc}}(x) = \Pi_{[c,d]}(x)\phi^{\text{aux}}(x + iL_{\text{aux}}) \tag{19.6.36}$$

To compute the convolution in Eq. 19.6.20 we can use the results from the previous section.
We call:

$$N_S = B - A \tag{19.6.37}$$
$$N_T = D - C \tag{19.6.38}$$
$$\tag{19.6.39}$$

The support of $\rho^{\text{aux}}(x)$ is:

$$[a + AL_{\text{aux}}, a + BL_{\text{aux}}] \text{ having size } N_S L_{\text{aux}} \tag{19.6.40}$$

The support of $G^{\text{aux}}(x)$ is:

$$[c - b + (C - B + 1)L_{\text{aux}}, c - b + (D - A)L_{\text{aux}}] \text{ having size } (N_S + N_T - 1)\, L_{\text{aux}} \tag{19.6.41}$$

Using a sampling step h_x, we can define:

$$N_1 = L_1/h_x \tag{19.6.42}$$
$$N_2 = L_2/h_x \tag{19.6.43}$$
$$N_{\text{aux}} = L_{\text{aux}}/h_x = N_1 + N_2 \tag{19.6.44}$$

The number of samples in the support of $G^{\text{aux}}(x)$ is

$$M_{\text{aux}} = (N_S + N_T - 1)N_{\text{aux}} \tag{19.6.45}$$

We define

$$G_m^{\text{aux}} = G^{\text{aux}}\left(c - b + (C - B + 1)L_{\text{aux}} + mh_x\right) \text{ for } 0 \leq m < M_{\text{aux}} \tag{19.6.46}$$

Replacing Eq. 19.6.17:

$$\begin{aligned} G_m^{\text{aux}} &= \sum_{l=C-B+1}^{D-A-1} G_l^{\text{tr, loc}}(c - b + (C - B + 1)L_{\text{aux}} + mh_x - lL_{\text{aux}}) && (19.6.47)\\ &= \sum_{l=C-B+1}^{D-A-1} G(c - b + (C - B + 1)L_{\text{aux}} + lP + h_x(m - lN_{\text{aux}})) \times && (19.6.48)\\ &\quad \Pi_{[c-b,\, d-a]}(c - b + (C - B + 1)L_{\text{aux}} + h_x(m - lN_{\text{aux}})) && (19.6.49) \end{aligned}$$

We define:

$$\begin{aligned} G_{l,n}^{\text{segm}} = G(c - b + (C - B + 1)L_{\text{aux}} + lP + nh_x)\Pi_{[c-b,\, d-a]}(c - b + (C - B + 1)L_{\text{aux}} + nh_x)\\ \text{for } 0 \leq n < N_{\text{aux}} \text{ and } (C - B + 1) \leq l < (D - A) \end{aligned} \tag{19.6.50}$$

So we can write:

$$G_m^{\text{aux}} = \sum_{l=C-B+1}^{D-A-1} G_{l,m-lN_{\text{aux}}}^{\text{segm}} \tag{19.6.51}$$

We define:

$$\rho_m^{\text{aux}} = \begin{cases} \rho^{\text{aux}}\left(a + AL_{\text{aux}} + mh_x\right) & \text{for } 0 \leq m < N_S N_{\text{aux}} \\ 0 & \text{for } N_S N_{\text{aux}} \leq m < M_{\text{aux}} \end{cases} \tag{19.6.52}$$

We can use the result from before linking the DFTs of these sequences:

$$\hat{\phi}_k^{\text{aux}} = h_x e^{j2\pi k \frac{(B-A-1)L_{\text{aux}} + (b-a)}{(N_S + N_T - 1)L_{\text{aux}}}} = h_x e^{j2\pi k \frac{(N_S-1)N_{\text{aux}} + N_1}{(N_S + N_T - 1)N_{\text{aux}}}} \hat{\rho}_k^{\text{aux}} \hat{G}_k^{\text{aux}} \tag{19.6.53}$$

The inverse DFT of $\hat{\phi}_k^{\text{aux}}$ provides:

$$\phi_m^{\text{aux}} = \phi^{\text{aux}}\left(c + CL_{\text{aux}} + mh_x\right) \quad \text{for } 0 \leq m < N_T N_{\text{aux}} \tag{19.6.54}$$

Bibliography

[1] MAD-X Project website. `http://cern.ch/madx`.

[2] F. C. Iselin. The mad program (methodical accelerator design) - physics methods manual. Technical Report CERN/SL/92-?? (AP), CERN, 1992.

[3] F. Schmidt. SIXTRACK: Single particle tracking code treating transverse motion with synchrotron oscillations in a symplectic manner. Technical Report 94-56, CERN, 1994.

[4] G. Ripken. Non-linear canonical equations of coupled synchro-betatron motion and their solutions within the framework of a non-linear six-dimensional (symplectic) tracking program for ultrarelativistic protons. Technical Report 85-084, DESY, 1985.

[5] D.P. Barber, G. Ripken, and F. Schmidt. A non-linear canonical formalism for the coupled synchro-betatron motion of protons with arbitrary energy. Technical Report 87-36, DESY, 1987.

[6] G. Ripken and F. Schmidt. A symplectic six-dimensional thin-lens formalism for tracking. Technical Report DESY 95-63 and CERN/SL/95-12(AP), DESY, CERN, 1995.

[7] K. Heinemann, G. Ripken, and F. Schmidt. Construction of nonlinear symplectic six-dimensional thin-lens maps by exponentiation. Technical Report 95-189, DESY, 1995.

[8] D.P. Barber, K. Heinemann, G. Ripken, and F. Schmidt. Symplectic thin-lens transfer maps for SIXTRACK: Treatment of bending magnets in terms of the exact hamiltonian. Technical Report 96-156, DESY, 1996.

[9] L.H.A. Leunissen, F. Schmidt, and G. Ripken. 6D beam-beam kick including coupled motion. Technical report, 2001.

[10] A. Latina and R. De Maria. RF multipole implementation. Technical report, CERN-ATS. 2012-088.

[11] E. Forest. *Beam Dynamics: A New Attitude and Framework*. Harcourt Academic Publisher, 1999.

[12] Andrzej Wolski. *Beam dynamics in high energy particle accelerators*. World Scientific, 2014.

[13] Haruo Yoshida. Construction of higher order symplectic integrators. *Physics Letters A*, 150(5):262–268, 1990.

[14] R Talman. Representation of thick quadrupoles by thin lenses. Technical report, Lawrence Berkeley Nat. Lab., Berkeley, CA, 1985.

[15] Helmut Burkhardt, Riccardo De Maria, Massimo Giovannozzi, and Thys Risselada. Improved TEAPOT Method and Tracking with Thick Quadrupoles for the LHC and its Upgrade. page MOPWO027, 2013.

[16] MAD-NG source code repository. `https://github.com/MethodicalAcceleratorDesign/MAD-NG`.

[17] Étienne Forest, Frank Schmidt, and Eric McIntosh. Introduction to the polymorphic tracking code: Fibre bundles, polymorphic taylor types and "exact tracking". Technical report, KEK and CERN, July 2002. `https://madx.web.cern.ch/doc/ptc_report_2002.pdf`.

[18] Étienne Forest, Simon C. Leemann, and Frank Schmidt. Fringe Effects in MAD PART I, Second Order Fringe in MAD-X for the Module PTC. *KEK-PREPRINT-2005-109, https://cds.cern.ch/record/2857004*.

[19] Silke Van Der Schueren. Impact of fringe fields on beam dynamics. *ABP-CAP Section Meeting, CERN, 4 Jul 2025, https://indico.cern.ch/event/1533185/*, 2025.

[20] Silke Van Der Schueren. Dipole fringing fields. *Meeting on fringe fields, CERN, 30 Sept 2024, https://indico.cern.ch/event/1462429*, 2024.

[21] David C. Sagan. *Bmad Reference Manual*. Cornell Laboratory for Accelerator-Based Sciences and Education, 2025. Available at `https://www.classe.cornell.edu/bmad/`.

[22] Helmut Poth. Electron cooling: theory, experiment, application. *Physics reports*, 196(3-4):135–297, 1990.

[23] F. Willeke and G. Ripken. Methods of beam optics. Technical Report 88-114, DESY, 1988.

[24] A. Franchi, L. Farvacque, F. Ewald, G. Le Bec, and K. B. Scheidt. First simultaneous measurement of sextupolar and octupolar resonance driving terms in a circular accelerator from turn-by-turn beam position monitor data. *Phys. Rev. ST Accel. Beams*, 17:074001, Jul 2014.

[25] Andrea Franchi, Simone Maria Liuzzo, and Zeus Marti. Analytic formulas for the rapid evaluation of the orbit response matrix and chromatic functions from lattice parameters in circular accelerators, 2023.

[26] H. Mais and G. Ripken. Theory of Coupled Synchro-Betatron Oscillations I. Technical Report DESY-M-82-05, DESY, 1982.

[27] V. A. Lebedev and S. A. Bogacz. Betatron Motion with Coupling of Horizontal and Vertical Degrees of Freedom. *Journal of Instrumentation*, 5:P10010, 2010.

[28] Y. Luo, P. Cameron, S. Peggs, and D. Trbojevic. Possible phase loop for the global betatron decoupling. Technical Report CAD/AP/174, Brookhaven National Laboratory, Upton, NY 11973, USA, October 4 2004.

[29] Rhodri Jones. Measuring Tune, Chromaticity and Coupling. 5 2020.

[30] Eirik Jaccheri Hoydalsvik, Tobias Hakan Bjorn Persson, and Rogelio Tomas Garcia. Evaluation of the closest tune approach and its MAD-X implementation. 2021.

[31] D. A. Edwards and L. C. Teng. Parametrization of Linear Coupled Motion in Periodic Systems. *IEEE Transactions on Nuclear Science*, 20:885–888, 1973.

[32] Laurent Deniau. Linear coupling treatment in MAD-X. *Presentation at ABP-HSS meeting, CERN, 25 Oct 2017, https://indico.cern.ch/event/672801/.*

[33] Laurent Deniau. Linear coupling treatment in MAD-X: part 2. *Presentation at ABP-HSS meeting, CERN, 22 Nov 2017, https://indico.cern.ch/event/679893/.*

[34] R. Calaga, R. Tomás, and A. Franchi. Betatron Coupling: Merging Hamiltonian and Matrix Approaches. *Physical Review Special Topics – Accelerators and Beams*, 8:034001, 2005.

[35] Albert Hofmann. *The Physics of Synchrotron Radiation*. Cambridge Monographs on Particle Physics, Nuclear Physics and Cosmology. Cambridge University Press, 2004.

[36] H Burkhardt. Monte Carlo generator for synchrotron radiation. Technical report, CERN, Geneva, 1990.

[37] Alexander W. Chao. Evaluation of beam distribution parameters in an electron storage ring. *Journal of Applied Physics*, 50(2):595–598, 07 2008.

[38] Georg H. Hoffstaetter. *High-Energy Polarized Proton Beams: A Modern View*, volume 218 of *Springer Tracts in Modern Physics*. Springer, Berlin, Heidelberg, 2006.

[39] A. W. Chao. Evaluation of Radiative Spin Polarization in an Electron Storage Ring. *Nucl. Instrum. Meth.*, 180:29, 1981.

[40] Ya. S. Derbenev and A. M. Kondratenko. Polarization kinematics of particles in storage rings. *Sov. Phys. JETP*, 37:968–973, 1973.

[41] Michael Boge. Analysis of spin depolarizing effects in electron storage rings. Other thesis, 5 1994.

[42] S. R. Mane. Electron Spin Polarization in High-Energy Storage Rings. 1. Derivation of the Equilibrium Polarization. *Phys. Rev. A*, 36:105–119, 1987.

[43] D. P. Barber and G. Ripken. Radiative polarization, computer algorithms and spin matching in electron storage rings. 7 1999.

[44] Zhe Duan, Mei Bai, Desmond P. Barber, and Qing Qin. A monte-carlo simulation of the equilibrium beam polarization in ultra-high energy electron (positron) storage rings. *Nuclear Instruments and Methods in Physics Research Section A: Accelerators, Spectrometers, Detectors and Associated Equipment*, 793:81–91, 2015.

[45] Silke Van der Schueren, Riccardo De Maria, Elena Benedetto, Daniel Barna, and Mauro Migliorati. Magnetic field modelling and symplectic integration of magnetic fields on curved reference frames for improved synchrotron design: first steps. In *Proceedings of the 15th International Particle Accelerator Conference (IPAC'24)*, pages 1649–1652, Nashville, TN, USA, 2024. `https://doi.org/10.18429/JACoW-IPAC2024-TUPS09`.

[46] J. P. Boris. Relativistic plasma simulation: optimization of a hybrid code. In *Proceedings of the Fourth Conference on Numerical Simulation of Plasmas*, pages 3–67, Washington, DC, 1970. Naval Research Laboratory.

[47] Hong Qin, Jian Xiao, Ruiliang Zhang, Yao He, Yajuan Sun, and William M. Tang. Why is boris algorithm so good? *Physics of Plasmas*, 20(8):084503, 2013.

[48] Ernst Hairer and Christian Lubich. Energy behaviour of the boris method for charged-particle dynamics. *BIT Numerical Mathematics*, 58(4):969–979, 2018.

[49] Peter H. Stoltz, John R. Cary, Gregory Penn, and Jonathan S. Wurtele. Efficiency of a boris-like integration scheme with spatial stepping. *Phys. Rev. ST Accel. Beams*, 5(9):094001, 2002.

[50] Gregory Penn, Peter H. Stoltz, John R. Cary, and Jonathan S. Wurtele. Boris push with spatial stepping. *Journal of Physics G: Nuclear and Particle Physics*, 29(8):1719–1722, 2003.

[51] Ernst Hairer, Syvert P. Nørsett, and Gerhard Wanner. *Solving Ordinary Differential Equations I: Nonstiff Problems*, volume 8 of *Springer Series in Computational Mathematics*. Springer, Berlin, Heidelberg, 2 edition, 1993. `https://doi.org/10.1007/978-3-540-78862-1`.

[52] Ernst Hairer, Christian Lubich, and Gerhard Wanner. *Geometric Numerical Integration: Structure-Preserving Algorithms for Ordinary Differential Equations*, volume 31 of *Springer Series in Computational Mathematics*. Springer, Berlin, Heidelberg, 2 edition, 2006. `https://doi.org/10.1007/3-540-30666-8`.

[53] John David Jackson. *Classical Electrodynamics*. Wiley, New York, 3 edition, 1998.

[54] K Hirata, H Moshammer, and F Ruggiero. A Symplectic Beam-Beam Interaction with Energy Change. *SLAC-PUB-10055*, Dec 2017.

[55] Kohji Hirata. Don't be afraid of beam-beam interactions with a large crossing angle. Technical Report SLAC-PUB-6375, 1994.

[56] G Iadarola, R De Maria, and Y Papaphilippou. Modelling and implementation of the "6D" beam-beam interaction. *CERN-ACC- SLIDES-2018-001*, Dec 2017.

[57] SixTrack Project website. `http://cern.ch/sixtrack`.

[58] SixTrackLib source code repository. `http://github.com/SixTrack/SixTrackLib`.

[59] G Iadarola, R De Maria, and Y Papaphilippou. 6D beam-beam interaction step-by-step. *CERN-ACC-NOTE-2018-0023*, Dec 2017.

[60] W Herr and T Pieloni. Beam-Beam Effects. *in Proceedings of CAS - CERN Accelerator School: Advanced Accelerator Physics Course, 18 - 29 Aug 2013, Trondheim, Norway, CERN-2014-009*, 2014.

[61] Mad-X beam-beam macros, source code repository. `https://github.com/lhcopt/beambeam_macros`.

[62] D. Griffiths. *Introduction to elementary particles*. 2nd rev. version, Wiley, 2008.

[63] C. Weizsäcker. Ausstrahlung bei Stössen sehr schneller Elektronen. *in Zeitschrift Für Physik, vol. 88, Sep. 1934, pp. 612-625.* `https://doi.org/10.1007/BF01333110`.

[64] E. Williams. Correlation of certain collision problems with radiation theory. *in Kong. Dan. Vid. Sel. Mat. Fys. Med., vol. 13N4, 1935, pp. 1-50.* `https://inspirehep.net/literature/1377275`.

[65] D. Schulte. Study of electromagnetic and hadronic background in the interaction region of the TESLA collider. Apr. 1997. `https://cds.cern.ch/record/331845`.

[66] F. Arutyunian and V. Tumanian. The Compton effect on relativistic electrons and the possibility of obtaining high energy beams. *in Physics Letters, vol. 4, 1963, pp. 176-178.* `https://doi.org/10.1016/0031-9163(63)90351-2`.

[67] M. Bassetti and G. Erskine. Closed expression for the electrical field of a two-dimensional Gaussian charge. 1980. `https://cds.cern.ch/record/122227`.

[68] F. Halzen and A. Martin. *Quarks and Leptons: An Introductory Course in Modern Particle Physics*. 1984. `http://www.gammaexplorer.com/wp-content/uploads/2014/03/Quarks-and-Leptons-An-Introductory-Course-in-Modern-Particle-Physics.pdf`.

[69] `GUINEA-PIG` repository. `https://gitlab.cern.ch/clic-software/guinea-pig-legacy`.

[70] I. Ginzburg, G. Kotkin, V. Serbo, and V. Telnov. Colliding ge and gg beams based on the single-pass e±e- colliders (VLEPP type). *in Nuclear Instruments And Methods In Physics Research, vol. 205, pp. 47-68.*, 1983. `https://www.sciencedirect.com/science/article/pii/0167508783901734`.

[71] Kaoru Yokoya. A Computer Simulation Code for the Beam-beam Interaction in Linear Colliders. 10 1985. https://inspirehep.net/literature/218375.

[72] Nicolas Mounet. The LHC Transverse Coupled-Bunch Instability, 2012. Presented 2012.

[73] A. W. Chao. *Physics of collective beam instabilities in high-energy accelerators*. 1993.

[74] H. L, Anderson. *AIP 50th Anniversary: Physics Vade Mecum*. American Institute of Physics, 1981.

[75] Sergei Nagaitsev. Intrabeam Scattering Formulas for Fast Numerical Evaluation. *Phys. Rev. ST Accel. Beams*, 8:064403, 5 2005.

[76] James Bjorken and Sekazi Mtingwa. Intrabeam scattering. In *Particle Accelerators*, pages 115–143. Gordon and Breach Science Publishers, 1983.

[77] F. Antoniou and F. Zimmermann. Revision of Intrabeam Scattering with Non-Ultrarelativistic Corrections and Vertical Dispersion for MAD-X. Technical report, Cern, Geneva, 2012.

[78] Shyh-yuan Lee. *Accelerator Physics (Fourth Edition)*. World Scientific Publishing Company, 2018.

[79] Ji-Gwang Hwang, Marten Koopmans, Markus Ries, Andreas Schälicke, and Roman Muller. Analytical and numerical analysis of longitudinally coupled transverse dynamics of pulse picking by resonant excitation in storage rings serving timing and high-flux users simultaneously. *Nuclear Instruments and Methods in Physics Research Section A: Accelerators, Spectrometers, Detectors and Associated Equipment*, 2019.

[80] Bruce R, Jowett J. M, Blaskiewicz M, and Fischer W. Time Evolution of the Luminosity of Colliding Heavy-Ion Beams in BNL Relativistic Heavy Ion Collider and CERN Large Hadron Collider. *Physical Review Special Topics - Accelerators and Beams*, 13(9), 2010.

[81] Zenkevich P, Boine-Frankenheim O, and Bolshakov A. A new Algorithm for the Kinetic Analysis of Intra-Beam Scattering in Storage Rings. *Nuclear Instruments and Methods in Physics Research Section A: Accelerators, Spectrometers, Detectors and Associated Equipment*, 561(2):284–288, 2006.

[82] M. Zampetakis, F. Antoniou, F. Asvesta, H. Bartosik, Y. Papaphilippou, and A.S. Hernández. Interplay of Space Charge and Intra-Beam Scattering in the LHC Ion Injector Chain. 2023.

[83] C. Bernardini, G. F. Corazza, G. Di Giugno, G. Ghigo, J. Haissinski, P. Marin, R. Querzoli, and B. Touschek. Lifetime and Beam Size in a Storage Ring. *Phys. Rev. Lett.*, 10:407–409, 5 1963.

[84] A. Xiao and M. Borland. Monte Carlo simulation of Touschek effect. *Phys. Rev. ST Accel. Beams*, 13:074201, 7 2010.

[85] M. Borland. elegant: A Flexible SDDS-Compliant Code for Accelerator Simulation. Technical Report APS LS-287, Advanced Photon Source, Argonne National Laboratory, 2000.

[86] Giacomo Broggi. *FCC-ee collimation system design*. PhD thesis, Sapienza Università di Roma, Rome, Italy, 2026.

[87] Chr. Møller. Zur Theorie des Durchgangs schneller Elektronen durch Materie. *Annalen der Physik*, 406(5):531–585, 1932.

[88] A. Piwinski. The Touschek Effect in Strong Focusing Storage Rings. Technical Report DESY-98-179, DESY, Hamburg, 1998. arXiv:physics/9903034.

[89] Ji Qiang, Miguel A. Furman, and Robert D. Ryne. A parallel particle-in-cell model for beam–beam interaction in high energy ring colliders. *Journal of Computational Physics*, 198(1):278–294, 2004.